Polaronic and Dynamic Effects in Ultracold Quantum Gases

DISSERTATION

zur Erlangung des Doktorgrades
der Naturwissenschaften

vorgelegt beim Fachbereich der Physik
der Johann Wolfgang Goethe-Universität
in Frankfurt am Main

von
M. Sc. Tao Yin
aus
Shandong (China)

Frankfurt am Main 2016
(D30)

vom Fachbereich Physik der
Johann Wolfgang Goethe-Universität
als Dissertation angenommen.

Dekan: Prof. Dr. Rene Reifarth

Gutachter: Prof. Dr. Walter Hofstetter
              Prof. Dr. Roser Valentí

Datum der Disputation:

Contents

Chapter 1

Introduction

The field of ultracold physics has explored a wide variety of phenomena in the last 20 years, after the first realization of Bose-Einstein condensate in 1995. Experimental setups consisting of ultracold atoms, ions or combinations of both have made remarkable achievements, demonstrating precise control over their properties [1, 2, 3, 4, 5]. In particular, the field has had many great successes due to the ability of ultracold experiments to tune across wide parameter regimes, to easily access and probe phase transitions [5, 4], as well as excitation spectra and dynamics of systems analog to condensed matter [6, 7, 8, 9]. Almost all parameters of the system such as the temperature, number of atoms, and the strength and sign of interaction can be varied by several orders of magnitude.

The desire of better understanding of condensed matters is one of the motivations for the fast development of ultracold quantum gases. In order to probe the dynamics of a complex quantum system and study its properties, we need to calculate the system exactly or make use of many unrealistic approximations. However, even for a simple system with two states for each particle, we need to deal with 2^N degrees of freedom, which is impossible for even small and modest values N. In 1982, Richard Feynman was the first to suggest that a complex quantum system could be simulated with another more easily controlled quantum system, introducing the idea of *quantum simulation* [10]. Due to the well control and high tunability, the system of ultracold quantum gases is one of the best experiment setups for quantum simulation. We can even simulate some purely important theoretical models and test their validity. In recent experiments, even features such as artificial gauge fields can be implemented for neutral atomic particles, allowing for the investigation of topological phases [11, 12].

This dissertation is broken into eight chapters. In chapter 1 I give a brief introduction and present basic concepts in quantum simulation.

In chapter 2 I firstly review the history and recent developments in quantum simulation with ultracold quantum gases. Then I discuss some important topics and background in detail, which are related to this thesis. I start with a single neutral atom and discuss methods through which it can be manipulated such as cooling, trapping techniques as well as geometry control. Then I discuss the behavior and tunability of interactions between two ultracold atoms in low energy limit. At the end of this chapter, I also discuss the open quantum system and the Lindblad master equation approach.

One of the important topics in quantum simulation as well as solid state physics is electron-phonon interaction, which plays a key role in superconductivity. In the first part of this thesis, I will discuss a single neutral impurity interacting with a quantum bath.

In chapter 3 I present the general overview of polaronic effects with a bosonic or fermionic bath. In this thesis I focus on the system in which the impurities are interacting with a bosonic bath. The theoretical description of this system is discussed. The bosonic bath is firstly treated by a Bogoliubov approximation in the weak boson-boson interaction limit, and then by the Gutzwiller mean-field approximation in all boson-boson interaction strengths. The polaron dynamics in an open quantum system are also discussed.

In chapter 4, I consider a specific system and focus on the dynamics and formation of a two-band polaron, in which an impurity living within two Bloch bands is dressed by a "cloud" of BEC phonons as a quasi-particle. Collaborators and I develop an effective model and apply a variational two-band Lang-Firsov polaron transformation to this system. The coherent polaron dynamics and inter-band relaxation are both discussed in this system.

In chapter 5 I study the system with multi-polaron coupled to a BEC. The previous method is generalized to a multi-impurity system including induced long-range interaction between polarons. It is able to describe the induced interactions and hopping renormalization within an extended Hubbard model, after applying the variational Lang-Firsov polaron transformation. The system is analyzed by the use of Hartree-Fock mean field theory. This system will be further studied by means of dynamical mean-field theory (DMFT) and is expected to show an interesting phase diagram.

In the second part of this thesis, I study another topic, namely hybrid atom-ion systems and periodically driven systems. In chapter 6, I introduce the Floquet theory and its basic concepts. Secondly, I apply these methods in a hybrid atom-ion system where the ions are trapped by a time-dependent Paul trap. The ionic micromotion plays an important role in such systems, as a consequence of the time-dependent trapping potential and atom-ion collisions. The effects of heating and decoherence arising from the ionic micromotion have been investigated.

In chapter 7, I discuss polaronic effects again in a hybrid atom-ion system with a trapped ion chain coupled to one-dimensional ultracold fermions [13]. Several solid-state models can be simulated by this system such as phonon excitation in ionic crystal and electron-phonon coupling. I calculate effective polaron hopping parameters and phonon-mediated interactions by means of the Lang-Firsov transformation. Dynamic properties and decoherence effects are also studied in this system.

In chapter 8 I summarize the results and conclude the thesis.

Chapter 2

Quantum Simulation with Ultracold Gases

At ultracold temperatures, the quantum world of identical particles of the same species can exhibit remarkably different behavior in contrast with the same system at high temperatures. Particles with integer spin are called bosons while particles with half-integer spin are called fermions. Bosons obey Bose-Einstein statistics in which any number of them can occupy the same single-particle state without restriction. The many-body wave function must be symmetric under the exchange of any two identical bosons. At low temperatures, this symmetry requirement of bosons becomes increasingly pronounced when the number of bosons is large. Below a transition temperature, a large number of identical bosons suddenly begin to condense into a single state, resulting in highly non-classical phenomena at low temperature.

The system formed at these low temperatures is called a Bose-Einstein Condensate (BEC). This is a quantum state of matter, in which a macroscopic number of bosonic particles occupy one single-particle state. Though the theory of BEC was already predicted in the 1920s by Bose and Einstein, it took more than 70 years of experimental advances to achieve the required low temperature and (relative) high density for quantum degeneracy region. Firstly, the atoms are cooled by interacting with laser beams to microkelvin temperatures and confined in a magneto-optical trap (MOT). Then temperature is further reduced by polarization gradient cooling and Sisyphus cooling down to the recoil energy limit. Finally in 1995, by applying the evaporative cooling method, the system reaches the temperature on the scale of a few nanokelvin while keeping the required densities of the BEC.

In many cases, the BEC plays an essential role in both superfluidity and superconductivity. However, it is important to note that there is no unique relationship between BEC and superfluidity. For example, an ideal gas BEC shows no superfluidity and a two-dimensional superfluid shows no BEC.

On the other hand, the many-body state must be antisymmetric when two identical fermionic particles are exchanged. At low temperature, fermions become degenerate below the Fermi temperature, where almost every quantum state below the Fermi energy is occupied by one fermion and the quantum states above the Fermi energy are empty. At even lower temperatures, fermionic systems may also undergo BEC by forming molecules or exhibit superfluidity by forming Cooper pairs. Unlike bosons, fermionic atoms are much harder to cool due to the Pauli exclusion principle which suppresses thermalization rates at low temperatures. The method of sympathetic cooling allows the fermionic gas to be cooled by adding another species, usually a cold bosonic gas after evaporate cooling, in order to enhance the thermalisation rates. Both molecular condensates [14] and Bardeen-Cooper-

Schrieffer (BCS) -type superfluids have been realized using alkali fermions, allowing us to study strongly correlated many-body Fermi gases in experiments.

The interaction between atoms plays an important role for phase transitions in most strongly correlated systems. For both bosons and fermions, the low-energy interaction behaviors can be modified by effectively coupling to a bound state in another or the same scattering channel. By ramping the effective detuning between scattering- and bound states, it is possible to exploit magnetic or optical Feshbach resonances to tune the strength and even the sign of the two-body scattering length [15]. For example, a two-component Fermi gas exhibits a crossover from BCS superfluid to molecular BEC by tuning the low-energy interactions from positive to negative scattering lengths.

A periodic potential for ultracold atoms can be produced by creating a so-called optical lattice through the interference of two counter-propagating laser beams. As was first proposed theoretically [2] and demonstrated experimentally [16], cold atoms in optical lattices can be used to simulate solid state physics. In a deep optical lattice, the Hamiltonian of the system is well described by Hubbard-type models. Besides, using different arrangements and polarization for the lasers, many different kinds of lattice geometries and dimensions can be controlled in the experiments. This high tunability of optical lattices allows us to simulate quantum many-body phases and dynamics in a wide parameter region.

A realistic quantum system is always coupled to its external environment and should be treated as an open quantum system. Ultracold quantum gases represent an excellent toolbox to simulate the dynamics and decoherence of an open quantum system. The coupling between system and environment, which was historically considered to be a disadvantage, can even be used to cool the atoms or drive the system into desired quantum states [17, 18].

2.1   Cooling and trapping

2.1.1   Doppler cooling and below

The first stage of producing an ultracold gas is to take the hot, fast atoms which are emitted from an oven and pass them through a Zeeman slower. In the Zeeman slower, an off-resonance laser with wave vector $\mathbf{k}$ propagates in the opposite direction of the atomic beam with velocity $\mathbf{v}$. Due to the Doppler effect, the laser frequency is shifted to a higher frequency in the atom's frame and becomes resonant. When the atom is excited by absorbing a photon, its velocity is reduced to $\mathbf{v} - \hbar\mathbf{k}/m$ and thus slowed down. A short time later, the atom emits a photon in a random direction. The atom is cooled since this random direction means that the momentum change averaged over emissions is negligible.

As the velocity of the atom changes as it is cooled, the setup must be adjusted continuously in order to satisfy the resonance condition. This can be done by applying an inhomogeneous
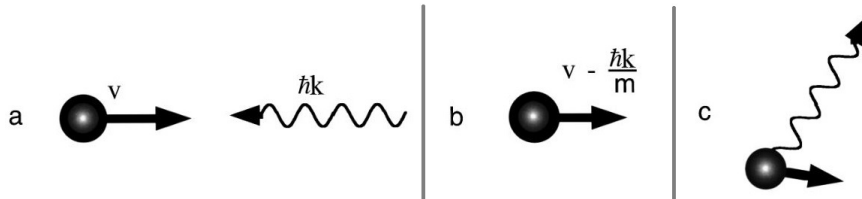
Figure 2.1: Doppler cooling illustration. (a) An atom with velocity $\mathbf{v}$ interacts with a laser with wave vector $\mathbf{k}$. (b) The atom is slowed by absorbing a photon. (c) The atom emits a photon with random momentum. The figure is from [19].

magnetic field to reduce the resonance frequency while keeping the laser frequency fixed. On the other hand, we can also adjust the frequency of cooling laser while maintaining the resonance frequency fixed. However, the system can only be cooled to a finite temperature, which arises from the fluctuations in the atom's momentum due to the randomized emission of photons. This temperature is called Doppler limit as

$$k_B T_D = \frac{\hbar \Gamma_e}{2}, \tag{2.1}$$

where Γ_e is the rate of spontaneous emission of the excited state. After passing the Zeeman slower, the atoms are slow enough to be captured by a magneto-optical trap (MOT).

It turns out that the experimentally achieved temperatures are even lower than the Doppler limit predicted by theory. These measurements motivated the understanding of cooling mechanisms below Doppler limit. By noticing that the achieved temperature depends on both the polarization of laser beams and the Zeeman level of atoms, people discovered a sub-Doppler cooling mechanism which can cool atoms to a thermal energy in order of the so-called recoil energy,

$$E_R = k_B T_R = \frac{\hbar^2 \mathbf{k}^2}{2m}, \tag{2.2}$$

where T_R is the corresponding recoil limit temperature. This is the lowest limiting temperature for laser-based cooling method and lies several orders of magnitude below the Doppler limit. These investigations showed that the phenomenon of Sisyphus cooling is occurring in the experiment, allowing for lower temperatures than expected. Further advances made use of these ideas to produce polarization gradient cooling.

2.1.2 Evaporative cooling

Unfortunately, the typical temperature ($\sim \mu$K) after laser cooling is still too "hot" and is not in the quantum degenerate regime. In experiments, the final step to achieving Bose–Einstein condensation is evaporative cooling, in which the temperature of the system is reduced through a repeated sequence of expelling the hottest atoms and subsequent rethermalisation. By adiabatically ramping down the trap depth, the atoms with high energy are able to escape due to elastic collisions. The remaining atoms will stay in a smaller volume of phase space after a small fraction of atom loss. The system is then rethermalized to a low temperature in the presence of interatomic interactions. In the end, this leads to an increase in the phase space density. In 1995, BEC was finally achieved in experiments with the temperature on the scale of few nanokelvin. Until now, the evaporative cooling method is still the most powerful cooling technology for cooling the system to quantum degeneracy.

For bosons, the achievable temperature after evaporative cooling is only limited by heating due to released internal energy and the changes of internal states. On the other hand, however, single species fermions are much more difficult to cool due to the absence of interatomic s-wave interactions. This is solved by adding another species, such as cold bosons or fermions in different internal states, to sympathetically cool the system.

2.1.3 Magneto-optical trap (MOT)

The slow atoms after cooling can be trapped by both magnetic field and laser beams. Due to the Zeeman effect, neutral atoms with dipoles can be trapped magnetically by a local field minimum or maximum. The magnetic field contribution to the energy shift will be

$$\Delta E = -\mu_l |B|. \tag{2.3}$$
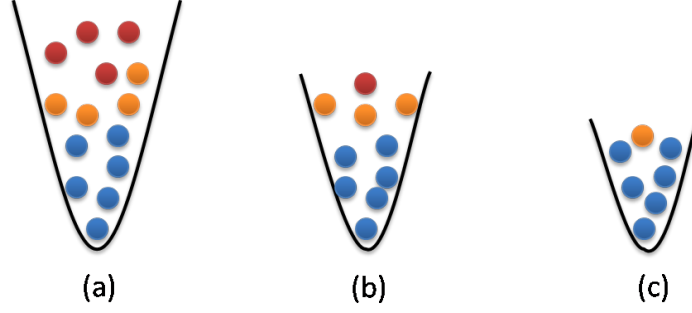
Figure 2.2: Evaporative cooling. (a) Atoms have a high temperature in a deep trap. (b) Hot atoms are escaping from the trap while decreasing the trap depth. (c) Atoms are cooled down to a lower temperature.

The atomic states with a positive magnetic moment will be driven to a higher field region as high-field seekers, while on the other hand the states with negative moments will be pushed to lower field region as low-field seekers. Since it is not possible to build a local magnetic field maximum in regions where there are no electrical currents, the only possible configuration is a magnetic trap with a local minimum field. Thus, only the low-field seekers of atom states can be trapped by purely magnetic fields.

The simple quadrupole trap is one of the configurations in which the magnetic field has a local minimum $|B| = 0$ at the center of the trap. This can be produced, for example, by a pair of opposed Helmholtz coils. Since the magnetic field varies linearly with distance, the trapping force is neither harmonic nor central. This unfortunately implies that the atomic angular momentum can not be conserved in the trap. Another disadvantage of simple quadrupole trap is the large atom loss in the trapping central where the magnetic field is zero. The low-field seeker states may transit to high-field seeker states around this point, thus leading to an effective "hole" near the trap center. This disadvantage can be overcame by using magnetic field configurations with non-zero minima as done in the time-averaged orbiting potential (TOP) trap. The Quic trap, which combines a quadropole and Ioffe coil, is another widely used trapping technique in ultracold atomic experiments.

The radiation pressure and dipole force from laser beams play a very important role in the cooling and manipulation of atoms. An optical trap is the potential created by the ac-Stark effect. This is a second-order process between the interaction of atom dipole moment $\mathbf{d}$ and electric field $\mathbf{E}(\mathbf{r})$. Consider two atomic energy levels $|g\rangle$ and $|e\rangle$ are coupled by a time-dependent electric field with frequency ω_l. If the frequency ω_l is sufficiently far from the resonance frequency ω_{eg} between these two energy levels, the excited state can be adiabatically eliminated. The detuning δ of the laser is defined as

$$\delta \equiv \omega_l - \omega_{eg} = \omega_l - \frac{E_e - E_g}{\hbar}, \tag{2.4}$$

and can be positive or negative, also known as blue or red detuning respectively. When the detuning is larger than the kinetic energy of the atoms, this process gives an effective potential of

$$V(\mathbf{r}) = -\frac{\hbar \Omega^2(\mathbf{r}) \delta}{\delta^2 + \Gamma_e^2/4}, \tag{2.5}$$
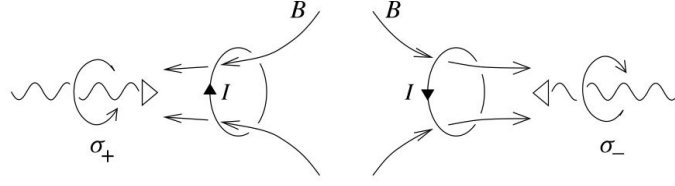
Figure 2.3: The magneto-optical trap (MOT). The figure is from [20].

where the effective Rabi frequency is given by

$$\Omega\left(\mathbf{r}\right) = \frac{\langle e|\mathbf{d} \cdot \mathbf{E}\left(\mathbf{r}\right)|g\rangle}{\hbar}. \tag{2.6}$$

The ground-state energy shifts are thus positive for blue detuning and negative for red detuning. In experiment, by tightly focusing far off-resonant laser beams, a conservative dipole potential will be formed. This potential can be used for trapping due to space dependent laser beam intensity.

In most experiments the atoms are trapped by a magneto-optical trap (MOT), which is done by a combination of a spatially varying magnetic field and laser beams.

2.2   Atomic interaction

In ultracold atomic systems, the interaction between atoms is dominated at long range by the interaction between induced dipoles of both atoms. This typical atomic interaction has an attractive tail at long distances as $V\left(r\right) \propto -C_6/r^6$ when $r \to \infty$. This van der Waals interaction has a characteristic length scale of $r_{\mathrm{vdW}} = \left(mC_6/\hbar^2\right)^{1/4}$. In typical systems, this characteristic length of atomic interaction is the order of $r_{\mathrm{vdW}} \approx 10^1\text{Å} = 10^{-9}\text{m}$. The average distance between atoms is $d \approx 10^{-6}-10^{-7}m$ with density of atom $n \approx 10^{18}-10^{22}\text{m}^3$. Hence, it is clear that only the long-range behavior, described by the induced dipole-dipole interaction, is important.

In the low-energy limit, the scattering behavior of two colliding atoms can be well described by a single parameter, known as the (s-wave) scattering length a_s. This scattering length is defined by the scattering amplitude. Consider two atoms with masses m_1 and m_2 and interaction $V\left(\mathbf{r}_1 - \mathbf{r}_2\right)$. The reduced mass is $m_* = m_1 m_2/(m_1 + m_2)$. The scattering process is described by a wave function $\psi\left(\mathbf{r}\right)$ where $\mathbf{r}$ is the distance between two atoms. This two-body system has a total energy

$$E = \hbar^2 \mathbf{k}^2/2m_* \tag{2.7}$$

with wave vector $\mathbf{k}$ in $\mathbf{z}$ direction. In a spherically symmetric single-channel model, the long range behavior for $\psi\left(\mathbf{r}\right)$ at $\mathbf{r} \to \infty$ can be expressed as

$$\psi(\mathbf{r}) = e^{ikz} + f_k(\theta)\frac{e^{i\mathbf{k}\cdot\mathbf{r}}}{|\mathbf{r}|}, \tag{2.8}$$

where $f_k(\theta)$ indicates the scattering amplitude with scattering angle θ between $\mathbf{k}$ and $\mathbf{r}$. The differential scattering cross section is related to the scattering amplitude through

$$\frac{d\sigma}{d\Omega} = |f_k(\theta)|^2. \tag{2.9}$$

For a spherically symmetric potential, we can break the scattering amplitude $f_k(\theta)$ into contributions from different partial waves as

$$
\begin{aligned}
f_k(\theta) =& \frac{1}{k} \sum_{\ell=0}^{\infty} (2\ell+1) \left(e^{i\delta_\ell(k)} \sin \delta_\ell(k) \right) P_\ell(\cos\theta) \\
=& \sum_{\ell=0}^{\infty} \frac{(2\ell+1)}{k \cot \delta_\ell(k) - ik} P_\ell(\cos\theta),
\end{aligned}
\tag{2.10}
$$

with phase shift $\delta_\ell(k)$ for $\ell-$th partial wave. We can expand the incident wave function e^{ikz} in Legendre polynomials:

$$
e^{ikz} = e^{ikr\cos\theta} = \sum_{\ell=0}^{\infty} (2\ell+1) i^\ell \jmath_\ell(kr) P_\ell(\cos\theta),
\tag{2.11}
$$

where $\jmath_\ell(kr)$ is spherical Bessel function with long-range behavior as

$$
\jmath_\ell(kr) \xrightarrow[r\to\infty]{} \frac{1}{kr} \sin(kr - \frac{1}{2}\ell\pi).
\tag{2.12}
$$

By combining Eq. (2.12) and Eq. (2.8), we get the boundary condition

$$
\begin{aligned}
\psi(\mathbf{r}) \xrightarrow[r\to\infty]{}& \frac{1}{kr} \sum_{\ell=0}^{\infty} (2\ell+1) \left[i^\ell \sin(kr - \frac{1}{2}\ell\pi) + \left(e^{i\delta_\ell(k)} \sin \delta_\ell(k) \right) e^{ikr} \right] P_\ell(\cos\theta) \\
=& \frac{1}{kr} \sum_{\ell=0}^{\infty} (2\ell+1) i^\ell e^{2i\delta_\ell} \sin(kr - \frac{1}{2}\ell\pi + \delta_\ell) P_\ell(\cos\theta).
\end{aligned}
\tag{2.13}
$$

The scattered wave function is only different from the incident wave function Eq. (2.11) by a phase shift $\delta_\ell(k)$ in each partial wave. In the asymptotic region, where the potential has vanished, the interaction $V(\mathbf{r})$ only affects the phase shift δ_ℓ. The scattering behavior at $r \to \infty$ in the system is fully described by phase shift $\delta_\ell(k)$ in each partial wave.

The system is in the low-energy limit when $\hbar^2 \mathbf{k}^2/2m_* \ll \hbar/2m_* r_0^2$ or $k \ll 1/r_0$, where r_0 is the characteristic length of atomic interaction. In the low energy limit $k \to 0$ with a short-range potential, the phase shift $\delta_\ell(k)$ approaches zero as $k^{2\ell+1}$. For two indistinguishable bosons, the s-wave ($\ell=0$) scattering process is dominated in this limit. For two indistinguishable fermions, the p-wave ($\ell=1$) scattering process is dominated due to the Pauli exclusion principle. Up to second order in k, the s-wave phase shift $\delta_\ell(k)$ is expressed as

$$
k \cot \delta_0(k) = -\frac{1}{a_s} + \frac{1}{2} r_s k^2 + \cdots,
\tag{2.14}
$$

with s-wave (two-body) scattering length a_s and effective range r_s.

In the case of a long-range interaction with an attractive tail

$$
V(\mathbf{r}) \xrightarrow[r\to\infty]{} -1/r^n, \; (n > 1),
$$

the phase shift $\delta_\ell(k)$ for higher partial wave approaches zero more slowly than in the short-range interaction case. For $\ell > (n-2)/2$, the phase shift $\delta_\ell(k)$ approaches zero as k^{n-1}. In particular for van der Waals interaction between two neutral atoms, the potential has a long-range tail as $-1/r^6$. Thus the phase shift $\delta_\ell(k)$ for $\ell=0$, 1, and 2 approach zero as

k, k^3, and k^5. As for the case of a short-range potential, this system is also well-described by $s-$wave ($\ell = 0$) scattering processes in the low-energy limit.

On the other hand, in the case of longer ranged interactions, the phase shift in higher partial waves is comparable with the s-wave phase shift. For example for a dipole-dipole type interaction with $n = 3$, all of the phase shifts $\delta_\ell(k)$ for $\ell > 1/2$ approach zero as k^2. Thus the system can not be described by only $s-$wave scattering even in the low-energy limit.

In dilute ultracold atomic systems in the low-energy limit, we are interested in the long-distance behavior of the wave function in the region $r_0 \ll r \ll 1/k$. In the zero-range limit with $r_0 \to 0$, the $s-$wave phase shift $\delta_0(k)$ takes the simple form

$$k \cot \delta_0(k) = -1/a_s. \tag{2.15}$$

In this limit, the properties of the system depend only on s-wave scattering length and not on any other detail of the interaction. In the low-energy and long-distance region we are interested in, two interactions are identical if they give the same scattering length a_s.

2.2.1 Pseudopotential method

From Eqs. (2.10, 2.13, 2.15), we get the scattering amplitude

$$f_k(\theta) = \frac{1}{-1/a_s - ik}, \tag{2.16}$$

and scattering wave function

$$\psi(\mathbf{r}) \propto \frac{1}{kr} \sin\left[kr + \delta_0(k)\right] \tag{2.17}$$

in the low-energy limit. In the region we are interested in, $r_0 \ll r \ll 1/k$, the wave function satisfies the Bethe-Peierls boundary condition

$$\lim_{r \to 0} \psi(\vec{r}) \propto 1 - \frac{a_s}{r} + \mathcal{O}(1). \tag{2.18}$$

As we discussed in previous section, one can use an identical effective description for the complicated atomic interaction as long as they have the same scattering length a_s. This effective description can be Bethe-Peierls boundary condition in Eq. (2.18) or a short-range pseudopotential. The Schrödinger equation is

$$\left(-\frac{\hbar^2 \nabla^2}{2m_*} + V_{\text{pseudo}}(\mathbf{r})\right) \psi(\mathbf{r}) = \frac{\hbar^2 \mathbf{k}^2}{2m_*} \psi(\mathbf{r}), \tag{2.19}$$

where $V_{\text{pseudo}}(\mathbf{r})$ is negligible except for $r \to 0$. By applying $s-$wave scattering wave function (2.17) and using the relation

$$-\nabla^2 \frac{1}{r} = 4\pi\delta(\mathbf{r}), \tag{2.20}$$

we get

$$
\begin{aligned}
V_{\text{pseudo}}(\mathbf{r})\psi(\mathbf{r}) \xrightarrow{r \to 0} & \frac{4\pi\hbar^2}{2m_*} \delta(\mathbf{r}) \frac{\sin(kr + \delta_0(k))}{k} \\
= & \frac{4\pi\hbar^2}{2m_*} \frac{-1}{k\cot(\delta_0)} \delta(\mathbf{r}) \frac{\partial}{\partial r} \left(\frac{\sin(kr + \delta_0(k))}{k}\right).
\end{aligned}
\tag{2.21}
$$

From the definition of scattering length in Eq. (2.15) we have

$$
\begin{aligned}
V_{\text{pseudo}}(\mathbf{r})\psi(\mathbf{r}) &= \frac{4\pi a_s \hbar^2}{2m_*}\delta(\mathbf{r})\frac{\partial}{\partial r}\left(r\frac{\sin(kr+\delta_0)}{kr}\right) \\
&= \frac{4\pi a_s \hbar^2}{2m_*}\delta(\mathbf{r})\frac{\partial}{\partial r}r\psi(\vec{r}),
\end{aligned}
\tag{2.22}
$$

which defines the pseudopotential to be

$$
V_{\text{pseudo}}(\mathbf{r}) \equiv \frac{4\pi a_s \hbar^2}{2m_*}\delta(\mathbf{r})\frac{\partial}{\partial r}r.
\tag{2.23}
$$

2.2.2 Feshbach resonance (FR)

An important tool to tune the interaction between atoms is known as a Feshbach resonance. The magnetic Feshbach resonance allows us to tune the strength and even the sign of inter-atomic interaction, by changing the external magnetic field.

A Feshbach resonance is an enhancement of scattering by the coupling of an open scattering channel with a closed (i.e. a bound) channel, representing a bound molecular state. Resonance occurs when the scattering state comes into resonance with the bound state. According to second-order perturbation theory, the energy shift is

$$
\Delta E = \frac{|\langle b|\hat{H}_{\text{int}}|s\rangle|^2}{E - E_b},
\tag{2.24}
$$

where $|i\rangle$ and $|b\rangle$ are the scattering and bound states and $\hat{H}_{\text{int}}$ is the interaction Hamiltonian that couples the closed and open channels.

The magnetic Feshbach resonance utilizes the fact that the bound state energy can be shifted by using an external magnetic field. In the presence of magnetic field B, the energy different between the bound state and open-channel threshold changes as

$$
E - E_b \propto (B - B_0),
\tag{2.25}
$$

since the different channels have different magnetic moments. The interaction between ultracold atoms is proportional to the scattering length. Near a Feshbach resonance, the scattering length depends on B as

$$
a = a_{\text{bg}}\left(1 - \frac{\Delta}{B - B_0}\right),
\tag{2.26}
$$

where a_{bg} is the background scattering without the presenting of B, and Δ is the width of the resonance. The magnitude and sign of the scattering length can thus be tuned by external magnetic field [15].

A scattering state may be brought into resonance with a bound state by other means. The resonance is called an optical Feshbach resonance if caused optically by the atom-light dipole interaction. A resonance can also be caused by coupling with a quasibound state, which is supported by the open-channel potential itself. Thus a shape resonance can occur in and around the regime of a shallow bound state.
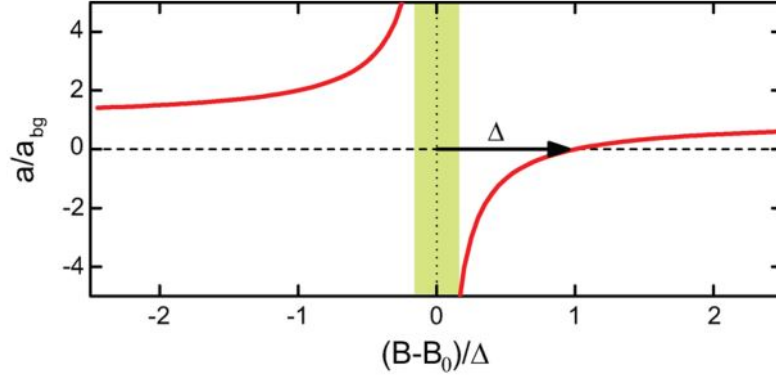
Figure 2.4: Illustration of a Feshbach resonance. The $s-$wave scattering length a is plotted as a function of the magnetic field B. The figure is from [21].

2.2.3 Confinement induced resonance (CIR)

The effective interaction can also be modified due to external atomic confinements. In quasi-low-dimensional systems, the effective scattering properties are strongly affected by the confining potential. The confinement-induced resonances(CIRs) were first predicted in 1998 [22] and observed in 2010 [23].

Consider a quasi-one dimensional (1D) system with tight optical trap $V_T(\mathbf{r})$ in x and y directions as

$$V_T(\mathbf{r}) = \sum_i \frac{1}{2} m \omega_\perp^2 \left(x^2 + y^2 \right).$$

The interaction between the atoms is described by the pseudo-potential

$$V(\mathbf{r}) = \frac{2\pi a_{3D} \hbar^2}{\mu} \delta(\mathbf{r}) \frac{\partial}{\partial r} r, \tag{2.27}$$

with the reduced mass $\mu \equiv m_1 m_2 / (m_1 + m_2)$ and free space three-dimensional (3D) scattering length a_{3D}. The system is approximated as an effective 1D system along z direction. The effective parameters of the 1D system should give the same wave function as calculated from a 3D system. According to scattering theory, the scattering amplitude in 1D system is

$$f(k_z) = -\frac{1}{1 + i k_z a_{1D}}, \tag{2.28}$$

with one-dimensional scattering length

$$a_{1D} \equiv -\frac{a_\perp^2}{2 a_{3D}} \left(1 - C \frac{a_{3D}}{a_\perp} \right)$$

where $a_\perp = \sqrt{\hbar / \mu \omega_\perp}$ and the constant

$$C = \lim_{s \to \infty} \left(\int_0^s \frac{ds'}{\sqrt{s'}} - \sum_{s'=1}^s \frac{1}{\sqrt{s'}} \right) \approx 1.4603.$$

This result is due to the resonant coupling between the incident channel of two particles and the transversal excited molecular state. Thus the 1D scattering length can be tuned by the
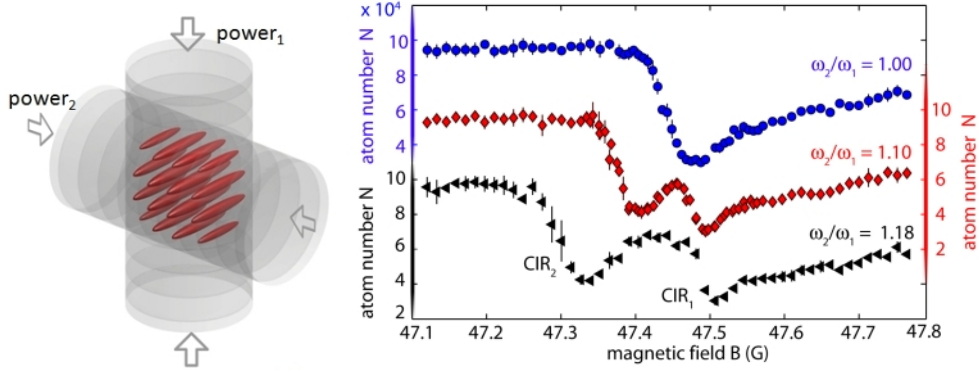
Figure 2.5: (Left) Quasi-one dimensional system with ultracold atoms. (Right) Atom number loss due to confinement induced resonances(CIR) and double-resonance due to different transversal frequency. The figure is from [23].
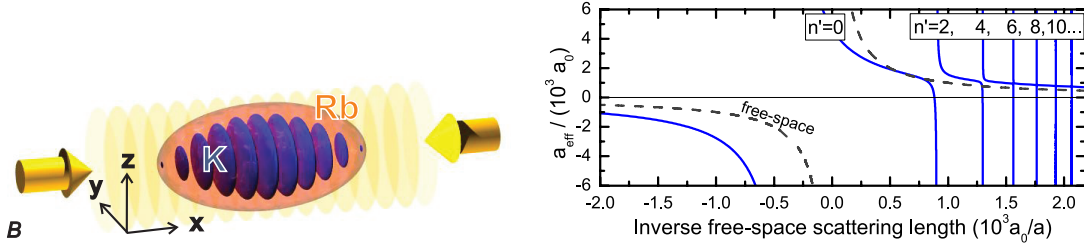
Figure 2.6: (Left) State-selective dipole potential (SSDP). (Right) Mixed-dimensional induced resonances (MDRs). The figure is from [25].

transversal confinement frequency. Also, by using a different transversal frequency $\omega_x \neq \omega_y$, a double-resonance is formed due to the loss of degeneracy [23].

The confinement effects also induce resonances in different systems. Experiments can build a state-selective dipole potential (SSDP) in which one species is confined in a two-dimensional plane (2D) or one-dimensional line (1D) while the other is free in the three-dimensional space (3D). When the characteristic confinement length $\sigma_\perp$ or $l_\perp$ is much smaller than any other length scale, the resulting system is mixed-dimensional. At low energies, the inter-species interaction is solely characterized by a single parameter, the effective mixed-dimensional scattering length a_{IB}^{eff}, whose value can be obtained numerically [24]. This mixed-dimensional induced resonances (MDRs) also allow us to arbitrarily tune the value of a_{IB}^{eff} by tuning the confinement strength, independent of tuning the magnetic Feshbach resonance.

2.3 Optical lattices and Bloch bands

2.3.1 Optical lattice

As discussed in Sec. 2.1, an optical potential can be created by laser beams due to ac-Stark effects. By using two counter propagating laser beams, we can build a periodic potential as optical lattice. The total electric field $\mathbf{E}(\mathbf{r})$ with two laser beams $\mathbf{E}_1(\mathbf{r})$ and $\mathbf{E}_2(\mathbf{r})$ is

$$\mathbf{E} = \mathbf{E}_1 \cos\left(\mathbf{k}_{l1} \cdot \mathbf{r} - \omega_1 t + \delta_1\right) + \mathbf{E}_2 \cos\left(\mathbf{k}_{l2} \cdot \mathbf{r} - \omega_2 t + \delta_2\right), \tag{2.29}$$
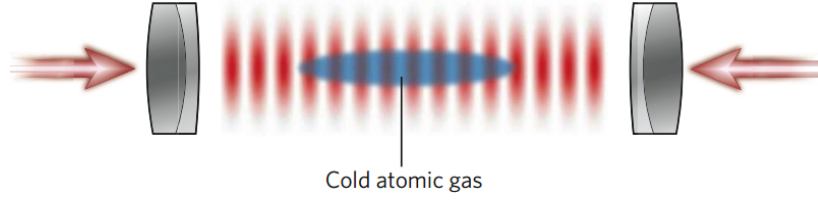
Figure 2.7: The formation of a one-dimensional (1D) optical lattice. An optical standing wave is generated by superimposing two laser beams. The figure is from [26].

with $(\omega_1 - \omega_2) \ll (\omega_1 + \omega_2)$. Thus after averaging out the fast term, we have

$$\langle \mathbf{E}^2 \rangle_t = \frac{1}{2} \mathbf{E}_1^2 + \frac{1}{2} \mathbf{E}_2^2 + \mathbf{E}_1 \cdot \mathbf{E}_2 \cos\left[(\mathbf{k}_{l1} - \mathbf{k}_{l2}) \cdot \mathbf{r} - (\omega_1 - \omega_2) t + (\delta_1 - \delta_2) \right]. \qquad (2.30)$$

In the case with same laser frequency $\omega_1 = \omega_2$, we can create a static lattice with wave vector $\mathbf{q}_l = \mathbf{k}_{l1} - \mathbf{k}_{l2}$ and lattice constant

$$d = \frac{2\pi}{|\mathbf{q}_l|} = \frac{\lambda}{(2 \sin(\theta/2))}, \qquad (2.31)$$

where $\lambda = 2\pi/k_l$ is the wavelength of the light and θ is the angle between $\mathbf{k}_{l1}$ and $\mathbf{k}_{l2}$. In the simple case with $\mathbf{k}_{l1} = -\mathbf{k}_{l2} = |k_l|\hat{e}_x$, the resulting optical lattice will be

$$V = \frac{V_0}{2} \cos\left(\frac{2\pi x}{d} \right) = \frac{V_0}{2} \cos\left(2k_l x \right) \propto V_0 \sin^2\left(k_l x \right), \qquad (2.32)$$

where $d = \lambda/2$ is equal to half wavelength of laser. As an example, for ^{87}Rb atoms with laser wave length $\lambda = 852$nm, the created lattice constant $d = 426.5$nm is much larger than the lattice constant in solid state systems. By varying the angle θ between the beams, we can also create different lattices with constant d larger than $\lambda/2$.

On the other hand, in the case of different laser frequency $\omega_1 \neq \omega_2$, the optical lattice can move with a velocity

$$v = \frac{\omega_1 - \omega_2}{|\mathbf{k}_{l1} - \mathbf{k}_{l2}|}, \qquad (2.33)$$

and the acceleration

$$a = \frac{dv}{dt} \approx \frac{1}{|\mathbf{k}_{l1} - \mathbf{k}_{l2}|} \frac{d\left(\omega_1 - \omega_2\right)}{dt}. \qquad (2.34)$$

By tuning the frequency with time, we can create an accelerating optical lattice or effectively a tilted optical lattice in space.

Due to the Gaussian form of the laser beam intensity profile

$$I(x, y, z) = \frac{2P}{\pi w^2(x)} \exp\left(-\frac{2\left(y^2 + z^2\right)}{w^2(x)} \right), \qquad (2.35)$$

there will be a minimum or maximum in the dipole potential. Here P is the total power of the laser beam, and $w(x) = w_0\sqrt{1 + x^2/x_R}$ is the $1/e^2$ radius with the beam waist w_0 and Rayleigh length $x_R = \pi\omega_0^2/\lambda$. The potential depth for a red-detuned beam has a local minimum and can be approximated as a harmonic potential

$$V_{\text{ext}} \approx -V_{\text{trap}} \left[1 - 2\left(\frac{y^2 + z^2}{\omega_0^2} \right) - \left(\frac{x}{x_R} \right)^2 \right]. \qquad (2.36)$$
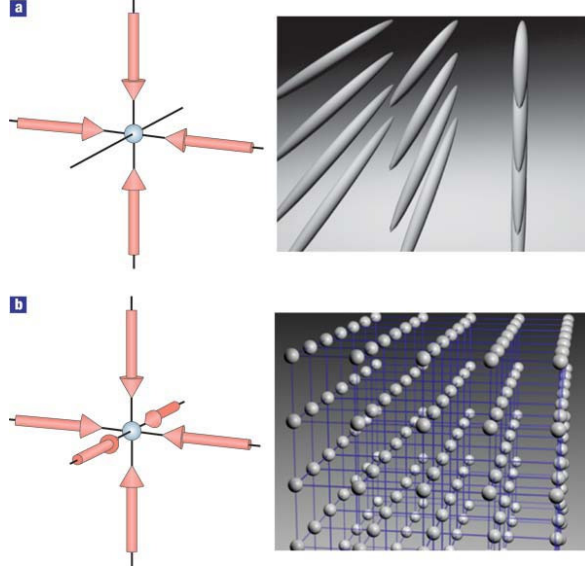
Figure 2.8: The two-dimensional (2D) and three-dimensional (3D) optical lattice. (a) In a 2D optical lattice, the atoms are confined in 1D tubes and (b) in a 3D lattice the atoms are confined in quantum dots. The figure is from [5].

This will provide an external harmonic potential besides the periodical optical lattice.

The high-dimensional optical lattice can be built in the same manner. For example, a three-dimensional (3D) cubic lattice is created by using three orthogonal, independent standing laser beams. The trapping potential can be approximated as the sum of a homogeneous periodic lattice potential as

$$V(\mathbf{r}) = V_0 \left(\sin^2(k_l x) + \sin^2(k_l y) + \sin^2(k_l z) \right). \tag{2.37}$$

In addition, there is also an external harmonic trapping due to the Gaussian intensity of the laser beams.

One important advantage of the optical lattice is the tunability for different geometries. On one hand, by using different laser setups and polarizations, a number of qualitatively different lattices have been realized such as hexagonal, trigonal, Kagome and honeycomb lattices. On the other hand, it is possible to realize different effective potentials for different atomic species or internal states. Thus a system with mixed-dimensional optical lattices can be created in which one species is confined in a particulate $n-$dimensional lattice while the other is confined in a different lattice or free in 3D space.

2.3.2   Bloch states

In this section we discuss the eigenstates for a single particle in 1D system with an optical lattice. The results can be straightforwardly generalized to high dimensional system. The Hamiltonian for this single particle is

$$\hat{H} = -\frac{\hbar^2}{2m} \frac{d^2}{dx^2} + \frac{V_0}{2} \cos\left(2k_l x\right), \tag{2.38}$$

with the potential period $d = \pi/k_l$. It is convenient to measure the lattice strength V_0 with particle recoil energy

$$E_R \equiv \frac{\hbar^2}{2m} k_l^2 = \frac{\pi^2 \hbar^2}{2md^2}. \tag{2.39}$$

The Schrödinger equation $\hat{H}\varphi(x) = E\varphi(x)$ can be expressed as

$$\left[\frac{1}{k_l^2}\frac{d^2}{dx^2} + \left(\frac{E}{E_R}\right) - \frac{1}{2}\left(\frac{V_0}{E_R}\right)\cos(2k_lx)\right]\varphi(x) = 0. \tag{2.40}$$

According to Bloch theory, the solution $\varphi(x)$ for the Schrödinger equation will take the form as

$$\varphi(x) = e^{ikx}\phi_k(x), \text{ with } \phi_k(x+d) = \phi_k(x). \tag{2.41}$$

The wave vector k lies in the range

$$-\frac{\pi}{d} \leq k \leq \frac{\pi}{d},$$

as first Brillouin zone and the quantity $\hbar k$ is called quasi-momentum.

The calculation of the Bloch states $\varphi(x)$ can be done by representing the periodic function $\phi(x)$ by its Fourier series:

$$\phi(x) = \sum_{n=-\infty}^{\infty} c_n e^{i\frac{2\pi}{d}nx}. \tag{2.42}$$

By using the fact that

$$\frac{d^2}{dx^2}\left(c_n e^{ikx}e^{in\frac{2\pi}{d}x}\right) = -\left(k + \frac{2\pi}{d}n\right)^2\left(c_n e^{ikx}e^{in\frac{2\pi}{d}x}\right), \tag{2.43}$$

and

$$\cos(2k_lx) = \frac{1}{2}\left(e^{i\frac{2\pi}{d}x} + e^{-i\frac{2\pi}{d}x}\right), \tag{2.44}$$

we end with the Schrödinger equations as

$$\left(\frac{k}{k_l} + 2n\right)^2 c_n - \frac{1}{4}\left(\frac{V_0}{E_R}\right)(c_{n+1} + c_{n-1}) = \left(\frac{E}{E_R}\right)c_n. \tag{2.45}$$

The eigenstates and eigenenergies can be calculated by diagonalizing these linear equations.

2.3.3   Bloch bands

The Schrödinger equation (2.40) for a single particle can be re-expressed as the standard form of the Mathieu equation [27] by changing k_lx to z as

$$\varphi''(z) + [a - 2q\cos(2z)]\varphi(z) = 0, \tag{2.46}$$

with

$$a = \frac{E}{E_R}; \quad q = \frac{V_0}{4E_R}. \tag{2.47}$$

The solutions of the Mathieu equation $\varphi(x) = e^{ikx}\phi(x)$ have $d-$periodic behavior as $\varphi(x+d) = \varphi(x)$ for $k = 0$, and $2d-$periodic behavior as $\varphi(x+d) = -\varphi(x)$ for $k = \pm\pi/d$. In this case the parameters a and q cannot be given independently: they must satisfy particular equations in order to allow $k = n(\pi/d)$, where n is an integer number. In this case for a given q, which means a given optical lattice depth V_0, all the discrete values for the parameter a are *characteristic values* for Mathieu equation. These characteristic values for a are expressed as $a_r(q)$ with $n = 2r$ for $d-$periodic function and $b_{r+1}(q)$ with $n = 2r + 1$ for $2d-$periodic odd function.
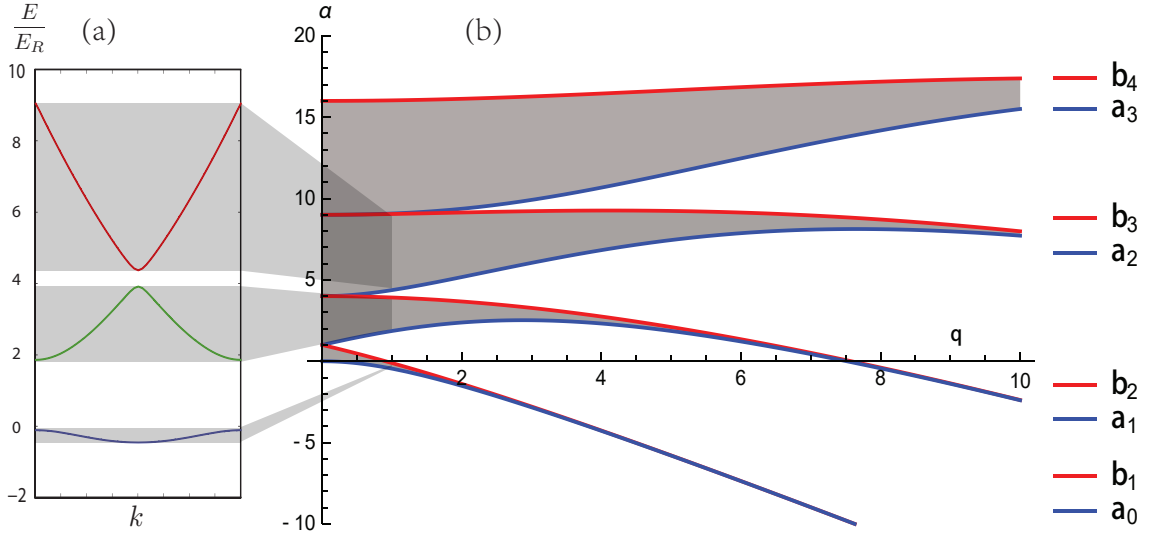
Figure 2.9: (a) Dispersion relation $E(k)$ in optical lattice for lowest three Bloch bands. These shadow areas show the band width for lattice depth $V_0 = 4E_R$. (b) Characteristic values for Mathieu equation where a_n corresponds to even Mathieu function and b_n corresponds to odd Mathieu function. These shadow areas show the band width for different $q = V_0/(4E_R)$.

In general, for the stable solutions of Mathieu equation with $-\pi/d \leq k \leq \pi/d$, the allowed values of a will form band structure. For $n = 0, 1, 2...$, the $n-$th energy bands $E_n = aE_R$ has a lower edge as

$$E_n^{\text{lower}} = a_n(q)E_R, \tag{2.48}$$

and an upper edge as

$$E_n^{\text{upper}} = b_{n+1}(q)E_R. \tag{2.49}$$

Due to the symmetry change for every new excited state, the state with $k = 0$ alternates between the lower and the upper edge from one band to another band [27]. The $n-$th band width is given as

$$W_n = (b_{n+1}(q) - a_n(q))E_R. \tag{2.50}$$

In the limit of deep lattice $V_0 \gg E_R$, the band width will be

$$W_n = \frac{2^{4n+5}}{n!} \left(\frac{2}{\pi}\right)^{\frac{1}{2}} q^{n+\frac{3}{4}} e^{-4\sqrt{q}} \left(1 - \frac{6n^2 + 14n + 7}{32\sqrt{q}}\right) E_R, \tag{2.51}$$

and thus for the lowest $(n = 0)$ band,

$$W_0 = 32 \left(\frac{2}{\pi}\right)^{\frac{1}{2}} \left(\frac{V_0}{4E_R}\right)^{\frac{3}{4}} \exp\left(-2\sqrt{\frac{V_0}{E_R}}\right) E_R. \tag{2.52}$$

2.3.4   Wannier functions

The Bloch states for single particle in an optical lattice are extending over the whole system with a phase factor e^{ikx}. Alternatively, we can use the Wannier functions as single-particle basis to describe the state. The Wannier function can be obtained by Fourier transformation from the Bloch state as

$$\phi_{n,k}(x) = \sqrt{\frac{d}{2\pi}} \sum_{x_i} w_n(x - x_i) e^{ikx_i}, \tag{2.53}$$

and

$$w_n(x - x_i) = \sqrt{\frac{d}{2\pi}} \int_{-\pi/d}^{\pi/d} dk \phi_{n,k}(x) e^{-ikx_i}, \tag{2.54}$$

with $w_n(x = x_i)$ is orthogonal and normalized Wannier function

$$\int dr w_n^*(x - x_i) w_{n'}(x - x_j) = \delta_{nn'}\delta_{i,j}. \tag{2.55}$$

It can be shown that, for each band at site x_i, there is one real Wannier function $w_n(x - x_i)$ falling off exponentially from x_i. These maximally localized Wannier functions are useful for describing local interactions between particles.

2.4 Hubbard model

The Hubbard model plays an important role in condensed matter physics. Even with only few parameters, the Hubbard model has great success in describing dynamics and phase transitions. In quantum simulation, the Hubbard model can be well realized by ultracold atoms in optical lattice. Due to the tunability of quantum gases, the effective parameters can be chosen in a wide region or even changed during the experiments.

The field operator for a single particle in an optical lattice at position $\mathbf{r}$ can be expressed as

$$\hat{\varphi}(\mathbf{r}) = \sum_{n,i} w_n(\mathbf{r} - \mathbf{R}_i) \hat{a}_{n,i}, \tag{2.56}$$

with the band index n. The Hamiltonian can be written as

$$H = \sum_{i,j} I_{i,j}^{nn'} \hat{a}_i^\dagger \hat{a}_j, \tag{2.57}$$

with integral

$$I_{i,j}^{nn'} = \int d\mathbf{r} w_n^*(\mathbf{r} - \mathbf{R}_i) \left[\frac{-\hbar^2 \nabla^2}{2m} + V(\mathbf{r}) \right] w_{n'}(\mathbf{r} - \mathbf{R}_j). \tag{2.58}$$

In a deep lattice with $V_0 \gg E_R$, the Wannier function $w_n^*(\mathbf{r} - \mathbf{R}_i)$ decays quickly from $\mathbf{R}_i$ so that only the terms with $|\mathbf{R}_i - \mathbf{R}_j| = d$ in the integral $I_{i,j}$ are affected. Under this tight-binding approximation, we only consider the nearest neighbor hopping terms as $\langle i,j \rangle$.

If the energy gap between lowest and first-excited band is much larger than other energy scales in the system, the particle will stay in the lowest Bloch band. The single band approximation allows us to describe the system with only lowest band index as $n = n' = 0$. Thus the effective Hamiltonian for the single particle will be

$$\hat{H} = -J \sum_{\langle i,j \rangle} \hat{a}_i^\dagger \hat{a}_j, \tag{2.59}$$

with $J = |I_{\langle i,j \rangle}|$. This single particle Hamiltonian can then be diagonalized in momentum space as

$$\hat{H} = \sum_{\mathbf{k}} \varepsilon_{\mathbf{k}} \hat{a}_{\mathbf{k}}^\dagger \hat{a}_{\mathbf{k}}, \tag{2.60}$$

with the dispersion relation

$$\varepsilon_{\mathbf{k}} = \varepsilon_0 - 2J \sum_{i=x,y,z} \cos\left(k_i d\right). \tag{2.61}$$

In this case, the Hubbard hopping J has a simple relation with lowest band width W_0 in Eq. (2.52) as $J = W_0/4$ and thus

$$J = \frac{4}{\sqrt{\pi}} E_r \left(\frac{V_0}{E_r}\right)^{3/4} \exp\left[-2\left(\frac{V_0}{E_r}\right)^{1/2}\right]. \tag{2.62}$$

On the other hand, the interaction term between two particles will be

$$\hat{H}_{\text{int}} = \int d\mathbf{r} d\mathbf{r}' \hat{\varphi}^{\dagger}\left(\mathbf{r}\right) \hat{\varphi}^{\dagger}\left(\mathbf{r}'\right) \frac{V\left(\mathbf{r} - \mathbf{r}'\right)}{2} \hat{\varphi}\left(\mathbf{r}'\right) \hat{\varphi}\left(\mathbf{r}\right). \tag{2.63}$$

By considering an on-site pseudo potential between neutral atoms, this term can be simplified as

$$\hat{H}_{\text{int}} = \frac{U}{2} \sum_i \hat{a}_i^{\dagger} \hat{a}_i^{\dagger} \hat{a}_i \hat{a}_i, \tag{2.64}$$

with

$$U = g \int d^3\mathbf{r} |w_0\left(\mathbf{r}\right)|^4. \tag{2.65}$$

Here we have

$$g = \frac{4\pi\hbar^2 a_s}{m}, \tag{2.66}$$

where a_s is $s-$wave scattering length between two particles in 3D space.

The different statistics between bosons and fermions make the interaction term different. For bosons this term will be

$$\hat{H}_{\text{int}} = \frac{U}{2} \sum_i \hat{n}_i \left(\hat{n}_i - 1\right), \tag{2.67}$$

and for fermions

$$\hat{H}_{\text{int}} = \frac{U}{2} \sum_i \hat{n}_i \left(1 - \hat{n}_i\right). \tag{2.68}$$

In the case with deep optical lattice when $V_0 \gg E_r$, the potential in each lattice can be approximated as harmonic potential with frequency

$$\hbar\omega_0 = 2\left(\frac{V_0}{E_R}\right)^{\frac{1}{2}} E_R. \tag{2.69}$$

In this harmonic approximation, the Wannier function at site i is described as harmonic oscillator

$$w_i\left(\mathbf{r}\right) = \left(\frac{1}{\pi\sigma^2}\right)^{\frac{3}{4}} e^{-(\mathbf{r}-\mathbf{R_i})^2/2\sigma^2} \tag{2.70}$$

with $\sigma_x \equiv \sqrt{\hbar/\left(m\omega_0\right)}$. Then the interaction parameter can be simplified as

$$U = g\sqrt{8\pi}\frac{a_s}{d}\left(\frac{V_0}{E_R}\right)^{\frac{3}{4}} E_R. \tag{2.71}$$

In most experiments, there is an additional harmonic potential due to the Gaussian form of laser profile. Under the local density approximation (LDA), this term can be treated as a modification to local chemical potential as

$$\mu_i = \mu_0 - V_{\text{ext}}\left(\mathbf{r}_i\right). \tag{2.72}$$

Finally, we end up with the single-band Bose-Hubbard model (BHM)

$$\hat{H}_{\text{BHM}} = -J \sum_{\langle i,j \rangle} \hat{a}_i^\dagger \hat{a}_j + \sum_i \mu_i \hat{n}_i + \frac{U}{2} \sum_i \hat{n}_i \left(\hat{n}_i - 1\right),$$

and the Fermi-Hubbard model (FHM)

$$\hat{H}_{\text{FHM}} = -J \sum_{\langle i,j \rangle} \hat{a}_i^\dagger \hat{a}_j + \sum_i \mu_i \hat{n}_i + \frac{U}{2} \sum_i \hat{n}_i \left(1 - \hat{n}_i\right).$$

From Eqs. (2.62, 2.71), it is possible to reach different coupling regimes U/J by either tuning the depth of the optical lattice or tuning the magnetic Feshbach resonances. This gives us a wide range of possibilities for strong correlation physics with cold atoms. For example, by simply tuning the depth of the optical lattice, the superfluid (SF) to Mott insulator (MI) transition for both bosons and fermions have been realized in experiments.

2.5   Open quantum systems

A small quantum system is called an open quantum system when coupled to an environment bath with a large number of degrees of freedom. The study of open quantum systems becomes an important aspect of ultracold quantum gases in recently years. In most quantum optical system or ultracold atomic system, the dynamics of an open quantum system can be described as a Lindblad master equation after applying reasonable approximations. In this section I will introduce some basic formulas regarding the Lindblad equation for an open quantum system.
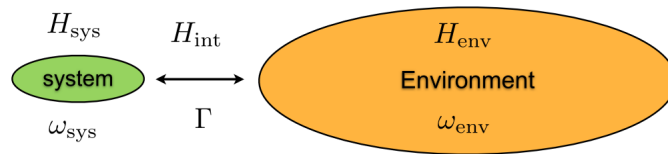
Figure 2.10: Illustration of open quantum system where a small quantum system interacts with its environment. This interaction leads to a combination of coherent and dissipative dynamics for the small system. The figure is from [18].

2.5.1   Lindblad master equation

Here we consider the general situation with a small system $\hat{H}_s$ coupled to an environment bath $\hat{H}_b$ with the interaction $\hat{H}_{\text{int}} = \sum_n \hat{A}_n \hat{B}_n$. Here $\hat{A}_n$ and $\hat{B}_n$ may indicate different systems and bath operators. Thus the Hamiltonian of the system is $\hat{H}_{\text{Tot}} = \hat{H}_0 + \hat{H}_{\text{int}}$ with $\hat{H}_0 = \hat{H}_s + \hat{H}_b$ the non-interacting part. The whole Hilbert space $\mathcal{H}$ will be the tensor product of system and bath as

$$\mathcal{H} = \mathcal{H}_s \otimes \mathcal{H}_b.$$

The time evolution of the system is determined by the equation of total density matrix ρ_{Tot} as

$$\frac{d\rho_{\text{Tot}}}{dt} = -\frac{i}{\hbar}\left[\hat{H}_{\text{Tot}}, \rho_{\text{Tot}}\right], \qquad (2.73)$$

with non-coupled initial condition

$$\rho_{\text{Tot}}\left(t=0\right) = \rho_s\left(t=0\right) \otimes \rho_b\left(t=0\right). \qquad (2.74)$$

In the interaction picture the time evolution should be

$$\frac{d\rho_{\text{Tot}}^I}{dt} = -\frac{i}{\hbar}\left[\hat{H}_{\text{int}}^I\left(t\right), \rho_{\text{Tot}}^I\left(t\right)\right], \qquad (2.75)$$

with

$$\hat{H}_{\text{int}}^I\left(t\right) = e^{i\hat{H}_0 t}\hat{H}_{\text{int}}e^{-i\hat{H}_0 t}; \quad \rho_{\text{Tot}}^I\left(t\right) = e^{i\hat{H}_0 t}\rho_{\text{Tot}}e^{-i\hat{H}_0 t}. \qquad (2.76)$$

The reduced density matrix ρ_s of the system can be obtained by tracing over the environment from the total density matrix ρ_{Tol} in $\mathcal{H}$. After the Born approximation, which expands the master equation up to second order of coupling, the reduced density matrix will follow as

$$\frac{d\rho_s^I}{dt} = -\frac{1}{\hbar^2}\int_0^t dt' Tr_B\left(\left[\hat{H}_{\text{int}}^I\left(t\right), \left[\hat{H}_{\text{int}}^I\left(t'\right), \rho_{\text{Tot}}^I\left(t\right)\right]\right]\right). \qquad (2.77)$$

The above equation can be further simplified after the Markov approximation as

$$\int_0^t dt' Tr_B \rightarrow \int_{-\infty}^t dt' Tr_B. \qquad (2.78)$$

This approximation assumes that the bath correlation function decays faster than any other time scale, i.e., the time evolution of the system does not depend on the history due to the short bath memory time.

Under Born-Markov approximation, the master equation in the interaction picture is:

$$\frac{d\rho_s^I\left(t\right)}{dt} = -i\left[H_{LS}, \rho_s^I\left(t\right)\right] + \mathcal{L}_I\left[\rho_s^I\left(t\right)\right], \qquad (2.79)$$

where the Hermitian operator H_{LS} is called Lamb-shift Hamiltonian, leading to a Lamb-type renormalization of the unperturbed energy levels induced by the system-reservoir coupling. The dissipative part of the master equation takes the form as

$$\mathcal{L}_I\left[\rho_s^I\left(t\right)\right] = \sum_n \gamma_n\left(\hat{A}_n\rho_s^I\left(t\right)\hat{A}_n^\dagger - \frac{1}{2}\left\{\hat{A}_n^\dagger\hat{A}_n, \rho_s^I\left(t\right)\right\}\right), \qquad (2.80)$$

with

$$\gamma\left(\omega\right) \equiv \int_{-\infty}^\infty d\tau e^{i\omega\tau}\langle B^\dagger\left(\tau\right)B\left(0\right)\rangle. \qquad (2.81)$$

In the Schrödinger picture, the reduced density operator follows the Lindblad equation

$$\frac{d\rho_s\left(t\right)}{dt} = -\frac{i}{\hbar}\left[\hat{H}_s + \hat{H}_{LS}, \rho_s\left(t\right)\right] + \sum_n \gamma_n\left(\hat{A}_n\rho_s\left(t\right)\hat{A}_n^\dagger - \frac{1}{2}\left\{\hat{A}_n^\dagger\hat{A}_n, \rho_I\right\}\right). \qquad (2.82)$$

2.5.2   Effective Hamiltonian with dissipation

The above Lindblad master equation (2.82) can also be expressed in convenient alternative form [18]

$$\frac{d\rho_s\left(t\right)}{dt} = -\frac{i}{\hbar}\left(\hat{H}_{\text{eff}}\rho_s - \rho_s\hat{H}_{\text{eff}}^\dagger\right) + \sum_n \hat{A}_n\rho_s\hat{A}_n^\dagger, \tag{2.83}$$

with renormalized jump operator $A_n \to \sqrt{\gamma_n}A_n$ and an effective Hamiltonian $\hat{H}_{\text{eff}}$ for the dissipative system:

$$\hat{H}_{\text{eff}} \equiv \left(\hat{H}_S + H_{LS}\right) - \frac{i\hbar}{2}\sum_n \hat{A}_n^\dagger\hat{A}_n. \tag{2.84}$$

The density matrix evolution follows from the non-Hermitian effective Hamiltonian. This indicates the decoherence or dephasing effects during the dynamics. The last term in the master equation $\hat{A}\rho_s\hat{A}^\dagger$ is often called the as recycling term, which will recycle the system population due to the non-Hermitian Hamiltonian.

2.5.3   Time evolution and steady states

For some simple systems, the time evolution for a Lindblad master equation can be solved analytically, to obtain expectation values of a given physical observable. In a small system, this can also be done numerically.

The Lindblad equation involves N^2 density matrix elements for a system with N quantum states. Then we can reduce this Lindblad equation to a linear differential equation as

$$\frac{d}{dt}\begin{pmatrix}\rho_{11}\\\rho_{21}\\\vdots\\\rho_{NN}\end{pmatrix} = \mathcal{L}\left[\rho\left(t\right)\right] = \underbrace{\begin{pmatrix}&&\\&\mathcal{L}&\\&&\end{pmatrix}}_{N\times N}\begin{pmatrix}\rho_{11}\\\rho_{21}\\\vdots\\\rho_{NN}\end{pmatrix}, \tag{2.85}$$

and then propagate the matrix with $N^2 \times N^2$ size.

On the other hand, if we want to calculate the steady states of Lindblad equation, we need to find the solution for $\frac{d}{dt}\rho\left(t\right) = 0$. This solution corresponds to the eigenvector with eigenvalue $\lambda = 0$ for the same $N^2 \times N^2$ matrix:

$$\underbrace{\begin{pmatrix}&&\\&\mathcal{L}&\\&&\end{pmatrix}}_{N\times N}\begin{pmatrix}\rho_{11}\\\rho_{21}\\\vdots\\\rho_{NN}\end{pmatrix} = \lambda\begin{pmatrix}\rho_{11}\\\rho_{21}\\\vdots\\\rho_{NN}\end{pmatrix}.$$

It is also possible to find several zero eigenvalues, which include the stable steady states solutions and unstable solutions.

However, for most many-body systems, it is impossible to obtain a simple solution even with relatively small particle-numbers. In order to numerically simulate the dissipative dynamics of the system, several groups [28, 29, 30, 31] developed the *quantum trajectory techniques* or *Monte Carlo wave function* method. By rewriting the master equation as a stochastic average over individual trajectories, these techniques treat the state evolution with stochastic sampling. Usually the quantum trajectory techniques need to be combined with many-body numerical methods in order to describe dynamics in a complex system [18].

Chapter 3

Polaron in Ultracold Quantum Systems

3.1 Introduction

An ingredient in the toolbox of ultracold techniques that has gathered increasing interest in recent years is the simulation of phonons and atom-phonon coupling [32, 33, 34, 35]. Of vital importance to real solid-state systems, such a coupling provides many interesting possibilities [36, 37]. For example, it can lead to effective Hamiltonians, such as extended Hubbard models or the Holstein model [38, 39, 40], as well as dissipative two-level systems [41, 42, 43].

Polaronic effects from electron-phonon interactions have also long been suggested to be the proponent behind high-T_c superconductivity in one- and two-band solid-state systems [44, 45, 46, 47]. In ultracold quantum gases, evidence of polarons has been found in systems with trapped ions [48] or systems with a single ion immersed in a degenerate quantum gas [49, 50, 51, 52, 53]. On the other hand, the atomic polaron has also been studied both experimentally and theoretically in systems of imbalanced Bose-Fermi mixtures [54, 55, 56, 57, 58] and Fermi-Fermi mixtures [59, 60, 61, 62, 63, 64]. In the particular case of a system with impurities immersed in a bosonic bath, these impurities coupled to bosonic excitations. For suitable parameters, polaronic phenomena arises generically in such systems [65, 66, 67, 68, 69, 70, 71, 72, 73, 74]. Such systems provide interesting features such as impurity-phonon coupling, induced long-range interactions between impurities, as well as dissipation and decoherence effects.

There are also other proposals for realizing atom-phonon couplings and polaronic effects, including crystals of dipole molecules [75, 76, 77], nanoparticles [78, 79] and hybrid atom-ion coupled systems [80].

3.2 Polarons in a Bose-Einstein condensate

In this section I discuss the effective Hamiltonian for a dilute set of impurities, weakly coupled to a Bose-Einstein condensate. By applying different trapping for the impurity and BEC atoms, the system can be realized with a different effective dimensionality and geometry. The polaron system in the strongly coupling limit will be discussed later in this chapter.

Here we consider the case where a dilute set of few neutral impurities with mass m_I interact with a Bose-Einstein condensate of another neutral species. The impurities can move in 3D space or be trapped by an optical lattice and their Hamiltonian is denoted by H_I. The homogeneous BEC system H_B is formed by another atomic species with mass m_B
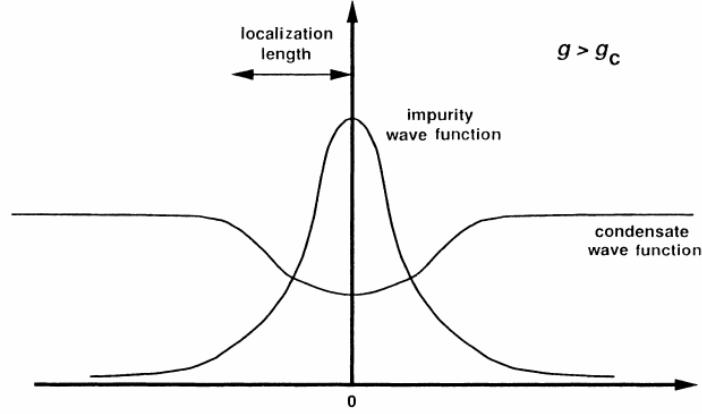
Figure 3.1: Self-trapping of polaron in a BEC with repulsive interaction. The figure is from [81].

and a weak repulsive interaction g_B. The impurity-BEC interaction H_{int} is caused by s-wave interactions between the different species, which can be tuned by Feshbach resonance techniques. The total Hamiltonian is hence

$$\hat{H} = \hat{H}_I + \hat{H}_B + \hat{H}_{\text{int}}.$$

In the case of a weak interaction between the impurities and the BEC, the Hamiltonian can be expressed as a Fröhlich-type Hamiltonian with an effective atom-(BEC) phonon interaction.

The simplest realization of such a system is a static impurity coupled to the BEC, which can be described by the Gross–Pitaevskii (GP) mean-field equation. The presence of impurity will repel or attract BEC particles and thus modify the GP ground state. On the other hand, the enhancement or reduction of the BEC density will create an effective potential that is attractive for the impurity. For example, an impurity with repulsive interaction can make a "hole" in the BEC ground state and thus be self-trapped in this "hole".

3.2.1 Impurities in an optical lattice

In this section, we consider a quasi-1D system with impurities trapped in an anisotropic 3D optical lattice:

$$V_I\left(\mathbf{r}\right) = V_I^x \sin^2\left(\frac{\pi}{d}x\right) + V_I^y \sin^2\left(\frac{\pi}{d}y\right) + V_I^z \sin^2\left(\frac{\pi}{d}z\right),$$

with lattice constant $d = \lambda/2$ and laser wavelength λ. We use the lattice constant d as the unit of length throughout this paper. The single impurity recoil energy is $E_R \equiv \pi^2 \hbar^2 / \left(2m_I d^2\right)$. The trapping strength in the transverse (y, z) directions are assumed to be much stronger than in the longitudinal (x) direction with $V_I^x \ll V_I^\perp \equiv V_I^y = V_I^z$. The impurities are therefore tightly trapped in the transverse direction, and remain in the ground state of the associated harmonic oscillator potential:

$$\phi^0\left(y\right) = 1/\left(\pi\sigma_\perp^2\right)^{\frac{1}{4}} e^{-y^2/\left(2\sigma_\perp^2\right)}, \tag{3.1}$$

with transverse characteristic length $\sigma_\perp \equiv \sqrt{\hbar/\left(m_I\omega_\perp\right)}$ and frequency $\hbar\omega_\perp \equiv 2\left(V_I^\perp E_R\right)^{1/2}$. In the longitudinal direction, on the other hand, the impurities will populate several lowest

states. In this chapter, we only consider the single band problem where impurities lie in the lowest band. The system with two bands occupied will be discussed in Chapter 4.

In principle, the exact Bloch wave functions need to be calculated numerically, which can then also be represented as linear combinations of Wannier states $\varphi_x^0(x)$. In a deep lattice, the Wannier functions can be approximated by the ground states of a harmonic oscillator

$$\varphi_x^0(x) \approx 1/\left(\pi\sigma_x^2\right)^{\frac{1}{4}} e^{-x^2/\left(2\sigma_x^2\right)}, \tag{3.2}$$

with longitudinal characteristic length $\sigma_x \equiv \sqrt{\hbar/(m_I\omega_x)}$ and oscillation frequency $\hbar\omega_x \equiv 2\left(V_I^x E_R\right)^{1/2}$.

In this highly anisotropic system, impurities can hop to their nearest-neighbor sites only along the longitudinal direction. A particle localized on lattice site j will be described by the wave function

$$W_j^0(\mathbf{r}) \equiv \varphi_x^0(x - x_j)\,\phi^0(y)\,\phi^0(z). \tag{3.3}$$

Due to the low density of impurities, their dynamics can be modeled by a non-interacting Hubbard Hamiltonian:

$$\hat{H}_I = -\sum_{\langle i,j\rangle} J\hat{a}_i^\dagger\hat{a}_j + \sum_i \varepsilon\hat{n}_i, \tag{3.4}$$

where J and ε are the hopping parameters and on-site energy.

3.2.2 Bosonic bath

The impurities are immersed in a homogeneous BEC with weakly repulsive boson-boson interaction g_B between the atoms. In a dilute system, this weak interaction can be described by the boson-boson scattering length a_B as $g_B = 4\pi\hbar^2 a_B/m_B$. For vanishing inter-species interaction g_{IB} between impurity and bath, the BEC can be described by standard Bogoliubov theory and treated as a phonon bath.

In the presence of impurities, the BEC becomes deformed once the impurity-boson interaction g_{IB} is introduced. This interaction is closely related to the impurity-boson scattering length and other system parameters such as the impurity-boson mass ratio and the impurity confinement strength. The relation can be determined by making use of scattering theory in the low-energy limit, such as the Lippmann-Schwinger equation or effective field theory [82]. For an unconfined impurity, the inter-species interaction g_{IB} can be derived as $g_{IB} \equiv 2\pi\hbar^2 a_{IB}/\mu$ with the reduced mass $\mu \equiv m_I m_B/(m_I + m_B)$ and 3D impurity-boson scattering length a_{IB}.

However, for the confined impurity, g_{IB} needs to be treated carefully due to lattice effects such as confinement induced resonances [22, 83]. In the specific system that we consider here, the impurity is confined in one-dimensional tube (quasi-1D) by an anisotropic optical lattice while the bosonic atoms are free in three-dimensional space (3D). When the transverse characteristic length $\sigma_\perp$ is much smaller than any other length scales, the resulting system is mixed-dimensional. At low energies, the inter-species interaction is solely characterized by a single parameter, the effective scattering length a_{IB}^{eff}, whose value can be obtained numerically [24]. This fact also allows us to arbitrarily tune the value of a_{IB}^{eff} by tuning the transverse confinement strength.

Here we use the approach in [66, 84], where the deformation is treated as a perturbation around the BEC ground state. The bosonic field operator is expanded as $\hat{\psi}(\mathbf{r}) = \psi_0(\mathbf{r}) + \hat{\vartheta}(\mathbf{r})$, where $\psi_0(\mathbf{r})$ is the order parameter in the absence of inter species interaction and $\hat{\vartheta}(\mathbf{r}) =$
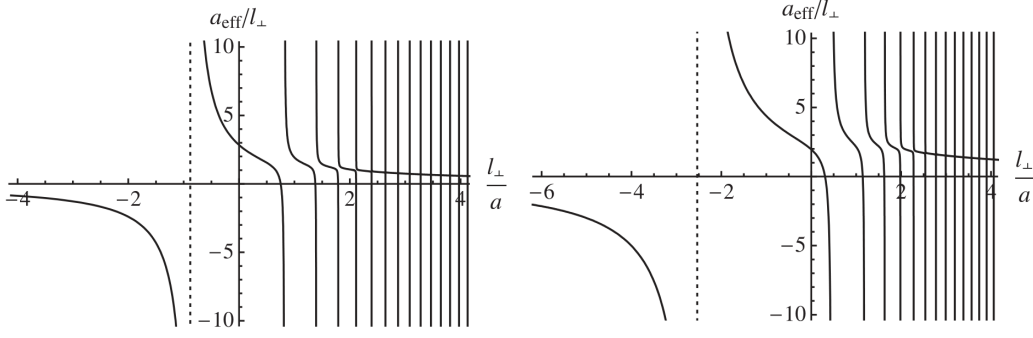
Figure 3.2: Effective scattering length a_{IB}^{eff} in mixed dimensional systems. (left) $a_{IB}^{\mathrm{eff}}/l_\perp$ as a function of $l_\perp/a_s$ for 2D-3D mixture. (right) $a_{IB}^{\mathrm{eff}}/l_\perp$ as a function of $l_\perp/a_s$ for 1D-3D mixture. Here $l_\perp = \sqrt{\hbar/m\omega_\perp}$. The figure is from [24].

$\vartheta(\mathbf{r}) + \hat{\zeta}(\mathbf{r})$ represents the perturbation itself, which consists of a correction to the order parameter, $\vartheta(\mathbf{r})$, and Bogoliubov excitation operators $\hat{\zeta}(\mathbf{r})$. The modified BEC ground state is described as $\psi_0(\mathbf{r}) + \vartheta(\mathbf{r})$, which is the Gross-Pitaevskii solution including the presence of impurities. This modification $\vartheta(\mathbf{r})$ shifts the equilibrium positions in order to minimize the total energy of the system. The small excitations $\hat{\zeta}(\mathbf{r})$, around the static GP ground state $\psi_0(\mathbf{r}) + \vartheta(\mathbf{r})$ of the condensate, can be described in the terms of Bogoliubov modes

$$\hat{\zeta}(\mathbf{r}) = \sum_{\mathbf{q}} \left[u_{\mathbf{q}} e^{i\mathbf{q}\cdot\mathbf{r}} \hat{\beta}_{\mathbf{q}} - v_{\mathbf{q}}^* e^{-i\mathbf{q}\cdot\mathbf{r}} \hat{\beta}_{\mathbf{q}}^\dagger \right], \tag{3.5}$$

with bosonic operators $\hat{\beta}_{\mathbf{q}}^\dagger$ ($\hat{\beta}_{\mathbf{q}}$) creating (annihilating) a Bogoliubov quasi-particle with momenta $\mathbf{q}$. The coefficients $u_{\mathbf{q}}(\mathbf{r})$ and $v_{\mathbf{q}}(\mathbf{r})$ can be determined by Bogoliubov-de Gennes equations:

$$u_{\mathbf{q}} = \sqrt{1/(2\Omega)\left[(\epsilon_{\mathbf{q}} + g_B n_0)/(\hbar\omega_{\mathbf{q}}) + 1 \right]};$$
$$v_{\mathbf{q}} = \sqrt{1/(2\Omega)\left[(\epsilon_{\mathbf{q}} + g_B n_0)/(\hbar\omega_{\mathbf{q}}) - 1 \right]},$$

with the system *quantization volume* Ω and the Bogoliubov phonon dispersion

$$\hbar\omega_{\mathbf{q}} \equiv \sqrt{\epsilon_{\mathbf{q}}(\epsilon_{\mathbf{q}} + 2g_B n_0)};$$
$$\epsilon_{\mathbf{q}} \equiv \frac{\hbar^2 |\mathbf{q}|^2}{2m_B}. \tag{3.6}$$

where $n_0 = |\psi_0|^2$ is the condensate density.

As pointed out in [84], the coefficients $u_{\mathbf{q}}(\mathbf{r})$, $v_{\mathbf{q}}(\mathbf{r})$ and Bogoliubov phonon spectrum $\omega_{\mathbf{q}}$ are not changed by the presence of the impurity, although the equilibrium positions of the modes are modified by $\vartheta(\mathbf{r})$. In [84], they express $\hat{\vartheta}(\mathbf{r}) = \vartheta(\mathbf{r}) + \hat{\zeta}(\mathbf{r})$ in terms of Bogoliubov modes around the state $\psi_0(\mathbf{r})$ as

$$\hat{\vartheta}(\mathbf{r}) = \sum_{\mathbf{q}} \left[u_{\mathbf{q}} e^{i\mathbf{q}\cdot\mathbf{r}} \hat{b}_{\mathbf{q}} - v_{\mathbf{q}}^* e^{-i\mathbf{q}\cdot\mathbf{r}} \hat{b}_{\mathbf{q}}^\dagger \right]. \tag{3.7}$$

In contrast to Eq. (3.5), the bosonic operators $\hat{b}_{\mathbf{q}}^\dagger$ ($\hat{b}_{\mathbf{q}}$) create (annihilate) a quasi-particle around the ground state $\psi_0(\mathbf{r})$ in the absence of the impurity rather than around the state

$\psi_0(\mathbf{r}) + \vartheta(\mathbf{r})$. The Hamiltonian (up to constant terms) for this effective phonon bath can be simply expressed as

$$\hat{H}_B = \sum_{\mathbf{q}} \hbar\omega_{\mathbf{q}} \hat{b}_{\mathbf{q}}^\dagger \hat{b}_{\mathbf{q}}, \tag{3.8}$$

if the impurity-BEC coupling g_{IB} satisfies condition $|\langle \vartheta(\mathbf{r}) \rangle| \ll \psi_0(\mathbf{r})$, which implies the dimensionless relation:

$$(|g_{IB}|/g_B) \ll n_0 \xi^D, \tag{3.9}$$

where $\xi \equiv \hbar/\sqrt{m_B g_B n_0}$ is the condensate healing length and $D = 3$ for a three dimensional homogeneous bosonic bath [66]. Strictly speaking, even when the coupling g_{IB} is stronger than this limit, the perturbation theory still qualitatively applies. For very strong interactions, however, the bath can not be properly described by Bogoliubov quasi-particles anymore. The above perturbative method can also be used in a system where the impurities and BEC are both trapped by optical lattices [68].

3.2.3   Fröhlich atom-phonon coupling

The impurity-BEC interaction of the Hamiltonian can be written as

$$\hat{H}_{\mathrm{int}} \quad = \quad \sum_{\mathbf{q}} \sum_{i,j} \hbar\omega_{\mathbf{q}} M_{i,j;\mathbf{q}} \hat{b}_{\mathbf{q}} \hat{a}_i^\dagger \hat{a}_j + h.c. \tag{3.10}$$

$$M_{i,j;\mathbf{q}} \quad = \quad \frac{g_{IB}}{\hbar\omega_{\mathbf{q}}} \sqrt{\frac{n_0}{\Omega}} \left(u_{\mathbf{q}} - v_{\mathbf{q}} \right) m_{i,j;\mathbf{q}}, \tag{3.11}$$

with $m_{i,j;\mathbf{q}} \equiv \int d^3 r\, e^{i\mathbf{q}\cdot\mathbf{r}} W_i^*(\mathbf{r}) W_j(\mathbf{r})$. This term describes the impurity coupling to the phonon bath by creating or annihilating phonons. The non-local coupling terms with $i \neq j$ are highly suppressed due to the local form of the interaction which requires overlap between localized Wannier functions. For these reasons, the above integrals $m_{i,j;\mathbf{q}}$ can be well approximated by $\delta_{ij} m_{\mathbf{q}} e^{i\mathbf{q}\cdot\mathbf{R}_i}$ such that the value depends only on $\mathbf{q}$. The dimensionless impurity-phonon coupling $M_{i;\mathbf{q}}$ can also be written as $M_{\mathbf{q}} e^{i\mathbf{q}\cdot\mathbf{R}_i}$ with

$$M_{\mathbf{q}} \equiv g_{IB} \sqrt{\frac{n_0 \epsilon_{\mathbf{q}}}{\Omega \left(\hbar\omega_{\mathbf{q}}\right)^3}} m_{\mathbf{q}}. \tag{3.12}$$

Note that the impurity-phonon coupling $M_{i,\mathbf{q}}$ obeys:

$$M_{i,\mathbf{q}}^* = M_{i,-\mathbf{q}}. \tag{3.13}$$

The integral factors $m_{\mathbf{q}}$ take the form

$$m_{\mathbf{q}} = \int d^3 r\, e^{i\mathbf{q}\cdot\mathbf{r}} |\varphi_x^0(x)|^2 |\phi^0(y)|^2 |\phi^0(z)|^2.$$

In a deep optical lattice, where the impurity Wannier functions in Eqs. (3.1) can be approximated as harmonic oscillator states, we can explicitly evaluate these factors

$$m_{\mathbf{q}} = e^{-\left(\sigma_\perp^2 q_\perp^2 + \sigma_x^2 q_x^2\right)/4},$$

by using the identity for Hermite polynomial integrals [85]. Here $q_\perp \equiv \sqrt{q_y^2 + q_z^2}$ indicates the transverse phonon momentum.

In order to describe polaronic effects resulting from the impurity-BEC coupling, we introduce a dimensionless coupling constant as in [86] and name it κ. This constant depends on the impurity-boson and boson-boson interactions g_{IB}, g_{BB} and the condensate parameters ξ and m_B as

$$\kappa \equiv \sqrt{\frac{g_{IB}^2 m_B}{g_B \hbar^2 \xi}}. \tag{3.14}$$

As described in [86], this constant is the ratio $\kappa = E_{IB}/E_{\mathrm{ph}}$ between the characteristic impurity-boson interaction $E_{IB} = g_{IB}\sqrt{n_0 \xi^{-3}}$ and the typical phonon energy $E_{\mathrm{ph}} = \hbar c/\xi$, where $c = \sqrt{g_B n_0/m_B}$ is the condensate speed of sound. In [67] an alternative dimensionless coupling constant is used as

$$\alpha \equiv \frac{a_{IB}^2}{a_{BB}\xi}, \tag{3.15}$$

or equivalently $\alpha = 4\pi n_0 a_{IB}^2 \xi$. These two coupling constants are related by $\alpha = (\kappa\mu/m_B)^2/\pi$, where μ is the reduced mass. There are also other coupling constants used [65, 87], which are slightly different from α or κ. By tuning the impurity-boson scattering length a_{IB}^{eff}, the coupling constant κ can be tuned continuously. However, the condition in Eq. (3.9) requires that the coupling constant satisfies the relation

$$\kappa \ll \kappa_c \equiv \frac{1}{2\sqrt{\pi}}\sqrt{\frac{\xi}{a_B}} = \left(64\pi^3 a_B^3 n_0\right)^{-\frac{1}{4}}. \tag{3.16}$$

This upper limit of the coupling constant κ_c depends only on the boson-boson scattering length a_B and the condensate density n_0 instead of the specific mass ratio m_I/m_B. In a typical BEC system, this maximum coupling constant is relatively small, such as $\kappa_c \approx 2.4$ for ^{87}Rb with $a_B = 100a_0$ and $n_0 \approx 10^{14}\mathrm{cm}^{-3}$. In order to reach larger values of κ_c in realistic systems, one needs to reduce the condensate density n_0 or the boson-boson scattering length a_B.

Finally the effective Hamiltonian with two-band Fröhlich impurity-phonon coupling is

$$\hat{H} = -\sum_{\langle i,j \rangle} J\hat{a}_i^\dagger \hat{a}_j + \sum_i \varepsilon \hat{n}_i + \sum_{\mathbf{q}} \hbar\omega_{\mathbf{q}} \hat{b}_{\mathbf{q}}^\dagger \hat{b}_{\mathbf{q}}$$
$$+ \sum_{i,\mathbf{q}} \hbar\omega_{\mathbf{q}} M_{i,\mathbf{q}} \left(\hat{b}_{\mathbf{q}} + \hat{b}_{-\mathbf{q}}^\dagger\right) \hat{a}_i^\dagger \hat{a}_i. \tag{3.17}$$

Here we used the relations in Eq. (3.13). This Hamiltonian describes a general single-band system with impurity-phonon coupling, which can also be realized by other experimental setups such as hybrid atom-ion systems [80]. We will further discuss such hybrid atom-ion system in Chapters 6 and 7.

3.3 Variational Lang-Firsov polaron transformation

This Hamiltonian in Eq. (3.17), with Fröhlich-type impurity-phonon coupling, cannot be solved analytically even for the case of a single impurity. The goal of this section is to find a simple but non-trivial variational method which can deal with the system (3.17) in general. We choose the Lang-Firsov polaron transformation approach and use its variational form.

Firstly we introduce the basic concept of the transformation. When a single impurity moves in a lattice and couples to a phonon bath, there are exact solutions in both the weak and strong coupling limits [39]. When the impurity-phonon interaction is much weaker than

the impurity kinetic energy, the impurity behaves as a free particle in a lattice. On the other hand, when the interaction is much larger than the kinetic part, the impurity will be tightly dressed by a "cloud" of phonons, forming a quasi-particle. The phonons are tied to the impurity such that the impurity cannot move on its own but must drag around a phonon cloud. This increases the effective mass of the quasiparticle. In the intermediate coupling region, the phonon dressing competes with the impurity dynamics. In order to describe this competition, a variational ground state can be used to connect between the weak and strong coupling limits [88, 89, 90, 91, 43, 92]. This variational ansatz is equivalent to a canonical transformation $\tilde{H} \equiv e^{\hat{S}} \hat{H} e^{-\hat{S}}$.

After the transformation, the Hamiltonian $\tilde{H}$ still cannot be solved analytically, but can be separated into a coherent part $\langle \tilde{H} \rangle_T$ and an incoherent part $\tilde{H}_{\text{inc}} \equiv \tilde{H} - \langle \tilde{H} \rangle_T$ where $\langle \cdots \rangle_T$ indicates a thermal average over the phonon bath. The coherent part, which is decoupled from the phonon bath, is of the form of an extended (polaronic) Hubbard model. The incoherent part describes the residual coupling between polaron quasi-particle and phonon bath. Compared to the initial "bare" impurity-phonon coupling, this incoherent part is significantly reduced by the polaron transformation. We first focus on the coherent part and neglect the incoherent terms. The variational parameters $\Lambda_{i,\mathbf{q}}$ are determined by minimizing the coherent Hamiltonian energy and approach $\Lambda_{i,\mathbf{q}} = M_{i,\mathbf{q}}$ in the strong coupling limit. Finally, the residual incoherent part can be included in a perturbative approach such as the Lindblad master equation.

We use a variational canonical transformation to decouple impurity-phonon coupling and connect between the weak and strong coupling limits. The Lang-Firsov polaron transformation takes the form $\tilde{H} \equiv e^{\hat{S}} \hat{H} e^{-\hat{S}}$ with

$$\hat{S} \equiv \sum_i \sum_{\mathbf{q}} \Lambda_{\mathbf{q}} e^{i\mathbf{q}\cdot\mathbf{R}_i} \left(\hat{b}^\dagger_{-\mathbf{q}} - \hat{b}_{\mathbf{q}} \right) \hat{n}_i, \tag{3.18}$$

where $\Lambda_{\mathbf{q}}$ are the variational parameters. By using the Baker-Campbell-Hausdorff formula, $e^{\hat{S}} \hat{A} e^{-\hat{S}} = \hat{A} + \left[\hat{S},\, \hat{A} \right] + \frac{1}{2!} \left[\hat{S},\, \left[\hat{S},\, \hat{A} \right] \right] + \cdots$, we can derive the transformed Hamiltonian with exponential quadratic operators. After the transformation, the impurity annihilation and creation operators can be expressed through

$$e^{\hat{S}} \hat{a}_i e^{-\hat{S}} = \hat{X}_i \hat{a}_i, \tag{3.19}$$

and similarly for the creation operators. The matrix operators $\hat{X}_i$ are found to be

$$\hat{X}_i \equiv e^{-\sum_{\mathbf{q}} \Lambda_{\mathbf{q}} e^{i\mathbf{q}\cdot\mathbf{R}_i} \left(\hat{b}^\dagger_{-\mathbf{q}} - \hat{b}_{\mathbf{q}} \right)}. \tag{3.20}$$

This canonical transformation is equivalent to defining a new quasi-particle, which represents an impurity dressed by the phonon cloud forming a polaron. This transformation also shifts the equilibrium position of the phonon bath by

$$e^{\hat{S}} \hat{b}_{\mathbf{q}} e^{-\hat{S}} = \hat{b}_{\mathbf{q}} + \sum_i \left(\hat{X}^\dagger_i \hat{b}_{\mathbf{q}} \hat{X}_i - \hat{b}_{\mathbf{q}} \right) \hat{a}^\dagger_i \hat{a}_i, \tag{3.21}$$

but it does not modify the phonon dispersion relation. The transformed polaronic Hamiltonian can be written as

$$\tilde{H} = - \sum_{\langle i,j \rangle} c^\dagger_i \hat{X}^\dagger_i J \hat{X}_j c_j + \sum_{\mathbf{q}} \omega_{\mathbf{q}} b^\dagger_{\mathbf{q}} b_{\mathbf{q}} + \sum_{i,\mathbf{q}} \hbar\omega_{\mathbf{q}} b_{\mathbf{q}} \left(M_{i,\mathbf{q}} - \Lambda_{i,\mathbf{q}} \right) n_i + h.c.$$
$$- \frac{1}{2} \sum_{i,j,\mathbf{q}} \hbar\omega_{\mathbf{q}} e^{i\mathbf{q}\cdot(\mathbf{R}_i - \mathbf{R}_j)} \left(2M_{\mathbf{q}} - \Lambda_{\mathbf{q}} \right) \Lambda_{\mathbf{q}} \hat{n}_i \hat{n}_j + h.c. \tag{3.22}$$

The last term, which is zero when only a single impurity is considered, describes induced polaron-polaron interactions due to the coupling with the phonon bath. Compared to the original Hamiltonian in Eq. (3.17), the hopping and on-site energies have been modified. As for the single band system, this Hamiltonian contains all interactions exactly and is hard to solve analytically. Motivated by the single-band system, we separate the Hamiltonian into coherent and incoherent parts, $\langle \tilde{H} \rangle_T$ and $\tilde{H} - \langle \tilde{H} \rangle_T$ respectively. The explicit form of the coherent terms, which conserve the number of phonons, is determined. After determining the variational parameters $\Lambda_{\mathbf{q}}$ by minimizing the free energy of the coherent part, we treat the residual polaron-bath coupling in the incoherent part as a perturbation and solve it by a Lindblad master equation.

3.3.1   Coherent polaronic Hamiltonian

The coherent part $\langle \tilde{H} \rangle_T$ is written as

$$\langle \tilde{H} \rangle_T = -\sum_{\langle i,j \rangle} J \langle \hat{X}_i^\dagger \hat{X}_j \rangle_T c_i^\dagger c_j + \sum_{\mathbf{q}} \omega_{\mathbf{q}} \hat{n}_{\mathbf{q}}$$
$$- \sum_{i,j,\mathbf{q}} \hbar \omega_{\mathbf{q}} \cos \left[\mathbf{q} \cdot (\mathbf{R}_i - \mathbf{R}_j) \right] (2M_{\mathbf{q}} - \Lambda_{\mathbf{q}}) \Lambda_{\mathbf{q}} \hat{n}_i \hat{n}_j, \qquad (3.23)$$

with

$$\langle \hat{X}_i^\dagger \hat{X}_j \rangle_T = \exp \left[\sum_{\mathbf{q}} -\left(\bar{N}_{\mathbf{q}} + \frac{1}{2} \right) |\Lambda_{i,\mathbf{q}} - \Lambda_{j,\mathbf{q}}|^2 \right] = \exp \left[-2 \sum_{\mathbf{q}} \left(2\bar{N}_{\mathbf{q}} + 1 \right) \Lambda_{\mathbf{q}}^2 \sin^2 \left(\frac{\mathbf{q} \cdot \mathbf{d}}{2} \right) \right],$$
$$(3.24)$$

and the incoherent part

$$H_I = -\sum_{\langle i,j \rangle} J \hat{T}_{i,j} c_i^\dagger c_j + \sum_{i,\mathbf{q}} \hbar \omega_{\mathbf{q}} b_{\mathbf{q}} \left(M_{i,\mathbf{q}} - \Lambda_{i,\mathbf{q}} \right) \hat{n}_i + h.c.,$$

where $\bar{N}_{\mathbf{q}}$ indicates the phonon number with momentum $\mathbf{q}$. For the simplest case, we can use the parameter $\Lambda_{i,\mathbf{q}} = M_{i,\mathbf{q}}$, and eliminate the linear phonon operators $b_{\mathbf{q}}$ and $b_{\mathbf{q}}^\dagger$ in H_I. This is an approximation and becomes exact when $J = 0$.

On the other hand, for $\Lambda_{i,\mathbf{q}} \neq M_{i,\mathbf{q}}$, one needs to fix the transformation parameters by attempting to minimize the approximation of the variational ansatz. The coherent Hamiltonian for a single polaron is

$$\langle \tilde{H} \rangle_T = -\sum_{\langle i,j \rangle} J \langle \hat{X}_i^\dagger \hat{X}_j \rangle_T c_i^\dagger c_j + \sum_{\mathbf{q}} \omega_{\mathbf{q}} \bar{N}_{\mathbf{q}} - \sum_{i,\mathbf{q}} \hbar \omega_{\mathbf{q}} \left(2M_{\mathbf{q}} - \Lambda_{\mathbf{q}} \right) \Lambda_{\mathbf{q}} \hat{n}_i$$
$$= -\sum_k \left[\epsilon_k + \sum_{\mathbf{q}} \hbar \omega_{\mathbf{q}} \left(2M_{\mathbf{q}} - \Lambda_{\mathbf{q}} \right) \Lambda_{\mathbf{q}} \right] \hat{n}_k + \sum_{\mathbf{q}} \omega_{\mathbf{q}} \bar{N}_{\mathbf{q}}, \qquad (3.25)$$

with

$$\epsilon_k = 2J \langle \hat{X}_i^\dagger \hat{X}_j \rangle_T \cos(kd) = 2J \cos(kd) \exp \left[-2 \sum_{\mathbf{q}} \left(2\bar{N}_{\mathbf{q}} + 1 \right) \Lambda_{\mathbf{q}}^2 \sin^2 \left(\frac{\mathbf{q} \cdot \mathbf{d}}{2} \right) \right].$$

From the Hamiltonian $\langle \tilde{H} \rangle_T$ above, we notice there is no change of the polaron dispersion except for a constant prefactor.

The single impurity is dressed by a coherent phonon cloud. It is easy to diagonalize the single-polaron coherent part in the momentum representation and minimize the free energy $F \equiv -k_{\mathrm{B}} T \ln \sum_k \exp\left(-E_k / k_{\mathrm{B}} T\right)$ for this system, with polaron dispersion

$$E_k = -2J_{\mathrm{P}} \cos\left(kd\right) + \varepsilon_{\mathrm{P}}, \tag{3.26}$$

with

$$J_{\mathrm{P}} = J \langle \hat{X}_i^\dagger \hat{X}_j \rangle_T,$$

and

$$\varepsilon_{\mathrm{P}} = -\sum_{\mathbf{q}} \hbar \omega_{\mathbf{q}} \left(2M_{\mathbf{q}} - \Lambda_{\mathbf{q}}\right) \Lambda_{\mathbf{q}},$$

where k is quasi-momentum in the longitudinal direction. Within the single polaron limit and after minimization of the the energy E_k, we can determine these variational parameters by the self-consistent equations:

$$\lambda_{\mathbf{q}} = \frac{\sum_k \exp\left(-E_k / k_{\mathrm{B}} T\right)}{\sum_k \left[1 - 2J_{\mathrm{P}} f_{\mathbf{q}} \cos(k \cdot d) / \omega_{\mathbf{q}}\right] \exp\left(-E_k / k_{\mathrm{B}} T\right)} \tag{3.27}$$

with $f_{\mathbf{q}} \equiv (2N_{\mathbf{q}} + 1)\left[1 - \cos\left(q_x d\right)\right]$.

One method to measure the polaron energy shift ε_{P} is by introducing an RF coupling into our system. The RF spectrum promotes the polaron particle into a free final state $|f\rangle$ without momentum transfer. The response function is given according to the Fermi's Golden Rule:

$$\Gamma\left(\omega\right) = A \sum_k \delta\left(\hbar \omega + E_k\right) = A \sum_k \delta\left(\hbar \omega + 2J_{\mathrm{P}} \cos\left(k \cdot d\right) + \varepsilon_{\mathrm{P}}\right). \tag{3.28}$$

3.3.2 Polaron phase transition

Before numerically calculating the variational parameters $\lambda_{\mathbf{q}}$, we firstly discuss some properties of this self-consistent equation. Considering a simplified model with momentum-independent variational parameters λ in a single band system, we choose to minimize only the ground state energy with $k = 0$. The self-consistent equation (3.27) in this case will be

$$\lambda = \left[1 + 2|J| \frac{\sum_{\mathbf{q}} f_{\mathbf{q}} |M_{\mathbf{q}}|^2}{\sum_{\mathbf{q}} \hbar \omega_{\mathbf{q}} |M_{\mathbf{q}}|^2} e^{-\lambda^2 \sum_{\mathbf{q}} f_{\mathbf{q}} |M_{\mathbf{q}}|^2}\right]^{-1}. \tag{3.29}$$

Such a form has been analyzed in [90, 91], where it was found that two locally stable solutions, λ_-, λ_+ exist, once the *adiabatic* regime is achieved when

$$2|J| \frac{\sum_{\mathbf{q}} f_{\mathbf{q}} |M_{\mathbf{q}}|^2}{\sum_{\mathbf{q}} \hbar \omega_{\mathbf{q}} |M_{\mathbf{q}}|^2} > \frac{e^{3/2}}{2}. \tag{3.30}$$

These two solutions λ_-, λ_+, corresponding to two local minimal of ground state energy, indicate the impurity is respectively loosely or tightly dressed by phonons. At a critical impurity-phonon coupling with $\sum_{\mathbf{q}} f_{\mathbf{q}} |M_{\mathbf{q}}|^2 = 27/8$, when the two minimal become equal, the lowest energy state solution abruptly switches from λ_- to λ_+, indicating a first-order *polaronic transition*. On the other hand, the solution of λ is a smooth and continuous crossover when the adiabatic condition is broken with a small value of $|J|$. This transition-crossover behavior also appears later when solving the self-consistent equation (3.27) numerically, although we

have considered a much more simplified model here. Strictly speaking, this sharp polaronic transition in the adiabatic regime is due to the mean-field approximation by thermal averaging of the phonon degrees of freedom. This drawback could be improved if we were to treat the incoherent dynamics properly, by taking into account fluctuations or using a master equation method.
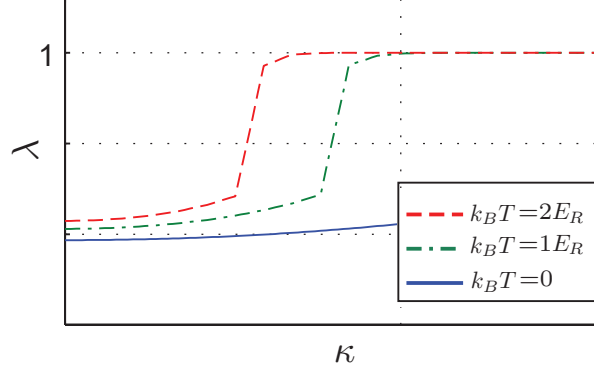
Figure 3.3: Polaronic transition for factors $\lambda \equiv \sum_{\mathbf{q}} \Lambda_{\mathbf{q}} / \sum_{\mathbf{q}} M_{\mathbf{q}}$ at different temperatures $k_{\mathrm{B}}T = 0, 1, 2E_R$. Maximum coupling constant $\kappa_c = 2.4$ for condensate density $n_0 = 1 \times 10^{14} \mathrm{cm}^{-3}$.

3.4   Dynamics of polaron in a tilted lattice

3.4.1   Polaronic Bloch oscillations

We show how a single polaron can be used to describe the decay of Bloch oscillations in a tilted lattice. From quantum mechanics, we learn that the eigenstates of a particle in a tilted lattice are Wannier-Stark states. In these states, the particle oscillates between the initially populated site and neighboring sites.

Without the coupling between polaron and bath, the coherent transport for a single polaron in a tilted lattice experiences Bloch oscillations. The Hamiltonian is

$$H_S = -J_{\mathrm{P}} \sum_{\langle i,j \rangle} \hat{c}_i^{\dagger} \hat{c}_j + \Omega_{\mathrm{tilted}} \sum_j j \hat{n}_j.$$

For a single particle, the dynamics produced by this Hamiltonian can be calculated analytically or numerically easily. Here we choose the Lindblad master equation and calculate the time-evolution of the density matrix:

$$\frac{d\rho_{sh}(t)}{dt} = -i\left[H_S, \rho_{sh}(t)\right] + \mathcal{L}_S\left[\rho_S(t)\right]. \tag{3.31}$$

In the case of coherent transport, the Lindblad term is identical to zero.

3.4.2   Decay of Bloch oscillations

From our previous section, by using the Lang-Firsov transformation $\tilde{H} = e^S H e^{-S}$, we can transform our low-energy effective Hamiltonian to an extended Hubbard model coupled with
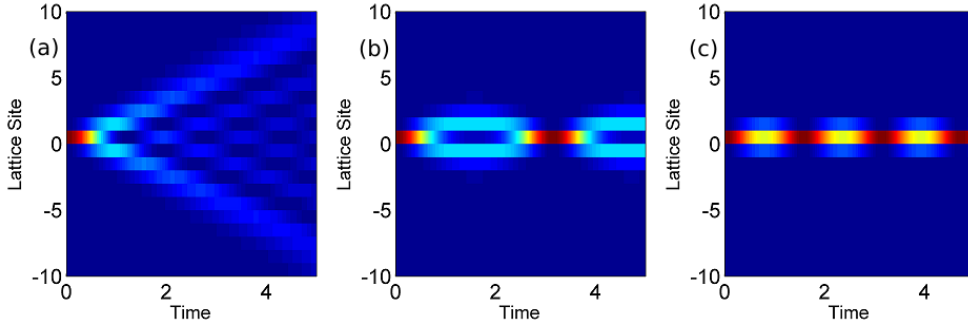
Figure 3.4: Bloch oscillation for single polaron in a tilted lattice with a) $\Omega = 0$, b) $\Omega = 2$ and c) $\Omega = 4$.

a phonon bath. The incoherent part can be written as

$$H_I = -J \sum_{<i,j>} \hat{c}_i^\dagger \hat{c}_j \left(\hat{X}_i^\dagger \hat{X}_j - \langle \hat{X}_i^\dagger \hat{X}_j \rangle \right) = \sum_{<i,j>} A_{ij} \otimes R_{ij}. \tag{3.32}$$

After the Born-Markov approximation, the master equation of system density matrix in the interaction picture is

$$\frac{d\rho_I(t)}{dt} = - \int_0^\infty d\tau Tr_B \left([H_I(t), [H_I(t-\tau), \rho_I(t) \otimes \rho_B]] \right) = \mathcal{L}_I[\rho_I(t)]. \tag{3.33}$$

In the interaction picture, the dynamics of polaron is in the quantum Brownian limit with

$$\hat{A}(-\tau) \approx \hat{A} - i\tau \left[H_S, \hat{A} \right], \tag{3.34}$$

thus

$$A_{ij}(-\tau) \approx -J\hat{c}_i^\dagger \hat{c}_j - (i\tau) \, JJ_{\mathrm{P}} \sum_{\delta_1,\delta_2=\pm 1} \left(\hat{c}_{i+\delta_1}^\dagger \hat{c}_j - \hat{c}_i^\dagger \hat{c}_{j+\delta_2} \right). \tag{3.35}$$

The Lindblad master equation can be calculated numerically for small systems. In the case of no tilt, $\Omega_{\mathrm{tilted}} = 0$, the incoherent Hamiltonian leads to decoherence of the quantum random walk. While in the case of a tilted lattice, $\Omega_{\mathrm{tilted}} \neq 0$, the incoherent part contributes to the decay of the oscillations as shown in Fig. 3.5.
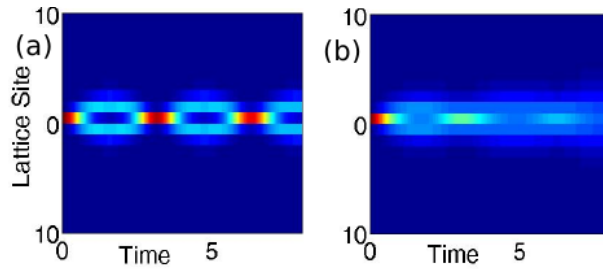
Figure 3.5: Bloch oscillation and decay for single polaron dynamics in a tilted lattice. (a) without and (b) with coupling between polaron and bath.

3.5   Polaron within a strongly interacting bosonic gas

In this section I consider a polaronic system with impurities coupling to a bosonic gas. Here we focus on the setup where impurities and bosonic gases are both trapped by an optical lattice. In order to include the case with strong impurity-boson coupling, we use Gutzwiller mean-field theory to describe the bosonic gas and coupled it to impurities.

As we know from the system with homogeneous BEC, the contact interactions between impurities and bosonic atoms U_{IB} will distort the density profile of the BEC and create a self-trapping potential minimum for each impurity. Effectively, there will be an induced long-range attractive interaction between different impurities. On the other hand, the BEC phonons will change the dynamics of impurity. We also would like to study whether such polaron effects still exist within a Gutzwiller treatment.

Here we write down the Hubbard Hamiltonian for the whole system with only a single Bloch band for impurities and bosonic gas $\hat{H} = \hat{H}_B + \hat{H}_I + \hat{H}_{I-B}$ with

$$\hat{H}_B = -J_B \sum_{\langle i,j \rangle} \left(\hat{b}_i^\dagger \hat{b}_j + h.c. \right) - \mu_B \hat{N}_B + \frac{U_{BB}}{2} \sum_i \hat{n}_i^B \left(\hat{n}_i^B - 1 \right), \tag{3.36}$$

$$\hat{H}_I = -J_I \sum_{\langle i,j \rangle} \left(\hat{c}_i^\dagger \hat{c}_j + h.c. \right) - \mu_I \hat{N}_I, \tag{3.37}$$

$$\hat{H}_{I-B} = U_{IB} \sum_i \hat{b}_i^\dagger \hat{b}_i \hat{c}_i^\dagger \hat{c}_i. \tag{3.38}$$

3.5.1   Gutzwiller mean-field theory

We start with solving the ground state of the bosonic gas and assuming the impurity-boson coupling term as a perturbation. For a bosonic gas in optical lattice, we apply the Gutzwiller wave function

$$|\Psi_{GW}\rangle = \prod_i |\psi_i\rangle = \prod_i \left(\sum_{n=0}^{N_c} \beta_n^i |n_i\rangle_i \right), \tag{3.39}$$

and minimize the variational ground state energy for all β_n^i. The energy of the bosonic Hamiltonian in Eq. (3.36) is

$$\langle \Psi_{GW} | H_B | \Psi_{GW} \rangle = -J_B \sum_{\langle i,j \rangle} | \left(\sum_{n=0}^{N_c} \sqrt{n+1} \beta_{n+1}^{i*} \beta_n^i \right)|^2 + \sum_i \sum_{n=0}^{N_c} \left(\frac{U_{BB}}{2} n(n-1) - \mu_B \right) |\beta_n^i|^2. \tag{3.40}$$

Alternatively the lattice bosonic system can be treated using mean-field techniques, and the Bose operator can be written as $\hat{b}_i = \langle \hat{b}_i \rangle + \left(\hat{b}_i - \langle \hat{b}_i \rangle \right)$. The mean-field Hamiltonian will be decoupled between the different sites as:

$$H_{MF}^B = \sum_i \left(H_{MF}^B \right)^i = -J_B \sum_i \left(\hat{b}_i^\dagger \eta_i + h.c \right) + \frac{J_B}{2} \sum_i \left(\langle \hat{b}_i^\dagger \rangle \eta_i + c.c \right)$$
$$+ \sum_i \left[\left(-\mu_B + V_i \right) \hat{n}_i^B + \frac{U_{BB}}{2} \hat{n}_i^B \left(\hat{n}_i^B - 1 \right) \right]. \tag{3.41}$$

with $\eta \equiv \sum_{n.n.i} \langle \hat{b}_i \rangle$. The ground state energy is

$$\langle \Psi_{MF} | H_{MF} | \Psi_{MF} \rangle = -\frac{J_B}{2} \sum_i \left(\langle \hat{b}_i^\dagger \rangle \eta_i + c.c \right) + \sum_i \left[\left(-\mu_B + V_i \right) \hat{n}_i^B + \frac{U_{BB}}{2} \hat{n}_i^B \left(\hat{n}_i^B - 1 \right) \right].$$

(3.42)

It can be shown that minimizing the ground state using the Gutzwiller method is identical to that using the mean-field (MF) method. Here we self-consistently calculate $\langle \hat{b}_i^\dagger \rangle$ by MF method instead of variationally calculating $\beta_{i,n}$ by Gutzwiller method.

In the MF Hamiltonian, the ground state can be calculated numerically or using second-order perturbation theory. Here we show how to self-consistently numerically calculate the mean-field order parameter $\langle \hat{b}_i \rangle \in C$. For each site i, the MF Hamiltonian in occupied Fock space is a matrix with elements:

$$\left(H_{MF}^0 \right)_{m,n}^i = -J_B \left(\sqrt{n+1} \eta_i \delta_{m,n+1} + \sqrt{n} \eta_i^* \delta_{m,n-1} \right)$$
$$-\tilde{\mu}_B \hat{n} + \frac{U_{BB}}{2} n (n-1) + \frac{J_B}{2} \left(\langle \hat{b}_i^\dagger \rangle \eta_i + \langle \hat{b}_i \rangle \eta_i^* \right),$$

(3.43)

where $\tilde{\mu}_B \equiv \mu_B - V_i$ and m, n indicate the particle number. The ground state energy and wave function will be the lowest eigenvalue and its eigenvector for the matrix:

$$\left(H_{MF}^0 \right)^i = \begin{bmatrix} 0 & -J_B \eta_i^* \sqrt{1} & & & \\ -J_B \eta_i^* \sqrt{1} & -\tilde{\mu}_B & -J_B \eta_i^* \sqrt{2} & & \\ & -J_B \eta_i^* \sqrt{2} & -2\tilde{\mu}_B + 2\frac{U_{BB}}{2} & \ddots & \\ & & \ddots & \ddots & -J_B \eta_i^* \sqrt{N_c} \\ & & & -J_B \eta_i^* \sqrt{N_c} & -N_c \tilde{\mu}_B + N_c (N_c - 1) \frac{U_{BB}}{2} \end{bmatrix}.$$

For an inhomogeneous system, as under discussion here, we need to calculate the mean-field order parameters $\langle \hat{b}_i \rangle$ for each site. Then we repeat the calculation until the results converge.

The Gutzwiller ansatz successfully describes the SF–MI transition of bosonic gas in a mean-field sense, and hence is exact only in the limit of infinite dimensionality. However, one needs to keep in mind the mean-field property of Gutzwiller ansatz and its limitations in accounting for the nontrivial correlations between particles. This limitation can be solved by applying a dynamic Gutzwiller mean-field analysis.

3.5.2 Impurity Gutzwiller method

There is a simple way to understand the polaron system with single impurity coupled to a bosonic gas: The density distribution of the bosonic bath acts as an effective potential for impurity with the form $U_{IB} \sum_i n_i^B \hat{c}_i^\dagger \hat{c}_i$, while the impurity density distribution also acts as an effective potential for the bosonic bath at the same time. Then we can iteratively calculate the ground state energy and density distribution until they converge.

Firstly, we pin an impurity in the middle of the system. The Gutzwiller ground state for the bosonic gas will be easily calculated in the present of this static impurity. By doing this, we minimize the energy with $H_B + H_{I-B}$. Secondly, the impurity wave function is calculated

with the new effective potential (due to bosonic bath). By doing this, we minimize the energy $H_I + H_{I-B}$. Then we calculate again the bosonic ground state using the new impurity density distribution. Finally, we repeat the calculation until it converges. The total energy should be simply adding the two parts together and removing one interaction term:

$$E_g = (H_I + H_{I-B}) + (H_B + H_{I-B}) - H_{I-B}. \tag{3.44}$$
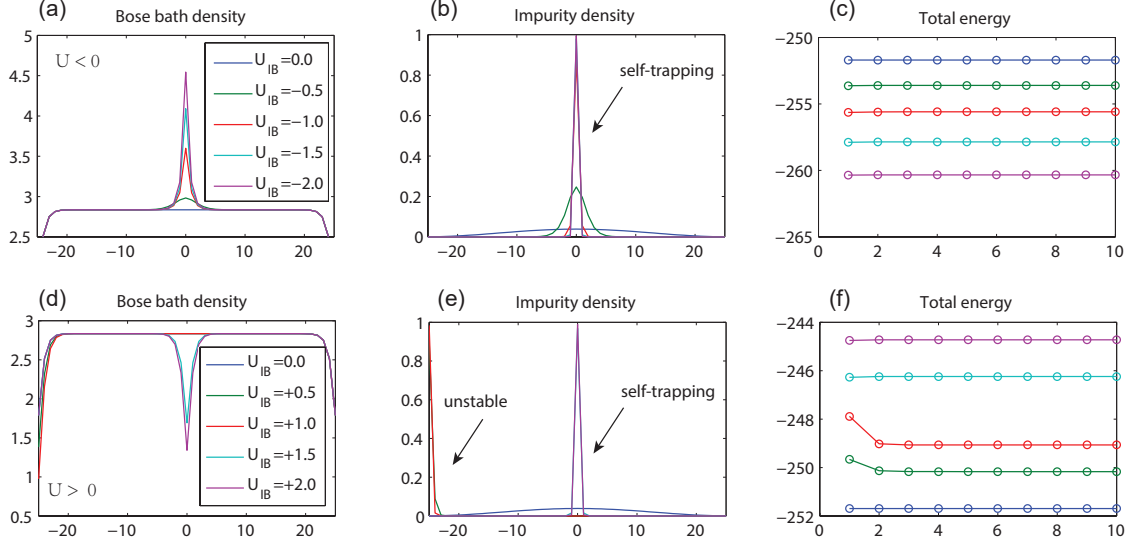
Figure 3.6: Calculation by the self-consistent impurity Gutzwiller method. (a, d) Bosonic bath density (b, e) impurity density and (c, f) total energy after several loops with different interactions. For attractive U_{IB}, the impurity is self-trapped in the center. For repulsive interaction $U_{IB} \leq 0.5$, the system is unstable while impurity is on the boundary of the system. For strongly repulsive $U_{IB} \geq 1$, the impurity is self-trapped in the middle of the system. We use 51 lattices and $U_{BB} = 1; J_{BB} = 1.5; \mu_B = 0.1$ (SF phase) and $J_I = 0.15$.

For a static impurity on site i, the impurity acts as a local potential at site i: $H_{I-B} = U_{IB} \sum_i \hat{b}_i^\dagger \hat{b}_i \hat{n}_i^I$. In this case, the Gutzwiller wave function $|\Psi_{GW}^{(i)}\rangle$ (in the presence of this impurity) can be easily solved by self-consistent method, by assuming single impurity localized on site i as

$$|\Psi_{GW}^{(i)}\rangle \equiv \prod_l \left(\sum_{n=0}^{N_c} \beta_n^l |n_l\rangle_l \right). \tag{3.45}$$

The ground state energy from $|\Psi_{GW}^{(i)}\rangle$ will be:

$$E_{GW}^{(i)} = \langle \Psi_{GW}^{(i)} | H_{\text{With impurity fixed on site } i} | \Psi_{GW}^{(i)} \rangle. \tag{3.46}$$

For single impurity moving in the system, the Gutzwiller wave function needs to be extended to to a state that is entangled with the impurity degrees of freedom:

$$|\Psi_{I-GW}\rangle = \left(\sum_i f_i \hat{c}_i^\dagger |vac\rangle \right) \otimes \prod_l \left(\sum_{n=0}^{N_c} \beta_n^l |n_l\rangle_l \right). \tag{3.47}$$

We can also write this as

$$|\Psi_{I-GW}\rangle = \sum_i f_i |\Psi_{I-GW}^{(i)}\rangle; \qquad (3.48)$$

$$|\Psi_{I-GW}^{(i)}\rangle \equiv \hat{c}_i^\dagger |vac\rangle |\Psi_{GW}^{(i)}\rangle = \hat{c}_i^\dagger |vac\rangle \otimes \prod_l \left(\sum_{n=0}^{N_c} \beta_n^l |n_l\rangle_l \right). \qquad (3.49)$$

The wave function for each site i describes one single impurity occupied site i, and the Gutzwiller wave function $|\Psi_{GW}^{(i)}\rangle$ in the presence of this impurity. In this basis, the total Hamiltonian can be expressed as a matrix with the elements:

$$\begin{aligned}
\mathcal{H}_{i,j} &= \langle \Psi_{GW}^{(i)} | \langle vac| \hat{c}_i H \hat{c}_j^\dagger |vac\rangle |\Psi_{GW}^{(i)}\rangle \\
&= \langle \Psi_{GW}^{(i)} | H_B |\Psi_{GW}^{(j)}\rangle \delta_{i,j} + \langle \Psi_{GW}^{(i)} | H_{I-B} |\Psi_{GW}^{(j)}\rangle \delta_{i,j} + \langle \Psi_{GW}^{(i)} | \langle vac| \hat{c}_i H_I \hat{c}_j^\dagger |vac\rangle \Psi_{GW}^{(j)}\rangle \\
&= E_{GW}^{(i)} \cdot \delta_{i,j} - J_I \langle \Psi_{GW}^{(i)} |\Psi_{GW}^{(j)}\rangle \left(\delta_{i,j+1} + \delta_{i,j+1} \right).
\end{aligned} \qquad (3.50)$$

We notice that the diagonal terms are $E_{GW}^{(i)}$, describing the static impurity, while the off-diagonal terms represent the hopping of the impurity. By diagonalizing this matrix, we can find the ground state and its energy for the system.

3.5.3 Generalization to variational Gutzwiller method

3.5.3.1 Variational Gutzwiller method

In a previous work [93], the authors studied one and two spinful impurities in a one-dimensional Bose lattice gas. Both the impurities and the Bose gas were contained in an optical lattice. With a single impurity, they proposed the following variational wave function for the system with momentum k:

$$|k\rangle = \sum_i |i\rangle e^{iki}, \qquad (3.51)$$

with

$$|i\rangle = A\hat{c}_i^\dagger |MF\rangle + \sum_j f_j \hat{c}_i^\dagger \hat{b}_{i+j} |MF\rangle. \qquad (3.52)$$

Here $|MF\rangle = \prod_i \left(\sum_{n=0} \beta_n |n_i\rangle_i \right)$ denotes the Gutzwiller mean-field ground state of the bosonic bath without impurity, as we discussed before. The amplitudes β_n for having n bosonic bath atoms on a site are determined by minimizing the energy. Variational parameters A encode the probability to find the single free impurity on site i, and f_j encodes how strongly the impurity binds with a hole at different distances j.

In their system, they used a simple variational wave function. They only considered the 1D system of a spin chain, in order to compare with a recent experiment [69, 93]. In addition, there are only repulsive interactions and $U_{IB} = U_{BB}$, which allows them to use a simple wave function. Finally, they only considered $\hat{b}_{i+j}$ excitations, which means only a single "hole" excitation $\hat{b}_{i+j}$ by one impurity on $\hat{c}_i^\dagger$. Because $U_{IB} = U_{BB}$, there are no double (and more) "hole" excitations.

By using this variational wave function, they calculated the polaron size, dispersion relation and impurity-hole correlations. In order to consider two-impurities system, they also used an extended variational wave function with zero total momentum:

$$|\psi\rangle = \sum_i |i\rangle = \sum_i \sum_{d\geq 0} \left(A(d) + \sum_l g(d,l) \hat{b}_{i+l} \right) \hat{c}_i^\dagger \hat{c}_{i+d}^\dagger |MF\rangle. \qquad (3.53)$$

They found that stable bi-polarons are formed when strong interactions are present [93].

3.5.3.2   Generalization to variational Gutzwiller

Our previous method yielded a ground state $|\Psi_{I-GW}\rangle = \sum_i f_i \hat{c}_i^\dagger |vac\rangle |\Psi_{GW}^{(i)}\rangle$, which is equivalent to a Gutzwiller based variational wave function:

$$|\Psi\rangle = \sum_i f_i \hat{c}_i^\dagger \hat{G}_i |MF\rangle, \tag{3.54}$$

with

$$\hat{G}_i |MF\rangle \equiv |\Psi_{GW}^{(i)}\rangle. \tag{3.55}$$

Here $\hat{G}_i$ is a group of operators acting on the mean-field ground state without impurity. Our method is a combination of different operators $\hat{G}_i$ on the ground state. Unlike other variational methods, we have already calculated $\hat{G}_i$ by the Gutzwiller method in advance. In order to extend our method for large impurity hopping, the wave function can be generalized to

$$|\Psi\rangle = \sum_i \left(A_i \hat{c}_i^\dagger |MF\rangle + f_i \hat{c}_i^\dagger \hat{G}_i |MF\rangle \right), \tag{3.56}$$

with A_i indicating a free impurity moving in a bosonic gas. Then we can work in a variational treatment, instead of diagonalizing the Hamiltonian. The ground state will be obtained by minimizing energy of this variational wave function, with variables A_i and f_i. In addition, the variational wave functions $|\Psi\rangle$ only have variables A_i, f_i by considering ground states $|\Psi_{GW}^{(i)}\rangle$ in the presence of impurity. We include excitations by adding terms as

$$\sum_i \sum_j \left(l_j \hat{c}_i^\dagger \hat{b}_{i+j} + k_j \hat{c}_i^\dagger \hat{b}_{i+j}^\dagger \right) |\Psi_{GW}^{(i)}\rangle,$$

with l_j, k_j indicating (single bosonic) excitations on the ground state $|\Psi_{GW}^{(i)}\rangle$.

3.5.3.3   Multi-polaron system

It is very straightforward to generalize the method to few-impurity system, by replacing the index i for the position of a single impurity, to an index n for the impurity's index of the Fock basis:

$$|\Psi_{I-GW}\rangle = \sum_n f_n |\Psi_{I-GW}^{(n)}\rangle; \tag{3.57}$$

$$|\Psi_{I-GW}^{(n)}\rangle \equiv |n\rangle |\Psi_{GW}^{(n)}\rangle. \tag{3.58}$$

Here $|n\rangle$ indicates the $n-$th basis for the Fock state of the impurities, and $|\Psi_{GW}^{(n)}\rangle$ is the ground state of bosonic gas when impurities are localized in $n-$th Fock state. However, by including multiple impurities, the Hilbert space becomes large very quickly, leaving the calculations impossible.

3.6   Polarons coupled to fermionic bath

For completeness of the discussion, we also briefly discuss the Fermi polaron system where the impurities are coupled to a fermionic bath. In the experiment work [60], they observed Fermi polarons, a spin-down impurity interacting with a spin-up Fermi sea. The experiment started with a spin-polarized cloud of ^{6}Li atoms in the lowest hyperfine state $|1\rangle$ with spin up. Then

they transferred a small fraction into state $|3\rangle$ with spin down. Those spin down impurities interact with the spin up Fermi sea and form polarons in this system. They perform RF spectroscopy on the impurity $|3\rangle$ and the environment Fermi sea $|1\rangle$. As the interaction between impurity and spin up environment leads to a shift of RF spectrum, the RF photon must supply additional energy to transfer a particle out of its attractive environment into the final, non-interacting state. By observing a narrow peak in the impurity spectrum that is not matched by the response of the environment, they were able to identify the formation of a Fermi polaron. There are also other experiments for Fermi polarons such as in [94, 95, 64].

The experimental results in [60] can be well explained by the variational Chevy ansatz [96, 97, 98, 59]. In order to calculate the impurity RF spectrum $\Gamma(\omega)$, they use the Chevy ansatz and Fermi's Golden Rule. In the dilute ultracold system, the interaction can be described by the short-range s-wave scattering length a. The many-body Hamiltonian for the system is:

$$\hat{H} = \sum_{k,\sigma} \epsilon_k c_{k\sigma}^\dagger c_{k\sigma} + \frac{g_0}{\nu} \sum_{k,k',q} c_{k+\frac{q}{2}\uparrow}^\dagger c_{-k+\frac{q}{2}\downarrow}^\dagger c_{k'+\frac{q}{2}\downarrow} c_{-k'+\frac{q}{2}\uparrow}. \tag{3.59}$$

The label σ denotes the spin state $\uparrow, \downarrow$,$\epsilon_k = \hbar^2 k^2/2m$, ν is the volume of the system and $c_{k\sigma}^\dagger, c_{k\sigma}$ are the creation and annihilation operators for fermions. The trial wave function for the Fermi polaron with zero momentum proposed by Chevy is:

$$|\Psi\rangle = \varphi_0 |0\rangle_\downarrow |FS\rangle_\uparrow + \sum_{q<k_F}^{k>k_F} \varphi_{kq} c_{k\uparrow}^\dagger c_{q\uparrow} |q-k\rangle_\downarrow |FS\rangle_\uparrow. \tag{3.60}$$

The energy will be minimized under variation of φ_0 and φ_{kq}. This wave function describes only single spin-down impurity interacting with a spin-up Fermi sea. By minimizing $\langle\Psi|\hat{H}|\Psi\rangle - E_\downarrow\langle\Psi|\Psi\rangle$, they get the particle-hole excitation amplitudes φ_{kq}, the quasiparticle weight $|\varphi_0|^2 = Z$, and the energy $E_\downarrow$ due to the addition of the down spin impurity.

On the other hand, in the case of weak interaction between polaron and bath, the system is described by Fermi liquid theory. Unless phase transitions occur, the system of interacting fermions will maintain the basic character of an ideal Fermi gas. The impurities evolve into quasiparticles (polarons) such that there is a one-to-one correspondence between the two spectra. In the adiabatic continuity limit, we can also label single-particle states of polarons in terms of those of free fermions.

Chapter 4

Polaron Effects in Two-band Quantum Lattice System

4.1 Introduction

Here we consider polaronic phenomena of multi-band systems with ultracold quantum gases. In such systems, the inter-band dynamics of polarons, as well as intra-band dynamics, lead to new effects which have no analog in single band systems. Motivated by recent experiments [99, 100, 101, 102], we consider a system of a few impurities in an optical lattice, populating the lowest two Bloch bands, immersed in a Bose-Einstein condensate. These impurities are coupled to Bogoliubov phonons (of the BEC) via both intra- and inter-band transitions. In order to decouple this Fröhlich-like term, we derive a generalized two-band Lang-Firsov polaron transformation. The transformed effective Hamiltonian still contains two bands, where the impurity is now dressed by phonons as a quasi-particle (polaron). We use a variational approach to connect the weak and strong coupling limits and calculate the dressing parameters. Polaronic effects modify both intra-band coherent transport and polaron energy shifts, and also induce a long-range interaction between different polarons.

We then focus on inter-band relaxation effects and specify our system as a single impurity trapped in a quasi-1D system. We study the residual incoherent coupling between polaron and bath by using a Lindblad master equation. The impurity inter-band relaxation process under this polaronic treatment is captured beyond a Fermi's Golden Rule description. These polaronic renormalization effects of the inter-band relaxation rate should be accessible in current experiments. On the other hand, for large impurity-phonon coupling, the polaron is tightly dressed in each band and cannot hop between different bands. In this limit, an *inter-band self-trapping* effect is expected.

In section 4.2, we introduce the effective two-band Hamiltonian of a realistic experimental setup, with a few impurities in a lattice, immersed in a Bose-Einstein condensate (BEC) of a different atomic species. In section 4.3, we describe in detail the generalized Lang-Firsov polaron transformation for the two-band system. The transformed Hamiltonian with two (polaron) bands can be separated into a coherent part and an incoherent part. The coherent part, arising from the thermal average over the phonon bath, is discussed in section 4.4. The inter-band relaxation and decoherence effects, which are all included in the incoherent part of this Hamiltonian, are discussed in section 4.5. We derive the Lindblad equation and correlation functions for the residual incoherent impurity-phonon coupling. The polaronic impurity dynamics is closely related to recent experiments.

4.2 Effective Hamiltonian

Here we consider a few neutral impurities with mass m_I interacting with a Bose-Einstein condensate of another neutral species. The impurities are trapped by a 3D optical lattice and their Hamiltonian is denoted by H_I. The homogeneous BEC system H_B is formed by another atomic species with mass m_B and a weak repulsive interaction g_B. The impurity-BEC interaction H_{int} is caused by s-wave interactions between the different species, which can be tuned by standard Feshbach resonance techniques. The total Hamiltonian is hence

$$H = H_I + H_B + H_{\text{int}}.$$

We describe these different terms in detail in the following parts of this section.

4.2.1 Impurities in an optical lattice

We consider a quasi-1D system with impurities trapped in an anisotropic 3D optical lattice. The same discussion is presented in the previous chapter.

In the longitudinal direction, on the other hand, the impurities populate both the lowest and the first excited band. In principle, exact Bloch wave functions need to be calculated numerically, which can then also be represented as linear combinations of Wannier states $\varphi_x^{0(1)}(x)$. In a deep lattice, the Wannier functions can be approximated by the lowest two eigenstates of a harmonic oscillator

$$\varphi_x^0(x) \quad \approx \quad 1/\left(\pi\sigma_x^2\right)^{\frac{1}{4}} e^{-x^2/\left(2\sigma_x^2\right)}, \tag{4.1}$$

$$\varphi_x^1(x) \quad \approx \quad 1/\left(\pi\sigma_x^2\right)^{\frac{1}{4}} \left(\sqrt{2}\cdot x/\sigma_x\right) e^{-x^2/\left(2\sigma_x^2\right)}, \tag{4.2}$$

with longitudinal characteristic length $\sigma_x \equiv \sqrt{\hbar/\left(m_I\omega_x\right)}$ and oscillation frequency $\hbar\omega_x \equiv 2\left(V_I^x E_R\right)^{1/2}$.

In this highly anisotropic system, impurities can hop to their nearest-neighbor sites only along the longitudinal direction. A particle localized on lattice site j will be described by the wave function

$$W_j^{0(1)}(\mathbf{r}) \equiv \varphi_x^{0(1)}(x - x_j)\,\phi^0(y)\,\phi^0(z). \tag{4.3}$$

Due to the low density of impurities, their dynamics can be modeled by a non-interacting two-band Hubbard Hamiltonian:

$$\hat{H}_I = -\sum_{\langle i,j\rangle}\sum_{\alpha} J^{\alpha}\hat{a}_i^{\alpha\dagger}\hat{a}_j^{\alpha} + \sum_i\sum_{\alpha}\varepsilon^{\alpha}\hat{n}_i^{\alpha}, \tag{4.4}$$

where J^{α} and ε^{α} are the hopping parameters and on-site energy for each band with index $\alpha = 0, 1$. In a deep lattice, the band gap $\varepsilon^{\Delta} \equiv \varepsilon^1 - \varepsilon^0$ can be approximated as the longitudinal oscillator frequency $\hbar\omega_x$. In this work we only consider inter-band dynamics between the lowest two Bloch bands and ignore higher band effects.

4.2.2 Bosonic bath and atom-phonon coupling

The impurities are immersed in a homogeneous BEC with weakly repulsive boson-boson interaction g_B between the atoms. In a dilute system, this weak interaction can be described by the boson-boson scattering length a_B as $g_B = 4\pi\hbar^2 a_B/m_B$. For vanishing inter-species interaction g_{IB} between impurity and bath, the BEC can be described by standard Bogoliubov theory and treated as a phonon bath.
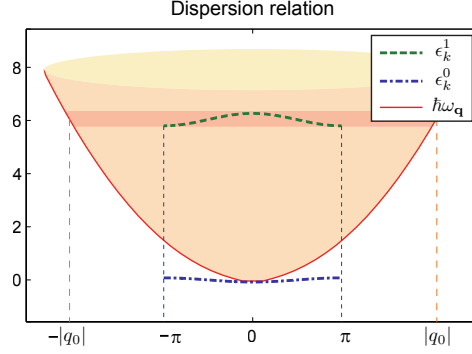
Figure 4.1: Dispersion relation for single impurity and phonon in longitudinal direction (in units of E_R). The impurity moves in the longitudinal direction of the system with two Bloch bands ϵ_k^0 (blue line) and ϵ_k^1 (green line). The dashed blue lines at $k = \pm\pi$ indicate the first Brillouin zone in longitudinal direction. The phonon dispersion $\hbar\omega_{\mathbf{q}}$ (red line) is described by Bogoliubov theory where $\mathbf{q} \equiv (q_x, q_y, q_z)$ is the phonon momentum. The dashed red lines at $q_x = \pm|q_0|$ indicate that the phonon energy matches with the impurity band gap $\hbar\omega_{|q_0|} \approx \varepsilon^\Delta$ with $\varepsilon^\Delta \equiv \varepsilon^1 - \varepsilon^0$.

Here we use the approach in [66, 84], where the deformation is treated as a perturbation around the BEC ground state. The Hamiltonian (up to constant terms) for this effective phonon bath can be simply expressed as

$$\hat{H}_B = \sum_{\mathbf{q}} \hbar\omega_{\mathbf{q}}\hat{b}_{\mathbf{q}}^\dagger\hat{b}_{\mathbf{q}}, \tag{4.5}$$

with the system *quantization volume* Ω and the Bogoliubov phonon dispersion

$$\hbar\omega_{\mathbf{q}} \equiv \sqrt{\epsilon_{\mathbf{q}}\left(\epsilon_{\mathbf{q}} + 2g_B n_0\right)};$$
$$\epsilon_{\mathbf{q}} \equiv \frac{\hbar^2|\mathbf{q}|^2}{2m_B}. \tag{4.6}$$

where $n_0 = |\psi_0|^2$ is the condensate density.

The impurity-BEC interaction of the Hamiltonian can be written as

$$\hat{H}_{\text{int}} = \sum_{\mathbf{q}}\sum_{\alpha,\beta}\sum_{i,j} \hbar\omega_{\mathbf{q}} M_{i,j;\mathbf{q}}^{\alpha\beta}\hat{b}_{\mathbf{q}}\hat{a}_i^{\alpha\dagger}\hat{a}_j^\beta + h.c., \tag{4.7}$$

$$M_{i,j;\mathbf{q}}^{\alpha\beta} = \frac{g_{IB}}{\hbar\omega_{\mathbf{q}}}\sqrt{\frac{n_0}{\Omega}}\left(u_{\mathbf{q}} - v_{\mathbf{q}}\right) m_{i,j;\mathbf{q}}^{\alpha\beta}, \tag{4.8}$$

with α, β indicating the impurity Bloch bands and $m_{i,j;\mathbf{q}}^{\alpha\beta} \equiv \int d^3\mathbf{r} \cdot e^{i\mathbf{q}\cdot\mathbf{r}} \cdot W_i^{\alpha*}(\mathbf{r}) W_j^\beta(\mathbf{r})$. This term describes the impurity coupling to the phonon bath by creating or annihilating phonons. The non-local coupling terms with $i \neq j$ are highly suppressed due to the local form of the interaction which requires overlap between localized Wannier functions. For these reasons, the above integrals $m_{i,j;\mathbf{q}}^{\alpha\beta}$ can be well approximated by $\delta_{ij}m_{\mathbf{q}}^{\alpha\beta}e^{i\mathbf{q}\cdot\mathbf{R}_i}$ such that the value depends only on α, β and $\mathbf{q}$. The dimensionless impurity-phonon coupling $M_{i;\mathbf{q}}^{\alpha\beta}$ can also be written as $M_{\mathbf{q}}^{\alpha\beta}e^{i\mathbf{q}\cdot\mathbf{R}_i}$ with

$$M_{\mathbf{q}}^{\alpha\beta} \equiv g_{IB}\sqrt{\frac{n_0\epsilon_{\mathbf{q}}}{\Omega\left(\hbar\omega_{\mathbf{q}}\right)^3}}m_{\mathbf{q}}^{\alpha\beta}. \tag{4.9}$$

Figure 4.2: Atom-phonon coupling matrix $M_s^{\alpha\beta}$ for inter- and intra-band hopping processes versus phonon momentum $\mathbf{s} = (s_x, s_y, s_y)$. The black dashed line indicates that the phonon energy matches with impurity band gap: $\hbar\omega_\mathbf{s} = \hbar\omega$. With $V_I^x = 16E_I^r, V_I^\perp = 25V_I^x$, $g_B = 0.3$; $g_{IB} = 0.5$; $m_I/m_B = 133/87$.

Note that the impurity-phonon coupling $M_{i,\mathbf{q}}^{\alpha\beta}$ obeys:

$$\left(M_{i,\mathbf{q}}^{\alpha\beta}\right)^* = M_{i,-\mathbf{q}}^{\alpha\beta}. \tag{4.10}$$

The integral factors $m_\mathbf{q}^{\alpha\beta}$ take the form

$$m_\mathbf{q}^{\alpha\beta} = \int d^3\mathbf{r} \cdot e^{i\cdot\mathbf{q}\cdot\mathbf{r}} \varphi_x^{\alpha*}(x)\, \varphi_x^\beta(x)\, |\phi^0(y)|^2 |\phi^0(z)|^2.$$

In a deep optical lattice, where the impurity Wannier functions in Eqs. (4.1-4.2) can be approximated as harmonic oscillator states, we can explicitly evaluate these factors:

$$\begin{aligned}
m_\mathbf{q}^{00} &= e^{-\left(\sigma_\perp^2 q_\perp^2 + \sigma_x^2 q_x^2\right)/4}, \\
m_\mathbf{q}^{01} &= e^{-\left(\sigma_\perp^2 q_\perp^2 + \sigma_x^2 q_x^2\right)/4}\left(iq_x\sigma_x/\sqrt{2}\right) = m_\mathbf{q}^{10}, \\
m_\mathbf{q}^{11} &= e^{-\left(\sigma_\perp^2 q_\perp^2 + \sigma_x^2 q_x^2\right)/4}\left(1 - q_x^2\sigma_x^2/2\right),
\end{aligned} \tag{4.11}$$

by using the identity for Hermite polynomial integrals [85]. Here $q_\perp \equiv \sqrt{q_y^2 + q_z^2}$ indicates the transverse phonon momentum.

In order to describe polaronic effects resulting from the impurity-BEC coupling, we again use the dimensionless coupling constant as in [86] and name it κ. This constant depends on the impurity-boson and boson-boson interactions g_{IB}, g_{BB} and the condensate parameters ξ and m_B as

$$\kappa \equiv \sqrt{\frac{g_{IB}^2 m_B}{g_B \hbar^2 \xi}}. \tag{4.12}$$

Finally the effective Hamiltonian with two-band Fröhlich impurity-phonon coupling is

$$\begin{aligned}
\hat{H} = &-\sum_{\langle i,j\rangle}\sum_\alpha J^\alpha \hat{a}_i^{\alpha\dagger}\hat{a}_j^\alpha + \sum_i\sum_\alpha \varepsilon^\alpha \hat{n}_i^\alpha \\
&+ \sum_\mathbf{q} \hbar\omega_\mathbf{q}\hat{b}_\mathbf{q}^\dagger\hat{b}_\mathbf{q} \\
&+ \sum_{i,\mathbf{q}}\sum_{\alpha,\beta} \hbar\omega_\mathbf{q} M_{i,\mathbf{q}}^{\alpha\beta}\left(\hat{b}_\mathbf{q} + \hat{b}_{-\mathbf{q}}^\dagger\right)\hat{a}_i^{\alpha\dagger}\hat{a}_i^\beta.
\end{aligned} \tag{4.13}$$

Here we used the relation in Eq. (4.10). This Hamiltonian describes a general two-band system with impurity-phonon coupling, which can also be realized by other experimental setups such as hybrid atom-ion systems [80].

4.3 Variational two-band polaron transformation

4.3.1 Transformation with exponential quadratic operators

This two-band Hamiltonian in Eq. (4.13), with Fröhlich-type impurity-phonon coupling, can not be solved analytically even for the case of a single impurity. The goal of this section is to find a simple but non-trivial variational method which can deal with the two-band system (4.13) in general. We choose the Lang-Firsov polaron transformation approach and generalize it to the two-band system. This canonical transformation was discussed in Chapter 3. In order to find a suitable variational transformation for the two-band system, we modify the Lang-Firsov polaron transformation $\tilde{H} = e^{\hat{S}}He^{-\hat{S}}$ by extending the impurity-phonon interaction to the two-band form. It takes the form:

$$\hat{S} \equiv \left[\sum_{i,\mathbf{q}} \sum_{\alpha,\beta} \Lambda_{i,\mathbf{q}}^{\alpha\beta} \left(\hat{b}_{-\mathbf{q}}^{\dagger} - \hat{b}_{\mathbf{q}} \right) \hat{a}_i^{\alpha\dagger} \hat{a}_i^{\beta} \right], \tag{4.14}$$

with $\Lambda_{i,\mathbf{q}}^{\alpha\beta} \equiv \Lambda_{\mathbf{q}}^{\alpha\beta} e^{i\cdot\mathbf{q}\cdot\mathbf{R}_i}$. A similar method was also applied in previous works [103, 104, 105, 106, 90] for a single-band system with non-local impurity-phonon coupling. Our initial guess for the variational parameters is the coupling element itself, $M_{\mathbf{q}}^{\alpha\beta}$, and we constrain the variational parameters to obey the same symmetry property as $M_{\mathbf{q}}^{\alpha\beta}$, namely that of Eq. (4.10). By using the Baker-Campbell-Hausdorff formula, $e^{\hat{S}}\hat{A}e^{-\hat{S}} = \hat{A} + \left[\hat{S},\ \hat{A}\right] + \frac{1}{2!}\left[\hat{S},\ \left[\hat{S},\ \hat{A}\right]\right] + \cdots$, we can derive the transformed Hamiltonian with exponential quadratic operators as outlined in Appendix B. For convenience, these expressions can be written in 2×2 matrix form via

$$\mathbf{\Lambda}_{\mathbf{q}} \equiv \left(\begin{array}{cc} \Lambda_{\mathbf{q}}^{00} & \Lambda_{\mathbf{q}}^{01} \\ \Lambda_{\mathbf{q}}^{10} & \Lambda_{\mathbf{q}}^{11} \end{array} \right); \ \hat{\mathbf{b}}_{\mathbf{q}} \equiv \left(\begin{array}{cc} \hat{b}_{\mathbf{q}} & 0 \\ 0 & \hat{b}_{\mathbf{q}} \end{array} \right), \tag{4.15}$$

and

$$\mathbf{M}_{i,\mathbf{q}} \equiv \left(\begin{array}{cc} M_{\mathbf{q}}^{00} & M_{\mathbf{q}}^{01} \\ M_{\mathbf{q}}^{10} & M_{\mathbf{q}}^{11} \end{array} \right) e^{i\cdot\mathbf{q}\cdot\mathbf{R}_i}. \tag{4.16}$$

After the transformation, the impurity annihilation and creation operators can be expressed through

$$e^{\hat{S}}\hat{a}_i^{\alpha}e^{-\hat{S}} = \sum_{\beta} \left(\hat{\mathbf{X}}_i \right)_{\alpha\beta} \hat{a}_i^{\beta}, \tag{4.17}$$

and similarly for the creation operators. The matrix operators $\hat{\mathbf{X}}_i$ are found to be

$$\hat{\mathbf{X}}_i \equiv e^{-\sum_{\mathbf{q}} \mathbf{\Lambda}_{\mathbf{q}} e^{i\cdot\mathbf{q}\cdot\mathbf{R}_i} \left(\hat{\mathbf{b}}_{-\mathbf{q}}^{\dagger} - \hat{\mathbf{b}}_{\mathbf{q}} \right)}. \tag{4.18}$$

In the same fashion as was described above for the single band system, this canonical transformation is equivalent to defining a new quasi-particle, which represents an impurity dressed by the phonon cloud forming a polaron. This transformation also shifts the equilibrium position of the phonon bath by

$$e^{\hat{S}}\hat{b}_{\mathbf{q}}e^{-\hat{S}} = \hat{b}_{\mathbf{q}} + \sum_{i,\alpha,\beta} \left(\hat{\mathbf{X}}_i^{\dagger} \hat{\mathbf{b}}_{\mathbf{q}} \hat{\mathbf{X}}_i - \hat{\mathbf{b}}_{\mathbf{q}} \right)_{\alpha\beta} \hat{a}_i^{\alpha\dagger} \hat{a}_i^{\beta}, \tag{4.19}$$

but it does not modify the phonon dispersion relation. In Appendix B, we show the derivations for Eqs. (4.17-4.19). The transformed polaronic Hamiltonian can be written as:

$$
\begin{aligned}
\tilde{H} = &-\sum_{\langle i,j \rangle} \sum_{\alpha\beta} \left(\hat{\mathbf{X}}_i^\dagger \mathbf{J} \hat{\mathbf{X}}_j \right)_{\alpha\beta} \hat{a}_i^{\alpha\dagger} \hat{a}_j^\beta + \sum_i \sum_{\alpha\beta} \left(\hat{\mathbf{X}}_i^\dagger \varepsilon \hat{\mathbf{X}}_i \right)_{\alpha\beta} \hat{a}_i^{\alpha\dagger} \hat{a}_i^\beta + \sum_{\mathbf{q}} \hbar\omega_{\mathbf{q}} \hat{b}_{\mathbf{q}}^\dagger \hat{b}_{\mathbf{q}} \\
&+ \sum_{i,\alpha,\beta} \sum_{\mathbf{q}} \hbar\omega_{\mathbf{q}} \left[\left(\hat{\mathbf{X}}_i^\dagger \hat{b}_{\mathbf{q}}^\dagger \mathbf{M}_{i,\mathbf{q}}^\dagger \hat{\mathbf{X}}_i \right) + \left(\hat{\mathbf{X}}_i^\dagger \mathbf{M}_{i,\mathbf{q}} \hat{b}_{\mathbf{q}} \hat{\mathbf{X}}_i \right) + \left(\hat{\mathbf{X}}_i^\dagger \hat{b}_{\mathbf{q}}^\dagger \hat{b}_{\mathbf{q}} \hat{\mathbf{X}}_i \right) - \hat{b}_{\mathbf{q}}^\dagger \hat{b}_{\mathbf{q}} \right]_{\alpha\beta} \hat{a}_i^{\alpha\dagger} \hat{a}_i^\beta \\
&+ \sum_{i,\alpha,\beta} \sum_{j,\alpha',\beta'} \sum_{\mathbf{q}} \frac{\hbar\omega_{\mathbf{q}}}{2} \left[\left(\hat{\mathbf{X}}_i^\dagger \hat{b}_{\mathbf{q}}^\dagger \hat{\mathbf{X}}_i - \hat{b}_{\mathbf{q}}^\dagger \right)_{\alpha\beta} \left(2\hat{\mathbf{X}}_j^\dagger \mathbf{M}_{j,\mathbf{q}}^\dagger \hat{\mathbf{X}}_j + \hat{\mathbf{X}}_j^\dagger \hat{b}_{\mathbf{q}} \hat{\mathbf{X}}_j - \hat{b}_{\mathbf{q}} \right)_{\alpha'\beta'} + h.c. \right] \hat{a}_i^{\alpha\dagger} \hat{a}_j^{\alpha'\dagger} \hat{a}_j^{\beta'} \hat{a}_i^\beta,
\end{aligned}
$$
$$(4.20)$$

where $\mathbf{J}$ and ε are the (diagonal) matrix forms of J^α and ε^α. Here we combine all single impurity contributions in the second line. The last term, which is zero when only a single impurity is considered, describes induced polaron-polaron interactions due to the coupling with the phonon bath. Compared to the original Hamiltonian in Eq. (4.13), the hopping and on-site energy have been modified. As for the single band system, this Hamiltonian contains all interactions exactly and is hard to solve analytically. Motivated by the single-band system, we separate the Hamiltonian into coherent and incoherent parts, $\langle \tilde{H} \rangle_T$ and $\tilde{H} - \langle \tilde{H} \rangle_T$ respectively. The explicit form of the coherent terms, which conserve the number of phonons, is determined in Appendix B. In Eqs. (B.16, B.17, B.24, B.27) we calculate all possible coherent terms in Eq. (4.20). After determining the variational parameters $\mathbf{\Lambda}_{\mathbf{q}}$ by minimizing the free energy of the coherent part, we treat the residual polaron-bath coupling in the incoherent part as a perturbation and solve it by a Lindblad master equation.

4.3.2 Diagonal transformation matrix

In Appendix B.2, we calculate the coherent part $\langle \tilde{H} \rangle_T$ by averaging over the phonon bath and assuming it is thermal. In contrast to the single-band case, these calculations are demanding when both intra- and inter-band phonon couplings are included. In order to determine the variational parameters $\mathbf{\Lambda}_{\mathbf{q}}$, we finally need to minimize the free energy of the full coherent Hamiltonian. Until now, we did not make any assumptions for our variational parameters $\mathbf{\Lambda}_{\mathbf{q}}$ except for the symmetry relations in Eq. (4.10).

Unfortunately, the general result of the transformed Hamiltonian in Eq. (4.20) and its corresponding coherent part are still quite complicated. It can be further simplified by making some approximations suitable to our specific system. Due to conservation of energy, the phonon-induced inter-band dynamics requires the phonon energy to match the impurity band gap, i.e. $\hbar\omega_{\mathbf{q}} \approx \varepsilon^\Delta$. This energy scale involves a phonon with particle-like dispersion and momentum $|\mathbf{q}| \approx \sqrt{2m_B\varepsilon^\Delta}/\hbar$ significantly far from zero. The inter-band coupling $M_{\mathbf{q}}^{01}$ for this large phonon momentum is highly reduced due to the Gaussian decay of $m_{\mathbf{q}}^{01}$ in Eq. (4.11). On the other hand, intra-band dynamics requires a phonon energy $\hbar\omega_{\mathbf{q}} \approx J^0; J^1$ with phonon-like dispersion and small momentum $|\mathbf{q}| \approx J^\alpha \sqrt{m_B/(g_B n_0)}/\hbar = J^\alpha/(\hbar c)$. The intra-band coupling $M_{\mathbf{q}}^{\alpha\alpha}$ is not reduced too much at this smaller momentum. In the polaron transformation, the parameters $\Lambda_{\mathbf{q}}^{\alpha\beta}$ reflect the dressing of the impurity by phonons and are closely related to $M_{\mathbf{q}}^{\alpha\beta}$. For this reason, we treat the inter-band coupling as small and approximate the matrices $\mathbf{\Lambda}_{\mathbf{q}}$ as diagonal:

$$
\mathbf{\Lambda}_{\mathbf{q}} = \left[\begin{array}{cc} \lambda_{\mathbf{q}}^0 M_{\mathbf{q}}^{00} & 0 \\ 0 & \lambda_{\mathbf{q}}^1 M_{\mathbf{q}}^{11} \end{array} \right],
$$

with variational parameters $\lambda_{\mathbf{q}}^0$ and $\lambda_{\mathbf{q}}^1$. Since the intra-band couplings $M_{\mathbf{q}}^{\alpha\alpha}$ are purely real numbers in our system, we assume $\lambda_{\mathbf{q}}^{\alpha}$ are also real. After the transformation with these diagonal matrices $\mathbf{\Lambda_q}$, we have then decoupled the intra-band impurity-phonon coupling and leave the (relatively) small inter-band coupling in the new polaronic two-band Hamiltonian. The coherent part, with phonons eliminated by thermal averaging, is a many-body Hamiltonian:

$$\langle \tilde{H} \rangle_T = - \sum_{\langle i,j \rangle, \alpha} J_{\mathrm{P}}^{\alpha} \hat{a}_i^{\alpha\dagger} \hat{a}_j^{\alpha} + \sum_{i,\alpha} \varepsilon_P^{\alpha} \hat{n}_i^{\alpha} + \sum_{\mathbf{q}} \hbar\omega_{\mathbf{q}} \langle \hat{b}_{\mathbf{q}}^{\dagger} \hat{b}_{\mathbf{q}} \rangle_T + \hat{V}_{\mathrm{P}}, \tag{4.21}$$

with renormalized polaronic hopping terms J_{P}^{α} and on-site energy $\varepsilon_{\mathrm{P}}^{\alpha}$ including the polaron energy shift:

$$\begin{aligned} J_{\mathrm{P}}^{\alpha} &\equiv J^{\alpha} \langle \left(\hat{\mathbf{X}}_i \right)_{\alpha\alpha}^{\dagger} \left(\hat{\mathbf{X}}_j \right)_{\alpha\alpha} \rangle_T, \\ \varepsilon_{\mathrm{P}}^{\alpha} &\equiv \varepsilon^{\alpha} - \sum_{\mathbf{q}} \hbar\omega_{\mathbf{q}} \left(\Lambda_{\mathbf{q}}^{\alpha\alpha} \right) \left(2M_{\mathbf{q}}^{\alpha\alpha} - \Lambda_{\mathbf{q}}^{\alpha\alpha} \right)^{*}. \end{aligned} \tag{4.22}$$

In the above formula, we use the fact that the operators $\hat{\mathbf{X}}_i$ have only diagonal terms. There are also induced interactions $\hat{V}_{\mathrm{P}}$ between multiple polarons, which can lead to strong correlations in the system and will be discussed in the next section. In the above calculations, we need to sum over all possible phonon momenta $\mathbf{q}$. In the thermodynamic limit of the phonon bath, we use the relation $\sum_{\mathbf{q}} \rightarrow \frac{\Omega}{(2\pi)^D} \int d\mathbf{q}$ with quantization volume Ω for the phonons, and write this explicitly in cylindrical coordinates: $\frac{\Omega}{(2\pi)^3} \int dq_{\perp} \int dq_x \left(2\pi q_{\perp} \right)$.

For the polaronic intra-band hopping J_{P}^{α}, we only need to calculate nearest-neighbor terms with $j = i \pm 1$ regardless of the specific value of i. By noting that

$$\langle \left(\hat{\mathbf{X}}_i \right)_{\alpha\alpha}^{\dagger} \left(\hat{\mathbf{X}}_j \right)_{\beta\beta} \rangle_T = e^{- \sum_{\mathbf{q}} (N_{\mathbf{q}} + 1/2) |\Lambda_{i,\mathbf{q}}^{\alpha\alpha} - \Lambda_{j,\mathbf{q}}^{\beta\beta}|^2}, \tag{4.23}$$

where $N_{\mathbf{q}} \equiv \left(\exp\left(\hbar\omega_{\mathbf{q}}/k_{\mathrm{B}}T \right) - 1 \right)^{-1}$ is the thermally averaged phonon occupation number, we define polaronic renormalization factors

$$S_T^{\alpha} \equiv \sum_{\mathbf{q}} \left(2N_{\mathbf{q}} + 1 \right) \left[1 - \cos\left(q_x \cdot d \right) \right] |\Lambda_{\mathbf{q}}^{\alpha\alpha}|^2 \tag{4.24}$$

for each band and thus $J_{\mathrm{P}}^{\alpha} = J^{\alpha} \exp\left(-S_T^{\alpha} \right)$.

We would like to note that this choice of the diagonal transformation matrices $\mathbf{\Lambda_q}$ works well when the inter-band coupling is less important than the intra-band coupling. By choosing diagonal matrices, we treat each of the two bands independently. This approach is similar as the one of the authors in Refs. [66, 84] for the single band problem, except that a variational treatment is used. On the other hand, when the off-diagonal terms in the coupling matrix $\mathbf{M_q}$ are comparable or larger than the diagonal terms, one must instead deal with the general transformed Hamiltonian in Eq. (4.20). For completeness, we describe a more general approximate technique in Appendix B, which may be useful for other types of systems. We intend to address the approximation introduced in this section more explicitly and quantitatively in some future studies.

4.4 Coherent polaron dynamics

4.4.1 Single polaron band structures

In the previous section, we derived a general form of the two-band polaron transformation and calculated the resulting coherent part of the Hamiltonian in Eq. (4.21). For the system

with a single polaron, there are only intra-band terms in the coherent Hamiltonian (4.21). The single impurity is dressed by a coherent phonon cloud in each band. The residual inter-band polaron-bath coupling will appear only in the incoherent Hamiltonian. It is easy to diagonalize the single-polaron coherent part in the momentum representation and minimize the free energy $F \equiv -k_B T \ln \sum_{\alpha,k} \exp\left(-E_k^\alpha/k_B T\right)$ for this two-band system, with the polaron dispersion

$$E_k^\alpha \equiv 2J_P^\alpha \cos\left(k \cdot d\right) + \varepsilon_P^\alpha. \tag{4.25}$$

Here k is quasi-momentum in longitudinal direction. These variational parameters, which are real numbers, can then be determined by the self-consistent equations

$$\lambda_{\mathbf{q}}^\alpha = \frac{\sum_{k,\alpha'} \exp\left(-E_k^{\alpha'}/k_B T\right)}{\sum_{k,\alpha'} \left[1 - 2J_P^\alpha f_{\mathbf{q}} \cos(k \cdot d)/\omega_{\mathbf{q}}\right] \exp\left(-E_k^{\alpha'}/k_B T\right)} \tag{4.26}$$

with $f_{\mathbf{q}} \equiv (2N_{\mathbf{q}} + 1)\left[1 - \cos\left(q_x \cdot d\right)\right]$.

We now compare the variational parameters $\lambda_{\mathbf{q}}^\alpha = \Lambda_{\mathbf{q}}^{\alpha\alpha}/M_{\mathbf{q}}^{\alpha\alpha}$ from Eq. (4.26) and polaron dressing effects for different system parameters. In Fig. 4.3(a) we show the coupling factor $\lambda_{\mathbf{q}}^\alpha$ in each band for the temperatures $k_B T = 0$, E_R, $2E_R$, where it can be seen that the variational parameters $\lambda_{\mathbf{q}}^\alpha$ are always smaller than 1. This shows the competition between intra-band dynamics and phonon dressing effects. These variational parameters are also different for the two bands, since the polaron is dressed differently in each band. We have focused on the results for momentum in the longitudinal direction with $\mathbf{q} = (q_x, 0, 0)$ and find that the low-momentum phonons are less dressed at higher temperatures $k_B T \approx E_R \gg J^\alpha$. Here E_R corresponds to a temperature of about 65nK for a ^{133}Cs impurity trapped by lasers with wavelength 1064nm. In Fig. 4.3(b, c) we also show the the factors $\lambda^\alpha \equiv \sum_{\mathbf{q}} \Lambda_{\mathbf{q}}^{\alpha\alpha} / \sum_{\mathbf{q}} M_{\mathbf{q}}^{\alpha\alpha}$. These factors λ^α thus indicate the differences between our initial guess for the variational parameters $\Lambda_{\mathbf{q}}^{\alpha\alpha} = M_{\mathbf{q}}^{\alpha\alpha}$, as is sometimes used for the transformation, and the full minimization of free energy for the variational parameters. As shown in Fig. 4.3, although these factors are different for each band and different temperatures, they always approach $\lambda^\alpha = 1$ in the limit of strong interaction. In order to reach larger values of the coupling constant, in Fig. 4.3(c) we show results with $\kappa_c = 7.6$ by assuming a condensate density $n_0 = 0.01 \times 10^{14}$cm^{-3}. In the upper plotting of Fig. 4.3(c), we notice that the parameter λ shows a polaronic transition behavior in the adiabatic regime at finite temperature, as discussed in Sec 3.3.2. While on the other hand, λ shows a smooth crossover behavior in the anti-adiabatic regime at zero temperature.

In the coherent part of the Hamiltonian Eq. (4.21), the single polaron band structure is modified by phonon dressing effects in Eq. (4.22). Effectively, the polaron is trapped in a deeper lattice, with larger mass. The effective mass of a single polaron (at $k_0 = 0$) in an optical lattice can be defined as

$$m_P^\alpha (k_0) \equiv \hbar^2 \left(\frac{\partial^2 E_k^\alpha}{\partial k^2} \mid_{k_0}\right)^{-1} = \frac{\hbar^2}{2J_P^\alpha}. \tag{4.27}$$

If the impurity-BEC coupling g_{IB} increases, the polaron effective mass will increase exponentially as $m_P^\alpha = m_0^\alpha \exp\left(S_T^\alpha\right)$, with m_0^α indicating the impurity effective mass at $\kappa = 0$. In Fig. 4.4 we compare energy spectrum E_k^α, renormalization of intra-band hopping J_P^α/J^α, polaron effective mass m_P^α/m_0^α and renormalization factor S_T^α for each band at different temperatures.

Due to phonon dressing effects, the polaronic band gap $\varepsilon_P^\Delta \equiv \varepsilon_P^1 - \varepsilon_P^0$ is also increased. This will affect the inter-band relaxation dynamics. In Fig. 4.5 we show the on-site polaron energy and band gap renormalization versus impurity-BEC coupling constant. In both
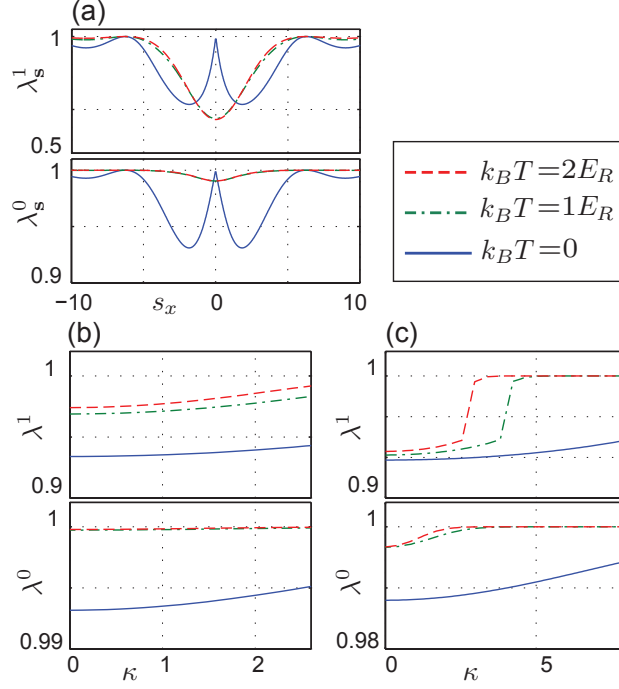
Figure 4.3: (a) Variational parameters $\lambda_{\mathbf{q}}^{\alpha}$ with $\mathbf{q} = (q_x, 0, 0)$ and $\kappa = 1$ in the higher band (upper) and lower band (lower) at different temperatures $k_{\mathrm{B}}T = 0$, E_R, $2E_R$. (b)(c) Factors $\lambda^{\alpha} \equiv \sum_{\mathbf{q}} \Lambda_{\mathbf{q}}^{\alpha\alpha} / \sum_{\mathbf{q}} M_{\mathbf{q}}^{\alpha\alpha}$ in each band at different temperatures. Maximum coupling constant $\kappa_c = 2.4$ for condensate density $n_0 = 1 \times 10^{14}\mathrm{cm}^{-3}$ (b) and $\kappa_c = 7.6$ for condensate density $n_0 = 0.01 \times 10^{14}\mathrm{cm}^{-3}$(c). Other parameters are: $m_I = 133$, $m_B = 87$, $V_I^x = 9E_R$, $V_I^{\perp} = 25V_I^x$ and $a_B = 100a_0$.

Fig. 4.4(a) and Fig. 4.5(a), without loss of any generality, we set the initial lower band on-site energy ε^0 to be zero. As shown in Fig. 4.5(b), the band gap renormalization is almost temperature independent. The quantities are only slightly affected by temperature due to different variational transformation matrices $\Lambda_{\mathbf{q}}$, as predicted in Eq. (4.22). Although the band gap is not significantly changed, this renormalization effect is important for inter-band resonance conditions, which are required for Landau-Zener tunneling to take place in a tilted lattice [107, 108].

4.4.2 Effective interactions between polarons

Here we briefly discuss interactions between polarons, by considering the additional interactions between impurities besides the original Hamiltonian (4.13), which are given by

$$\hat{V}_0 = \sum_i \sum_{\alpha\beta} U^{\alpha\beta} \hat{n}_i^{\alpha} \left(\hat{n}_i^{\beta} - \delta_{\alpha\beta} \right), \tag{4.28}$$

with the impurity on-site intra-/inter-band Hubbard-type interaction $U^{\alpha\beta}$. After the polaron transformation, the coherent Hamiltonian Eq. (4.21) for the multi-polaron system contains effective interactions $\hat{V}_{\mathrm{P}}$ with both intra- and inter-band terms. In principle, the variational parameters $\lambda_{\mathbf{q}}$ should be determined by minimizing the total free energy. This is hard for the many-impurity system. Here we assume that the polaron parameters are not modified
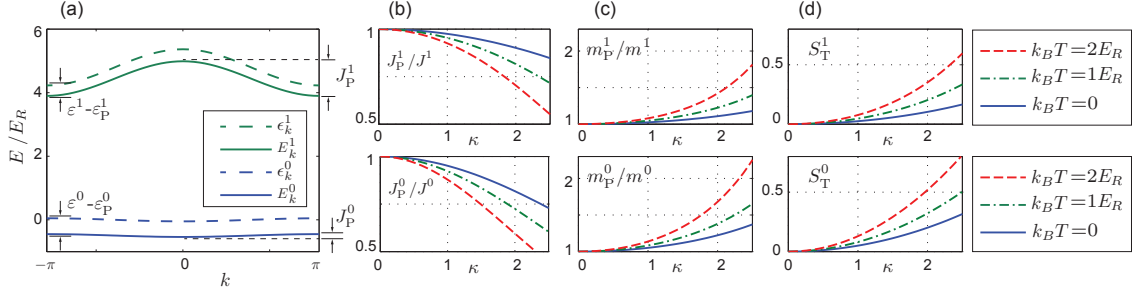
Figure 4.4: (a) Dispersion relation for the bare impurity ϵ_k^α and for the polaron E_k^α with $\kappa = \kappa_c$; (b) renormalized hopping J_P^α / J^α; (c) polaron effective mass m_P^α / m_0^α; (d) renormalization factor S_T^α for each band at different temperatures $k_B T = 0$; E_R; $2 E_R$. Other parameters are $m_I = 133$, $m_B = 87$; $V_I^x = 9 E_R$, $V_I^\perp = 25 V_I^x$; $a_B = 100 a_0$, $n_0 = 1 \times 10^{14} \text{cm}^{-3}$ and $\kappa_c = 2.4$.
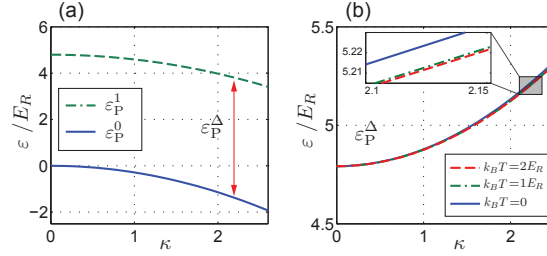
Figure 4.5: (a) On-site energy ε_P^α including polaron energy shift at zero temperature; (b) renormalized band gap $\varepsilon_P^\Delta \equiv \varepsilon_P^1 - \varepsilon_P^0$ at different temperatures $k_B T = 0$; E_R; $2 E_R$. The energy renormalization is almost temperature-independent. Other parameters are $m_I = 133$, $m_B = 87$; $V_I^x = 9 E_R$, $V_I^\perp = 25 V_I^x$; $a_B = 100 a_0$, $n_0 = 1 \times 10^{14} \text{cm}^{-3}$ and $\kappa_c = 2.4$.

from the single polaron case, due to the low density of impurities in our dilute system. The effective interaction terms $\hat{V}_P$ in Hamiltonian Eq. (4.21) take the form:

$$\hat{V}_P = \sum_i \sum_{\alpha\beta} \left(U^{\alpha\beta} + V_{ii}^{\alpha\beta} \right) \hat{n}_i^\alpha \left(\hat{n}_i^\beta - \delta_{\alpha\beta} \right)$$
$$+ \sum_{i \neq j} \sum_{\alpha\beta} \left(V_{i,j}^{\alpha\beta} \hat{n}_i^\alpha \hat{n}_j^\beta + \sum_{\beta' \neq \beta} V_{i,j}^{\alpha;\beta\beta'} \hat{n}_i^\alpha \hat{a}_j^{\beta\dagger} \hat{a}_j^{\beta'} \right) \tag{4.29}$$

with long-range bath-induced interaction terms:

$$V_{i,j}^{\alpha\beta} \equiv - \sum_{\mathbf{q}} \hbar \omega_{\mathbf{q}} \cos \left[q_x (i-j) d \right] \left(\Lambda_{\mathbf{q}}^{\alpha\alpha} \right) \left(2 M_{\mathbf{q}}^{\beta\beta} - \Lambda_{\mathbf{q}}^{\beta\beta} \right), \tag{4.30}$$

and

$$V_{i,j}^{\alpha;\beta\beta'} \equiv - \sum_{\mathbf{q}} \hbar \omega_{\mathbf{q}} \sin \left[q_x (i-j) d \right] \left(\Lambda_{\mathbf{q}}^{\alpha\alpha} \right) \left(2 i \cdot M_{\mathbf{q}}^{\beta\beta'} \right) \langle \hat{K}_{j,j}^{\beta\beta'} \rangle_T, \tag{4.31}$$

with

$$\hat{K}_{i,j}^{\alpha\beta} \equiv \left(\hat{\mathbf{X}}_i \right)_{\alpha\alpha}^\dagger \left(\hat{\mathbf{X}}_j \right)_{\beta\beta} = e^{- \sum_{\mathbf{q}} \left(\Lambda_{i,\mathbf{q}}^{\alpha\alpha} - \Lambda_{j,\mathbf{q}}^{\beta\beta} \right)^* \hat{b}_{\mathbf{q}}^\dagger - h.c.}. \tag{4.32}$$
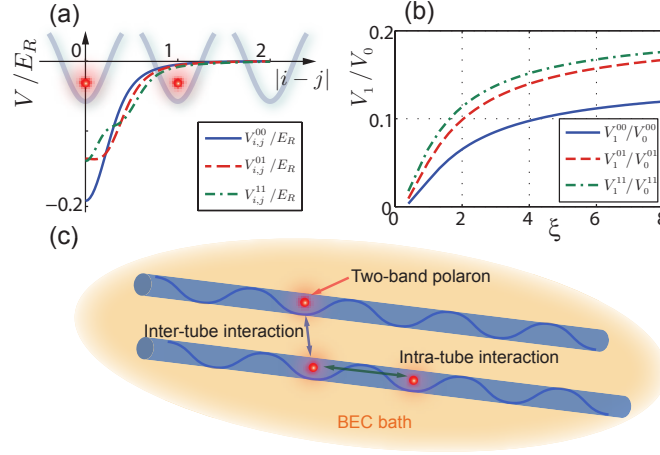
Figure 4.6: (a) Induced density-density interactions $V_{i,j}^{\alpha\beta}$ between different band at $\kappa = 1$. (b) Ratio between induced on-site and nearest neighbor interaction terms. The healing length ξ is increased by reducing the condensate density n_0 from $1 \times 10^{14} \text{cm}^{-3}$ to $0.01 \times 10^{14} \text{cm}^{-3}$ while keeping the coupling constant $\kappa = 0.3\kappa_c$. (c) Effective polaronic interactions in a multiple tube setup with two Bloch bands. Other parameters are $m_I = 133, m_B = 87$; $V_I^x = 9E_R$, $V_I^\perp = 25V_I^x$ and $a_B = 100a_0$; $n_0 = 1 \times 10^{14} \text{cm}^{-3}$.

As it was shown in [66, 109], these induced density-density interactions $V_{i,j}^{\alpha\beta}$ are always attractive with $V_{i,j}^{\alpha\beta} < 0$ and take the form of Yukawa-type interactions. The first line in Eq. (4.29) contains on-site effective interactions between polarons, also within different bands. Due to these attractive interactions $V_{i,j}^{\alpha\beta}$, the total on-site interactions $\left(U^{\alpha\beta} + V_{ii}^{\alpha\beta}\right)$ must be repulsive for bosonic impurities in order to keep the system stable. The second part in Eq. (4.29) describes the long-range part of these induced interactions. There are also density-induced inter-band transitions, which are due to the inter-band polaron-bath coupling.

In Fig. 4.6(a) we show the induced density-density interactions $V_{i,j}^{\alpha\beta}$ versus distance $|i-j|$ between polarons in different bands. Since these interactions are induced by the impurity-BEC coupling, the long-range behavior is related to the condensate healing length ξ. Here we assume we can obtain large values for ξ by tuning the boson-boson scattering length a_B to a small positive value or by keeping the condensate density n_0 small. In Fig. 4.6(b) we also show the ratio of $V_{i,j}^{\alpha\beta}$ between on-site and nearest neighbor terms versus ξ. These ratios increase with the BEC healing length, indicating a longer effective range of the interactions. The effects of these interactions, which are beyond this section, might include new ordered polaronic phases in our system with Hamiltonian Eq. (4.21). As shown in Fig. 4.6(c), if we consider that the transverse confinement is due to a very deep optical lattice instead of a single well, different 1D tubes could then interact due to the bath-induced long-range (attractive) interactions. A richer phase diagram is expected in such mixed-dimensional systems coupled to a bosonic bath [110, 111, 112, 113].

4.5   Lindblad equation and inter-band dynamics

The incoherent part of the Hamiltonian $\tilde{H}_{\text{inc}} = \tilde{H} - \langle\tilde{H}\rangle_T$ includes the residual coupling between polarons and phonon bath:

$$
\begin{aligned}
\tilde{H}_{\text{inc}} = &-\sum_{\langle i,j\rangle}\sum_{\alpha}\left(J^{\alpha}\hat{T}_{i,j}^{\alpha\alpha}\right)\hat{a}_i^{\alpha\dagger}\hat{a}_j^{\alpha} + \sum_i\sum_{\alpha}\left[\sum_{\mathbf{q}}\hbar\omega_{\mathbf{q}}\hat{b}_{\mathbf{q}}^{\dagger}\left(M_{i,\mathbf{q}}^{\alpha\alpha}-\Lambda_{i,\mathbf{q}}^{\alpha\alpha}\right)^* + h.c.\right]\hat{a}_i^{\alpha\dagger}\hat{a}_i^{\alpha} \\
&+\sum_i\sum_{\alpha\neq\beta}\left\{\sum_{\mathbf{q}}\hbar\omega_{\mathbf{q}}\left[\hat{b}_{\mathbf{q}}^{\dagger}\left(M_{i,\mathbf{q}}^{\alpha\beta}\right)^*\left(\hat{K}_{i,i}^{\alpha\beta}\right)-\left(\Lambda_{i,\mathbf{q}}^{\alpha\alpha}\right)\left(M_{i,\mathbf{q}}^{\alpha\beta}\right)^*\left(\hat{T}_{i,i}^{\alpha\beta}\right)\right]+h.c.\right\}\hat{a}_i^{\alpha\dagger}\hat{a}_i^{\beta} \\
&-\sum_{i\neq j}\sum_{\alpha}\sum_{\alpha'\neq\beta'}\left\{\sum_{\mathbf{q}}\hbar\omega_{\mathbf{q}}\left[\left(\Lambda_{i,\mathbf{q}}^{\alpha\alpha}\right)\left(M_{j,\mathbf{q}}^{\alpha'\beta'}\right)^*\left(\hat{T}_{j,j}^{\alpha'\beta'}\right)\right]+h.c.\right\}\hat{a}_i^{\alpha\dagger}\hat{a}_i^{\alpha}\hat{a}_j^{\alpha'\dagger}\hat{a}_j^{\beta'}. \qquad (4.33)
\end{aligned}
$$

with $\hat{T}_{i,j}^{\alpha\beta}\equiv\hat{K}_{i,j}^{\alpha\beta}-\langle\hat{K}_{i,j}^{\alpha\beta}\rangle_T$. There are three different coupling terms in Eq. (4.33): 1) an intra-band part due to hopping of the polaron to nearest neighbor sites and residual phonon dressing effects; 2) an inter-band part due to polaron dynamics between two bands; and 3) a mixed many-body term due to effective interactions between polarons.

The coherent part of the Hamiltonian Eq. (4.21), as calculated before, is a two-band Hubbard Hamiltonian. In order to focus on inter-band relaxation effects, we restrict our investigations to the case of a single polaron and ignore the interaction part $\hat{V}_{\text{P}}$. The incoherent Hamiltonian part Eq. (4.33) can be treated by a Lindblad master equation. After applying the Born-Markov approximation, the Lindblad equation has the form

$$
\frac{d\rho(t)}{dt} = -i\left[\langle\tilde{H}\rangle_T, \rho(t)\right] + \mathcal{L}_I\left[\rho(t)\right], \qquad (4.34)
$$

with reduced density operator $\rho(t)$ of the polaron system. All decoherence effects in the system are described by the dissipator

$$
\mathcal{L}_I\left[\rho(t)\right] = \sum_{\alpha\beta}\sum_{\alpha'\beta'}\sum_{i,j}\sum_{i',j'}\gamma_{ij;i'j'}^{\alpha\beta;\alpha'\beta'}\left(C_{i'j'}^{\alpha'\beta'}\rho C_{ij}^{\alpha\beta\dagger}-\frac{1}{2}\left\{C_{ij}^{\alpha\beta\dagger}C_{i'j'}^{\alpha'\beta'}, \rho\right\}\right), \qquad (4.35)
$$

with the quantum jump operators $C_{ij}^{\alpha\beta}\equiv\left(\hat{a}_i^{\alpha\dagger}\hat{a}_j^{\beta}\right)$. These jump operators describe the dynamics of polarons instead of bare impurities, since they include the creation and annihilation operators of the polaron. In the interaction picture with $\hat{O}(t)\equiv e^{-i\langle\tilde{H}\rangle_T t/\hbar}\hat{O}e^{i\langle\tilde{H}\rangle_T t/\hbar}$, the decoherence rates are defined as:

$$
\gamma_{ij;i'j'}^{\alpha\beta;\alpha'\beta'}\equiv 2\cdot\text{Re}\int_0^{\infty}d\tau e^{i\omega\tau}g_{ij;i'j'}^{\alpha\beta;\alpha'\beta'}(\tau), \qquad (4.36)
$$

and the correlation functions $g_{ij;i'j'}^{\alpha\beta;\alpha'\beta'}(\tau)$ are defined in Appendix C.

In this section, we focus our study on inter-band spontaneous relaxation of the polaron. Due to longitudinal trapping, the energy scales for intra- and inter-band dynamics are mismatched as $J^0; J^1 \ll \varepsilon_{\text{P}}^{\Delta}$. This allows us to use the rotating wave approximation (RWA) for inter-band dynamics and decouple it from intra-band dynamics in Eq. (C.4). We then use the short-hand notation $\gamma_{i,j}^{01}\equiv\gamma_{ii;jj}^{01;01}$ and $C_i^{01}\equiv\left(\hat{a}_i^{0\dagger}\hat{a}_i^1\right)$ to describe the polaron relaxation processes. Due to the coupling with the bath, a polaron in the upper band can spontaneously relax to the lower band with rate $\gamma_{i,j}^{01}$ and emit a phonon. In our system, the corresponding phonon energy $\hbar\omega_{\mathbf{q}}$ for inter-band dynamics is much larger than the BEC temperature

$k_{\rm B}T$. For inter-band dynamics, the phonon bath temperature is thus effectively zero. In the interaction picture, this process is described by the master equation

$$\frac{d}{dt}\hat{\rho} \equiv \sum_{i,j} \gamma_{i,j}^{01} \left(C_j^{01} \hat{\rho} C_i^{01\dagger} - \frac{1}{2} \left\{ C_i^{01\dagger} C_j^{01}, \ \hat{\rho} \right\} \right).$$

The single polaron spontaneous relaxation rate $\gamma_{i,j}^{01}$ is calculated in Eq. (C.14). It is convenient to write the master equation for relaxation processes in momentum space, as long as $\gamma_{i,j}^{01}$ only depends on the value of $(i-j)$:

$$\frac{d}{dt}\hat{\rho} \equiv \sum_q \gamma_q \left(C_q^{01} \hat{\rho} C_q^{01\dagger} - \frac{1}{2} \left\{ C_q^{01\dagger} C_q^{01}, \ \hat{\rho} \right\} \right),$$

with $C_q^{01} \equiv \sum_k \left(\hat{a}_{k-q}^{0\dagger} \hat{a}_k^1 \right)$ and $\hat{a}_k^\alpha$ is the polaron annihilation operator in momentum space [114, 115]. Here, k, $k-q$ are the quasi-momenta in the first Brillouin zone and $C_q \equiv C_{q+zG}$, $z \in \mathbb{Z}$, $G = 2\pi/d$. The relaxation rate is written as a function of longitudinal phonon momentum:

$$\gamma_q = \frac{1}{N} \sum_{(i-j)} \gamma_{i,j}^{01} e^{-iq(i-j)d}, \tag{4.37}$$

where N is lattice number. When $qd \gg 2\pi$, the sum over with $i \neq j$, involving polaron relaxation effects over different sites, decays rapidly with $|i-j|$.

The total relaxation rate γ is a sum over longitudinal phonon momenta, $\gamma \equiv \sum_q \gamma_q$ [115]. From the expression for the correlation function $g_{ij}^{01}(\tau)$ in Eq. (C.12), the polaronic inter-band relaxation contains two terms. The first term in (C.12) is a single-phonon process, with the polaron absorbing (emitting) one phonon from (to) the bath. This term is similar to Fermi's Golden Rule except a renormalization factor $\langle \hat{K}_{i,i}^{10}(\tau) \hat{K}_{j,j}^{01}(0) \rangle_T$. The second term describes a higher order process involving two phonons absorption (emission), which are absent in Fermi's Golden Rule. In the total relaxation rate, we will only consider the leading-order single-phonon process in Eqs. (C.5, C.14) and neglect higher orders. At zero temperature, only spontaneous emission of phonons is allowed with the single polaron spontaneous relaxation rate

$$\gamma^{\rm P} = 2 \cdot {\rm Re} \int_0^\infty d\tau e^{i\varepsilon_{\rm P}^\Delta \tau/\hbar} \sum_{\mathbf{q}} \omega_{\mathbf{q}}^2 |M_{\mathbf{q}}^{01}|^2 e^{-i\omega_{\mathbf{q}}\tau} \langle \hat{K}_{i,i}^{10}(\tau) \hat{K}_{i,i}^{01}(0) \rangle_T, \tag{4.38}$$

where $\langle \hat{K}_{i,i}^{10}(\tau) \hat{K}_{i,i}^{01}(0) \rangle_T$ is defined in Eq. (C.13) as a renormalization factor for inter-band relaxation dynamics.

In order to investigate how polaron effects affect the inter-band dynamics, we also derive a Lindblad equation for the original "bare" Hamiltonian in Eq. (4.13), before the Lang-Firsov transformation is applied. The corresponding single-impurity spontaneous relaxation rate in this case is

$$\gamma^0 = 2{\rm Re} \int_0^\infty d\tau e^{i\varepsilon^\Delta \tau/\hbar} \sum_{\mathbf{q}} \omega_{\mathbf{q}}^2 |M_{\mathbf{q}}^{01}|^2 e^{-i\omega_{\mathbf{q}}\tau}, \tag{4.39}$$

and reduces to Fermi's Golden Rule formula:

$$\gamma^0 = 2\pi \sum_{\mathbf{q}} \omega_{\mathbf{q}}^2 |M_{\mathbf{q}}^{01}|^2 \delta\left(\hbar\omega_{\mathbf{q}} - \varepsilon^\Delta \right). \tag{4.40}$$

Comparing Eq. (4.38) and Eq. (4.39), we observe that the renormalization of the band gap from ε^Δ to $\varepsilon_{\rm P}^\Delta$ increases the energy of the phonon which is created, due to energy conservation.

The polaron relaxation rate γ^{P} is also reduced by an additional exponential factor, since the coupling between impurity and bath is also renormalized.

Before we discuss the numerical results for the relaxation rate, let us first look at the behavior of γ_q as a function of phonon momentum in the longitudinal direction. For the bare particle relaxation rate, the prediction of Fermi's Golden rule gives

$$
\begin{aligned}
\gamma_q^0 \equiv & 2 \cdot \operatorname{Re} \int_0^\infty d\tau e^{i\varepsilon^\Delta \tau/\hbar} \sum_{q_y,q_z} \omega_{\mathbf{q}}^2 |M_{\mathbf{q}}^{01}|^2 e^{-i\omega_{\mathbf{q}}\tau} \\
\approx & 2\pi \sum_{q_\perp} \omega_{\mathbf{q}}^2 |M_{\mathbf{q}}^{01}|^2 \delta\left(\hbar\omega_{\mathbf{q}} - \varepsilon^\Delta\right).
\end{aligned}
\tag{4.41}
$$

In a deep lattice, the impurity-phonon coupling matrices $M_{\mathbf{q}}^{\alpha\beta}$ can be approximated by Gaussian functions in Eq. (4.11). Then the value of Fermi's golden rule for γ_q^0 in Eq. (4.41) is found to be

$$
\gamma_q^0 \approx \left(\frac{m_B}{\hbar^2}\right) \frac{n_0}{L_x} g_{IB}^2 \left(q^2\sigma_x^2/2\right) e^{-\left(q^2\sigma_x^2 + q_\perp^2\sigma_\perp^2\right)/2}
\tag{4.42}
$$

where L_x is the phonon quantization length (analogous to the quantization volume Ω) in the longitudinal direction. The phonon momentum in the transverse direction $q_\perp$ is fixed by energy conservation $\hbar\omega_{\mathbf{q}} = \varepsilon^\Delta \approx \hbar\omega_x$, where $|\mathbf{q}|^2 = q^2 + q_\perp^2$ and ω_x is the longitudinal oscillation frequency. An additional consequence of energy conservation is that γ_q is cut off when $\hbar\omega_{\mathbf{q}}\left(|\mathbf{q}| = q\right) = \hbar\omega_x$. The cut-off is

$$
|q\sigma_x| \approx \sqrt{2\frac{m_B}{m_I}},
\tag{4.43}
$$

which only depends on the mass ratio m_I/m_B between the impurity and the atoms in the BEC.

On the other hand, the polaron relaxation rate γ_q^{P} versus longitudinal phonon momentum needs to be calculated numerically from Eq. (4.37) and Eq. (C.14). As we discussed before for the total relaxation rate Eq. (4.38), we consider only the single-phonon emission process and calculate γ_q^{P} as:

$$
\gamma_q^{\mathrm{P}} \approx 2\operatorname{Re} \int_0^\infty d\tau e^{i\varepsilon_{\mathrm{P}}^\Delta \tau/\hbar} \sum_{q_y,q_z} \omega_{\mathbf{q}}^2 |M_{\mathbf{q}}^{01}|^2 e^{-i\omega_{\mathbf{q}}\tau} \langle \hat{K}_{i,i}^{10}(\tau) \hat{K}_{i,i}^{01}(0)\rangle_T.
\tag{4.44}
$$

Compared with Eq. (4.41), the polaron relaxation rate has a similar behavior except for an additional renormalization factor. Due to energy conservation, γ_q^{P} also has a cut-off when $\hbar\omega_{\mathbf{q}}\left(|\mathbf{q}| = q\right) = \varepsilon_{\mathrm{P}}^\Delta$. The renormalized polaron band gap $\varepsilon_{\mathrm{P}}^\Delta$, which is larger than the bare gap ε^Δ, will shift this cut-off position to higher phonon momentum. At the same time, the renormalization factor in Eq. (4.44) will reduce the value of γ_q^{P}.

In Fig. 4.7 we show the behavior of the relaxation rate γ_q^{P} and γ_q^0 as functions of longitudinal momentum $q\sigma_x$ with different impurity-BEC mass ratios. In order to compare the differences between γ_q^{P} and γ_q^0 at different coupling, we divide both γ_q^{P} and γ_q^0 by κ^2 and then normalize them. In this way, the Fermi's golden rule value γ_q^0 always stays the same for different coupling constants κ. As shown in Fig. 4.7, the dashed black lines indicate normalized γ_q^0 from Eq. (4.42), while the cut-off of $|q\sigma_x|$ in Eq. (4.43) is indicated by black lines. The total relaxation rate $\gamma^0 = \sum_q \gamma_q^0$ from Fermi's golden rule is the gray area below the black curve. At $\kappa = 0$, the polaronic relaxation rate γ_q^{P} is identical to the results from Fermi's golden rule.
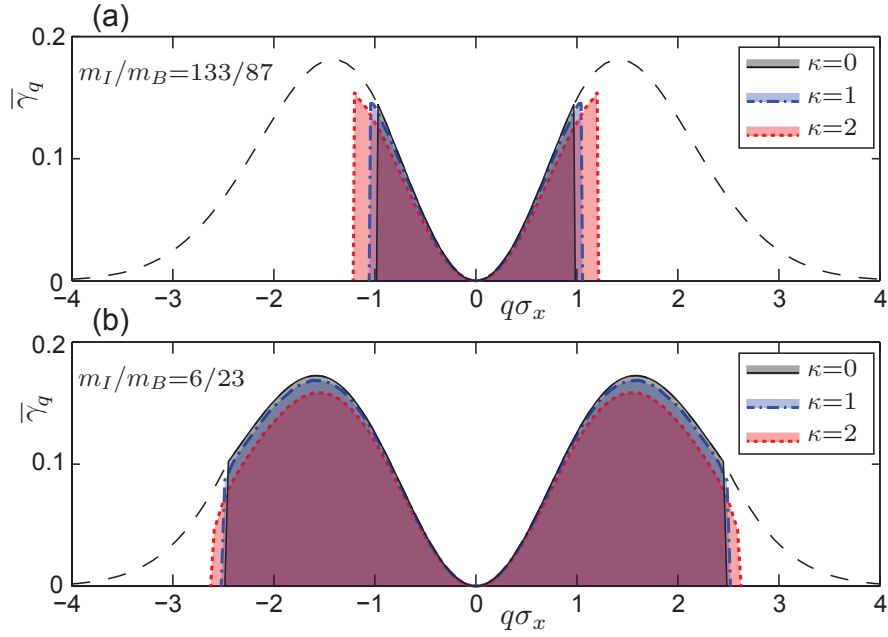
Figure 4.7: Normalized relaxation rate γ_q^{P} and γ_q^0 as functions of longitudinal momentum $q\sigma_x$ for different impurity-BEC mass ratios. The dashed black lines indicate the Fermi's Golden Rule result for γ_q^0 from Eq. (4.42) with momentum cut-off given by the solid black line ($\kappa = 0$). The blue (red) curves indicate the normalized polaron relaxation rate γ_q^{P} at coupling $\kappa = 1\,(2)$. The total relaxation rate $\gamma = \sum_q \gamma_q$ is shown as the area below the corresponding curves. (a) System with $m_I/m_B = 133/87$, i.e. ^{133}Cs impurity in ^{87}Rb BEC. (b) System with $m_I/m_B = 6/23$, i.e. ^{6}Li impurity in ^{23}Na BEC. Other parameters are $V_I^x = 9E_R$, $V_I^\perp = 25V_I^x$ and $a_B = 100a_0$, $n_0 = 1 \times 10^{14}$cm^{-3}.
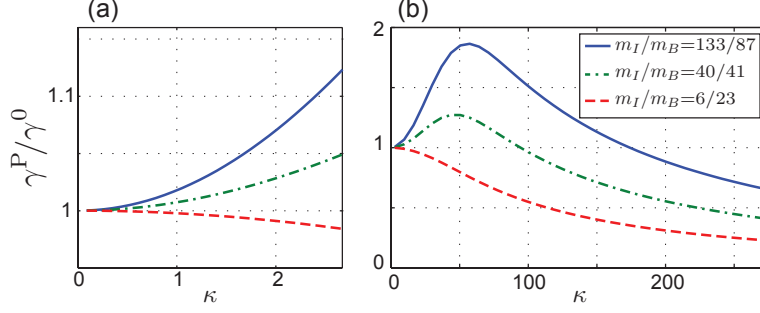
Figure 4.8: Ratio between polaron inter-band relaxation rate γ^{P} and Fermi Golden Rule result γ^0 at different impurity-BEC mass ratios. (a) In the weak coupling regime, this ratio is increased with the coupling constant κ for a heavy impurity coupled to a light BEC bath, and decreased for a light impurity coupled to a heavy BEC bath. The boson-boson scattering length here is chosen as $a_B = 100a_0$ and $\kappa_c = 2.4$. (b) In the strong coupling regime, the polaron inter-band relaxation processes for any impurity-BEC mass ratio are suppressed. This leads to an inter-band self-trapping effect. The boson-boson scattering length here is $a_B = 0.2a_0$ and $\kappa_c = 255$. We use $m_I = 133$, $m_B = 87$ for a ^{133}Cs impurity and ^{87}Rb BEC (blue line), $m_I = 40$, $m_B = 41$ for a ^{40}K impurity and ^{41}K BEC (green line), and $m_I = 6$, $m_B = 23$ for a ^{6}Li impurity and ^{23}Na BEC (red line). Other parameters are $V_I^x = 9E_R$, $V_I^\perp = 25V_I^x$ and $n_0 = 1 \times 10^{14}$cm^{-3}.

On the other hand, as the impurity-BEC coupling is increased, the polaron relaxation rate γ_q^{P} from Eq. (4.44) is renormalized by the polaron band gap $\varepsilon_{\mathrm{P}}^\Delta$ and the renormalization factor. The increased polaron band gap will involve more phonons by shifting the cut-off momentum (4.43), while the renormalization factor reduces the whole momentum range. In Fig. 4.7 we also show the polaron relaxation rate γ_q^{P} by the blue (red) curve at $\kappa = 1(2)$ and the total relaxation rate γ^{P} by the blue (red) area.

As shown in Fig. 4.7, the renormalization of the relaxation rate is different for various impurity-BEC mass ratios. For larger mass ratio (heavy impurity) as in a system of single ^{133}Cs impurity coupled to a ^{87}Rb BEC, the polaron relaxation processes will be enhanced by the shift of the cut-off momentum and increase the total rate. On the other hand, for smaller mass ratio (light impurity) such as a ^{6}Li impurity coupled to a ^{23}Na BEC, the higher momentum cut-off for $|q\sigma_x|$ is less important due to Gaussian decay of γ_q. In this case, the renormalization factor will reduce γ_q^{P} as well as the total relaxation rate γ^{P}. We can also expect that, for extremely strong impurity-BEC coupling, the total relaxation rate will be reduced due to this renormalization factor for any mass ratio.

Finally we compare the polaronic inter-band relaxation rate γ^{P} and Fermi Golden Rule results γ^0 in Fig. 4.8 as a function of coupling constant for different impurity-BEC mass ratios. As we have already seen in Fig. 4.7, the polaron formation will renormalize the inter-band relaxation rate differently, depending on the mass ratio.

We first consider the weak impurity-BEC coupling regime with small κ in Fig. 4.8(a). For a heavy impurity coupled to a light BEC bath, the inter-band relaxation process involves more phonon modes and will be enhanced. The difference in the ratio $\gamma^{\mathrm{P}}/\gamma^0$ between polaronic relaxation and the Fermi Golden Rule result increases with coupling constant κ. On the other hand, for a light impurity coupled to a heavy BEC, the impurity is dressed by heavy phonons in each band and tends to localize in the same band. Although the inter-band relaxation

process does involve more phonon modes than the Fermi Golden Rule result, this effect is highly suppressed due to Gaussian decay of γ_q with high momentum. The ratio γ^P/γ^0 will be reduced in this system. We also notice that the ratio γ^P/γ^0 is not sensitive to the longitudinal trapping potential.

On the other hand, we can access the strong coupling regime by tuning the Bose-Bose scattering a_B to a small positive value, since the allowed maximum coupling constant in Eq. (3.16) goes as $\kappa_c \propto 1/\left(n_0 a_B^3\right)^{1/4}$. For the strong impurity-BEC coupling region with large κ in Fig. 4.8(b), though the Lindblad master equation might not be accurate enough for such strong inter-band coupling, we can still obtain some qualitative insight. In each band, the polaron is tightly dressed by phonons with different coupling strengths, such that the polaron behaves as a quasi-particle with rather different properties in each band. Also, the band gap ε_P^Δ is enhanced in comparison to the bare case, so the polaron cannot hop between bands by creating or annihilating phonons. As shown in Fig. 4.8(b), we indeed obtain a suppressed inter-band relaxation process. This *inter-band self-trapping* effect is expected in a strongly coupled impurity-BEC system. In a realistic impurity-BEC system, this effect might be also observed together with the well known *self-trapping* effect due to deformation of BEC [81, 65, 116, 117, 118, 119, 99].

Chapter 5

Interacting Polarons in a BEC

5.1 Introduction

In this section I consider a many-body system with multiple impurities coupled to a BEC. The impurities are trapped by an optical lattice in two-dimensional space, while the BEC does not feel the optical lattice and can be treated as homogeneous. An impurity immersed in a dilute BEC can create a potential well in which the impurity is self-trapped even without an external trapping. The impurity distorts the density of the surrounding BEC, thereby creating the self-trapping potential minimum. With the presence of an optical lattice, this self-trapping potential will contribute to additional trapping effects for impurity.

In a system with multiple impurities, the contact interactions between impurities and bosonic atoms V_{IB} will also modify the density of the BEC and create a self-trapping potential minimum for each impurity. Effectively, there will be an interaction between two different impurities when they both are coupled to the same BEC bath. This induced interaction is long-range attractive and tunable. If the impurity-boson interaction V_{IB} is an s-wave density-density interaction, the induced interaction will always be attractive and take the form of a Yukawa-type interaction, i.e. $V_{i,j}^{\alpha\beta} \propto \exp\left(-2|i-j|/\xi\right)$, where ξ is the healing length of the BEC. Similar systems have been studied in several works for bosonic impurities [109, 92], fermionic impurities [120, 121, 122, 123] as well as classical impurities [119, 124].

In this chapter we will study how the many-body phase diagram of impurities is affected due to these interactions. The ground state is studied by a mean field approach while the long-range interactions are treated by the Hartree approximation.

5.2 Effective multi-polaron Hamiltonian

5.2.1 System and Hamiltonian

Here we consider impurities with mass m_I interacting with a BEC with mass m_B. The impurities are trapped by an optical lattice. Without loss of generality, we use a two-species model of the impurity, where α and β indicate different species, hyperfine states or Bloch bands. In a deep optical lattice, the Hamiltonian H_I is described by the Hubbard model:

$$\hat{H}_I = -\sum_{\langle i,j \rangle}\sum_{\alpha} J_{i,j}^{\alpha} \hat{c}_i^{\alpha\dagger} \hat{c}_j^{\alpha} - \sum_{i}\sum_{\alpha} \mu^{\alpha} c_i^{\alpha\dagger} c_i^{\alpha} + \sum_{i}\sum_{\alpha\beta} \frac{U_0}{2} \hat{c}_i^{\alpha\dagger} \hat{c}_i^{\beta\dagger} \hat{c}_i^{\beta} \hat{c}_i^{\alpha}, \tag{5.1}$$

with on-site interactions U_0. The lattice constant is $d = \lambda/2$ with trapping laser wavelength λ. We use the lattice constant d as the unit of length. The single impurity recoil energy is

$E_R \equiv \pi^2\hbar^2 / \left(2m_I d^2\right)$. The trapping strength in the transverse (z) direction is much stronger than in the parallel (x, y) directions with $V_I^x = V_I^y \ll V_I^\perp \equiv V_I^z$ and $V_I^x = n_\parallel E_I^r; V_I^\perp = n_\perp E_I^r$. The system is thus quasi-2D with hopping parameter J and on-site interaction U_0. For a deep lattice, J is obtained from the lowest band solution of the Mathieu equation as

$$J \approx \frac{4}{\sqrt{\pi}} E^r \left(n_\parallel\right)^{\frac{3}{4}} \exp\left(-2\sqrt{n_\parallel}\right), \tag{5.2}$$

In the harmonic approximation, the Wannier function for impurity is described as

$$W_i^\alpha \left(\mathbf{r}\right) = \left(\frac{1}{\pi\sigma^2}\right)^{\frac{1}{2}} e^{-\frac{1}{2\sigma^2}\left(x^2 + y^2\right)} \left(\frac{\sqrt{n_\perp/n_\parallel}}{\pi\sigma^2}\right)^{\frac{1}{4}} e^{-\frac{\sqrt{n_\perp/n_\parallel}}{2\sigma^2}z^2},$$

with $\sigma = \sqrt{\frac{\hbar}{m_I\omega_\parallel}} = \frac{1}{\pi n_x^{1/4}}d$. The on-site interaction is written as

$$U_I = g_{II} \int d^3\mathbf{r}|W_j\left(\mathbf{r}\right)|^4 \approx \sqrt{8\pi}\frac{a_{II}^{\text{eff}}}{d}\left(n_\parallel\right)^{\frac{1}{2}}\left(n_\perp\right)^{\frac{1}{4}} E_I^r, \tag{5.3}$$

where E^r is impurity recoil energy and V_0 is trapping amplitude. The effective scattering length between impurities is a_{II}^{eff}, which can be tuned by a Feshbach resonance or a confinement induced resonance.

On the other hand, the BEC with weak repulsive interaction g_B can be described by Bogoliubov theory and treated as a phonon bath:

$$H_B = \sum_\mathbf{q} \hbar\omega_\mathbf{q}\hat{b}_\mathbf{q}^\dagger\hat{b}_\mathbf{q}, \tag{5.4}$$

where the BEC healing length is $\xi \equiv \hbar/\sqrt{2m_B g_B n_0}$. Here we use the approach of [66, 84], where the deformation is treated as a perturbation around the BEC ground state. As shown in [125], the impurity-BEC interaction term can be written as a Fröhlich impurity-phonon coupling:

$$\hat{H}_{\text{int}} = \sum_{i,\alpha} \sum_\mathbf{q}{}' \hbar\omega_\mathbf{q}M_\mathbf{q}^\alpha e^{i\cdot\mathbf{q}\cdot\mathbf{R}_i}\left(\hat{b}_\mathbf{q} + \hat{b}_{-\mathbf{q}}^\dagger\right)\hat{c}_i^{\alpha\dagger}\hat{c}_i^\alpha + h.c. \tag{5.5}$$

with

$$M_\mathbf{q}^\alpha = g_{IB}^\alpha\sqrt{\frac{n_0\epsilon_\mathbf{q}}{\Omega\left(\hbar\omega_\mathbf{q}\right)^3}}\exp\left(-\frac{q_\rho^2\sigma^2}{4} - \frac{q_z^2\sigma_\perp^2}{4}\right),$$

and $q_\rho^2 \equiv q_x^2 + q_y^2$ and $g_{IB}^\alpha = 2\pi\hbar^2 a_{IB}^{\alpha(\text{eff})}/\mu$. Finally the effective Hamiltonian with two-species Fröhlich impurity-phonon coupling can be combined as

$$\hat{H} = H_I + H_B + H_{\text{int}}.$$

5.2.2   Variational Lang-Firsov transformation

To deal with the non-local Fröhlich impurity-phonon coupling, we use a variational canonical transformation to decouple the impurity-phonon coupling and connect between the weak and

strong coupling limit. The Lang-Firsov polaron transformation takes the form $\tilde{H} \equiv e^{\hat{S}} \hat{H} e^{-\hat{S}}$ with

$$\hat{S} \equiv \sum_{i,\alpha} \sum_{\mathbf{s}} \lambda_{\mathbf{s}}^{\alpha} M_{\mathbf{s}}^{\alpha} e^{i \cdot \mathbf{s} \cdot R_i} \left(\hat{b}_{-\mathbf{s}}^{\dagger} - \hat{b}_{\mathbf{s}} \right) \hat{n}_i^{\alpha}, \tag{5.6}$$

where $\lambda_{\mathbf{s}}^{\alpha}$ are the variational parameters for species α. The transformed Hamiltonian $\tilde{H}$ still cannot be solved analytically, but can be separated into a coherent part $\langle \tilde{H} \rangle$ and an incoherent part $\tilde{H}_{\text{Inc}} \equiv \tilde{H} - \langle \tilde{H} \rangle$. The coherent part, which is decoupled from the phonon bath, is of the form of an extended (polaronic) Hubbard model. The incoherent part describes the residual coupling between polaron quasi-particle and phonon bath. Compared with the initial "bare" impurity-phonon coupling, this incoherent part is significantly reduced by the polaron transformation. We first focus on the coherent part and neglect the incoherent terms. The variational parameters $\lambda_{\mathbf{s}}^{\alpha}$ are determined by minimizing the coherent Hamiltonian energy and approach $\lambda_{\mathbf{s}}^{\alpha} = 1$ in the strong coupling limit. Finally, the residual incoherent part can be included by a perturbative approach such as the Lindblad master equation.

5.2.3   Coherent polaronic Hamiltonian

The coherent part $\langle \tilde{H} \rangle$ of the Hamiltonian is an extended polaronic Hubbard model

$$\hat{H}_{\text{P}} \equiv \langle \tilde{H} \rangle = -\sum_{\langle i,j \rangle} \sum_{\alpha} J_{\text{P}}^{\alpha} \hat{c}_i^{\alpha \dagger} \hat{c}_j^{\alpha} - \sum_i \sum_{\alpha} \mu_P^{\alpha} \hat{n}_i^{\alpha} + \sum_{\mathbf{q}} \omega_{\mathbf{q}} \hat{b}_{\mathbf{q}}^{\dagger} \hat{b}_{\mathbf{q}}$$
$$+ \sum_{i \neq j} \sum_{\alpha \beta} \frac{V_{i,j}^{\alpha \beta}}{2} \hat{n}_i^{\alpha} \hat{n}_j^{\beta} + \sum_i \sum_{\alpha} \left(\frac{U_0}{2} \hat{n}_i^{\alpha} \hat{n}_i^{\bar{\alpha}} + \frac{V_i^{\alpha \bar{\alpha}}}{2} \hat{n}_i^{\alpha} \hat{n}_j^{\bar{\alpha}} \right) \tag{5.7}$$

with renormalized polaronic hopping and on-site energy terms including the polaron energy shift:

$$J_{\text{P}}^{\alpha} \equiv J^{\alpha} \exp \left(-S_T^{\alpha} \right), \tag{5.8}$$

$$S_T^{\alpha} \equiv \sum_{\mathbf{q}}' \left(2N_{\mathbf{q}} + 1 \right) \left[1 - \cos \left(\mathbf{q} \cdot \mathbf{d} \right) \right] |\lambda_{\mathbf{q}}^{\alpha} M_{\mathbf{q}}^{\alpha}|^2 \tag{5.9}$$

$$\mu_{\text{P}}^{\alpha} \equiv \mu^{\alpha} + \sum_{\mathbf{q}}' \omega_{\mathbf{q}} \lambda_{\mathbf{s}}^{\alpha} \left(2 - \lambda_{\mathbf{q}}^{\alpha} \right) |M_{\mathbf{q}}^{\alpha}|^2. \tag{5.10}$$

For nearest-neighbor hopping, $\mathbf{d}$ can be $\hat{e}_x$ or $\hat{e}_y$, which gives the same results. There are also induced interactions $V_{i,j}^{\alpha \beta}$ between polarons:

$$V_{i,j}^{\alpha \beta} \equiv -\sum_{\mathbf{q}}' \hbar \omega_{\mathbf{q}} \cos \left[\mathbf{q} \cdot \left(\mathbf{R}_i - \mathbf{R}_j \right) \right] \left[M_{\mathbf{q}}^{\alpha} M_{\mathbf{q}}^{\beta} \left(\lambda_{\mathbf{q}}^{\alpha} \right) \left(2 - \lambda_{\mathbf{q}}^{\beta} \right) + h.c. \right]. \tag{5.11}$$

From the geometry of the system, we expect that the variational parameters $\lambda_{\mathbf{q}}^{\alpha}$ should depend only on q_{ρ} and q_z.

In this calculation, we need to sum over all possible phonon momenta $\mathbf{s}$. In the thermodynamic limit of the phonon bath, we use the relation $\sum_{\mathbf{s}} \to \frac{\Omega}{(2\pi)^D} \int d\mathbf{s}$ with quantization volume Ω for the phonons, and write this explicitly in cylindrical coordinates in our 2D system:

$$\sum_{\mathbf{s}} \to \frac{\Omega}{(2\pi)^3} \int ds_{\rho} \int ds_z \int d\theta s_{\rho}.$$

By noting that only the part $\cos\left(\mathbf{s}\cdot\mathbf{r}\right) = \cos\left(s_\rho\left(\sin\theta r_x + \cos\theta r_y\right)\right)$ is θ dependent, we can calculate these terms $\sum_{\mathbf{s}} f\left(\mathbf{s}\right)\cos\left(\mathbf{s}\cdot\mathbf{r}\right)$ as

$$
\frac{\Omega}{(2\pi)^3}\int_0^\infty ds_\rho \int_{-\infty}^\infty ds_z \int_0^{2\pi} d\theta s_\rho f\left(\mathbf{s}\right)\cos\left(s_\rho\cdot\left(\sin\theta r_x + \cos\theta r_y\right)\right)
$$

$$
= \frac{\Omega}{(2\pi)^3}\int_0^\infty ds_\rho \int_{-\infty}^\infty ds_z \cdot s_\rho f\left(\mathbf{s}\right)2\pi\mathcal{J}_0\left(s_\rho|\mathbf{r}|\right), \tag{5.12}
$$

where $\mathcal{J}_0\left(x\right)$ is the Bessel function of first kind $\mathcal{J}_n\left(x\right)$ with $n=0$.

In principle, the variational parameters $\lambda_{\mathbf{s}}^\alpha$ should be determined by minimizing the whole coherent Hamiltonian energy. In the dilute limit, we use the parameters for single polaron results, thus minimizing the free energy $F^\alpha \equiv -k_{\mathrm{B}}T\ln\sum_{\mathbf{k}}\exp\left(-E_{\mathbf{k}}^\alpha/k_{\mathrm{B}}T\right)$ for this two-species system, with the polaron dispersion:

$$
E_{\mathbf{k}}^\alpha \equiv 2J_{\mathrm{P}}^\alpha\left[\cos\left(k_x d\right) + \cos\left(k_y d\right)\right] + \varepsilon_{\mathrm{P}}^\alpha, \tag{5.13}
$$

The minimization gives us

$$
\sum_{\mathbf{k}} e^{-\beta E_{\mathbf{k}}^\alpha}\left(\frac{\partial}{\partial\lambda_{\mathbf{s}}^\alpha}E_{\mathbf{k}}^\alpha\right) = 0,
$$

where $\mathbf{k} = (k_x, k_y)$ is quasi-momentum in parallel direction. These variational parameters, which are real numbers, can then be determined by the self-consistent equations:

$$
\lambda_{\mathbf{s}}^\alpha = \frac{\sum_{\mathbf{k}}\exp\left(-E_{\mathbf{k}}^\alpha/k_{\mathrm{B}}T\right)}{\sum_{\mathbf{k}}\left[1 - 2J_{\mathrm{P}}^\alpha f_{\mathbf{s}}\left[\cos\left(k_x d\right) + \cos\left(k_y d\right)\right]/\omega_{\mathbf{s}}\right]\exp\left(-E_{\mathbf{k}}^\alpha/k_{\mathrm{B}}T\right)}, \tag{5.14}
$$

with $f_{\mathbf{s}} \equiv (2N_{\mathbf{s}} + 1)\left[1 - \cos\left(\mathbf{s}\cdot\mathbf{d}\right)\right]$ and $\mathbf{d}$ can be $d\cdot\hat{e}_x$ or $d\cdot\hat{e}_y$. The parameters converge to 1 for strong coupling limit when $J_{\mathrm{P}}^\alpha/\left(\varepsilon^\alpha - \varepsilon_{\mathrm{P}}^\alpha\right) \ll 1$. Since $\lambda_{\mathbf{s}}^\alpha$ depends on (s_ρ, s_z) only, the above equation will be equal to

$$
\lambda^\alpha\left(s_\rho, s_z\right) = 1/\left\{1 - 2J_{\mathrm{P}}^\alpha F\left(s_\rho, s_z\right)\frac{\sum_{\mathbf{k}}\left[\cos\left(k_x d\right) + \cos\left(k_y d\right)\right]\exp\left(-E_{\mathbf{k}}^\alpha/k_{\mathrm{B}}T\right)}{\sum_{\mathbf{k}}\exp\left(-E_{\mathbf{k}}^\alpha/k_{\mathrm{B}}T\right)}\right\}, \tag{5.15}
$$

with

$$
F\left(s_\rho, s_z\right) = \sum_\theta (2N_{\mathbf{s}} + 1)\left[1 - \cos\left(s_\rho\left(\sin\theta\hat{e}_x d\right)\right)\right] = (2N_{\mathbf{s}} + 1)\left[1 - \mathcal{J}_0\left(s_\rho d\right)\right]. \tag{5.16}
$$

5.3 Effective interactions between polarons

5.3.1 Induced interactions

After the polaron transformation, the induced interaction takes the form

$$
V_{i,j}^{\alpha\beta} = \sum_{\mathbf{q}}' \frac{1}{2}V_{\mathbf{q}}^{\alpha\beta}\left(\left(\lambda_{\mathbf{q}}^\alpha\right)\left(2 - \lambda_{\mathbf{q}}^\beta\right) + h.c.\right)\cos\left[\mathbf{q}\cdot\left(\mathbf{R}_i - \mathbf{R}_j\right)\right], \tag{5.17}
$$

with

$$
g_{IB}^\alpha\sqrt{\frac{n_0\epsilon_{\mathbf{q}}}{\Omega\left(\hbar\omega_{\mathbf{q}}\right)^3}}\exp\left(-\frac{q_\rho^2\sigma^2}{4} - \frac{q_z^2\sigma_\perp^2}{4}\right),
$$
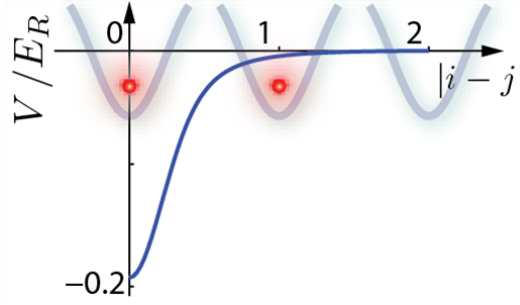
Figure 5.1: Induced interaction between polarons. At large distances, the induced interaction takes the form of a Yukawa potential.

and

$$V_{\mathbf{q}}^{\alpha\beta} \equiv -2\hbar\omega_{\mathbf{q}}M_{\mathbf{q}}^{\alpha}M_{\mathbf{q}}^{\beta} = \frac{g_{IB}^{\alpha}g_{IB}^{\beta}}{g_{BB}\Omega}\frac{1}{1+\xi^2\mathbf{q}^2/2}\exp\left(-\frac{q_{\rho}^2\sigma^2}{2}-\frac{q_z^2\sigma_{\perp}^2}{2}\right). \qquad (5.18)$$

In case of a deep lattice $n_{\perp} \gg n_{\parallel} \gg 1$, the impurities are highly localized. The induced interaction is shown in Fig. 5.1. At large distances, the induced interaction takes the form of a Yukawa potential

$$V_{i,j}^{\alpha\beta} = -\left(\frac{g_{IB}^{\alpha}g_{IB}^{\beta}}{g_{BB}}\right)\frac{1}{2\pi\xi^2}\frac{1}{|r|}e^{-\sqrt{2}|r|/\xi}, \qquad (3D) \qquad (5.19)$$

with $|r| \equiv |\mathbf{R}_i - \mathbf{R}_j|$.

On the other hand, in case of a BEC in low-dimensions, the long range behavior of induced interaction will be

$$V_{i,j}^{\alpha\beta} = -\left(\frac{g_{IB}^{\alpha}g_{IB}^{\beta}}{g_{BB}}\right)\frac{1}{\sqrt{2}\xi}e^{-\sqrt{2}|r|/\xi}; \qquad (1D) \qquad (5.20)$$

$$V_{i,j}^{\alpha\beta} = -\left(\frac{g_{IB}^{\alpha}g_{IB}^{\beta}}{g_{BB}}\right)\frac{1}{\pi\xi^2}\mathrm{K}_0\left(\frac{\sqrt{2}|r|}{\xi}\right). \qquad (2D) \qquad (5.21)$$

The total interaction is the combination of original and induced interactions as

$$\hat{H}_V = \sum_i\sum_{\alpha}\left(\frac{U_0}{2}+\frac{V_{i,i}^{\alpha\bar{\alpha}}}{2}\right)\hat{n}_i^{\alpha}\hat{n}_i^{\bar{\alpha}} + \sum_{i\neq j}\sum_{\alpha,\beta}\frac{V_{i,j}^{\alpha\beta}}{2}\hat{n}_i^{\alpha}\hat{n}_j^{\beta}. \qquad (5.22)$$

The on-site energy shift is $\mu^{\alpha} - \mu_{\mathrm{P}}^{\alpha} = V_{i,i}^{\alpha\alpha}/2$. The interaction strength depends on the scattering length between impurity and bosonic bath as $V_{i,j}^{\alpha\beta} \propto -a_{IB}^{\alpha}a_{IB}^{\beta}$. The index $\bar{\alpha}$ indicates $\bar{\alpha} \equiv -\alpha$. The interaction range depends on the bosonic healing length ξ. Under suitable conditions the interaction U_0 and V_{ij} can be of the same order.

It is interesting to have two-species impurities, where one species has attractive impurity-BEC interaction and the other has repulsive interaction, i.e., $a_{IB}^{\alpha} = -a_{IB}^{\beta}$. Thus the induced interactions $V_{i,j}^{\alpha\beta}$ will be positive. These two-species impurities will be automatically repulsive to each other at large distances, even in the absence of on-site repulsive interaction. This may support possible exotic new phases or phase separation between two-species fermions. These inter-species polaronic interactions can be tuned by Feshbach resonance.

5.4   Mean field analysis

The effective polaron Hamiltonian (5.7) can be reexpressed in momentum space as

$$\hat{H}_{\mathrm{P}} = \sum_{\mathbf{k}\alpha} (\epsilon_{\mathbf{k}}^{\alpha} - \mu_P^{\alpha})\, \hat{c}_{\mathbf{k}}^{\alpha\dagger} \hat{c}_{\mathbf{k}}^{\alpha} + \frac{1}{2N} \sum_{\mathbf{k}_1, \mathbf{k}_2, \mathbf{p}} \sum_{\alpha\beta} V_{\mathrm{eff}}^{\alpha\beta}\,(\mathbf{k}_1 - \mathbf{k}_2) \cdot \hat{c}_{\mathbf{k}_1}^{\alpha\dagger} \hat{c}_{-\mathbf{k}_1+\mathbf{p}}^{\beta\dagger} \hat{c}_{-\mathbf{k}_2+\mathbf{p}}^{\beta} \hat{c}_{\mathbf{k}_2}^{\alpha}, \qquad (5.23)$$

where $\epsilon_{\mathbf{k}}^{\alpha} = 2J_{\mathrm{P}}^{\alpha} \left(\cos k_x d + \cos k_y d\right)$ and N is the system size.

5.4.1   Superfluid order

5.4.1.1   Mean field Hamiltonian

Two polarons can pair with each other and form superfluid states [120, 126]. The mean field (MF) Hamiltonian can be written as

$$\hat{H}_{\mathrm{SF}} = \sum_{\mathbf{k},\alpha} (\epsilon_{\mathbf{k}}^{\alpha} - \mu_P^{\alpha})\, \hat{c}_{\mathbf{k}}^{\alpha\dagger} \hat{c}_{\mathbf{k}}^{\alpha} + \sum_{\mathbf{k}} \sum_{\alpha\beta} \left(\frac{\Delta_{\mathbf{k}}^{\alpha\beta}}{2} \hat{c}_{-\mathbf{k}}^{\beta} \hat{c}_{\mathbf{k}}^{\alpha} + \frac{\Delta_{\mathbf{k}}^{\alpha\beta*}}{2} \hat{c}_{\mathbf{k}}^{\alpha\dagger} \hat{c}_{-\mathbf{k}}^{\beta\dagger} \right)$$

$$- \sum_{\mathbf{k}} \sum_{\alpha\beta} \frac{\Delta_{\mathbf{k}}^{\alpha\beta}}{2} g_{\mathbf{k}}^{\alpha\beta*}, \qquad (5.24)$$

with the superfluid (SF) order parameters

$$\Delta_{\mathbf{k},(\mathbf{p})}^{\alpha\beta} \equiv \frac{1}{N} \sum_{\mathbf{k}',\mathbf{p}} V_{\mathrm{eff}}^{\alpha\beta}\,(\mathbf{k} - \mathbf{k}') \langle \hat{c}_{\mathbf{k}'}^{\alpha\dagger} \hat{c}_{-\mathbf{k}'+\mathbf{p}}^{\beta\dagger} \rangle, \qquad (5.25)$$

and

$$g_{\mathbf{k},(\mathbf{p})}^{\alpha\beta} \equiv \langle \hat{c}_{\mathbf{k}'}^{\alpha\dagger} \hat{c}_{-\mathbf{k}'+\mathbf{p}}^{\beta\dagger} \rangle.$$

At the moment we only consider paring with zero total momentum $\mathbf{p} = 0$. The above MF Hamiltonian can be diagonalized by a Bogoliubov transformation for fermions [120, 127]:

$$\hat{H}_{\mathrm{SF}} = \sum_{\mathbf{k},\beta} \frac{1}{2} \left(\epsilon_{\mathbf{k}}^{\beta} - \mu_P^{\beta} \right)$$

$$+ \frac{1}{2} \sum_{\mathbf{k}} \sum_{\alpha\beta} \left(\begin{array}{cc} \hat{c}_{\mathbf{k}}^{\alpha\dagger} & \hat{c}_{-\mathbf{k}}^{\beta} \end{array} \right) \left(\begin{array}{cc} (\epsilon_{\mathbf{k}}^{\alpha} - \mu_P^{\alpha}) & \Delta_{\mathbf{k}}^{\alpha\beta*} \\ \Delta_{\mathbf{k}}^{\alpha\beta} & -\left(\epsilon_{\mathbf{k}}^{\beta} - \mu_P^{\beta} \right) \end{array} \right) \left(\begin{array}{c} \hat{c}_{\mathbf{k}}^{\alpha} \\ \hat{c}_{-\mathbf{k}}^{\beta\dagger} \end{array} \right) - \sum_{\mathbf{k}} \sum_{\alpha\beta} \frac{\Delta_{\mathbf{k}}^{\alpha\beta}}{2} g_{\mathbf{k}}^{\alpha\beta*}.$$

$$(5.26)$$

In the simple case with $|g_{IB}^{\alpha}| = |g_{IB}^{\beta}|$, the polaronic renormalization prefactors are the same and $\epsilon_{\mathbf{k}} \equiv \epsilon_{\mathbf{k}}^{\alpha} = \epsilon_{\mathbf{k}}^{\beta}$; $\mu_P \equiv \mu_P^{\alpha} = \mu_P^{\beta}$. The transformation can be done by

$$\left(\begin{array}{c} \hat{c}_{\mathbf{k}}^{\alpha} \\ \hat{c}_{-\mathbf{k}}^{\beta\dagger} \end{array} \right) = \left(\begin{array}{cc} u_{\mathbf{k}} & v_{\mathbf{k}} \\ v_{-\mathbf{k}} & -u_{-\mathbf{k}} \end{array} \right) \left(\begin{array}{c} \hat{d}_{\mathbf{k}}^{\alpha} \\ \hat{d}_{-\mathbf{k}}^{\beta\dagger} \end{array} \right) = \left(\begin{array}{c} u_{\mathbf{k}} \hat{d}_{\mathbf{k}}^{\alpha} + v_{\mathbf{k}} \hat{d}_{-\mathbf{k}}^{\beta\dagger} \\ v_{-\mathbf{k}} \hat{d}_{\mathbf{k}}^{\alpha} - u_{-\mathbf{k}} \hat{d}_{-\mathbf{k}}^{\beta\dagger} \end{array} \right), \qquad (5.27)$$

with

$$u_{\mathbf{k}}^2 = \frac{1}{2} \left(1 + \frac{\epsilon_{\mathbf{k}} - \mu_P}{E_{\mathbf{k}}} \right); \qquad (5.28)$$

$$v_{\mathbf{k}}^2 = \frac{1}{2} \left(1 - \frac{\epsilon_{\mathbf{k}} - \mu_P}{E_{\mathbf{k}}} \right). \qquad (5.29)$$

The diagonalized Hamiltonian will be:

$$
\hat{H}_{\mathrm{SF}} = \sum_{\mathbf{k}} (\epsilon_{\mathbf{k}} - \mu_P) + \frac{1}{2} \sum_{\mathbf{k}} \sum_{\alpha\beta} \left(\begin{array}{cc} \hat{d}_{\mathbf{k}}^{\alpha\dagger} & \hat{d}_{-\mathbf{k}}^{\beta} \end{array} \right) \left(\begin{array}{cc} E_{\mathbf{k}} & 0 \\ 0 & -E_{\mathbf{k}} \end{array} \right) \left(\begin{array}{c} \hat{d}_{\mathbf{k}}^{\alpha} \\ \hat{d}_{-\mathbf{k}}^{\beta\dagger} \end{array} \right)
$$

$$
+ \sum_{\mathbf{k}} \sum_{\alpha\beta} \frac{|\Delta_{\mathbf{k}}^{\alpha\beta}|^2}{4E_{\mathbf{k}}} \tanh \left(\frac{E_{\mathbf{k}'}}{2T} \right)
$$

$$
= (E_{\mathrm{SF}} - \mu n_f N) + \sum_{\mathbf{k},\alpha} E_{\mathbf{k}} \hat{d}_{\mathbf{k}}^{\alpha\dagger} \hat{d}_{\mathbf{k}}^{\alpha}, \tag{5.30}
$$

with the MF ground state energy E_{SF} for the superfluid phase:

$$
E_{\mathrm{SF}} \equiv \sum_{\mathbf{k}} (\epsilon_{\mathbf{k}} - \mu_P - E_{\mathbf{k}}) + \mu n_f N + \sum_{\mathbf{k}} \sum_{\alpha\beta} \frac{|\Delta_{\mathbf{k}}^{\alpha\beta}|^2}{4E_{\mathbf{k}}}, \tag{5.31}
$$

and single particle excitation energy

$$
E_{\mathbf{k}} = \sqrt{(\epsilon_{\mathbf{k}} - \mu_P)^2 + |\Delta_{\mathbf{k}}^{\alpha\beta}|^2}. \tag{5.32}
$$

The gap equation is given by

$$
\Delta_{\mathbf{k}}^{\alpha\beta} = -\frac{1}{N} \sum_{\mathbf{k}'} V_{\mathrm{eff}}^{\alpha\beta} \left(\mathbf{k} - \mathbf{k}' \right) \frac{\Delta_{\mathbf{k}'}^{\alpha\beta}}{2E_{\mathbf{k}'}} \tanh \left(\frac{E_{\mathbf{k}'}}{2T} \right), \tag{5.33}
$$

with total density

$$
n_f = \frac{1}{N} \sum_{\mathbf{k}',\alpha} \langle \hat{c}_{\mathbf{k}'}^{\alpha\dagger} \hat{c}_{\mathbf{k}'}^{\alpha} \rangle = 1 - \frac{1}{N} \sum_{\mathbf{k}'} \frac{\epsilon_{\mathbf{k}'} - \mu_P}{E_{\mathbf{k}'}} \tanh \left(\frac{E_{\mathbf{k}'}}{2T} \right). \tag{5.34}
$$

5.4.1.2   Order parameters

The above order parameters need to be calculated numerically for all momenta $\mathbf{k}$. These different parameters $\Delta_{\mathbf{k}}^{\alpha\beta}$ can be simplified by system symmetries. Noting that the induced interaction decays exponentially, we only consider $V_{\mathrm{eff}}^{\alpha\beta} \left(\mathbf{k} - \mathbf{k}' \right)$ with onsite and nearest-neighbor terms. Thus in momentum space,

$$
V_{\mathrm{eff}}^{\alpha\beta} \left(\mathbf{k} - \mathbf{k}' \right) = \left(U_0 + V_0^{\alpha\beta} \right) \delta_{\alpha,-\beta} + \frac{V_1^{\alpha\beta}}{4} \left(\gamma_{\mathbf{k}} \gamma_{\mathbf{k}'} + \eta_{\mathbf{k}} \eta_{\mathbf{k}'} \right)
$$

$$
+ 2V_1^{\alpha\beta} \left(\sin k_x \sin k_x' + \sin k_y \sin k_y' \right), \tag{5.35}
$$

with lattice size $d = 1$, $\gamma_{\mathbf{k}} \equiv 2 \left(\cos k_x + \cos k_y \right)$ and $\eta_{\mathbf{k}} \equiv 2 \left(\cos k_x - \cos k_y \right)$. From [128, 120], it is straightforward to use an ansatz for the order parameters as

$$
\Delta_{\mathbf{k}}^{\alpha\beta} = \delta_{\alpha,-\beta} \left[\Delta_{s0} + \Delta_{s1} \gamma_{\mathbf{k}} + \Delta_d \eta_{\mathbf{k}} \right]
$$

$$
+ \delta_{\alpha,\beta} \left[\Delta_{px} \sin k_x + \Delta_{py} \sin k_y \right], \tag{5.36}
$$

where Δ_{s0} and Δ_{s1} are the onsite and extended $s-$wave superfluid phase, while $\Delta_{p(d)}$ is the $p - (d-)$ wave superfluid phase.

The singlet superfluid phase contains $s-$wave and $d-$wave pairing with order parameters $\Delta_{\mathbf{k}}^{\alpha\bar{\alpha}} = \Delta_{s0} + \Delta_{s1}\gamma_{\mathbf{k}} + \Delta_d\eta_{\mathbf{k}}$. The gap and density equations are reduced to

$$\Delta_{s0} = -\frac{1}{N}\left(U_0 + V_0^{\alpha\bar{\alpha}}\right)\sum_{\mathbf{k}'}\frac{(\Delta_{s0} + \Delta_{s1}\gamma_{\mathbf{k}'} + \Delta_d\eta_{\mathbf{k}'})}{2E_{\mathbf{k}'}}\tanh\left(\frac{E_{\mathbf{k}'}}{2T}\right); \qquad (5.37)$$

$$\Delta_{s1} = -\frac{1}{N}\left(V_1^{\alpha\bar{\alpha}}/4\right)\sum_{\mathbf{k}'}\frac{\gamma_{\mathbf{k}'}(\Delta_{s0} + \Delta_{s1}\gamma_{\mathbf{k}'} + \Delta_d\eta_{\mathbf{k}'})}{2E_{\mathbf{k}'}}\tanh\left(\frac{E_{\mathbf{k}'}}{2T}\right); \qquad (5.38)$$

$$\Delta_d = -\frac{1}{N}\left(V_1^{\alpha\bar{\alpha}}/4\right)\sum_{\mathbf{k}'}\frac{\eta_{\mathbf{k}'}(\Delta_{s0} + \Delta_{s1}\gamma_{\mathbf{k}'} + \Delta_d\eta_{\mathbf{k}'})}{2E_{\mathbf{k}'}}\tanh\left(\frac{E_{\mathbf{k}'}}{2T}\right); \qquad (5.39)$$

$$n_f = 1 - \frac{1}{N}\sum_{\mathbf{k}'}\frac{\epsilon_{\mathbf{k}'} - \mu_P}{E_{\mathbf{k}'}}\tanh\left(\frac{E_{\mathbf{k}'}}{2T}\right). \qquad (5.40)$$

with

$$E_{\mathbf{k}} = \sqrt{(\epsilon_{\mathbf{k}} - \mu_P)^2 + |\Delta_{s0} + \Delta_{s1}\gamma_{\mathbf{k}'} + \Delta_d\eta_{\mathbf{k}'}|^2}. \qquad (5.41)$$

On the other hand, the triplet superfluid phase contains $p-$wave pairing with order parameters $\Delta_{\mathbf{k}}^{\alpha\alpha} = \Delta_{px}\sin k_x + \Delta_{py}\sin k_y$ in x and y directions. The gap and density equations are reduced to

$$1 = -\frac{1}{N}\left(2V_1^{\alpha\alpha}\right)\sum_{\mathbf{k}'}\frac{\sin^2 k_x'}{2E_{\mathbf{k}'}}\tanh\left(\frac{E_{\mathbf{k}'}}{2T}\right); \qquad (5.42)$$

$$1 = -\frac{1}{N}\left(2V_1^{\alpha\alpha}\right)\sum_{\mathbf{k}'}\frac{\sin^2 k_y'}{2E_{\mathbf{k}'}}\tanh\left(\frac{E_{\mathbf{k}'}}{2T}\right); \qquad (5.43)$$

$$n_f = 1 - \frac{1}{N}\sum_{\mathbf{k}'}\frac{\epsilon_{\mathbf{k}'} - \mu_P}{E_{\mathbf{k}'}}\tanh\left(\frac{E_{\mathbf{k}'}}{2T}\right). \qquad (5.44)$$

with

$$E_{\mathbf{k}} = \sqrt{(\epsilon_{\mathbf{k}} - \mu_P)^2 + |\Delta_{px}\sin k_x + \Delta_{py}\sin k_y|^2}. \qquad (5.45)$$

5.4.1.3   Transition temperature

The transition temperature T_c can be solved numerically from the gap and density equations by setting $\Delta_{\mathbf{k}}^{\alpha\beta} \to 0$ and

$$\Delta_{\mathbf{k}}^{\alpha\beta} = -\frac{1}{N}\sum_{\mathbf{k}'}V_{\text{eff}}^{\alpha\beta}\left(\mathbf{k} - \mathbf{k}'\right)\frac{\Delta_{\mathbf{k}'}^{\alpha\beta}}{2E_{\mathbf{k}'}}\tanh\left(\frac{E_{\mathbf{k}'}}{2T}\right); \qquad (5.46)$$

$$n_f = 1 - \frac{1}{N}\sum_{\mathbf{k}'}\frac{\epsilon_{\mathbf{k}'} - \mu_P}{E_{\mathbf{k}'}}\tanh\left(\frac{E_{\mathbf{k}'}}{2T}\right). \qquad (5.47)$$

5.4.2   Charge density wave and spin density wave

At half-filling, the Fermi surface exhibits perfect nesting, when translated by the nesting wave vector $\mathbf{Q} = (\pi, \pi)$ in momentum space [129]. However, away from half-filling, the superfluid phases for the commensurate wave vector may be less favorable than density wave phases at incommensurate wave-vectors [120]. In the simple case with $|g_{IB}^{\alpha}| = |g_{IB}^{\beta}|$, the induced interactions have the same amplitude as $|V_{\text{eff}}^{\alpha\alpha}| = |V_{\text{eff}}^{\beta\beta}| = |V_{\text{eff}}^{\alpha\bar{\alpha}}|$. The Hartree mean field

Hamiltonian including both charge density wave (CDW) and spin density wave (SDW) orders is written as

$$
\begin{aligned}
\hat{H}_{\mathrm{DW}} = \sum_{\mathbf{k},\alpha} & \left[\epsilon_{\mathbf{k}} - \mu_P + n_f \left(V_{\mathrm{eff}(0)}^{\alpha\alpha} + V_{\mathrm{eff}(0)}^{\alpha\bar{\alpha}} \right) \right] \hat{c}_{\mathbf{k}}^{\alpha\dagger} \hat{c}_{\mathbf{k}}^{\alpha} \\
& + 2 n_{\mathbf{Q}} \left(V_{\mathrm{eff}(\mathbf{Q})}^{\alpha\alpha} + V_{\mathrm{eff}(\mathbf{Q})}^{\alpha\bar{\alpha}} \right) \sum_{\mathbf{k},\alpha} \hat{c}_{\mathbf{k}}^{\alpha\dagger} \hat{c}_{\mathbf{k}+\mathbf{Q}}^{\alpha} + 2 m_{\mathbf{Q}} \left(V_{\mathrm{eff}(\mathbf{Q})}^{\alpha\alpha} - V_{\mathrm{eff}(\mathbf{Q})}^{\alpha\bar{\alpha}} \right) \sum_{\mathbf{k},\alpha} \alpha \hat{c}_{\mathbf{k}}^{\alpha\dagger} \hat{c}_{\mathbf{k}+\mathbf{Q}}^{\alpha} \\
& - \frac{1}{2} \left(V_{\mathrm{eff}(0)}^{\alpha\alpha} + V_{\mathrm{eff}(0)}^{\alpha\bar{\alpha}} \right) n_f^2 - 2 \left(V_{\mathrm{eff}(\mathbf{Q})}^{\alpha\alpha} + V_{\mathrm{eff}(\mathbf{Q})}^{\alpha\bar{\alpha}} \right) |n_{\mathbf{Q}}|^2 - 2 \left(V_{\mathrm{eff}(\mathbf{Q})}^{\alpha\alpha} - V_{\mathrm{eff}(\mathbf{Q})}^{\alpha\bar{\alpha}} \right) |m_{\mathbf{Q}}|^2,
\end{aligned}
\tag{5.48}
$$

with CDW and SDW order parameters:

$$
n_{\mathbf{Q}} \equiv \frac{1}{2N} \sum_{\mathbf{k},\alpha} \langle \hat{c}_{\mathbf{k}+\mathbf{Q}}^{\alpha\dagger} \hat{c}_{\mathbf{k}}^{\alpha} \rangle = \frac{1}{2} \sum_{i,\alpha} (-1)^i \langle \hat{c}_i^{\alpha\dagger} \hat{c}_i^{\alpha} \rangle,
\tag{5.49}
$$

$$
m_{\mathbf{Q}} \equiv \frac{1}{2N} \sum_{\mathbf{k},\alpha} \alpha \langle \hat{c}_{\mathbf{k}+\mathbf{Q}}^{\alpha\dagger} \hat{c}_{\mathbf{k}}^{\alpha} \rangle = \frac{1}{2} \sum_{i,\alpha} (-1)^i \alpha \langle \hat{c}_i^{\alpha\dagger} \hat{c}_i^{\alpha} \rangle,
\tag{5.50}
$$

and

$$
\langle \hat{c}_i^{\alpha\dagger} \hat{c}_i^{\alpha} \rangle = \frac{n_f}{2} + (-1)^i n_{\mathbf{Q}} + \alpha (-1)^i m_{\mathbf{Q}}.
\tag{5.51}
$$

5.4.3   Hartree-Fock mean field with symmetry broken

In the above sections, we have applied the mean field approximation to calculate the fermionic superfluid phases and the competing SDW/CDW phases separately. As shown in [130], using Wick's theorem, the expectation value of two fermionic operators can be expressed as sums of all products with one-particles terms as

$$
\langle \hat{O}_1 \hat{O}_2 \hat{O}_3 \hat{O}_4 \rangle = \langle \hat{O}_1 \hat{O}_2 \rangle \langle \hat{O}_3 \hat{O}_4 \rangle + \langle \hat{O}_1 \hat{O}_4 \rangle \langle \hat{O}_2 \hat{O}_3 \rangle - \langle \hat{O}_1 \hat{O}_3 \rangle \langle \hat{O}_2 \hat{O}_4 \rangle.
\tag{5.52}
$$

From [128, 131], the Hartree-Fock treatment with broken symmetry gives the mean field-Hamiltonian:

$$
\begin{aligned}
& V_{\mathrm{eff}}^{\alpha\beta} (\mathbf{k}_1 - \mathbf{k}_2) \cdot \hat{c}_{\mathbf{k}_1}^{\alpha\dagger} \hat{c}_{-\mathbf{k}_1+\mathbf{p}}^{\beta\dagger} \hat{c}_{-\mathbf{k}_2+\mathbf{p}}^{\beta} \hat{c}_{\mathbf{k}_2}^{\alpha} \\
= & V_{\mathrm{eff}}^{\alpha\beta} (\mathbf{k}_1 - \mathbf{k}_2) \left[\langle \hat{c}_{\mathbf{k}_1}^{\alpha\dagger} \hat{c}_{-\mathbf{k}_1+\mathbf{p}}^{\beta\dagger} \rangle \hat{c}_{-\mathbf{k}_2+\mathbf{p}}^{\beta} \hat{c}_{\mathbf{k}_2}^{\alpha} + \hat{c}_{\mathbf{k}_1}^{\alpha\dagger} \hat{c}_{-\mathbf{k}_1+\mathbf{p}}^{\beta\dagger} \langle \hat{c}_{-\mathbf{k}_2+\mathbf{p}}^{\beta} \hat{c}_{\mathbf{k}_2}^{\alpha} \rangle - \langle \hat{c}_{\mathbf{k}_1}^{\alpha\dagger} \hat{c}_{-\mathbf{k}_1+\mathbf{p}}^{\beta\dagger} \rangle \langle \hat{c}_{-\mathbf{k}_2+\mathbf{p}}^{\beta} \hat{c}_{\mathbf{k}_2}^{\alpha} \rangle \right] \\
+ & V_{\mathrm{eff}}^{\alpha\beta} (\mathbf{k}_1 - \mathbf{k}_2) \left[\langle \hat{c}_{\mathbf{k}_1}^{\alpha\dagger} \hat{c}_{\mathbf{k}_2}^{\alpha} \rangle \hat{c}_{-\mathbf{k}_1+\mathbf{p}}^{\beta\dagger} \hat{c}_{-\mathbf{k}_2+\mathbf{p}}^{\beta} + \hat{c}_{\mathbf{k}_1}^{\alpha\dagger} \hat{c}_{\mathbf{k}_2}^{\alpha} \langle \hat{c}_{-\mathbf{k}_1+\mathbf{p}}^{\beta\dagger} \hat{c}_{-\mathbf{k}_2+\mathbf{p}}^{\beta} \rangle - \langle \hat{c}_{\mathbf{k}_1}^{\alpha\dagger} \hat{c}_{\mathbf{k}_2}^{\alpha} \rangle \langle \hat{c}_{-\mathbf{k}_1+\mathbf{p}}^{\beta\dagger} \hat{c}_{-\mathbf{k}_2+\mathbf{p}}^{\beta} \rangle \right] \\
- & V_{\mathrm{eff}}^{\alpha\beta} (\mathbf{k}_1 - \mathbf{k}_2) \left[\langle \hat{c}_{\mathbf{k}_1}^{\alpha\dagger} \hat{c}_{-\mathbf{k}_2+\mathbf{p}}^{\beta} \rangle \hat{c}_{-\mathbf{k}_1+\mathbf{p}}^{\beta\dagger} \hat{c}_{\mathbf{k}_2}^{\alpha} + \hat{c}_{\mathbf{k}_1}^{\alpha\dagger} \hat{c}_{-\mathbf{k}_2+\mathbf{p}}^{\beta} \langle \hat{c}_{-\mathbf{k}_1+\mathbf{p}}^{\beta\dagger} \hat{c}_{\mathbf{k}_2}^{\alpha} \rangle - \langle \hat{c}_{\mathbf{k}_1}^{\alpha\dagger} \hat{c}_{-\mathbf{k}_2+\mathbf{p}}^{\beta} \rangle \langle \hat{c}_{-\mathbf{k}_1+\mathbf{p}}^{\beta\dagger} \hat{c}_{\mathbf{k}_2}^{\alpha} \rangle \right].
\end{aligned}
$$

In this Hamiltonian, the first term is the Bogoliubov superfluid term with order parameters at half filling

$$
\begin{aligned}
\Delta_{\mathbf{k}}^{\alpha\beta} = & \delta_{\alpha,-\beta} \left[\Delta_{s0} + \Delta_{s1} \gamma_{\mathbf{k}} + \Delta_d \eta_{\mathbf{k}} \right] \\
& + \delta_{\alpha,\beta} \left[\Delta_{px} \sin k_x + \Delta_{py} \sin k_y \right],
\end{aligned}
\tag{5.53}
$$

where Δ_{s0} and Δ_{s1} are the onsite and extended s-wave paring gaps, while $\Delta_{p/d}$ is the $p-$/$d-$wave pairing gap. Away from half filling, the system may also support nonuniform $s-$wave order as

$$
\Delta_{\pi} \equiv \frac{U_0}{\Omega} \sum_{\mathbf{k}} \langle \hat{c}_{\mathbf{k}+\pi}^{\alpha\dagger} \hat{c}_{-\mathbf{k}}^{\bar{\alpha}\dagger} \rangle = \frac{U_0}{\Omega} \sum_i (-1)^i \langle \hat{c}_i^{\alpha\dagger} \hat{c}_i^{\bar{\alpha}\dagger} \rangle.
$$

While Δ_π will vanish identically in the case of half-filling due to particle-hole symmetry.

The second term is the Hartree mean field including charge density wave and spin density wave order

$$n_{\mathbf{Q}} = \frac{1}{2N} \sum_{\mathbf{k},\alpha} \langle \hat{c}_{\mathbf{k+Q}}^{\alpha\dagger} \hat{c}_{\mathbf{k}}^{\alpha} \rangle = \frac{1}{2} \sum_{i,\alpha} (-1)^i \langle \hat{c}_i^{\alpha\dagger} \hat{c}_i^{\alpha} \rangle, \tag{5.54}$$

$$m_{\mathbf{Q}} = \frac{1}{2N} \sum_{\mathbf{k},\alpha} \alpha \langle \hat{c}_{\mathbf{k+Q}}^{\alpha\dagger} \hat{c}_{\mathbf{k}}^{\alpha} \rangle = \frac{1}{2} \sum_{i,\alpha} (-1)^i \alpha \langle \hat{c}_i^{\alpha\dagger} \hat{c}_i^{\alpha} \rangle. \tag{5.55}$$

The last term contains the Fock exchange energy. The term including $\alpha = \beta$ describes the fermionic exchange self-energy

$$\Sigma_{\mathbf{k}}^{\alpha} = -(2/N) \sum_{\mathbf{p}} V_{\text{eff}}^{\alpha\alpha} (\mathbf{k} - \mathbf{p}) \langle \hat{c}_{\mathbf{p}}^{\alpha\dagger} \hat{c}_{\mathbf{p}}^{\alpha} \rangle, \tag{5.56}$$

which should be considered in addition to the on-site self-energy terms.

5.5   DMFT implementation

We plan to use dynamical mean field theory (DMFT) to investigate the system and calculate the free energy with the effective Hamiltonian after the Lang-Firsov transformation. The effective Hamiltonian is an extended Hubbard model

$$\hat{H}_{\text{P}} = -\sum_{\langle i,j \rangle} \sum_{\alpha} J_{\text{P}}^{\alpha} \hat{c}_i^{\alpha\dagger} \hat{c}_j^{\alpha} - \sum_{i,\alpha} \mu_P^{\alpha} \hat{n}_i^{\alpha} + \sum_i \sum_{\alpha} \left(\frac{U_0}{2} + \frac{V_{i,i}^{\alpha\bar{\alpha}}}{2} \right) \hat{n}_i^{\alpha} \hat{n}_i^{\bar{\alpha}} + \sum_{i \neq j} \sum_{\alpha,\beta} \frac{V_{i,j}^{\alpha\beta}}{2} \hat{n}_i^{\alpha} \hat{n}_j^{\beta}, \tag{5.57}$$

where $\alpha(\beta) = \sigma(\sigma') = \uparrow (\downarrow)$ indicate different spins, species or hyperfine states.

Within DMFT we decouple the induced interaction in local and non-local terms and treat the non-local term by the Hartree approximation. By keeping Hartree terms $\hat{n}_i^{\alpha} \hat{n}_j^{\beta} \approx \langle \hat{n}_i^{\alpha} \rangle \hat{n}_j^{\beta} + \hat{n}_i^{\alpha} \langle \hat{n}_j^{\beta} \rangle - \langle \hat{n}_i^{\alpha} \rangle \langle \hat{n}_j^{\beta} \rangle$ and considering only nearest-neighbor and second-nearest-neighbor interactions, the long-range interaction can be approximated as

$$\sum_{i \neq j} \sum_{\alpha\beta} \frac{V_{i,j}^{\alpha\beta}}{2} \hat{n}_i^{\alpha} \hat{n}_j^{\beta} = \sum_{\langle i,j \rangle} \sum_{\alpha\beta} \frac{V_{i,j}^{\alpha\beta}}{2} \hat{n}_i^{\alpha} \hat{n}_j^{\beta} + \sum_{\langle\langle i,j \rangle\rangle} \sum_{\alpha\beta} \frac{V_{i,j}^{\alpha\beta}}{2} \hat{n}_i^{\alpha} \hat{n}_j^{\beta} + ...$$

$$\approx \sum_{i,\alpha} \hat{n}_i^{\alpha} \left(\sum_{j \in n.n.i} \sum_{\beta} V_{i,i\pm1}^{\alpha\beta} \langle \hat{n}_j^{\beta} \rangle + \sum_{j \in n.n.n.i} \sum_{\beta} V_{i,i\pm2}^{\alpha\beta} \langle \hat{n}_j^{\beta} \rangle + ... \right) + \mathcal{C}, \tag{5.58}$$

with

$$\mathcal{C} \equiv -\frac{1}{2} \sum_{i \neq j} \sum_{\alpha\beta} V_{i,j}^{\alpha\beta} \langle \hat{n}_i^{\alpha} \rangle \langle \hat{n}_j^{\beta} \rangle. \tag{5.59}$$

Up to an energy shift, the mean field Hamiltonian is thus expressed as

$$\hat{H}_{\text{MF}} = -\sum_{\langle i,j \rangle} \sum_{\alpha} J_{\text{P}}^{\alpha} \hat{c}_i^{\alpha\dagger} \hat{c}_j^{\alpha} - \sum_{i,\alpha} \mu_{i,\alpha}^{\text{MF}} \hat{n}_i^{\alpha} + \sum_i \sum_{\alpha} \left(\frac{U_0}{2} + \frac{V_{i,i}^{\alpha\bar{\alpha}}}{2} \right) \hat{n}_i^{\alpha} \hat{n}_i^{\bar{\alpha}}, \tag{5.60}$$

with effective chemical potential

$$\mu_{i,\alpha}^{\mathrm{MF}} \equiv \mu_P^\alpha - \left(\sum_{j \in n.n.i} \sum_\beta V_{i,i\pm 1}^{\alpha\beta} \langle \hat{n}_j^\beta \rangle + \sum_{j \in n.n.n.i} \sum_\beta V_{i,i\pm 2}^{\alpha\beta} \langle \hat{n}_j^\beta \rangle + ... \right). \tag{5.61}$$

In the simple case with identical interaction amplitude $|a_{IB}^\uparrow| = |a_{IB}^\downarrow|$, the polaron energy shifts and induced interactions have the relations $\varepsilon_P^\uparrow = \varepsilon_P^\downarrow$ and $V_{|i-j|} \equiv V_{ij}^{\uparrow\uparrow} = V_{ij}^{\downarrow\downarrow} = \pm V_{ij}^{\uparrow\downarrow}$. Note that $V_{|i-j|}$ is always negative. The effective chemical potential in a 2D lattice can be simplified as

$$\mu_{i,\uparrow}^{\mathrm{MF}} = \mu_P^\uparrow - V_1 \sum_{j \in n.n.i} \left(\langle \hat{n}_j^\uparrow \rangle \pm \langle \hat{n}_j^\downarrow \rangle \right) - V_2 \sum_{j \in n.n.n.i} \left(\langle \hat{n}_j^\uparrow \rangle \pm \langle \hat{n}_j^\downarrow \rangle \right); \tag{5.62}$$

$$\mu_{i,\downarrow}^{\mathrm{MF}} = \mu_P^\downarrow - V_1 \sum_{j \in n.n.i} \left(\pm \langle \hat{n}_j^\uparrow \rangle + \langle \hat{n}_j^\uparrow \rangle \right) - V_2 \sum_{j \in n.n.n.i} \left(\pm \langle \hat{n}_j^\uparrow \rangle + \langle \hat{n}_j^\uparrow \rangle \right). \tag{5.63}$$

The total occupancies $\langle \hat{n} \rangle$ are derived from the full interacting Green's function, and hence must be obtained self-consistently. The free energy for Hamiltonian $\hat{H}_{\mathrm{MF}}$ and phase diagram can be investigated by dynamical mean field theory.

Chapter 6

Floquet Theory and Hybrid Atom-Ion Simulators

6.1 Introduction

Starting from this chapter, I switch the attention to hybrid systems with trapped ions and atoms. Trapped ultracold ions alone feature a remarkable degree of control over both the preparation and read-out of vibrational and internal degrees of freedom. Many other measurable quantities can also be mapped to these systems [132, 133, 134].

In this chapter, I present a study of heating and decoherence effects in a hybrid atom-ion system, in which the atom and ion are trapped by a harmonic trap and Paul trap, respectively. The classical heating model for this system shows a fundamental limit to sympathetic atom-ion cooling. This limitation arises from the long-range atom-ion interaction, even with the atom gas at zero temperature in a perfect dc- and rf- compensated Paul trap [135]. The interaction with the atom displaces the ion from the rf node, leading to micro-motion and heating.

We consider the entangled state of one ion strongly coupled to one atom. As a consequence of the time-dependent trapping potential and short-range atom-ion collisions, the ionic micromotion plays an important role in such systems. We investigate the dynamic properties of this system by the Floquet formalism and calculate the effects of heating and decoherence arising from the ionic micromotion.

6.2 Single ion in a Paul trap

It is impossible to trap a charged particle in all three directions by a static electric field due to Earnshaw's theorem [136]. In a real system, the ion is trapped by a 3D time-dependent Paul trap. By choosing suitable parameters, the experiments can create an average confining force for ions in all three directions.

In this chapter we consider a simplified one-dimensional Paul trap for a single ion. The Hamiltonian is given by

$$\hat{H}(t) = \frac{p^2}{2m_i} + \frac{1}{2}m_i x^2 K(t),$$ (6.1)

where the effective spring constant

$$K(t) = \frac{1}{4}\omega^2[a + 2q\cos(\omega t)]$$ (6.2)
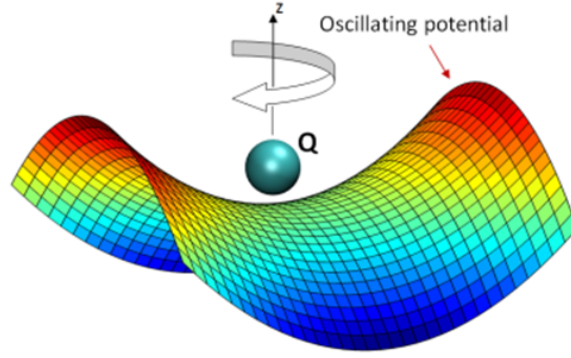
Figure 6.1: Illustration of Paul trap. The figure is from ORNL (https://www.ornl.gov/).
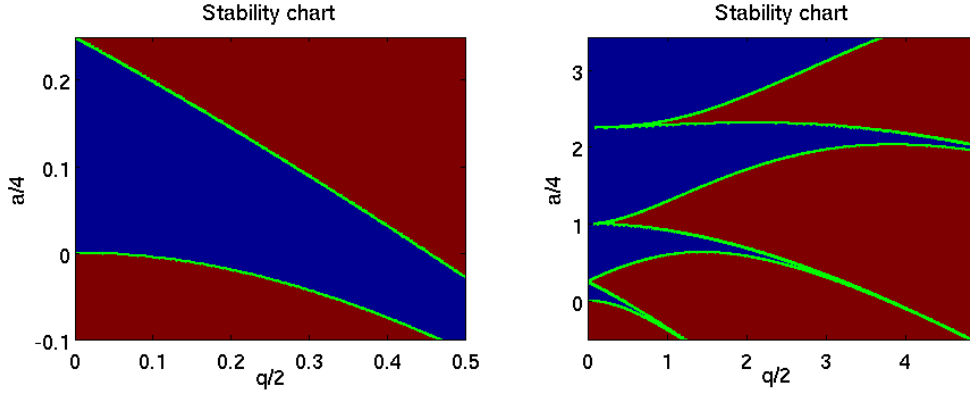
Figure 6.2: Stability chart for the classical Mathieu equation. In the blue regions the solutions are stable (bounded for arbitrary initial conditions), while in the red regions the system is unstable with $\text{Im}(\mu) \neq 0$.

is a periodic function of time with $K(t + T) = K(t)$ and $T = 2\pi/\omega$.

6.2.1 Classical Mathieu equation

The classical equation of motion

$$\ddot{f}(t) + K(t) f(t) = 0 \tag{6.3}$$

is 1D Mathieu equation with the following solution

$$f(t) = e^{i\mu t}\phi(t); \ \phi(t + T) = \phi(t), \tag{6.4}$$

and another independent solution given by the complex conjugate $f^*(t)$. The function $\phi(t)$ is periodic and can be represented as a Fourier series as

$$\phi(t) = \sum_{n=-\infty}^{\infty} c_n e^{in\omega t}. \tag{6.5}$$

As shown in appendix D, the problem is mapped to the tridiagonal recurrence relation

$$\left[\omega^2 a - 4(\mu + n\omega)^2\right] c_n + \omega^2 q(c_{n+1} + c_{n-1}) = 0, \tag{6.6}$$
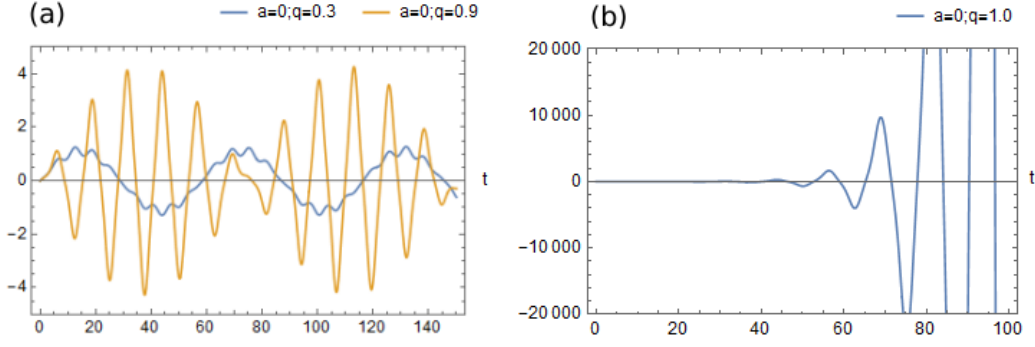
Figure 6.3: Solution of the classical Mathieu equation in the stable region with $a = 0$, $q = 0.3(0.9)$ (left) and in the unstable region with $a = 0$, $q = 1.0$ (right).

which can also be expressed as a tridiagonal matrix H_ν. The linear equations have a non-trivial solution only if $\det(H_\nu) = 0$, which is an equation for μ. These equations can be solved numerically for given a and q. The coefficients c_n are also found by numerical diagonalization. These solutions are stable (bounded for arbitrary initial conditions) when μ/ω is a real non-integer number. The classical function $\psi(t)$ is stable only when $\mu \in \mathbb{R}$. We plot the stability chart of the classical Mathieu equation with $a - q$ in Fig. 6.2. In the blue regions the solutions are stable (bounded for arbitrary initial conditions), while in the red regions the system is unstable with $\text{Im}(\mu) \neq 0$. In Fig. 6.3 we show the solutions of the classical Mathieu equation in the stable region with $a = 0$, $q = 0.3(0.9)$ and the unstable region with $a = 0$, $q = 1.0$.

6.2.2 Quantum solution from unitary transformation

In order to solve the quantum-mechanical problem, we follow the method in [137, 138] and apply the canonical unitary transformation. The transformed Hamiltonian will be

$$\tilde{H}(t) = U^{-1} H(t) U - i\hbar U^{-1} \frac{\partial}{\partial t} U, \tag{6.7}$$

with the transformed wave function $|\tilde{\psi}\rangle = U^{-1}|\psi\rangle$ and unitary transformation

$$U = \exp\left[+\frac{i}{4\hbar} \left(mx^2 \frac{d}{dt} - px - xp \right) \ln|f(t)|^2 \right], \tag{6.8}$$

Then the transformed Hamiltonian is

$$\tilde{H}(t) = \frac{W}{|f(t)|^2} \left(\hat{b}^\dagger \hat{b} + \frac{1}{2} \right), \tag{6.9}$$

with

$$\hat{b} \equiv \sqrt{\frac{mW}{2}} x + i\sqrt{\frac{1}{2mW}} p, \tag{6.10}$$

and a time-independent Wronskian as

$$2iW \equiv \dot{f}(t) f^*(t) - f(t) \dot{f}^*(t). \tag{6.11}$$

From the solutions in Appendix D, the wave function for $n-$th excited state is

$$\Psi_n(x,t) = e^{-i\left(n + \frac{1}{2}\right)\mu t} \psi_n(x,t), \tag{6.12}$$

with

$$\psi_n\left(x\right) = \frac{1}{\sqrt{2^n n!}} \left(\frac{mW}{\pi\hbar}\right)^{\frac{1}{4}} \frac{1}{\sqrt{\phi\left(t\right)}} \left[\frac{\phi^*\left(t\right)}{\phi\left(t\right)}\right]^{\frac{n}{2}+\frac{1}{4}} H_n\left(\sqrt{\frac{mW}{\hbar\left|f\left(t\right)^2\right|}}x\right) \exp\left[-\frac{m\mu}{2\hbar}\left(1 - \frac{i}{\mu}\frac{\dot{\phi}\left(t\right)}{\phi\left(t\right)}\right)x^2\right].$$

(6.13)

6.2.3 Secular approximation and quasienergy

Alternatively, one can apply a different unitary transformation to the Hamiltonian (6.1) with

$$U\left(x,t\right) \equiv \exp\left[-\frac{i}{4\hbar}m_i q\omega x^2 \sin(\omega t)\right],$$

(6.14)

where $U\left(x,t\right)$ indicates fast moving term of ion [139].

The effective Hamiltonian after transformation will be

$$H_{\text{eff}}\left(t\right) = -\frac{\hbar^2}{2m_i}\frac{\partial^2}{\partial x^2} + \frac{1}{2}m_i\omega_0^2 x^2 + \left[-m_i(\gamma\omega_0)^2 x^2\cos(2\omega t) + 2i\hbar\gamma\omega_0\left(x\frac{\partial}{\partial x} + \frac{1}{2}\right)\sin(\omega t)\right]$$

$$= H_0 + H_{\text{mm}}\left(t\right),$$

(6.15)

where ω_0 is the secular frequency

$$\omega_0 \equiv \frac{\omega}{2}\sqrt{a + \frac{q^2}{2}},$$

(6.16)

with the factor $\gamma \equiv 1/\sqrt{2\left(1 + \frac{2a}{q^2}\right)}$.

In the limite $a \ll 1$ and $q \ll 1$, we can consider only the time-independent terms H_0 in Eq. (6.15) as harmonic approximation or secular approximation. This describes a harmonic oscillator with frequency ω_0. The time-dependent terms in H_{eff} are the micromotion terms as

$$H_{\text{mm}}(t) = -m_i(\gamma\omega_0)^2 x^2\cos(2\omega t) - \gamma\omega_0\{x,\, p\}\sin(\omega t).$$

(6.17)

The magnitudes of time-dependent terms are reduced by a factor ω_0/ω compare to Eq. (6.1). The full dynamics of the total Hamiltonian $H_0 + H_{\text{mm}}\left(t\right)$ can be solved by Floquet theory.

6.3 Floquet theory

6.3.1 Floquet quasienergies and eigenstates

The system with periodic driving can be described by Floquet theory. Consider such a quantum system with time-periodic Hamiltonian

$$\hat{H}\left(t+T\right) = \hat{H}\left(t\right)$$

(6.18)

with periodic T. From the time-dependent Schrödinger equation

$$i\hbar\frac{\partial}{\partial t}|\psi\left(t\right)\rangle = \hat{H}\left(t\right)|\psi\left(t\right)\rangle,$$

(6.19)

the evolution operator will take the form

$$\hat{U}\left(t_2, t_1\right) = \mathcal{T}_t \exp\left[-\frac{i}{\hbar}\int_{t_1}^{t_2}\tilde{H}\left(\tau\right)d\tau\right].$$

(6.20)

This unitary operator fulfills the relation $\hat{U}(t_2, t_1) = \hat{U}(t_2 + T, t_1 + T)$ due to time-periodicity of the Hamiltonian.

The eigenstates $|\psi_n(t)\rangle$ of the time evolution operator from time t to $t + T$ fulfill

$$\hat{U}(t+T,t)|\psi_n(t)\rangle = a_n(t)|\psi_n(t)\rangle. \tag{6.21}$$

Since $\hat{U}(t+T,t)$ is unitary, the eigenvalues $a_n(t)$ are only phase factors as $|a_n(t)| = 1$. By applying the relation $\hat{U}(t,t')\hat{U}(t',t) = 1$ to the previous equation, the eigenvalues for $\hat{U}(t'+T,t')$ can be found as

$$\begin{aligned}
\hat{U}(t'+T,t')|\psi_n(t')\rangle =& \hat{U}(t'+T,t+T)\hat{U}(t+T,t)\hat{U}(t,t')\hat{U}(t',t)|\psi_n(t)\rangle \\
=& \hat{U}(t',t)\left(\hat{U}(t+T,t)|\psi_n(t)\rangle\right) \\
=& a_n(t)\hat{U}(t',t)|\psi_n(t)\rangle \\
=& a_n(t)|\psi_n(t')\rangle,
\end{aligned} \tag{6.22}$$

which is the same as in Eq. (6.21). These eigenvalues, which do not depend on the time t from which the evolution over one driving period starts, can be expressed as $a_n(t) = e^{-i\varepsilon_n T/\hbar}$ with *Floquet quasienergy* ε_n. Then the eigenstates after one period T will satisfy

$$|\psi_n(t+T)\rangle = \hat{U}(t+T,t)|\psi_n(t)\rangle = e^{-i\varepsilon_n T/\hbar}|\psi_n(t)\rangle. \tag{6.23}$$

These eigenstates are defined as *Floquet eigenstates* with

$$|\psi_n(t)\rangle = e^{-i\varepsilon_n t/\hbar}|u_n(t)\rangle, \tag{6.24}$$

where $|u_n(t)\rangle$ is the time-periodic *Floquet mode*

$$|u_n(t)\rangle = e^{+i\varepsilon_n t/\hbar}|\psi_n(t)\rangle = |u_n(t+T)\rangle. \tag{6.25}$$

The quasienergy spectrum can be obtained by computing and diagonalizing $\hat{U}(t_0 + T, t_0)$ for an arbitrary t_0. By choosing a complete orthonormal basis $|u_n(t)\rangle$, the time evolution operator can be written as

$$\hat{U}(t_2, t_1) = \sum_n e^{-i\varepsilon_n(t_2-t_1)/\hbar}|u_n(t_2)\rangle\langle u_n(t_1)|. \tag{6.26}$$

The the time evolution for an initial state is

$$|\psi(t)\rangle = \sum_n c_n e^{-i\varepsilon_n(t-t_0)/\hbar}|u_n(t_0)\rangle, \tag{6.27}$$

with time-independent coefficients $c_n \equiv \langle u_n(t_0)||\psi(t_0)\rangle$. The detailed discussion can be found in the paper by Eckardt and Anisimovas [140].

6.3.2 Floquet Hamiltonian

In order to study the dynamics over a long time after several periods T, one can ignore the micromotion by studying the time evolution in the stroboscopic picture in steps of the driving period. Such a stroboscopic time evolution is described by the time-independent Floquet Hamiltonian $\hat{H}_F[t_0]$ with t_0 as a "gauge". The Floquet Hamiltonian is defined such that it generates the time evolution over one period

$$\exp\left(-\frac{i}{\hbar}T\hat{H}_F[t_0]\right) \equiv \hat{U}(t_0 + T, t_0), \tag{6.28}$$

and thus

$$\hat{H}_F[t_0] = \sum_n \varepsilon_n |u_n(t_0)\rangle\langle u_n(t_0)|. \tag{6.29}$$

The parametric dependence on the initial time t_0 is periodic, $\hat{H}_F[t_0+T] = \hat{H}_F[t_0]$, and related to the micromotion. From a Floquet Hamiltonian $\hat{H}_F[t_0]$ obtained for the initial time t_0, one can construct a Floquet Hamiltonian for a different initial time t_0' by applying a unitary transformation

$$\hat{H}_F[t_0'] = \hat{U}^\dagger\left(t_0, t_0'\right)\hat{H}_F[t_0]\hat{U}\left(t_0, t_0'\right). \tag{6.30}$$

One can notice that the quasienergy ε_n, which is obtained by diagonalizing the Floquet Hamiltonian, is gauge-independently.

If the Floquet states and their quasienergies are known, e.g. from computing and diagonalizing the time evolution operator over one period, one can immediately write down the Floquet Hamiltonian. However, it can also be computed directly, without computing the Floquet states and the quasienergies beforehand. The Floquet modes $|u_n(t_0)\rangle$ and their quasienergies ε_n can, in a subsequent step, be obtained from the diagonalization of $\hat{H}_F[t_0]$.

6.3.3 Extended Hilbert space

Here we calculate the Floquet quasi-energy by numerically diagonalizing the Hamiltonian in the extended Hilbert space. The Floquet eigenstates satisfy the time-dependent Schrödinger equation

$$i\hbar\frac{\partial}{\partial t}|\psi_n\left(t\right)\rangle = \hat{H}\left(t\right)|\psi_n\left(t\right)\rangle, \tag{6.31}$$

with $|\psi_n\left(t\right)\rangle = e^{-i\varepsilon_n t/\hbar}|u_n\left(t\right)\rangle$. Based on Floquet theory, these Floquet states are obtained by solving the eigenvalue equation

$$\left[\hat{H}\left(t\right) - i\hbar\frac{\partial}{\partial t}\right]u_n\left(t\right) = \varepsilon_n u_n\left(t\right); \quad \hat{H}_F \equiv \hat{H}\left(t\right) - i\hbar\frac{\partial}{\partial t}. \tag{6.32}$$

The phase factors $e^{-i\varepsilon_n T/\hbar}$ and the Floquet states $|\psi_n\left(t\right)\rangle$ are uniquely defined. However, the quasienergies ε_n and the Floquet modes $|u_n(t)\rangle = e^{i\varepsilon_n t/T}|\psi_n\left(t\right)\rangle$ are not defined uniquely. The quasienergies ε_n are defined up to an integer multiple of $\hbar\omega$. If $|u_n\left(t\right)\rangle$ is a Floquet state with eigenvalue ε_n, then $|u_n\left(t\right)\rangle e^{ik\omega t}$ is also a T-periodic eigensolution with quasienergy $\varepsilon_n + k\hbar\omega$. The quasienergy spectrum of a periodically time-dependent quantum system thus possesses a Brillouin zone-like structure with the width $\hbar\omega$ of one zone. One can choose all quasienergies within a single Brillouin zone as $\varepsilon_n \in [0, \hbar\omega]$. We label ε_n and $|u_n\left(t\right)\rangle$ as $\varepsilon_{n,k}$ and $|u_{n,k}\left(t\right)\rangle$ with

$$\varepsilon_{n,k} = \varepsilon_n + k\hbar\omega; \quad |u_{n,k}\left(t\right)\rangle = |u_n\left(t\right)\rangle e^{ik\omega t}, \tag{6.33}$$

where the index n indicates physically different classes and k denotes different members in a class.

The Schrödinger equation refers to an extended Hilbert space $\mathcal{F} = \mathcal{H}\otimes\mathcal{L}_T$. This space is given by the product space of the state space $\mathcal{H}$ of a quantum system and the space of quare-integrable $T-$ periodically time-dependent functions $\mathcal{L}_T$. Time is treated as a coordinate under open or periodic boundary conditions. The scalar product in that space is given by

$$\langle\langle u\left(\vec{r}, t\right)|v\left(\vec{r}, t\right)\rangle\rangle \equiv \frac{1}{T}\int_0^T dt\langle u\left(\vec{r}, t\right)|v\left(\vec{r}, t\right)\rangle, \tag{6.34}$$

i.e., by the usual scalar product combined with time averaging over one period. Hence the quasienergies are obtained by computing the matrix elements of the operator $\hat{H}_F \equiv \hat{H}(t) - i\hbar\frac{\partial}{\partial t}$ in the Floquet basis, and diagonalizing.

We use a complete set of orthogonal basis states $|\alpha, k\rangle\rangle$ in $\mathcal{F}$ space as a basis to evaluate the matrix elements of the Floquet Hamiltonian. This basis is constructed by combining a complete set of orthogonal basis states $|\alpha\rangle$ of $\mathcal{H}$ with the complete set of time-periodic functions $e^{ik\omega t}$ as

$$|\alpha, k\rangle\rangle = |\alpha\rangle e^{ik\omega t}. \tag{6.35}$$

The time-periodic Hamiltonian $\hat{H}(t)$ can be expressed as $\hat{H}(t) = \sum_{l \in \mathbb{Z}} \hat{H}_l e^{il\omega t}$ where $\hat{H}_l$ is the Fourier transform

$$\hat{H}_l = \frac{1}{T} \int_0^T dt e^{-il\omega t} \hat{H}(t) = \hat{H}_{-l}^{\dagger}. \tag{6.36}$$

Thus the Floquet matrix elements in extended Hilbert space can be calculated as

$$\begin{aligned}\langle\langle\alpha, k|\hat{H}_F|\alpha', j\rangle\rangle =& \frac{1}{T} \int_0^T dt e^{-ik\omega t} \langle\alpha'| \left(\hat{H}_0 - i\hbar\frac{\partial}{\partial t}\right) + \sum_{l \neq 0} \hat{H}_l e^{il\omega t} |\alpha'\rangle e^{ij\omega t} \\ =& \left(\langle\alpha|\hat{H}_0|\alpha'\rangle + k\hbar\omega\delta_{\alpha\alpha'}\right)\delta_{k,j} + \sum_{l \neq 0}\langle\alpha|\hat{H}_l|\alpha'\rangle\delta_{k,j+l}.\end{aligned} \tag{6.37}$$

By defining the identity matrix $\mathbf{I}$ and matrix $\mathbf{H}_l$ in $\mathcal{H}$ space with elements

$$(\mathbf{H}_l)_{\alpha\alpha'} = \langle\alpha|\hat{H}_l|\alpha'\rangle, \tag{6.38}$$

the Floquet matrix is written as

$$\begin{array}{c} \begin{array}{ccccc} j=-2 & -1 & 0 & 1 & 2 \end{array} \\ \begin{array}{c} k=-2 \\ \\ -1 \\ \\ 0 \\ \\ 1 \\ \\ 2 \end{array} \left(\begin{array}{ccccccc} \ddots & \cdots & \cdots & \cdots & \cdots & \cdots & \cdot^{\cdot^{\cdot}} \\ \cdots & \mathbf{H}_0 - 2\hbar\omega\mathbf{I} & \color{red}{\mathbf{H}_{-1}} & \color{blue}{\mathbf{H}_{-2}} & \color{green}{\mathbf{H}_{-3}} & \color{cyan}{\mathbf{H}_{-4}} & \cdots \\ \cdots & \color{red}{\mathbf{H}_1} & \mathbf{H}_0 - \hbar\omega\mathbf{I} & \color{red}{\mathbf{H}_{-1}} & \color{blue}{\mathbf{H}_{-2}} & \color{green}{\mathbf{H}_{-3}} & \cdots \\ \cdots & \color{blue}{\mathbf{H}_2} & \color{red}{\mathbf{H}_1} & \mathbf{H}_0 & \color{red}{\mathbf{H}_{-1}} & \color{blue}{\mathbf{H}_{-2}} & \cdots \\ \cdots & \color{green}{\mathbf{H}_3} & \color{blue}{\mathbf{H}_2} & \color{red}{\mathbf{H}_1} & \mathbf{H}_0 + \hbar\omega\mathbf{I} & \color{red}{\mathbf{H}_{-1}} & \cdots \\ \cdots & \color{cyan}{\mathbf{H}_4} & \color{green}{\mathbf{H}_3} & \color{blue}{\mathbf{H}_2} & \color{red}{\mathbf{H}_1} & \mathbf{H}_0 + 2\hbar\omega\mathbf{I} & \cdots \\ \cdot^{\cdot^{\cdot}} & \cdots & \cdots & \cdots & \cdots & \cdots & \ddots \end{array}\right). \end{array} \tag{6.39}$$

The Floquet quasienergy ε_n and eigenstates can be obtained after diagonalization and thus

$$|\psi_n(t)\rangle = e^{-i\varepsilon_n t/\hbar}|u_n(t)\rangle = e^{-i\varepsilon_{n,k} t/\hbar}|u_{n,k}(t)\rangle. \tag{6.40}$$

The Floquet mode $|u_n(t)\rangle$ corresponding to the n-th quasienergy is

$$|u_n(t)\rangle = \sum_{\alpha,k} c_{\alpha,k}^n |\alpha, k\rangle. \tag{6.41}$$

6.3.4   Magnus expansion

The evolution operator over one period is given by

$$\hat{U}(t_0 + T, t_0) = \mathcal{T}_t \exp\left[-\frac{i}{\hbar}\int_{t_0}^{t_0+T}\tilde{H}(\tau)\,d\tau\right] = \exp\left(-\frac{i}{\hbar}T\hat{H}_F[t_0]\right). \tag{6.42}$$

Taking the logarithm of both sides of the equation above and expanding the exponents in a Taylor series, which is justified if the period is sufficiently short, one can represent the stroboscopic Floquet Hamiltonian as [141, 142]:

$$H_F[t_0] = \sum_{n=0}^{\infty} H_F^{(n)}[t_0]. \tag{6.43}$$

The super-index (n) means that $H_F^{(n)}[t_0]$ is of order ω^{-n} with $\omega = 2\pi/T$. The first few terms are given by

$$H_F^{(0)} = \frac{1}{T}\int_{t_0}^{T+t_0} dt\, H(t) = H_0; \tag{6.44}$$

$$H_F^{(1)} = \frac{1}{2!T(i\hbar)}\int_{t_0}^{T+t_0} dt_1 \int_{t_0}^{t_1} dt_2\,[H(t_1),\,H(t_2)]; \tag{6.45}$$

$$H_F^{(2)} = \frac{1}{3!T(i\hbar)^2}\int_{t_0}^{T+t_0} dt_1 \int_{t_0}^{t_1} dt_2 \int_{t_0}^{t_2} dt_3\,([H(t_1),\,[H(t_2),\,H(t_3)]] + [H(t_3),\,[H(t_2),\,H(t_1)]]). \tag{6.46}$$

We take the gauge $t_0 = 0$ and expand the time-periodic Hamiltonian in its Fourier series as $\hat{H}(t) = \sum_{l\in\mathbb{Z}}\hat{H}_l e^{il\omega t}$.

As calculated in appendix E, the first few terms in the Magnus expansion take the form

$$H_F^{(0)} = H_0;$$
$$H_F^{(1)} = \frac{1}{\omega}\sum_{l=1}^{\infty}\frac{1}{l}\left([H_l,\,H_{-l}] - [H_l,\,H_0] + [H_{-l},\,H_0]\right); \tag{6.47}$$

The higher order such as $H_F^{(2)}$ can also be found in Appendix E.

6.4   Micromotion-induced heating and instability

6.4.1   Quasienergy from exactly diagonalization

For our single-ion Hamiltonian in Eq. (6.15), the Fourier series is $H(t) = \sum_{l\in\mathbb{Z}} H_l e^{il\omega t}$ with

$$H_0 = \frac{1}{2m_i}p^2 + \frac{1}{2}m_i\omega_0^2 x^2; \tag{6.48}$$

$$H_1 = -H_{-1} = +\frac{i}{2}\gamma\omega_0\{x,\,p\}; \tag{6.49}$$

$$H_2 = +H_{-2} = -\frac{1}{2}m_i(\gamma\omega_0)^2 x^2. \tag{6.50}$$

We use a complete set of orthogonal basis states $|\alpha, k\rangle\rangle = |\alpha\rangle e^{ik\omega t}$ in $\mathcal{F}$ space as a basis to evaluate the matrix elements of the Floquet Hamiltonian. We choose $|\alpha\rangle$ as the eigenbasis of H_0, i.e., 1D quantum Harmonic oscillator states:

$$|\alpha\rangle = \frac{1}{\sqrt{2^\alpha \alpha!}} \left(\frac{m_i\omega_0}{\pi\hbar}\right)^{\frac{1}{4}} e^{-\frac{m\omega_0 x^2}{2\hbar}} H_\alpha \left(\sqrt{\frac{m\omega_0}{\hbar}}x\right), \qquad (6.51)$$

and thus

$$\langle\alpha|H_0|\beta\rangle = \left(\alpha + \frac{1}{2}\right)\hbar\omega_0\delta_{\alpha\beta}.$$

From the relations

$$x|\alpha\rangle = \sqrt{\frac{\hbar}{2m_i\omega_0}}\left(\sqrt{\alpha+1}|\alpha+1\rangle + \sqrt{\alpha}|\alpha-1\rangle\right);$$

$$p|\alpha\rangle = i\sqrt{\frac{m_i\omega_0\hbar}{2}}\left(\sqrt{\alpha+1}|\alpha+1\rangle - \sqrt{\alpha}|\alpha-1\rangle\right), \qquad (6.52)$$

we have

$$\langle\alpha|H_1|\beta\rangle = -\langle\alpha|H_{-1}|\beta\rangle$$
$$= -\frac{\gamma\hbar\omega_0}{2}\left(\sqrt{(\beta+1)(\beta+2)}\langle\alpha|\beta+2\rangle - \sqrt{\beta(\beta-1)}\langle\alpha|\beta-2\rangle\right), \qquad (6.53)$$

and

$$\langle\alpha|H_2|\beta\rangle = \langle\alpha|H_{-2}|\beta\rangle$$
$$= -\frac{\gamma^2\hbar\omega_0}{4}\left(\sqrt{(\beta+1)(\beta+2)}\langle\alpha|\beta+2\rangle + (2\beta+1)\langle\alpha|\beta\rangle + \sqrt{\beta(\beta-1)}\langle\alpha|\beta-2\rangle\right). \qquad (6.54)$$

Thus the Floquet matrix elements in extended Hilbert space are calculated as

$$\langle\langle\alpha, k|\hat{H}_F|\beta, j\rangle\rangle = \left(\left(\alpha + \frac{1}{2}\right)\hbar\omega_0 + k\hbar\omega\right)\delta_{\alpha\beta}\delta_{k,j} + \sum_{l\neq 0}\langle\alpha|\hat{H}_l|\beta\rangle\delta_{k,j+l}. \qquad (6.55)$$

6.4.2 Quasienergy from Magnus expansion method

The Magnus expansion for the ionic Hamiltonian (6.15) is calculated up to second order of $1/\omega$.

For $H_F^{(1)}$ we have

$$H_F^{(1)} = \frac{1}{\omega\hbar}\sum_{l=1}^{\infty}\frac{1}{l}\left([H_l, H_{-l}] - [H_l, H_0] + [H_{-l}, H_0]\right)$$
$$= \frac{1}{2m_i}P^2\left(4\frac{\gamma\omega_0}{\omega}\right) - \frac{1}{2}m_i\omega_0^2 X^2\left(4\frac{\gamma\omega_0}{\omega}\right). \qquad (6.56)$$

We also notice that, the Floquet Hamiltonian only contains a shift relative to the harmonic approximation. For $H_F^{(2)}$ we use the results in appendix E and obtain

$$H_F^{(2)} = \frac{1}{\omega^2\hbar^2}\left(\frac{1}{2}[H_0, [H_2, H_0]] - \frac{1}{4}[H_2, [H_2, H_0]] + 3[H_1, [H_1, H_0]] + [H_1, [H_1, H_2]]\right)$$
$$= \frac{1}{2m_i}P^2\left[11\left(\frac{\gamma\omega_0}{\omega}\right)^2\right] + \frac{1}{2}m_i\omega_0^2 X^2 \cdot \left[\left(13 - \frac{7}{2}\gamma^2\right)\left(\frac{\gamma\omega_0}{\omega}\right)^2\right]. \qquad (6.57)$$
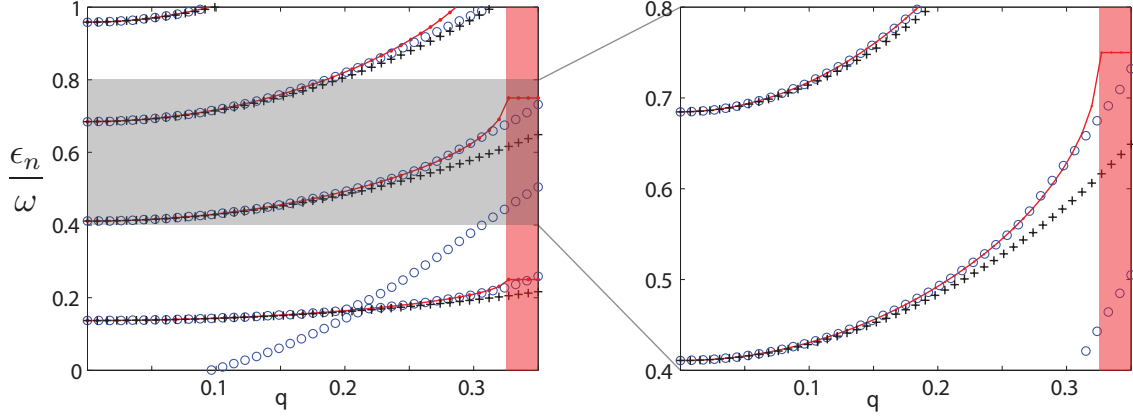
Figure 6.4: Comparison of Floquet quasienergies from diagonalization (blue circles) and Magnus expansion (black crosses) to exact solution (red lines). The system is unstable in the red region.

The effective Floquet Hamiltonian $H_F \approx H_F^{(0)} + H_F^{(1)} + H_F^{(2)}$ is a modified 1D harmonic oscillator

$$H_F = \frac{1}{2m_F}P^2 + \frac{1}{2}m_F\omega_F^2 X^2 \tag{6.58}$$

with

$$m_F \equiv m_i \left[1 - 4\left(\frac{\gamma\omega_0}{\omega}\right) + 5\left(\frac{\gamma\omega_0}{\omega}\right)^2 + \mathcal{O}\left(\frac{\gamma\omega_0}{\omega}\right)^3\right], \tag{6.59}$$

and

$$\omega_F = \omega_0 \left[1 + 0\cdot\left(\frac{\gamma\omega_0}{\omega}\right) + \left(4 - \frac{7}{4}\gamma^2\right)\left(\frac{\gamma\omega_0}{\omega}\right)^2 + \mathcal{O}\left(\frac{\gamma\omega_0}{\omega}\right)^3\right]. \tag{6.60}$$

From Eqs. (6.58 - 6.60) we notice that the Magnus expansion only shifts the quasienergy from $\hbar\omega_0(n+1/2)$ to $\hbar\omega_F(n+1/2)$ and the effective mass from m to m_F. As shown in Fig. 6.4, when the condition $\omega_0 \ll \omega$ is satisfied, the micromotion does not play an important role and thus the Magnus expansion results are valid.

As an application for the Magnus expansion, the single-ion system with excess micromotion is also studied in appendix F.

6.4.3 Heating effects

In order to describe the heating effects, we calculate the expectation value of H_0 after a long time $t = NT$ with $N \to \infty$ [143, 144]. We use the Floquet evolution operator

$$\hat{U}_F(T) = e^{-iH_F T} = \sum_n |u_n\rangle e^{-i\varepsilon_n T}\langle u_n|, \tag{6.61}$$
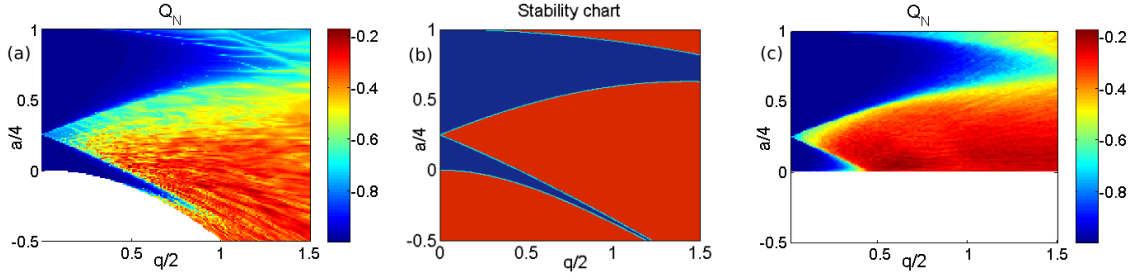
Figure 6.5: (a) Normalized quantity Q_N after infinitely long time, calculated by numerical diagonalization. The blue area with $Q_N = -1$ shows that the ion is not heated even after a long time. The red area shows that the ion is heated, $Q_N \approx 0$, which means the system approaches a thermal state with infinite temperature $\beta = 0$. The white area has $\omega_0^2 < 0$ and thus unstable. Here we use $n_f = 10, n_p = 25$. (b) Stability chart for the classical Mathieu equation. The Floquet results fit well with the classical stability results. (c) Q_N calculated directly from Eq. (6.1). With $a \gg 1; q \gg 1$, Q_N is slow to converge.

where ε_n is the Floquet quasienergy and $|u_n\rangle$ is the eigenstate of $e^{-iH_F T}$. Starting from the initial state $|\Psi_i\rangle$, the expectation value of H_0 after long time is

$$
\begin{aligned}
\langle H_0 \rangle (t = NT) &= \langle \Psi_i | \hat{U}_F^\dagger (NT) H_0 \hat{U}_F (NT) |\Psi_i\rangle \\
&= \sum_{m,n} \langle \Psi_i | u_m \rangle e^{+i\varepsilon_m NT} \langle u_m | H_0 | u_n \rangle e^{-i\varepsilon_n NT} \langle u_n | \Psi_i \rangle \\
&\approx \sum_n |\langle \Psi_i | u_n \rangle|^2 \langle u_n | H_0 | u_n \rangle,
\end{aligned}
\tag{6.62}
$$

where the so-called *diagonal ensemble* is used in the last step for $N \to \infty$ [145, 146]. If the system is driven to high energy, the final $\langle H_0 \rangle$ will behave as a thermal distribution with infinite temperature $\mathcal{T} = \infty$ or $\beta \equiv 1/k\mathcal{T} = 0$.

To quantify the heating effects, we calculate a normalized quantity Q_N as [143]

$$
Q_N \equiv \frac{\langle H_0 \rangle (t = NT) - \langle H_0 \rangle_{\beta=0}}{\langle H_0 \rangle_{\beta=0} - \langle H_0 \rangle (t = 0)}.
\tag{6.63}
$$

The value $Q_N = -1$ indicates that the system is not heated at all, while $Q_N = 0$ indicates that the system is heated to a thermal state with infinite temperature.

By exact diagonalization of the Floquet Hamiltonian, we numerically calculate the quasienergy ϵ_m^F and the Floquet state $|u_m(t)\rangle = \sum_{n,k}^m c_{n,k} |n\rangle e^{ik\omega t}$, where $|n\rangle$ is the n-th harmonic oscillator state.

In Fig. 6.5 we show the results for Q_N by numerical diagonalization for different values of q and a. We use the ground state $|n\rangle$ as the initial state $|\Psi_i\rangle$. The blue area with $Q_N = -1$ shows that the ion is not heated even after a long time $t = NT$, while the red area shows that the ion is heated to a thermal state with infinite temperature $\beta = 0$. Further studies indicate that in the heated region, the final state does not depend on the initial state. The system always approaches the infinite temperature thermal state.

In Fig. 6.5, we also compare the results to diagonalizaing the original Hamiltonian (6.1) before secular approximation. Then we have the time-independent part

$$
H_0 = -\frac{\hbar^2}{2m_i} \frac{\partial^2}{\partial x^2} + \frac{1}{2} m_i \omega_0^2 x^2,
\tag{6.64}
$$

with $\omega_0 = \sqrt{a/4}\,\omega$ and the micromotion part:

$$H_{\mathrm{mm}}(t) = m_i \left(\frac{q\omega^2}{4} \right) x^2 \cos(\omega t). \tag{6.65}$$

Similar to the previous calculation, we express the Hamiltonian as $H(t) = \sum_{l \in \mathbb{Z}} H_l e^{il\omega t}$ with

$$H_1 = m_i \left(\frac{q\omega^2}{8} \right) x^2.$$

In the diagonalization, a larger matrix is needed in order to achieve convergence, since the off-diagonal parts are larger compared to the transformed Hamiltonian. We set up the Floquet matrix as

$$\langle n|H_0|m \rangle = \left(n \frac{\omega}{2} \sqrt{a} + \frac{1}{2} \right) \delta_{mn};$$

$$\langle n|H_1|m \rangle = \frac{q\omega}{8\sqrt{a}} \left(\sqrt{(m+1)(m+2)}\langle n|m+2 \rangle + (2m+1)\langle n|m \rangle + \sqrt{m(m-1)}\langle n|m-2 \rangle \right).$$

The results in Fig. 6.5 show good aggrement with previous calculations.

6.5 Hybrid system with single ion and single atom

6.5.1 Atom-ion interaction and energy spectrum

Now we consider a hybrid atom-ion system with an additional atom trapped by a harmonic potential. We start with the effective Hamiltonian in the rotating frame, and consider the presence of atom-ion interaction:

$$H(t) = \frac{p_a^2}{2m_a} + \frac{1}{2}m_a\omega_a^2 x_a^2 + \frac{p_i^2}{2m_i} + \frac{1}{2}m_i\omega_0^2(x_i - d)^2 - \frac{\alpha e^2}{2(x_i - x_a)^4} + H_{\mathrm{mm}}(t), \tag{6.66}$$

with the micromotion part

$$H_{\mathrm{mm}}(t) = -m_i(\gamma\omega_0)^2(x_i - d)^2 \cos(2\omega t) - \gamma\omega_0\{x_i - d, p_i\}\sin(\omega t), \tag{6.67}$$

where d is the distance between the center of trapping for atom and ion.

Firstly we consider a simple case and assume the atom is fixed at the center of its trap, then we have $x_a = 0$ and the following Hamiltonian

$$H(t) = \frac{p_i^2}{2m_i} + \frac{1}{2}m_i\omega_0^2(x_i - d)^2 - \frac{\alpha e^2}{2x_i^4} + H_{\mathrm{mm}}(t). \tag{6.68}$$
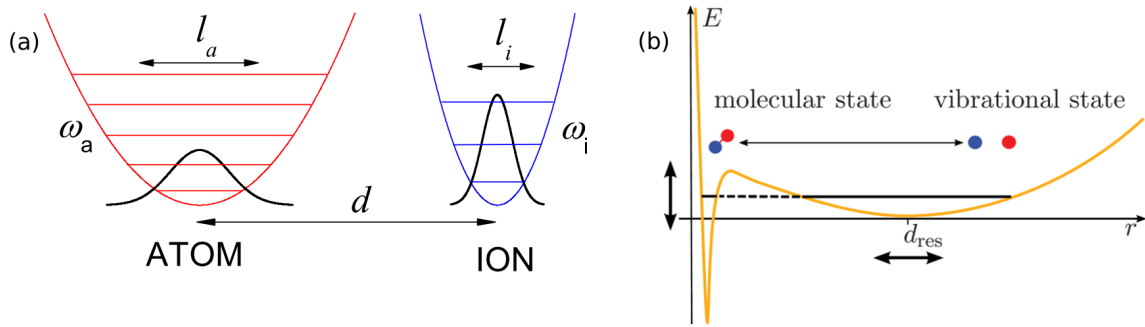
Figure 6.6: (a) Hybrid system with a trapped atom and ion. (b) Effective interaction and different two-body states. The figures are from [147, 148].

6.5.2 Energy spectrum

Firstly we calculate the above Hamiltonian without micromotion. We choose the Numerov method as our numerical approach to solve the 1D Schrödinger equation with the Hamiltonian

$$H_0 = \frac{p_i^2}{2m_i} + \frac{1}{2}m_i\omega_0^2(x_i - d)^2 - \frac{\alpha e^2}{2x_i^4}. \tag{6.69}$$

At short distance, we apply quantum defect theory (QDT) [147] and describe the radial wave functions as

$$R_l(r, k) \sim \sin[R^*/r + \varphi_l(k)], \quad r \ll \sqrt{R^*/k}. \tag{6.70}$$

For $R_0 \ll R^*$ we assume that the $\varphi_l(k)$ are independent of energy and angular momentum, i.e. $\varphi_l(k) = \varphi$, which reduces the description of the short-range interaction to the single quantum-defect parameter. In a 1D system, the wave functions have asymptotic behavior as

$$\Psi_e(z, k) \sim |z| \sin[R^*/|z| + \varphi_e(k)], \quad z \ll \sqrt{R^*/k}; \tag{6.71}$$

$$\Psi_o(z, k) \sim z \sin[R^*/|z| + \varphi_o(k)], \quad z \ll \sqrt{R^*/k}. \tag{6.72}$$

and $\Psi_{1D}(z)$ is a linear combination of odd and even waves

$$\Psi_{1D}(z) = c_e\Psi_e(z) + c_o\Psi_o(z). \tag{6.73}$$

From the Numerov method, the energy spectrum is found with $d = 0$ as $E_\alpha^{(d=0)}$ for the Hamiltonian $H_0^{(d=0)}$. For the case $d \neq 0$, the energies are calculated by diagonalizing $H_0^{(d)}$ in the Hilbert space of $|\alpha\rangle$, where $|\alpha\rangle$ is the eigenbasis of $H_0^{(d=0)}$. The matrix elements are calculated as

$$\langle\alpha|H_0^{(d)}|\beta\rangle = \langle\alpha|\left(H_0^{(d=0)} + \frac{1}{2}m\omega_0^2 d^2 - m\omega_0^2 dx\right)|\beta\rangle$$

$$= \left(E_\alpha^{(d=0)} + \frac{1}{2}m\omega_0^2 d^2\right)\delta_{\alpha,\beta} - m\omega_0^2 d\langle n|x|\beta\rangle. \tag{6.74}$$

Here we use the ion harmonic oscillator length $l_i = \sqrt{\hbar/m_i\omega_0}$ as length unit and choose the same parameters as in [149]. The energy spectrum is shown in Fig. 6.7.

6.5.3 Floquet quasienergies

We study the total Hamiltonian (6.68) by the Floquet method. There are two methods to calculate the exact quasienergies: time-propagation and exact diagonalization. The difference between these two methods is the dimension of the Hamiltonian.

The time evolution operator satisfies the Schrödinger equation $i\frac{\partial}{\partial t}U(t, 0) = H(t)U(t, 0)$. It has the following properties, $U(t + T, 0) = U(t + T, T)U(T, 0) = U(t, 0)U(T, 0)$. The eigenvalue λ of $U(T, 0)$ is related to the quasi-energy ϵ_n by, $\lambda_n = e^{-i\epsilon_n T}$. Therefore, we need to obtain $U(T, 0)$ and diagonalize it to get the eigenenergies. We compute $U(T, 0)$ by using the propagation scheme,

$$U(t + \Delta t, 0) = \exp\left[-i\int_t^{t+\Delta t} dt' H(t')\right]U(t, 0) + \mathcal{O}(\Delta t^3) \tag{6.75}$$

which is a second-order method.
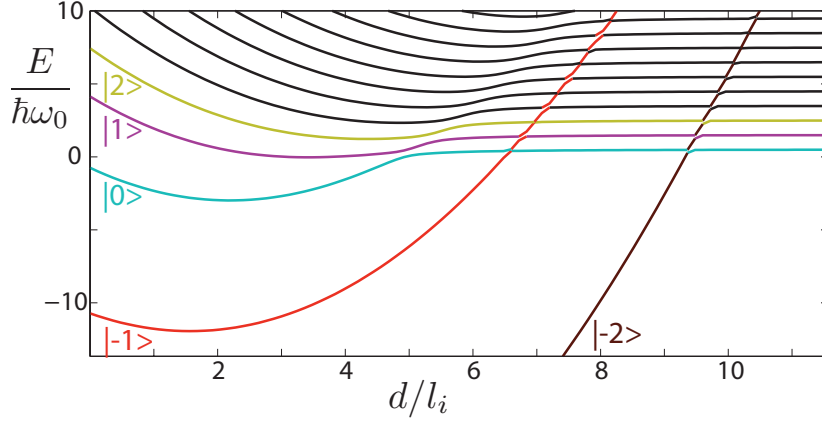
Figure 6.7: Energy spectrum (in units of ω_0) for 1D atom-ion system. We use 53 even + 53 odd states as basis to diagonalize the Hamiltonian.

On the other hand, the exact diagonalization method obtains the quasienergies directly from the eigenvalues $E_{n,k} = \epsilon_n + k\hbar\omega$, where n indicates different classes and k indicates the number of different members in every class. For large enough double-well separation d, the avoided crossing is relatively small, which justified the use of secular (time-independent) approximation. For a smaller d, many avoided-crossings are present, and thus more Floquet states are required to reach convergence.

At the moment, we use exact diagonalization method and obtain the Floquet quasienergies by diagonalizing the Floquet matrix. By re-expressing the Hamiltonian (6.68) in its Fourier series as $H(t) = \sum_{l \in \mathbb{Z}} H_l e^{il\omega t}$, the Floquet matrix can be calculated as

$$\langle \alpha | H_0 | \beta \rangle = \left(E_\alpha^{(d=0)} + \frac{1}{2} m \omega_0^2 d^2 \right) \delta_{\alpha,\beta} - m\omega_0^2 d \langle n | x | \beta \rangle \tag{6.76}$$

and for the $l \neq 0$ case

$$H_1 = -H_{-1} = +\frac{i}{2} \gamma \omega_0 \{ x_i - d, \, p_i \} ; \tag{6.77}$$

$$H_2 = +H_{-2} = -\frac{1}{2} m_i (\gamma \omega_0)^2 (x_i - d)^2, \tag{6.78}$$

From the relation

$$\{ x_i - d, \, p_i \} = -\frac{m}{i\hbar} \left[H_0^{(d=0)}, \, (x_i - d)^2 \right], \tag{6.79}$$

we have

$$\langle \alpha | H_1 | \beta \rangle = -\frac{1}{2} \frac{m}{\hbar} \gamma \omega_0 \langle \alpha | (\left[H_0^{(d=0)}, \, (x_i - d)^2 \right]) | \beta \rangle$$

$$= \frac{1}{2} \frac{m}{\hbar} \gamma \omega_0 (E_\beta^{(d=0)} - E_\alpha^{(d=0)}) \langle \alpha | (x_i - d)^2 | \beta \rangle, \tag{6.80}$$

and

$$\langle \alpha | H_2 | \beta \rangle = -\frac{1}{2} m_i (\gamma \omega_0)^2 \langle \alpha | (x_i - d)^2 | \beta \rangle. \tag{6.81}$$

Magnus expansion

It is interesting to check the results from Magnus expansion method. Up to second order, the effective Floquet Hamiltonian H_F is

$$
\begin{aligned}
H_{ME} \approx & H_{ME}^{(0)} + H_{ME}^{(1)} + H_{ME}^{(2)} \\
= & + \frac{1}{2m_i} p_i^2 \left[1 + 4 \left(\frac{q}{4} \right) + 11 \left(\frac{q}{4} \right)^2 \right] + \frac{1}{2} m_i \omega_0^2 (x_i - d)^2 \left[1 - 4 \left(\frac{q}{4} \right) + \left(13 - \frac{7}{2} \gamma^2 \right) \left(\frac{q}{4} \right)^2 \right] \\
& - \frac{\alpha e^2}{2 x_i^4} \left[1 + 8 \left(\frac{x_i - d}{x_i} \right) \left(\frac{q}{4} \right) + \left(-14 \cdot \left(\frac{x_i - d}{x_i} \right) + 60 \cdot \left(\frac{x_i - d}{x_i} \right)^2 \right) \left(\frac{q}{4} \right)^2 \right],
\end{aligned}
\tag{6.82}
$$

where the first two parts can also be written as $1/(2m_F) \cdot p_i^2 + 1/2 \cdot m_F \omega_F^2 (x_i - d)^2$.

Unlike in the single ion system, the last term in Eq. (6.82) does not decrease with higher driving frequency. There is always a higher order of $1/x_i$, which keeps the system from converging. In principle, this means that we have to include infinitely high orders of $(1/\omega)$ in H_F. When the trap distance d is smaller than a characteristic distance d_{mm}, this micromotion becomes significant and may lead to chaotic behavior of the system.

6.5.4 Heating and instability

We use the Floquet evolution operator

$$
\hat{U}_F (T) = e^{-iH_F T} = \sum_n |u_n\rangle e^{-i\epsilon_n T} \langle u_n|
\tag{6.83}
$$

where ϵ_n are the Floquet quasienergies and $|u_n\rangle$ are the eigenstates of $e^{-iH_F T}$. Starting from the initial state $|\Psi_i\rangle$, the final energy $\langle H_0 \rangle (t)$ can be calculated as a function of time $t = NT$. The expectation value of H_0 after a long time is

$$
\langle H_0 \rangle (t = NT) \approx \sum_n |\langle \Psi_i | u_n \rangle|^2 \langle u_n | H_0 | u_n \rangle,
\tag{6.84}
$$

where the diagonal ensemble is used for $N \to \infty$.

The energy gain from driving can be calculated as

$$
\Delta E (NT) = \langle H_0 \rangle (t) - E_i.
\tag{6.85}
$$

On the other hand, the fidelity of this system after time t is defined as

$$
F(t) \equiv |\langle \psi (t) | \Psi_i \rangle|^2.
\tag{6.86}
$$

After long evolution time, it can be calculated as

$$
\begin{aligned}
F(t \to NT) = & |\langle \Psi_i | \hat{U}_F^\dagger (NT) | \Psi_i \rangle|^2 \\
= & | \left(\sum_n |\langle \Psi_i | u_n \rangle|^2 e^{+i\epsilon_n NT} \right) |^2.
\end{aligned}
\tag{6.87}
$$

In Fig. 6.8 we show the fidelities for different trap distance d if the system is initially in the ground vibrational state $|0\rangle$. For a large trap distance $d > 7 l_i$, the system keeps a high fidelity. For smaller distances $d \approx 0$ and $d \approx 3.5 l_i$, the ionic micromotion reduces the
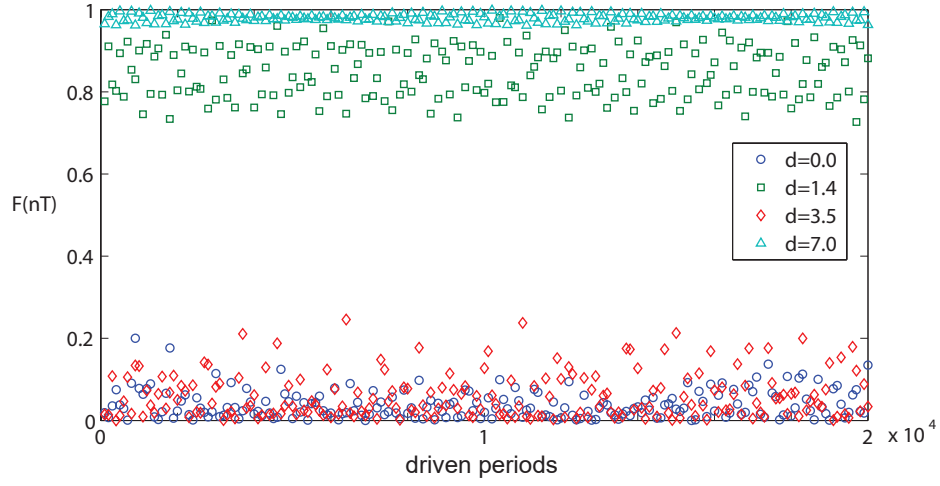
Figure 6.8: Fidelity after long driving time for different trap distances d. Initially we start from the ground vibrational state $|0\rangle$.
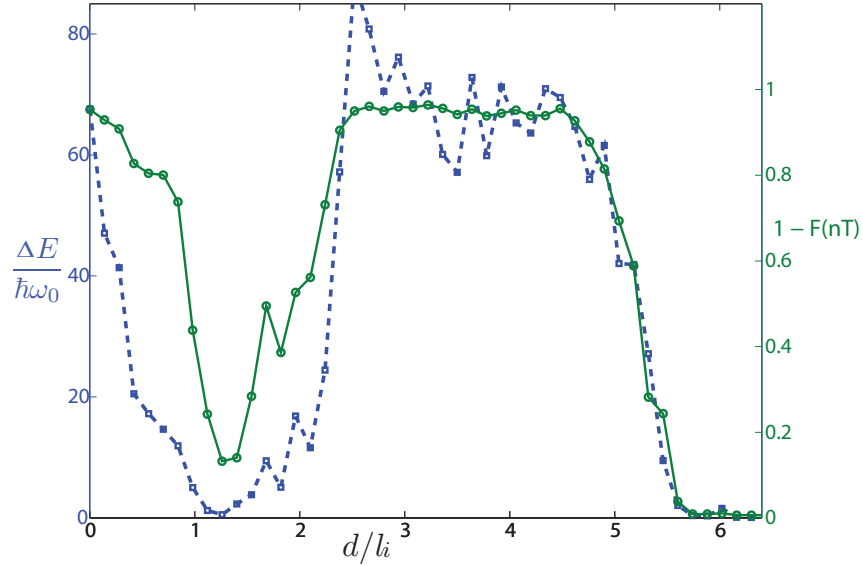
Figure 6.9: Energy gain and averaged fidelity after long driving time for different trap distances d. Initially we start from the ground vibrational state $|0\rangle$.
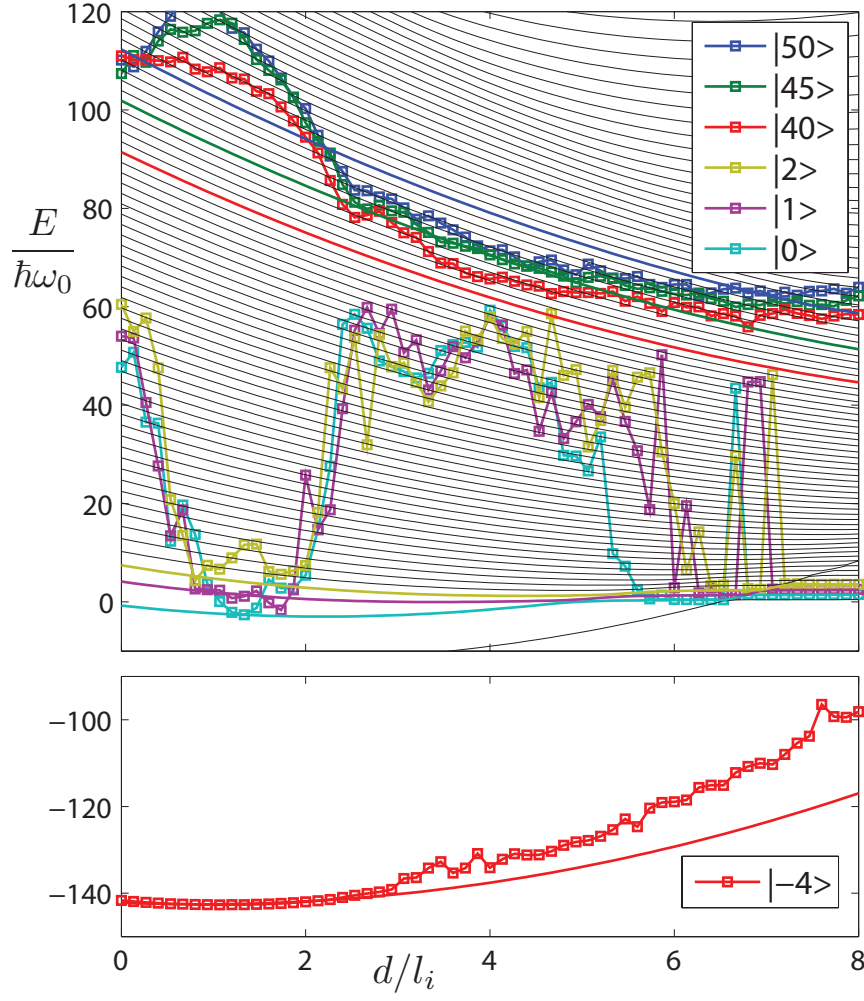
Figure 6.10: Energy gain after long driving time for different trap distances d and different initial states $|n\rangle$.

fidelities to a small value. However for a distance $d \approx 1.4l_i$, the system keeps a relative high fidelity even after a very long driving time.

These results are shown in Fig. 6.9 and compared with energy gain from driving. It shows that the system fidelity is lost whenever the heating happens. It also shows that the system maintains high fidelities for large trap distance d and for $d \approx 1.4l_i$.

Our main results are presented in Fig. 6.10 as energy gain for different trap distances d and different initial states $|n\rangle$.

For low vibrational states, the system is heated at short distances $d \approx 0$ and intermediate distances $2l_i < d < 6l_i$. In these regions, the system is driven to a high-temperature thermal state. The final states do not depend on the initial state, and thus, the fidelity is also lost. For large distances $d > 7l_i$, the ion and atom are separated and thus ionic micromotion does not play an important role in these regions. These vibration states are stable and the harmonic approximation is valid in these regions. However, for a relatively short distance $d \approx 1.4l_i$, the system is not heated and shows a similar behavior as for large distance d. The system with this distance d should be further investigated systematically.

For high vibrational states, on the other hand, the system is easily heated to a thermal state due to large overlap between vibrational states and atom-ion mocecular states.

Bypass micromotion

There are several molecule states $|-n\rangle$ in this system, which describe the tight bound states with atom and ion. As shown in Fig. 6.10, a deep molecule state $|-4\rangle$ is more stable for short and intermediate distances when $d < 7l_i$, due to its large energy gap between vibrational states. It is possible to bypass micromotion effects by flipping the vibrational state to a molecule state [149]. Then we can study strongly coupled atom-ion systems at a short distance d, while reducing the effects from micromotion. For example, a) at larger distance $d \approx 7l_i$ before the micromotion becomes important, the ground vibrational state $|0\rangle$ is transferred to a deep molecule state $|-4\rangle$ by electromagnetic field. b) The trap distance is adiabatically reduced while the molecule state is not affected by micromotion. c) The molecule state is transferred back to the ground vibrational state at short distance $d \approx 1.4l_i$. Finally, we can prepare a strongly coupled atom-ion system in the absence of micromotion effects arising from the intermediate distances $2l_i < d < 6l_i$.

Chapter 7

Interacting Neutral Atom-Ion System

7.1 Introduction

In order to study the many-body physics in a hybrid atom-ion system, recent work [80] has proposed a hybrid ion and neutral atom system that naturally gives rise to phonons and atom-phonon coupling, both of which can be tuned to a large degree. Several atom-phonon coupling models such as the Fröhlich or Holstein model can be simulated by such a system. This system can be realized with, e.g., ^{6}Li atoms and ^{174}Yb$^+$ ions to produce a large mass ratio, and as they exhibit comparable length scales (in their natural units) this mimics the physics of real solid-state systems.

In this chapter, we generate an effective low energy Hamiltonian based on the proposal [80] where the ions are trapped in a 1D chain and induce a periodic potential for the atoms, while phonons arise from fluctuations of the ionic positions. We also describe the explicit realizations of our experimental setup, which can be built by either overlapping traps or separated traps. By using the Lang-Firsov transformation, we demonstrate an extended Hubbard model of polarons, which can result from such a system in different tunable regimes. This Hamiltonian is then solved for the periodic system in the thermodynamic limit by a master equation approach. We also calculate the dynamic properties of several polarons in a finite system.

7.2 Low energy Hamiltonian

7.2.1 Ion chain and phonon excitation

We consider the ions to be trapped in a 1D chain in a Paul trap. They feel the Paul trap $V_{\text{ion trap}}(\boldsymbol{R}_i)$ and each other via the Coulomb repulsion, where $\boldsymbol{R}_i$ denotes the position and $\boldsymbol{P}_i$ the momentum of ion i with mass m_I:

$$\hat{H}_{\text{ion}} = \sum_i \left[\frac{\boldsymbol{P}_i^2}{2m_I} + V_{\text{ion trap}}(\boldsymbol{R}_i) \right] + \sum_{i,j\neq i} \frac{e^2}{4\pi\epsilon_0} \frac{1}{|\boldsymbol{R}_i - \boldsymbol{R}_j|}. \tag{7.1}$$

For a periodic linear chain consisting of N_I ions per unit cell, we consider trapping only in the radial direction: $V_{\text{ion trap}}(\boldsymbol{R}_i) = \frac{1}{2}m_I\omega_{\perp\text{ion}}^2(X_i^2 + Y_i^2)$ where we place the axial direction along the z axis.

To obtain the phonon spectrum, we first determine the classical equilibrium positions of the ions, denoted by $\bar{\boldsymbol{R}}_i$ and then expand the Hamiltonian up to second order in the
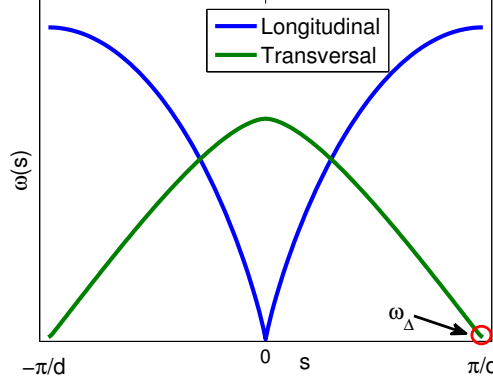
Figure 7.1: Sample phonon spectrum for $d = 1 \, \mu$m, $\omega_{\perp \mathrm{ion}} = 10$ kHz, where ω_Δ is smallest transverse phonon energy at $k = \pi/d$.

displacements $\delta \boldsymbol{R}_i = \boldsymbol{R}_i - \bar{\boldsymbol{R}}_i$ [80]. Finally, we obtain an ion Hamiltonian including phonon excitations as

$$\hat{H}_{\mathrm{ion}} = E_I^{(0)} + \sum_{\mathbf{s}} \omega_{\mathbf{s}} (\hat{b}_{\mathbf{s}}^\dagger \hat{b}_{\mathbf{s}} + \frac{1}{2}) + \frac{\mathcal{P}^2}{2\tilde{m}} + O(\alpha^3), \tag{7.2}$$

where $\mathbf{s} = \{\gamma, s\}$ is a combined index label which is respectively the phonon mode label (e.g. transverse or longitudinal) and quasimomentum. The term $\mathcal{P}^2/2\tilde{m}$ describes the center of mass motion and $E_I^{(0)}$ is a constant energy shift – these two terms will be henceforth neglected. Of importance in the phonon spectra is the disparity that is present with the atomic energies, which will become apparent later in section 7.3. While the lowest energy phonon modes will be similar in energy to atomic transitions, for a small discrete number of ions, only one or two phonon energies are relevant. We assume the ions are equally spaced at a distance of d and can then obtain the phonon spectrum as shown in Fig. 7.1. By tuning the trapping $\omega_{\perp \mathrm{ion}}$, we can adjust the energy of the smallest transverse phonon to be within $\omega_\Delta = \omega_{s=\pi/d} \approx 10$ kHz. Realistically, an experiment will consider the regime $d > 1 \, \mu$m.

In contrast, a finite system includes only a limited number of ions and an additional trapping potential along the axial direction. In the experiment this is generated by static direct current (DC) electric fields using sets of segments in two blades of the Paul trap to trap ions. This configuration allows the creation of a standard harmonic trap $V \sim z^2$ or a double-well trap $V \sim (z^2 - q^2)^2$ along the axial direction. The double well trap is useful to appropriately space the ions in the middle of the trap and prepare an approximately equally spaced ion chain.

7.2.2   Atom Hamiltonian

The atoms alone, without the interactions with the ions, are confined by an optical dipole trap and are described by the following Hamiltonian in the case of a periodic system:

$$\hat{H}_{\mathrm{atom}} = \sum_i \left[\frac{\boldsymbol{p}_i^2}{2m_A} + V_{\mathrm{atom,trap}}(\boldsymbol{r}_i) \right] + \sum_{i,j \neq i} V_{\mathrm{int}}(|\boldsymbol{r}_i - \boldsymbol{r}_j|), \tag{7.3}$$

with $V_{\mathrm{atom\,trap}}(\boldsymbol{R}_i) = \frac{1}{2} m_A \omega_{\perp \mathrm{atom}}^2 (x_i^2 + y_i^2)$. For the moment, we will ignore effects of atom-atom interactions and set $V_{\mathrm{int}}(\boldsymbol{r}) = 0$.

7.2.3 Atom-ion interaction

The interesting component of this setup is the interaction between the ions and atoms. A single ion and single atom interact at long-range via a $1/r^4$ type potential, due to the ionic charge and the polarization of the atom:

$$V_{AI}(\boldsymbol{R}_i, \boldsymbol{r}_j) = \frac{-C_4}{|\boldsymbol{r}_j - \boldsymbol{R}_i|^4}. \tag{7.4}$$

This potential also allows us to define natural length and energy scales, namely $R^* = \sqrt{2m_A C_4/\hbar^2}$ and $E^* = \hbar^4/(4m_A^2 C_4)$. Along with the choice of $\hbar = 1$ to complete our choice of units.

To treat this potential using phonon operators, we expand it in terms of the displacement operators $\boldsymbol{\delta R}_i = \boldsymbol{R}_i - \bar{\boldsymbol{R}}_i$:

$$V_{AI}(\boldsymbol{R}_i, \boldsymbol{r}_j) = V_{AI}^{(0)}(\bar{\boldsymbol{R}}_i, \delta\boldsymbol{R}_i, \boldsymbol{r}_j) + V_{AI}^{(1)}(\bar{\boldsymbol{R}}_i, \delta\boldsymbol{R}_i, \boldsymbol{r}_j) + O(\delta\boldsymbol{R}_i^2), \tag{7.5}$$

where

$$V_{AI}^{(0)}(\bar{\boldsymbol{R}}_i, \delta\boldsymbol{R}_i, \boldsymbol{r}_j) = \frac{-C_4}{|\boldsymbol{r}_j - \bar{\boldsymbol{R}}_i|^4} \tag{7.6}$$

gives the classical potential produced by the equilibrium positions of the ions and felt by the atoms, and

$$V_{AI}^{(1)}(\bar{\boldsymbol{R}}_i, \delta\boldsymbol{R}_i, \boldsymbol{r}_j) = \frac{4C_4(\boldsymbol{r}_j - \bar{\boldsymbol{R}}_i) \cdot \delta\boldsymbol{R}_i}{|\boldsymbol{r}_j - \bar{\boldsymbol{R}}_i|^6} \tag{7.7}$$

is the subsequent atom-phonon coupling. Hence, the many-body atom-ion interaction up to first order in the phonon modes is

$$H_{AI} = \sum_{ij} \left[\frac{-C_4}{|\boldsymbol{r}_j - \bar{\boldsymbol{R}}_i|^4} + \frac{4C_4(\boldsymbol{r}_j - \bar{\boldsymbol{R}}_i) \cdot \delta\boldsymbol{R}_i}{|\boldsymbol{r}_j - \bar{\boldsymbol{R}}_i|^6} \right]. \tag{7.8}$$

The term $V_{AI}^{(0)}$ produces a lattice potential felt by the atoms. Hence, we can treat the part of the Hamiltonian that contains

$$H_{\text{atom latt}} = H_{\text{atom}} + \sum_{ij} \frac{-C_4}{|\boldsymbol{r}_j - \bar{\boldsymbol{R}}_i|^4}, \tag{7.9}$$

and from this determine the atomic Bloch states, which then leaves us with the following representation:

$$H_{\text{atom latt}} = \sum_k \epsilon_{k,\beta} \hat{c}_{k,\beta}^\dagger \hat{c}_{k,\beta}, \tag{7.10}$$

where $\epsilon_{k,\beta}$ is the atomic dispersion for Bloch band index β.

7.2.4 Atom-phonon coupling

The atom-phonon coupling, resulting from the potential $V_{AI}^{(1)}$, can now be expressed in terms of the phonon and particle operators. After some maths, we arrive at

$$H_{\text{ph coup}} = \sum_{ij} \frac{4C_4(\boldsymbol{r}_j - \bar{\boldsymbol{R}}_i) \cdot \delta\boldsymbol{R}_i}{|\boldsymbol{r}_j - \bar{\boldsymbol{R}}_i|^6} = \sum_{ks\gamma\beta\beta'} \frac{\lambda_{k,s}^{(\gamma),\beta,\beta'}}{\sqrt{N_I}} b_{\gamma,s} c_{k+s,\beta}^\dagger c_{k,\beta'} + h.c., \tag{7.11}$$

where the constant $\lambda_{k,s}^{(\gamma),\beta,\beta'}$ depends only on N_I through the form of the Bloch states, and for the periodic system is found via:

$$\lambda_{k,s}^{(\gamma),\beta,\beta'} = 4C_4 \sum_n \frac{v_n^{(\gamma)} - u_n^{(\gamma)}}{\sqrt{2m_I \Omega_n / N_I}} \int d^3\boldsymbol{r} V_n(\boldsymbol{r}) \phi_k^*(\boldsymbol{r}) \phi_{k+s}(\boldsymbol{r}), \qquad (7.12)$$

where $v_n^{(s)}$, $u_n^{(s)}$ and Ω_n are parts of the phonon transformation and

$$V_n(\boldsymbol{r}) = \frac{(\boldsymbol{r}_j - \bar{\boldsymbol{R}}_i) \cdot \boldsymbol{e}_D}{|\boldsymbol{r}_j - \bar{\boldsymbol{R}}_i|^6}, \qquad (7.13)$$

where $\boldsymbol{e}_D$ is the spatial direction of the phonon mode.

Combining together all of the pieces above, we arrive at the following Hamiltonian:

$$\hat{H} = \sum_{k\beta} \epsilon_{k,\beta} \hat{c}_{k,\beta}^\dagger \hat{c}_{k,\beta} + \sum_{\mathbf{s}} \omega_s (\hat{b}_{\mathbf{s}}^\dagger \hat{b}_{\mathbf{s}} + \frac{1}{2}) + \sum_{ks\gamma\beta\beta'} \left[\frac{\lambda_{k,s}^{(\gamma),\beta,\beta'}}{\sqrt{N_I}} \hat{b}_{\mathbf{s}} \hat{c}_{k+s,\beta}^\dagger \hat{c}_{k,\beta'} + h.c. \right]. \qquad (7.14)$$

7.3   Explicit realizations

In the experiment, we have the option of two distinct setups, see Fig. 7.2. The natural choice is to place the atom and ion traps at the same origin and this choice is implicit in the equations above. The other choice is to displace the two traps from one another by a distance Δ_r, which is equivalent to using the trapping potential $V_{\text{ion trap}}(\boldsymbol{R}_i) = \frac{1}{2} m_I \omega_{\perp \text{ion}}^2 ((X_i + \Delta_r)^2 + Y_i^2)$ for the ions.

In both cases one can consider three different atom-ion combinations. The pairing of ^{6}Li-^{174}Yb$^+$ gives rise to a large mass ratio and the natural units of $E^* = 166$ kHz and $R^* = 71$ nm. The pairing ^{40}K-^{40}Ca$^+$ is more favorable in regards to trapping of the atoms as well as micromotion and has natural units of $E^* = 2.1$ kHz and $R^* = 245$ nm. The opposite mass ratio can also be achieved with a pairing of ^{40}K-^{4}Be$^+$, with the same E^* and R^* as ^{40}K-^{40}Ca$^+$.

7.3.1   Overlapping traps

If the traps have exactly the same origin (Fig. 7.2 c), then the atoms can "fall into" the wells generated by the ions. This leads to very strong atom-phonon coupling and an interesting
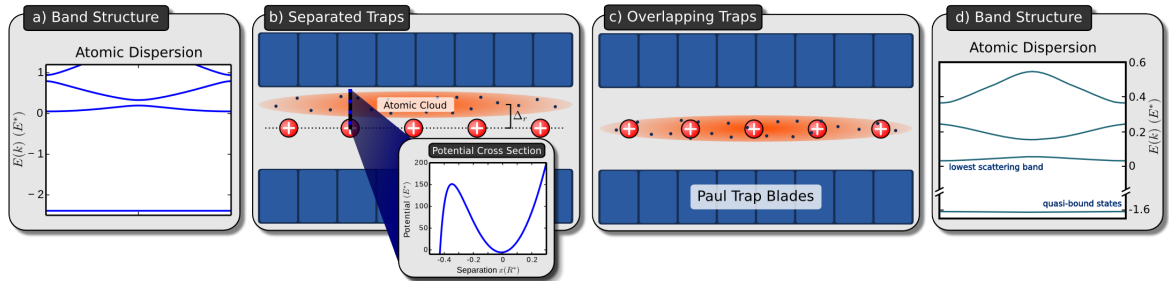

Figure 7.2: Illustration of the two setups possible and corresponding band structures in the experiment. a) b) Separated traps, where the atomic and ionic systems have the same origin. c) d) Overlapping traps, where the atomic trap is displaced a distance Δ_r perpendicularly from the ionic trap.

atomic band structure that mimics many aspects of a real solid-state material. In previous calculations the atomic bands were divided into two distinct groups: those that originate from "free" atoms that are not localized to any ion, and those that originate from the bound states of an atom-ion pair. As one can see from Fig. 7.2(d), the "bound" bands have a very flat dispersion, as well as being well separated from other bands. Hence, it is reasonable to expect that loading of the ionic lattice will populate the "scattering" bands only. Cooling should then place the atoms into the lowest of these scattering bands. However, the disadvantage of the overlapped system for experimental realization is that losses can occur from micromotion [135, 149].

7.3.2   Separated traps

By displacing the traps from one another (Fig. 7.2 b), a situation can be created which avoids the issues mentioned above. In particular, the atomic cloud does not overlap significantly with the ionic system and hence reduces the heating effects of micromotion. Also, theoretically this case is much more convenient to investigate, as the Bloch states can be well approximated by a 1D function, in the lowest transverse harmonic oscillator state of the confining potential.

Of course, to achieve such a separation requires a tight optical dipole trap, for example of the order of $\omega_{\perp,\mathrm{atom}} = 200$ kHz. Even for such a tight trap, the atoms can only be brought to within a distance $\Delta_{r,\mathrm{min}}$ of the ionic trap, otherwise no local minimal will exist in the classical ionic potential felt by the atoms. For the combination of ^{40}K-^{40}Ca$^+$ we find approximately $\Delta_{r,\mathrm{min}} = 0.55\,R^*$. An example profile of the trapping is given in Fig. 7.2(b) for a separation of $\Delta_{r,\mathrm{min}} = 0.65\,R^*$.

The band structure at the same separation is also shown in Fig. 7.2(a). One can see that the lowest band is rather narrow. However, in contrast to the overlapped trap case, we would expect the system to be prepared within this lowest band. If a cold gas of atoms in a tight tube is brought adiabatically towards the ion trap, then it is not until their wave functions overlap with the "bound" eigenstates of the ions that Landau-Zenner tunneling can take place. Hence, the atoms will remain close to the ground state and populate this lowest band.

The phonon-coupling felt by the atoms in such a configuration is illustrated in Fig. 7.3. One can show, for the approximation of a 1D system above, that the phonon mode in the $\boldsymbol{e}_y$ direction will be completely decoupled from the atomic system. As well, one can see from the coupling magnitudes in Fig. 7.3, that the longitudinal phonons are only negligibly coupled and can easily be neglected.

The atom-phonon coupling of the lowest atomic band to the transverse mode in the $\boldsymbol{e}_x$ direction ($\lambda_{k,s}^{1,1}$) is however much stronger, at least for the dominant phonon mode at $s = \pi/d$. Furthermore, the coupling, while weaker, is still present for the coupling within the second band ($\lambda_{k,s}^{2,2}$), as well as the coupling between the first and second bands ($\lambda_{k,s}^{1,2}$). Also, the different couplings have different dependencies on the atom momentum k, with the lowest band having a negligible dependence $\lambda_{k,s}^{1,1} \approx \lambda_s^{1,1} \approx \lambda_s^{1,1}\delta_{s,\pi/d}$.

7.4   Polaron transformation

To better capture the behavior of the system, we can switch to a description of polarons which consist of one atom with a local disturbance of the ion chain, by using the Lang-Firsov transformation. We note that, although Hamiltonian (7.14) has the form of a Fröhlich Hamiltonian, the structure of the coupling constant $\lambda_{k,s}^{(\gamma),\beta,\beta'}$ lends itself to a better representation
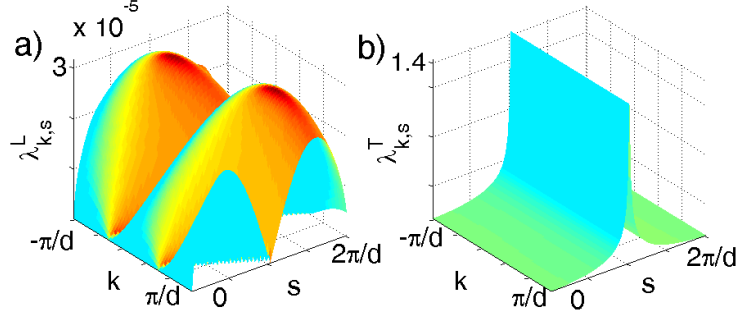
Figure 7.3: Atom-phonon coupling strengths for the periodic system and the case of separated traps ($\Delta_r = 0.75\,R^*$) within the approximation of a 1D ansatz for the atomic system. a) Coupling to the longitudinal phonon mode and b) coupling to the transversal phonon mode along the direction of the separation. Note that the coupling to the transversal phonon mode in the perpendicular direction vanishes due to the 1D approximation. The trapping frequency of the ions $\omega_{\perp,\text{ion}}$ has been tuned such that $\omega_\Delta = 30\,E^*$, which corresponds to $\omega_\Delta \approx 60$ kHz for a K-Ca$^+$ system.

in the tight binding form:

$$
\begin{aligned}
H_{\text{low energy}} = &- J \sum_{i\delta\beta} \hat{c}^\dagger_{i+\delta,\beta}\hat{c}_{i,\beta} + \sum_{\mathbf{s}} \omega_{\mathbf{s}}(\hat{b}^\dagger_{\mathbf{s}}\hat{b}_{\mathbf{s}} + \frac{1}{2}) \\
&+ \sum_{ij\gamma s} \left[\hbar\omega_{\gamma,s} M^{\gamma,\beta,\beta'}_{i,j,s} \hat{b}_{\gamma,s}\hat{c}^\dagger_i\hat{c}_j + h.c. \right],
\end{aligned}
\tag{7.15}
$$

where we have assumed that the next-nearest-neighbour bare-atom hopping terms can be neglected. The coupling

$$
M^{\gamma\beta\beta'}_{ijs} = \frac{e^{isR_i}}{\hbar\omega_{\gamma s}N_I^{3/2}} \sum_k \lambda^{\gamma\beta\beta'}_{ks} e^{ik(R_i-R_j)}
\tag{7.16}
$$

has a trivial dependence on i, and a dependence on the site separation $i-j$ that is connected directly to the k-dependence of $\lambda^{\gamma\beta\beta'}_{ks}$. When $M^{1,1}_{ijs} = M^{1,1}_{is}\delta_{ij}$, we can see that this model reduces to coupling the onsite atomic density with each boson mode. This is true only if the atom-phonon interaction does not depend on the Bloch momentum, i.e. $\lambda^{\beta,\beta'}_{k,s} = \lambda^{\beta,\beta'}_s$, which is valid for the lowest band coupling $\lambda^{\perp 1,1}_s$ in the case of separated atoms as considered here. This form then implies that the atom-phonon coupling creates or annihilates phonons, without moving the atoms. In contrast, for the first excited band, we find that $M^{2,2}_{i,j,s}$ can be well approximated by $M^{2,2}_{ijs}(\delta_{ij} + \delta_{i,j\pm1})$, leading to the presence of assisted hopping events. In fact, we may Fourier transform the atom-phonon coupling with respect to k, to determine which couplings are relevant, shown in Fig. 7.4 for the lowest two atomic bands. This is similar to obtaining the hopping coefficients J_{nn}, J_{nnn}, and so on from a Fourier transform of the atomic dispersion.

The Lang-Firsov transformation for the lowest band only, where we assume $M_{ijs} = M_{is}$, then reads:

$$
H = e^{-S}\tilde{H}e^S,
\tag{7.17}
$$

where

$$
S = \sum_{j,s} \left[M^*_{j,s}\hat{b}^\dagger_s - M_{j,s}\hat{b}_s \right] \hat{n}_j.
\tag{7.18}
$$
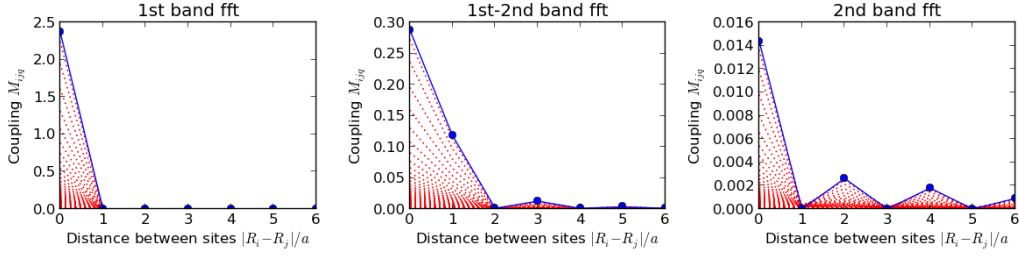
Figure 7.4: Fourier transform of the atom-phonon coupling in the transverse direction, $\sum_k \hbar\omega_s \lambda_{ks}^{\perp\beta\beta'} e^{ik(R_i - R_j)}$, which gives the value of the atom-phonon coupling in the tight-binding picture $M_{|i-j|s}^{\perp\beta\beta'}$, up to a phase factor. The Fourier transform for $s = \pi/d$ is shown in solid blue, whereas the other values of s are shown in dashed red, to illustrate the range of values that can be found. It is clear to see that the lowest band has no assisted tunneling terms, that is $M_{ijs}^{\perp1,1} = M_{is}^{\perp1,1}\delta_{ij}$. The second band coupling and the first-second band mixing show a more complicated behavior.

This results in an effective Hamiltonian of the form:

$$H = -J \sum_{i,\delta} \left(\hat{X}_{i+\delta}\hat{c}_{i+\delta}\right)^\dagger \left(\hat{X}_i\hat{c}_i\right) + \sum_s \hbar\omega_s \left(\hat{b}_s^\dagger\hat{b}_s + \frac{1}{2}\right)$$

$$-\frac{1}{2}\sum_{i\neq j}\tilde{V}_{i,j}\hat{n}_i\hat{n}_j - E_p\sum_j \hat{n}_j. \tag{7.19}$$

Here the coupling between bare atoms and bare phonons has been transformed into a coupling between polarons and polaronic-phonons via the displacement operators

$$\hat{X}_i \equiv \exp\left[\sum_s \left(M_{j,s}^*\hat{b}_s^\dagger - M_{j,s}\hat{b}_s\right)\right]. \tag{7.20}$$

The remaining terms,

$$\tilde{V}_{ij} = \sum_s \hbar\omega_s \left(M_{i,s}M_{j,s}^* + M_{i,s}^*M_{j,s}\right), \tag{7.21}$$

the phonon-mediated long-range interaction and the polaron energy shift $E_p = \frac{1}{2}V_{j,j}$, constitute an extended Hubbard model.

Hamiltonian (7.19) is equivalent to (7.15) with no approximation made to the individual terms beyond a restriction to the lowest band. However, if we consider the atom to be static in the ion crystal, then the hopping term J vanishes and Hamiltonian (7.19) can be solved exactly. In this case, the static impurity is dressed by Bogoliubov phonons and forms localized polarons. In general, when the polaron shift energy is much larger than the hopping J of the impurity, that is

$$\zeta \equiv \frac{J}{E_p} \ll 1,$$

then the impurity will be surrounded by a phonon cloud which moves together as a quasi-particle, forming a polaron in the system. Under this condition, the phonon cloud can react quickly to the moving impurity and for our experimental parameters considered here, this requirement $\zeta \equiv \frac{J}{E_p} \ll 1$ is always satisfied.

A phonon-mediated long-range interaction V_{ij} has arisen from the transformation, which typically has a very slow decay over distance and alternates sign with each site. One particular
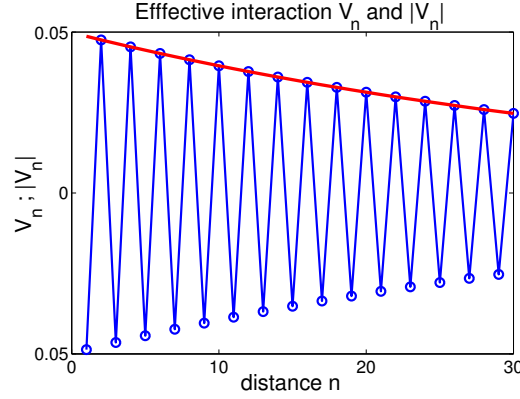
Figure 7.5: Phonon-mediated long-range interaction $V_{i,j}$ of the polaronic system resulting from realistic experimental parameters. Blue circle line: interaction $V_{i,j}$, which alternates sign with each site. Red line: absolute value of $V_{i,j}$, which has a slow exponentially decay behavior.

example, for a separated trap system, is shown in Fig. 7.5. The magnitude and slow decay are due to a very small range of phonon modes which are non-negligibly coupled to the atomic system.

The first term of the transformed Hamiltonian (7.19), which is small for current experimental parameters, describes the hopping of polarons from one site j to the neighboring site i. This hopping event can be divided into incoherent and coherent hopping processes, in which the number of phonons before and after the hopping are either changed or remain the same respectively [38]. At low temperatures $k_B T \ll E_p$, the incoherent phonon scattering is highly suppressed and the coherent transport is the most likely hopping event. In this case, the particle will hop from site to site while retaining phase coherence, and can be well aproximated by a Bloch particle which forms energy bands. On the other hand, phonons are emitted and absorbed during hopping at high temperatures $E_p \ll k_B T$ when the incoherent processes become dominant, and simple pictures of renormalised fermions break down.

Due to the small number of participating phonon modes, it is possible to perform an exact diagonalization on a small system at low temperature. However, to determine a solution for large ion or atom number, we must approximate the incoherent hopping terms that have arisen. When we consider an infinite periodic system, we may take the standard approach to approximate the incoherent processes through the use of a Markovian bath, and build a master equation. This approach only makes sense, if the number of ions is large, and there exists a continuum of phonon energies that are coupled, something which is not fulfilled in the finite sized system.

7.5 Thermodynamic limit

In this section, we consider a periodic ion chain. In this limit, the phonon modes can be assumed as continuous and the phonon number in each state is determined by a thermal average, $N_s = 1/\left(e^{\hbar\omega_s/k_B T} - 1\right)$. To approach this thermodynamic limit, we make use of a master equation formalism by treating the coupled phonon energies as an environment bath. The ions are assumed to form an infinite chain, from which the bath spectra and correlators are determined for the corresponding phonon bath at temperature T. We then consider a periodic atomic system with a finite number of atoms in each ionic period.

7.5.1 Master equation

The Hamiltonian after the Lang-Firsov transformation (7.19) represents the exact system Hamiltonian, including both the atoms and the phonons, but is better suited for an approximation of the phononic system via a bath. As mentioned previously, hopping processes in the Hamiltonian (7.19) can be distinguished as coherent processes and incoherent processes. The amplitude of all processes together is $J\langle f|\hat{X}_{i+\delta}^\dagger \hat{X}_i|i\rangle$, where $|i\rangle$ and $|f\rangle$ describe the phonon numbers in the initial and final states after polaron hopping. One can identify coherent processes $J\langle \hat{X}_{i+\delta}^\dagger \hat{X}_i\rangle c_{i+\delta}^\dagger c_i$, which do not change the number of phonons, and incoherent processes which include all remaining possibilities. To construct a master equation, we choose to approximate the phononic part of the system by a thermal bath, such that the coherent processes may be succinctly described by a renormalized hopping parameter

$$\tilde{J} = J\langle \hat{X}_{i+\delta}^\dagger \hat{X}_i\rangle_T = Je^{-S_T}, \tag{7.22}$$

where $\langle\rangle_T$ indicates a partial trace over the phonon bath at temperature T. The explicit value of S_T is

$$S_T \equiv \sum_s M_{i+\delta,s}^* M_{is} \coth\left(\frac{\hbar\omega_s}{2k_B T}\right) \tag{7.23}$$

and this will increase with temperature and atom-phonon coupling strength $|M_{i,s}|$. The increase of S_T corresponds to a decay of the polaronic hopping parameter, which indicates the increase of the effective polaron mass. We emphasize that even at zero temperature, where the phonon number in the bath is zero, the hopping parameter $\tilde{J}$ is renormalized by the virtual creation and annihilation of phonons. In our experimental setup, S_T can be varied from 0 to 0.03 at $T = 0$, and reaches 0.7 at temperature $k_B T = 200$. This allows $\tilde{J} = Je^{-S_T}$ to take values from J to $0.5J$.

With this, the system Hamiltonian, containing the fermions with coherent processes included, becomes:

$$H_S = -\tilde{J}\sum_{i,\delta} \hat{c}_{i+\delta}^\dagger \hat{c}_i - \frac{1}{2}\sum_{i\neq j} \tilde{V}_{i,j}\hat{n}_i\hat{n}_j - E_p\sum_j \hat{n}_j. \tag{7.24}$$

The Hamiltonian of the bath is simply described by

$$H_B = \sum_s \hbar\omega_s\left(\hat{b}_s^\dagger\hat{b}_s + \frac{1}{2}\right), \tag{7.25}$$

and the remaining incoherent couplings are represented by

$$H_I = -J\sum_{i,\delta} \hat{c}_{i+\delta}^\dagger \hat{c}_i\left(\hat{X}_{i+\delta}^\dagger \hat{X}_i - \langle \hat{X}_{i+\delta}^\dagger \hat{X}_i\rangle_T\right). \tag{7.26}$$

The master equation after the Born-Markov approximation can hence be written, in the interaction picture with respect to $H_0 = H_S + H_B$, as

$$\frac{d\rho(t)}{dt} = -\int_0^\infty d\tau Tr_B\left([H_I(t),[H_I(t-\tau),\rho(t)\otimes\rho_B]]\right)$$

$$= \sum_{i,\delta}\sum_{j,\delta'}\int_0^\infty d\tau\left(g_{ij}^{\delta,\delta'}(\tau,T)A_{i,\delta}(t)\left[A_{j,\delta'}(t-\tau),\rho_S(t)\right]\right.$$

$$\left. -g_{ij}^{\delta,\delta'*}(\tau,T)\left[A_{j,\delta'}(t-\tau),\rho_S(t)\right]A_{i,\delta}(t)\right), \tag{7.27}$$
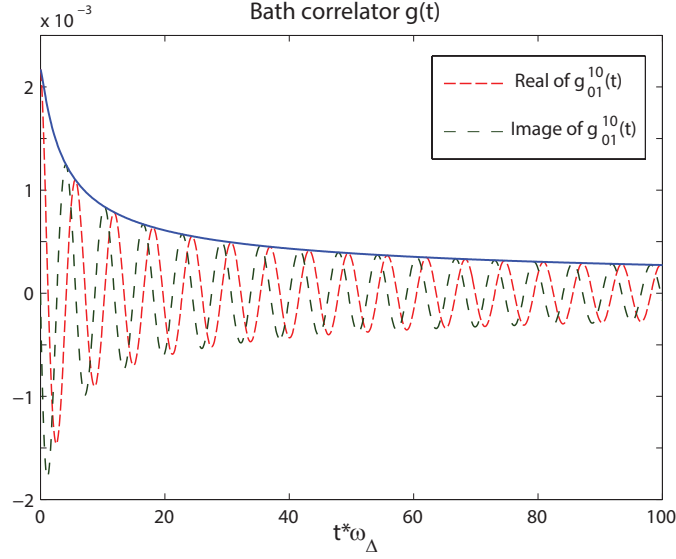
Figure 7.6: Phonon bath correlator $g_{ij}^{\delta,\delta'}(\tau, T)$ for the system in the thermodynamic limit with $i = j$, $\delta = \delta'$.

with $A_{ij}(t) \equiv -J\hat{c}_i^\dagger(t)\hat{c}_j(t)$ and the bath correlators

$$
\begin{aligned}
g_{ij}^{\delta,\delta'}(\tau, T) &= \langle \hat{X}_{i+\delta}^\dagger(\tau)\,\hat{X}_i(\tau)\,\hat{X}_{j+\delta'}^\dagger\hat{X}_j \rangle_T - -\langle \hat{X}_{i+\delta}^\dagger(\tau)\,\hat{X}_i(\tau) \rangle_T \cdot \langle \hat{X}_{j+\delta'}^\dagger\hat{X}_j \rangle_T \\
&= e^{-2S_T} \left[e^{\phi_{ij}^{\delta,\delta'}(\tau,T)} - 1 \right]
\end{aligned}
\tag{7.28}
$$

with

$$
\phi_{ij}^{\delta,\delta'}(\tau, T) = \sum_s M_{i+\delta,s}^* M_{is} \theta_{ij}^{\delta,\delta'} \left[(N_s + 1)\,e^{-i\omega_s t} + N_s e^{i\omega_s t} \right],
\tag{7.29}
$$

and

$$
\begin{aligned}
\theta_{ij}^{\delta,\delta'} &\equiv \cos\left[s\left(R_{i+\delta} - R_j\right)\right] + \cos\left[s\left(R_i - R_{j+\delta'}\right)\right] \\
&\quad - \cos\left[s\left(R_{i+\delta} - R_{j+\delta'}\right)\right] - \cos\left[s\left(R_i - R_j\right)\right].
\end{aligned}
\tag{7.30}
$$

We can continue working with the exact form of the master equation with the bath spectra $\Gamma_{ij}^{\delta,\delta'}(\omega) = \int d\tau\, e^{i\omega\tau} g_{ij}^{\delta,\delta'}(\tau, T)$. Finally, the master equation can be written down in the Lindblad form:

$$
\begin{aligned}
\mathcal{L}\left[\rho(t)\right] = &- i \left[\sum_{i,\delta} \sum_{j,\delta'} \sum_{\omega\omega'} I(\omega)\, A_{i,\delta}(\omega) A_{j,\delta'}(\omega'),\ \rho(t) \right] \\
&- \left\{ \sum_{i,\delta} \sum_{j,\delta'} \sum_{\omega\omega'} R(\omega)\, A_{i,\delta}(\omega) A_{j,\delta'}(\omega'),\ \rho(t) \right\} \\
&+ 2 \sum_{i,\delta} \sum_{j,\delta'} \sum_{\omega\omega'} R(\omega)\, A_{i,\delta}(\omega)\rho(t)\, A_{j,\delta'}(\omega'),
\end{aligned}
\tag{7.31}
$$
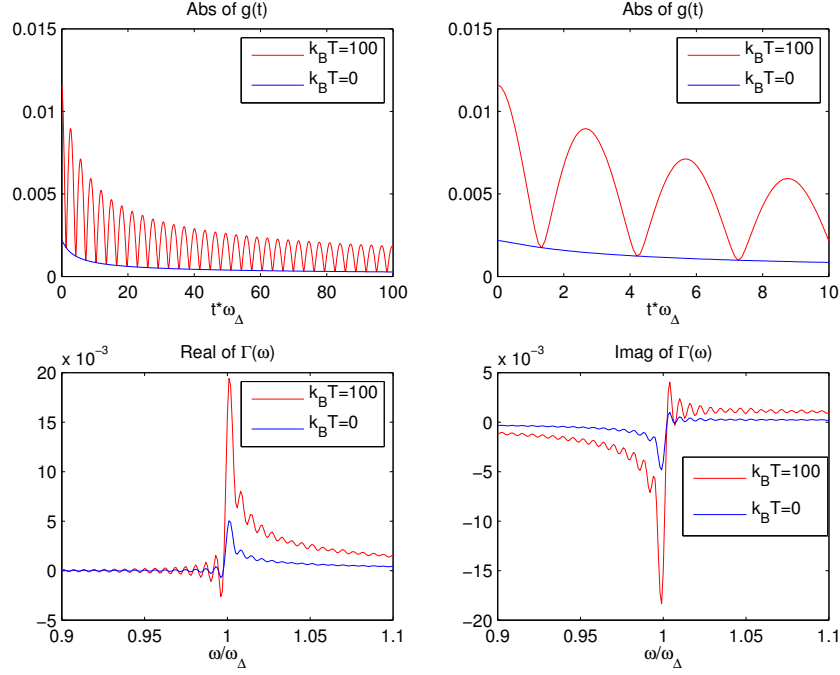
Figure 7.7: Correlation function $g(t)$ and spectra $\Gamma(\omega)$ of a thermal phonon bath at $T = 0$ and at $T = 100/k_B$. The effect of temperature only produces an overall multiplicative factor and a very high-frequency peak at $\omega = \omega_\Delta$. Parameters: $d = 8.17R^*, \Delta = 0.55R^*, \omega_\Delta = 29.7E^*$.

with $\Gamma_{ij}^{\delta,\delta'}(\omega) = R(\omega) + iI(\omega)$ and the frequency resolved operators are such that $A_{i,\delta}(\omega) = \sum_{\epsilon,\epsilon'} \Pi_\epsilon A_{i,\delta} \Pi_{\epsilon'} \delta_{\epsilon-\epsilon',\omega}$ where Π_ϵ is a projector onto eigenstates with energy ϵ. Then the master equation in the Schrödinger picture is

$$\frac{d\rho(t)}{dt} = -i[H_S, \rho(t)] + \mathcal{L}[\rho(t)]. \tag{7.32}$$

One can obtain much more information in this form, due to the spectra of $\Gamma_{ij}^{\delta,\delta'}(\omega)$, and hence also determine which excitations and transitions are important to the system. However, the disadvantage of this form is that we must work with the frequency resolved operators $A_{i,\delta}(\omega)$ which require in general the exact eigenstates of the system H_S. In the limit of a single polaron or a many-body system, we obtain a large separation of energy scales and can easily approximate these operators.

The precise values of $\Gamma_{ij}^{\delta,\delta'}(\omega)$ play an important role in determining the behavior of the system. In particular, we can separate the part $\mathrm{Re}(\Gamma_{ij}^{\delta,\delta'})$, which provides dissipative time evolution, and $\mathrm{Im}(\Gamma_{ij}^{\delta,\delta'}(\omega))$ which produces effective corrections to the energy levels of the system and hence the unitary dynamics of the master equation. We plot in Fig. 7.7 these spectra for a phonon bath at $T = 0$. Higher temperature baths produce very similar results, except for an overall multiplicative factor and a very high-frequency peak.

For the separated traps in our experiment, we can tune the separation between the ionic trap and the atomic trap Δ_r, the distance between trapped ions, and the lowest phonon energy ω_Δ. Then we can tune our system from larger J but weaker phonon coupling to stronger coupling but smaller J.

As shown in Fig. 7.7, the Fourier transformations have peaks at $\omega = \omega_\Delta$. Below this energy value, the real part, $\mathrm{Re}(\Gamma_{ij}^{\delta,\delta'})$, which corresponds to dissipation in the master equation, is almost zero, and the imaginary part, $\mathrm{Im}(\Gamma_{ij}^{\delta,\delta'})$, which corresponds to corrections to the unitary time evolution, has a small but finite value. The peak at $\omega = \omega_\Delta$ suggests that the particles can interact strongly with the phonon bath through energy differences of ω_Δ. If we only consider the lowest particle band, it is impossible to reach such regimes of energy, due to the small hopping coefficient J and narrow band width. However, if we include the hopping between lowest and second band, by choosing suitable parameters, particles can fit this energy difference by hopping between the bands.

Alternatively, we can approximate the time evolution in a similar fashion in [76], by expanding the time evolution of the system operators $c_i(t) \approx c_i - i\,[H_S, c_i]\,\tau/\hbar + O(\tau^2)$. This is valid in the quantum Brownian limit, when the bath response time is much faster than the system. This is also the validity requirement of the polaron limit, where the phonons have to move much faster than the particles. In our system, this limit is satisfied due to small hopping J for all experimental parameters. If we include this operator into the master equation, we can finally write our master equation of Brownian motion:

$$
\begin{aligned}
\frac{d\rho\,(t)}{dt} = & - i\left[H_S + J^2 \sum_{i,j} \sum_{\delta,\delta'} \Delta_{ij}^{\delta,\delta'} \hat{c}_{i+\delta}^\dagger \hat{c}_i \hat{c}_{j+\delta'}^\dagger \hat{c}_j,\ \rho\,(t)\right] \\
& - \left\{J^2 \sum_{i,j} \sum_{\delta,\delta'} \Gamma_{ij}^{\delta,\delta'} \hat{c}_{i+\delta}^\dagger \hat{c}_i \hat{c}_{j+\delta'}^\dagger \hat{c}_j,\ \rho\,(t)\right\} \\
& + 2J^2 \sum_{i,j} \sum_{\delta,\delta'} \Gamma_{ij}^{\delta,\delta'} \hat{c}_{i+\delta}^\dagger \hat{c}_i \rho\,(t)\, \hat{c}_{j+\delta'}^\dagger \hat{c}_j \\
& - J^2 \tilde{J} \sum_{i,j} \sum_{\delta,\delta'} \delta_{ij}^{\delta,\delta'} \left[\hat{c}_{i+\delta}^\dagger \hat{c}_i, \left[\left(\hat{c}_{j+\delta'\pm1}^\dagger \hat{c}_j - \hat{c}_{j+\delta'}^\dagger \hat{c}_{j\pm1}\right),\ \rho\,(t)\right]\right] \\
& - iJ^2 \tilde{J} \sum_{i,j} \sum_{\delta,\delta'} \gamma_{ij}^{\delta,\delta'} \left[\hat{c}_{i+\delta}^\dagger \hat{c}_i, \left[\left(\hat{c}_{j+\delta'\pm1}^\dagger \hat{c}_j - \hat{c}_{j+\delta'}^\dagger \hat{c}_{j\pm1}\right),\ \rho\,(t)\right]\right],
\end{aligned}
\tag{7.33}
$$

with

$$
\begin{aligned}
\Gamma_{ij}^{\delta,\delta'} &= \mathrm{Re}\left[\int_0^\infty d\tau\, g_{ij}^{\delta,\delta'}(\tau)\right]; \quad \Delta_{ij}^{\delta,\delta'} = \mathrm{Im}\left[\int_0^\infty d\tau\, g_{ij}^{\delta,\delta'}(\tau)\right]; \\
\gamma_{ij}^{\delta,\delta'} &= \mathrm{Re}\left[\int_0^\infty d\tau\, \tau g_{ij}^{\delta,\delta'}(\tau)\right]; \quad \delta_{ij}^{\delta,\delta'} = \mathrm{Im}\left[\int_0^\infty d\tau\, \tau g_{ij}^{\delta,\delta'}(\tau)\right].
\end{aligned}
\tag{7.34}
$$

7.6   Polaron induced Peierls transition

Now we consider several polarons in the system. Due to the phonon-mediated long-range interaction V_{ij} that arises from the transformation, the many-body system shows interesting behavior even without incoherent coupling to the phonon bath. As shown in Fig. 7.8, the dynamics of multiple polarons is highly sensitive to initial states due to the oscillation behavior of the induced interaction.

At low filling, the system experiences a Peierls transition due to polaron effects. The effective coherent Hamiltonian is an extended Hubbard model

$$
H_S = -\tilde{J} \sum_{<i,j>} \hat{c}_i^\dagger \hat{c}_j + \frac{1}{2} \sum_{i \neq j} \tilde{V}_{i,j} \hat{n}_i \hat{n}_j - E_p \sum_j \hat{n}_j,
\tag{7.35}
$$
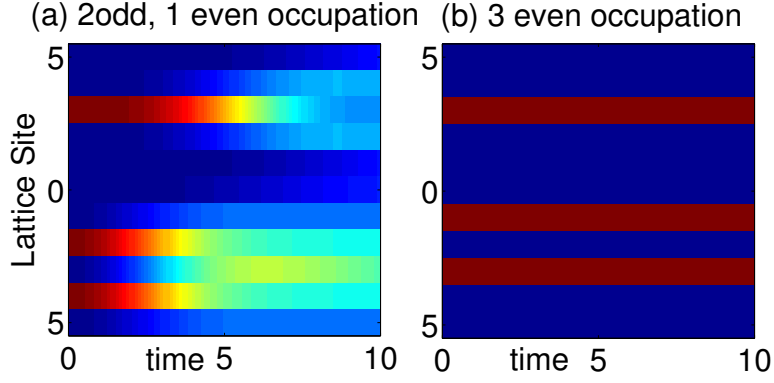
Figure 7.8: Dynamics for three polarons with different initial states. (a) Polarons hop between sites for an initial state with two odd sites and one even site occupied. (b) Polarons are localized for an initial state with three even sites occupied.

where $\tilde{V}_{i,j}$ is an induced long-range polaron-polaron interaction. In this case, the fermionic polarons will feel a new lattice potential, shifted by an effective interaction $\tilde{V}_{i,j}$. This new effective potential will be an asymmetric double potential with period $2d$. Thus the fermionic dispersion will open a gap at $k = \pi/(2d)$, which corresponds to a Peierls transition in this system. The system with half filling will support a charge density wave (CDW) phase of polarons. As shown in Fig. 7.9, this CDW phase is enhanced for larger system size due to the long-range interactions.
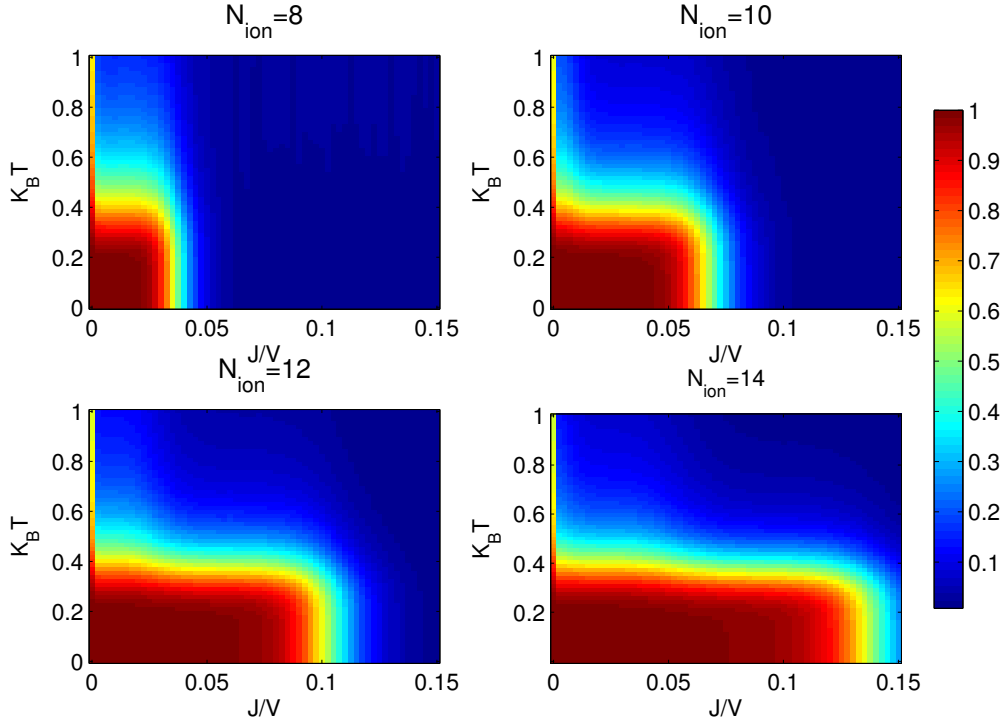
Figure 7.9: Charge density wave phase for polaron half filling, with charge density wave order $\Delta = \sum_n |\langle (n_1 - n_2) \rangle|^2 e^{-E_n/K_B T}/\Xi$.

On the other hand, the ions could also interact with a bosonic gas in our system. After the polaron transformation, the bosonic quasiparticles will feel the same effective potential as fermions. However, due to the different statistical properties, these bosonic particles will form different phases. As the impurity-phonon coupling increases, there will be a phase transition from a superfluid to a charge density wave. If the impurity-phonon coupling becomes large enough, there will be a collapse of the bosons.

In conclusion, in this chapter we consider polaronic effects in a hybrid system with trapped ions coupled to ultracold fermions. The low-energy effective Hamiltonian is based on previous work [80]. By using a Lang-Firsov transformation, we calculate the effective polaron Hamiltonian and phonon-mediated long-range interaction. We also investigate the polaronic dynamics in the thermodynamic limit and the formation of a charge density wave in a finite-sized system.

Chapter 8

Summary and Conclusion

In this thesis, I study the dynamics and polaronic effects of ultracold quantum systems with atoms and ions. In the first part, I focus on polaronic and dynamic effects in ultracold quantum systems where few impurities are interacting with a bosonic or fermionic bath. Such systems provide interesting aspects such as impurity-phonon coupling, induced long-range interactions between impurities, as well as dissipation and decoherence effects. In the second part, I study hybrid atom-ion systems and interacting quantum systems with periodic driving, such as hybrid atom-ion simulators with ions in a Paul trap. The dynamical properties of this system, as well as ionic micromotion effects, are investigated by the Floquet formalism.

Polaronic effects in ultracold quantum system

In the first part I am mainly focusing on polaronic effects in ultracold quantum systems both theoretically and numerically. Firstly we introduce the basic concepts about the polaronic system and some theory approaches. The system with impurities coupled to a BEC is studied based on a Lang-Firsov polaron transformation. We have investigated the dynamics of polarons as well as Bloch oscillations. The decoherence of Bloch oscillations due to incoherent transport has been studied by the Lindblad master equation approach. A variational method based on Gutzwiller mean-field theory is applied to investigate strongly correlated systems.

I study a two-band Hamiltonian with Fröhlich-type impurity-phonon coupling with both intra- and inter-band terms. Such a Hamiltonian is realized in experiments where few impurities are immersed in a Bose-Einstein condensate of another species. The impurities are trapped by an anisotropic optical lattice and behave as quasi-1D particles. Based on the Lang-Firsov transformation, we have derived and applied a variational two-band polaron transformation. We have calculated the coherent part of the resulting effective Hamiltonian with two (polaron) bands. In each band the impurity is dressed by phonons as a quasi-particle (polaron) with different properties. The polaronic intra-band coherent transport and polaron effective mass are both renormalized. Due to the coupling with bath, there are also induced on-site polaron energy shifts and long-range interactions between different polarons.

In order to account for the residual incoherent coupling between polaron and bath, we have derived a Lindblad master equation and focused on the single-polaron inter-band relaxation dynamics. Comparing with Fermi's Golden Rule calculations for the bare impurities, we found the renormalization of the relaxation rate to depend on the mass ratio of impurity and BEC particles. These polaronic effects in the inter-band relaxation dynamics might be observed in ongoing experiments. In the strong coupling limit of the two-band Fröhlich Hamiltonian, the impurity is *inter-band self-trapped* and can not tunnel between bands by

creating or annihilating phonons.

In another work, in order to further investigate many-polaron phenomena and novel quantum phases, we have considered a Fermi-Bose mixture, where the fermionic impurities are trapped by a 2D optical lattice and interacting with a 3D Bose-Einstein condensate. The impurity-(BEC) phonon coupling will induce effective long-range interactions between polarons. We can describe the induced interactions and hopping renormalization within an extended Hubbard model, after applying the variational Lang-Firsov polaron transformation. This system will be further studied using mean field (MF) or dynamical mean field Theory (DMFT) and is expected to show a rich interacting phase diagram.

Hybrid atom-ion quantum simulator

Another topic of this thesis is a hybrid atom-ion system with periodic driving, where the ions are confined by a Paul trap. In particular, I consider the entangled state of one ion strongly coupled to one atom and investigate the dynamical properties of this system by the Floquet formalism. The effects of heating and decoherence arising from the ionic micromotion are calculated. Also, I study the validity of the secular approximation for different atom-ion mass ratios and have derived effective descriptions of the system by including the micromotion effects. These results can be used to explain and design experiments on hybrid atom-ion simulators of this type. Additionally, periodically driven system of this kind provide exotic possibilities such as artificial gauge fields and topological phases, which can be addressed by Floquet theory and the Magnus expansion method.

Based on a previous work [80], I have studied polaronic effects in a hybrid system with a trapped ion chain coupled to one-dimensional ultracold fermions. Several solid-state models can be simulated by this system such as phonon excitation in ionic crystals and electron-phonon coupling. By using the Lang-Firsov transformation, we calculated the effective polaron hopping parameters and the phonon-mediated interaction. In the thermodynamic limit, we studied dynamical properties for the single polaron case, as well as a charge density wave phase at half filling. The decoherence effects are also studied in this system.

Zusammenfassung

Einleitung

In den letzten 20 Jahren seit der ersten Realisierung eines Bose-Einstein Kondensates im Jahr 1995 wurden im Rahmen ultrakalter Quanten physik eine Vielzahl an Phänomenen studiert. In der Welt der Quanten können selbst identische Teilchen völlig unterschiedliche Arten von Verhalten aufweisen, in starkem Kontrast zu hohen Temperaturen. Teilchen mit ganzzahligem Spin werden Bosonen genannt, Teilchen mit halbzahligem Spin sind Fermionen. Bosonen unterliegen der Bose-Einstein Statistik, nach der eine beliebige Anzahl an Teilchen den gleichen Einteilchenzustand belegen kann. Die Vielteilchen Wellenfunktion muss symmetrisch unter Vertauschung zweier beliebiger identischer Bosonen sein. Diese Symmetrieeigenschaft wird zunehmend wichtiger bei tiefen Temperaturen, wenn die Zahl der Teilchen ist groß. Unterhalb einer kritischen Temperatur kondensiert eine große Anzahl identischer Bosonen in einen einzigen Zustand, was in einem hochgradig nicht-klassischen Tieftemperatur-Phänomen resultiert.

Dieses sogenannte Bose-Einstein Kondensat (BEC) ist ein Quantenzustand, in dem eine makroskopische Anzahl von Bosonen einen einzigen Einteilchenzustand besetzt. Obwohl die theoretische Vorhersage des BEC bereits in den 1920ern von Bose und Einstein gemacht wurde, benötigte man mehr als 70 Jahre, um in Experimenten die nötigen tiefen Temperaturen und (relativ) hohen Dichten des quantenmechanisch entarteten Regimes zu erreichen. Hierzu werden die Atome zunächst mittels Laserkühlung in den Mikro-Kelvin Bereich gekühlt und dann in einer magneto-optischen Falle (MOT) gefangen. Die Temperatur wird dann weiter bis zur sogenannten „rückstoßenergie " reduziert durch Anwendung von „Polarisationsgradientenkühlung" und „Sisyphus kühlung". 1995 konnte man durch erfolgreiche Anwendung der Verdampfungskühlung die notwendige Temperaturskala von wenigen Nanokelvin bei gleichzeitig hoher Dichte erreichen. In vielen Bereichen spielt die Bose-Einstein Kondensation eine entscheidende Rolle für Suprafluidität und Supraleitung, wobeies wichtig ist anzumerken, dass es keine eindeutige Beziehung zwischen BEC und Suprafluidität gibt. So ist ein BEC, das sich wie ein ideales Gas verhält, nicht suprafluid, und ein zweidimensionales Suprafluid kein BEC.

Unter Vertauschung zweier identischer Fermionen muss der Vielteilchen-Zustand antisymmetrisch sein. Bei tiefen Temperaturen, unterhalb der Fermitemperatur, werden Fermionen „entartet", wobei beinahe jeder Zustand unterhalb der Fermienergie von einem Fermion besetzt ist und die Zustände oberhalb frei sind. Bei noch tieferen Temperaturen können auch Fermionen zu BECs, etwa durch Molekülbildung, oder durch Bildung von Cooper Paaren zu Suprafluiden werden. Im Gegensatz zu Bosonen ist es deutlich schwieriger, fermionische Atome mittels Verdampfungskühlung zu kühlen, da diese das Pauli Ausschlussprinzip einhalten müssen. Die Methode des „sympathetic cooling" erreicht die Kühlung fermionischer Atome durch Beifügen einer anderen Teilchensorte, üblicherweise ein bereits gekühltes bosonisches Gas, um durch thermische Wechselwirkung die Temperatur der Fermionen zu re-

duzieren. Sowohl molekulare Kondensate als auch Suprafluide vom Bardeen-Cooper-Schrieffer (BCS) Typ konnten mit alkalischen Fermionen realisiert werden. Dies ermöglichte die experimentelle Untersuchung stark korrelierter Vielteilchen Fermigase.

Wechselwirkungen zwischen Atomen spielen eine wichtige Rolle für Phasenübergänge in den meisten stark korrelierten Systemen. In beiden Fällen, Bosonen oder Fermionen, kann die Niedrigenergie Physik durch Kopplung an gebundene Zustände in einem anderen oder demselben Streukanal modelliert werden. Durch Änderung der Energiedifferenz zwischen Streu- und gebundenen Zuständen ist es möglich, die Größe und sogar das Vorzeichen der Zweiteilchen Streulänge (mittels sogenannter Feshbach Resonanzen) zu verändern. Beispielsweise erfährt ein zweikomponentiges Fermionengas einen Übergang von der BCS Supraflüssigkeit zum molekularen BEC durch Verringerung der Wechselwirkungen.

Systeme aus ultrakalten Atomen und Ionen können beeindruckende Erfolge in verschiedensten realisierung mit hoher Kontrollierbarkeit vorweisen. Insbesondere erreichen konnte man verschiedenste Parameter-Regimes durch regelung experimenteller Parameter, was es ermöglichte, Phasenübergänge, angeregte Zustände sowie die Dynamik von Systemen analog zur Festkörperphysik zu realisieren und zu untersuchen. Fast alle Parameter des Experiments, wie Temperatur, Teilchenzahl, Stärke und Vorzeichen der Wechselwirkung, können um mehrere Größenordnungen verändert werden.

Um die Dynamik eines komplexen Quantensystems zu verstehen und seine Eigenschaften zu untersuchen, müssen die Rechnungen entweder exakt durchgeführt werden oder durch oft unrealistische Näherungen vereinfacht werden. Selbst bei einem System mit nur zwei Zuständen pro Teilchen beträgt die Zahl der Freiheitsgrade 2^N, was selbst für kleine N unmöglich zu lösen ist. Richard Feynman schlug 1982 zuerst vor, solche komplexen Systeme durch experimentell kontrollierbare Quantensysteme zu simulieren und führte damit das Konzept der Quantensimulation ein. Durch die hohe Kontrollierbarkeit sind Systeme ultrakalter Quantengase eine der besten experimentellen Möglichkeiten für *Quantensimulatoren*.

Durch Interferenz mehrerer entgegenlaufender Laserstrahlen können periodische Potentiale für Atome erzeugt werden, die optischen Gitter. Kalte Atome in optischen Gittern können daher benutzt werden, um Festkörper zu simulieren. Der Hamiltonoperator in tiefen optischen Gittern lässt sich gut durch Modelle vom Hubbard Typ beschreiben. Verschiedene Ausrichtungen und Polarisierungen der Laser erlauben die Realisierung verschiedener Gitter-Geometrien und Dimensionen. Diese hohe Kontrolle über das System erlaubt die Simulation der Phasen und Dynamik von Quanten Vielteilchensystemen über große Parameterbereiche hinweg. Sogar rein theoretische Modelle können simuliert und validiert werden. In neuen Experimenten konnten sogar künstliche Eichfelder für neutrale Teilchen implementiert werden, sodass topologische Phasen studiert werden können.

Ein realistisches System koppelt an seine Umgebung und sollte daher als offenes System betrachtet werden. Ultrakalte Quantengase stellen eine hervorragende Toolbox dar, um die Dynamik und Dekohärenz von offenen Quantensystemen zu simulieren. Die Kopplung zwischen System und Umgebung, die in vielen Fällen als Nachteil angesehen wird, kann sogar genutzt werden, um Atome zu kühlen oder das System in gewünschte Quantenzustände zu zwingen.

Überblick

In dieser Arbeit habe ich die Dynamik und polaronischen Effekte in ultrakalten Quantensystemen mit Atomen und Ionen untersucht. Im ersten Teil liegt der Fokus auf polaronischen und dynamischen Effekten in ultrakalten Quantensystemen, in denen einige wenige Verunreinigungen oder Störstellen mit einem bosonischen oder fermionischen Bad wechselwirken. Solche Systeme zeigen interessante Effekte wie Störstellen-Phonon Kopplung, langreichweitige Wechselwirkungen zwischen Störstellen und Dissipations- und Dekohärenz-Effekte. Im zweiten Teil der Arbeit gehe ich auf wechselwirkende periodisch getriebene Quantensysteme ein, wie etwa hybride Atom-Ion Simulatoren, in denen Ionen in einer Paul Falle gefangen sind. Die Dissertation ist in acht Kapitel unterteilt. Im ersten Kapitel wird eine kurze Einführung in Quantensimulatoren gegeben und es werden die grundlegenden Konzepte vorgestellt.

In Kapitel 2 skizzieren wir zunächst die Geschichte und kürzliche Entwicklungen in Quantensimulationen und besprechen einige wichtige Themen und Hintergründe im Detail, die mit dieser Arbeit in Verbindung stehen. Wir gehen von einem einzigen neutralen Atom aus und diskutieren die Manipulationsmöglichkeiten wie Kühlung, Fallenpotentiale und geometrische Kontrolle. Danach besprechen wir Verhalten und Kontrolle von Wechselwirkungen zwischen zwei kalten Atomen im Niedrigenergie Limit. Am Ende des Kapitels besprechen wir außerdem offene Quantensysteme und die Lindblad Master-Gleichung.

In Kapitel 3 präsentieren wir einen generellen Überblick über polaronische Effekte in Bose- oder Fermi-Bädern. In dieser Arbeit fokussieren wir uns auf Systeme mit Störstellen, die mit einem bosonischen Bad wechselwirken und besprechen die theoretische Beschreibung dieser Systeme. Das bosonische Bad wird zunächst durch die Bogoliubov Approximation im Grenzfall schwacher Boson-Boson Wechselwirkungen beschrieben und danach durch die Gutzwiller Molekularfeld Näherung für alle Wechselwirkungsstärken. Außerdem besprechen wir die polaronische Dynamik in offenen Quantensystemen.

In Kapitel 4 beschränken wir uns auf die Dynamik und Erzeugung eines zwei-Band Polarons, worin eine Störstelle aus zwei Bloch Bändern mit einer „Wolke" von BEC Phononen als Quasiteilchen angereichert wird. Wir haben ein effektives Modell entwickelt und eine variationelle zwei-Band Lang-Firsov Polaron Transformation auf das System angewendet. Die kohärenten Anteile und die interband Relaxation werden beide für dieses System diskutiert.

In Kapitel 5 studieren wir ein System vieler Polaronen, die an ein BEC koppeln. Wir wenden unsere Methode auf multi-Impurity Systeme an und untersuchen die langreichweitige Wechselwirkung zwischen Polaronen. Dabei können wir die Wechselwirkung und renormierten Tunnelamplituden im Rahmen eines erweiterten Hubbard-Modells beschreiben, nach Anwendung einer Lang-Firsov Polaron Transformation. Das System wird mittels Hartree-Fock Molekularfeld-Theorie analysiert. Zukunftige Anwendung der sogenannten real-space dynamischen Molekularfeld-Theorie (R-DMFT), verspricht hier ein interessantes Phasendiagramm.

In Kapitel 6 präsentieren wir ein weiteres Thema dieser Arbeit: periodisch getriebene Systeme und hybride Atom-Ion Simulatoren. Zunächst geben wir eine Einführung in die Floquet Theorie und grundlegende Konzepte. Danach wenden wir diese Methoden auf ein hybrides Atom-Ion System an, wobei die Ionen in einer zeitabhängigen Paul Falle gefangen sind. Die Mikrobewegung der Ionen, eine Folge des zeitabhängigen Fallenpotentials, spielteine wichtige Rolle in diesen Systemen wegen Atom-Ion Kollisionen. Die Effekte von Erhitzung und Dekohärenz, die durch die ionische Mikrobewegung entstehen, wurden berechnet. Am Ende habe ich die Gültigkeit der säkularen Näherung für verschiedene Atom-Ion Massenverhältnisse untersucht und durch Inklusion der Mikrobewegungen eine effektive Beschreibung für das System hergeleitet.

In Kapitel 7 studieren wir erneut polaronische Effekte in einem hybriden Atom-Ion System mit einer Ionenkette, die an eindimensionale ultrakalte Fermionen koppelt. Verschiedene Festkörpermodelle können durch ein solches System simuliert werden, wie beispielsweise Phonon-Anregungen in ionischen Kristallen und Elektron-Phonon Kopplung. Wir berechnen die effektiven Polaron „Hüpfparameter" und die durch Phononen induzierten Wechselwirkungen im Rahmen einer Lang-Firsov Transformation. Dynamische Eigenschaften und Dekohärenz-Effekte werden für dieses System ebenfalls untersucht.

Polaronische Effekte in ultrakalten Quantensystemen

Im Bereich ultrakalter Quantenszsteme ist eine Eigenschaft von besonderer und über die letzten Jahre vermehrt zunehmender Bedeutung, da diese eine wesentliche Zutat im Vergleich zum Vorbild realer Festkörper darstellt: Phononen sowie die Atom-Phonon-Wechselwirkung. Zum einen können diese effektive Hamiltonians erzeugen, wie zum Beispiel erweiterte Hubbard Modelle oder das Holstein Model, zum anderen ergeben sich dissipative Zwei-Niveau-Systeme. Polaronische Effekte, bedingt durch Elektron-Phonon-Kopplungen, werden ebenfalls schon lange als Ursache von Hoch-T_c Supraleitung, sowohl in Ein- und Zwei-Band Festkörpersystemen, vorgeschlagen.

Im Bereich ultrakalter Quantengase sind Polaronen bereits in Systemen gefangene Ionen sowie für ein einzelnes Ion innerhalb eines entarteten Quantengases nachgewiesen worden. Weiterhin wurde das atomare Polaron bereits sowohl experimentell als auch theoretisch in Bose-Fermi- sowie Fermi-Fermi-Mischungen untersucht. Für den speziellen Fall eines Systems von atomaren Defekten innerhalb eines bosonischen Bades, koppeln diese Störungen an die bosonischen Anregungen des Bades. Bei geeigneten Parametern zeigen sich ganz allgemein polaronische Phänomene in solchen Systemen. Es existieren auch weitere Vorschläge zur Realisierung von Atom-Phonon Kopplungen und polaronischen Effekten, welche Kristalle dipolarer Moleküle, Nanoteilchen sowie hybride Atom-Ion Systeme einschließen.

Im ersten Teil werden wir den Schwerpunkt hauptsächlich auf die theoretische und numerische Beschreibung polaronische Effekte in ultrakalten Quantensystemen legen. Zuerst führen wir die grundlegenden Konzepte polaronischer Systeme ein und geben einige theoretische Ansätze. Das System von Fremdteilchen, gekoppelt an ein BEC, wird analysiert anhand einer Lang-Firsov Polaronentransformation. Wir haben die Dynamik der Polaronen sowie Bloch-Oszillationen studiert. Die Dekohärenz der Bloch-Oszillationen, bedingt durch inkohärenten Transport, wurde mittels des Ansatz einer Lindblad- Mastergleichung bestimmt. Zur Erforschung stark gekoppelter Systeme habe ich eine variationelle Methode, basierend auf der Gutzwiller Molekularfeld Theorie, verwendet.

Keine dieser vorhergehenden Arbeiten berücksichtige polaronische Phänomene von Multi-band-Systemen in ultrakalten Quantengasen. In solchen Systemen führen sowohl die inter-band als auch die intra-Band-Dynamik der Polaronen zu neuartigen Effekten ohne Entsprechung in Ein-Band Systemen. Angeregt durch neuartige Experimente betrachten wir ein System weniger Fremdatome in einem optischen Gitter, welche die beiden tiefliegendsten Blochbänder bevölkern, eingebettet in ein Bose-Einstein-Kondensat. Diese Störstellen koppeln an die Bogoliubov-Phononen (des BEC) durch intra- und inter-Band Übergänge. Wir haben einen Zwei-Band Hamiltonian mit Störstellen-Phonon Kopplungstermen vom Fröhlich-Typ analysiert. Solch ein Hamiltonian kann experimentell realisiert werden, indem einige Fremdatome in ein Bose-Einstein-Kondensat einer anderen Spezies eingebracht werden. Die Fremdatome,

welche eingefangen sind mittels eines anisotropen optischen Gitters, verhalten sich wie Quasi-1D Teilchen. Basierend auf der Lang-Firsov-Transformation, haben wir eine variationelle Zwei-Band Polaronentransformation hergeleitet und angewendet. Wir haben den kohärenten Teil des resultierenden effektiven Hamiltonians zweier polarahischer Bänder berechnet. In jedem Band wird das Fremdatom "gedresst" durch Phononen, und dadurch ein Quasiteilchen (Polaron) mit verschiedenartigen Eigenschaften. Der kohärente polaronische intra-Band-Transport und die effektive Polaronmasse sind beide renormiert. Bedingt durch die Kopplung mit dem Bad existieren auch induzierte lokale Verschiebungen der Polaronenergien, sowie langreichweitige Wechselwirkungen zwischen Polaronen.

Um der verbleibenden inkohärenten Kopplung zwischen Polaron und Bad Rechung zu tragen, haben wir eine Lindblad Mastergleichung hergeleitet und uns auf die inter-Band Relaxationsdynamik eines einzelnen Polarons konzentriert. Im Vergleich zu Berechnungen nach Fermis Goldener Regel für die unrenormierten Fremdatome haben wir herausgefunden, dass die Renormierung der Relaxationsrate von dem Massenverhältnis der Fremdteilchen und der BEC-Teilchen abhängt. Diese polaronischen Effekte der inter-Band Relaxationsdynamik könnte in gegenwärtig laufenden Experimenten beobachtet werden. Im Grenzfall starker Kopplung des Zwei-Band Fröhlich-Hamiltonians ist die Störstelle *zwischen den Bändern selbstgefangen* und kann nicht durch die Erzeugung oder Vernichtung von Phononen zwischen den Bändern tunneln.

In einer weiteren Arbeit haben wir, zur Erforschung von Multipolaron Phänomenen und neuartigen Quantenphasen, eine Fermi-Bose Mischung untersucht, bei der fermionische Störstellen in einem 2D optischen Gitter gefangen sind und mit einem 3D Bose-Einstein-Kondensat wechselwirken. Die Störstellen-(BEC) Phononenwechselwirkung wird hier langreichweitige effektive Kopplungen zwischen Polaronen induzieren. Es ist uns möglich, diese induzierten Kopplungen und die Renormierung der Hüpfamplituden nach Anwendung einer variationellen Lang-Firsov-Polaronentransformation innerhalb eines erweiterten Hubbard-Models zu beschreiben. Dieses System wird mit Hilfe der Ortsraum (real-space) Dynamischen Molekularfeld Theorie (R-DMFT) studiert, wobei ein reichhaltiges wechselwirkendes Phasendiagramm erwartet wird.

Hybrider Atom-Ion Quantensimulator

In diesem Kapitel verschieben wir unsere Aufmerksamkeit auf hybride Systeme gefangener Ionen und Atome. Gefangene ultrakalte Ionen zeichnen sich aus durch einen bemerkenwerten Grad der Kontrolle sowohl über die Präparation als auch das Auslesen von Schwingungs- und inneren Freiheitsgraden, wobei viele weitere Messgrößen auf diese zurückgeführt werden können. Die wohl bemerkenswerteste Eigenschaft ist, dass Ionensysteme einen Baustein eines universellen digitalen Quantensimulators darstellen, und es ist einzig die Einschränkung der Skalierbarkeit dieser Systeme zu einer großen Ionenanzahl, welche die Konstruktion derartiger Simulatoren noch verhindert. Das System, welches wir in dieser Arbeit betrachten, ist eigentlich ein analoger und kein digitaler Quantensimulator, aber die Vorteile der präzisen Kontrolle über die Ionen bleiben bestehen.

Ich habe Heiz- und Dekohärenzeffekte in einem hybriden Atom-Ion System studiert, in welchem die Atome und Ionen mittels einer anharmonischen und einer Paul-Falle gefangen sind. Das klassische Modell der Erwärmung weist bei diesem System eine fundamentale Grenze der Atom-Ion-Mitkühlung auf, welche durch die langreichweitige Atom-Ion-

Kopplung bedingt ist, selbst dann wenn das Atomgas sich am Temperaturnullpunkt in einer idealen dc- und rf-kompensierten Paul-Falle befindet. Das Atom verdrängt das Ion vom rf-Knotenpunkt der Falle, was zu Mikrobewegungen führt, deren Störung die Erwärmung verursacht. Ich betrachte den verschränkten Zustand eines Ions in starker Kopplung an ein Atom und untersuche die dynamischen Eigenschaften dieses Systems mittels des Floquetformalismus. Die Effekte der Erwärmung und Dekohärenz, die sich aus der ionischen Mikrobewegung ergeben, wurden dabei berechnet. Im weiteren habe ich die Gültigkeit der einfachen (bekannten) Näherung für verschiedene Atom-Ion-Massenverhältnisse studiert und habe effektive Beschreibungen des Systems unter Mitberücksichtigung der Effekte durch Mikrobewegung hergeleitet. Weiterhin eröffnen periodisch angetriebene Systeme dieser Art exotische Möglichkeiten, wie zum Beispiel künstlicher Eichfelder und topologischer Phasen, welche in der Floquet-Theorie und der Magnus-Entwicklungsmethode beschreibbar sind.

Basierend auf der vorangegangenen Arbeit [80] habe ich polaronische Effekte in einem hybriden System, bestehend aus einer gefangenen Ionenkette in Wechselwirkung mit eindimensionalen ultrakalten Fermionen studiert. Dieses hybride System von Ionen und neutralen Atomen ermöglicht aus sich heraus Phononen und eine Atom-Phonon-Wechselwirkung, die beide in einem weiten Bereich eingestellt werden können. Mehrere Festkörpermodelle lassen sich durch dieses System simulieren, wie zum Beispiel Phononanregungen in einem ionischen Kristall. Dieses System lässt sich beispielweise mit ^{6}Li Atomen und ^{174}Yb$^+$ Ionen realisieren, um ein großes Masseverhältnis zu erzeugen. Da diese (in natürlichen Einheiten) vergleichbare Längenskalen aufweisen, imitiert ein solches System die Physik des realen Festkörper Systems. Durch die Anwendung der Lang-Firsov-Transformation haben wir effektive Polaron-Hüpfamplituden sowie durch Phononen vermittelte Wechselwirkungen berechnet. Im thermodynamischen Grenzfall haben wir sowohl die dynamischen Eigenschaften eines Einzelpolarons als auch Ladungsdichtewellephasen bei Halbfüllung studiert. In diesem System haben wir auch dynamische Eigenschaften und Dekohärenzeffekte analysiert.

Appendix A

General form of Lindblad master equation

Here we consider the general form for the Lindblad equation, with the Hamiltonian $H = H_0 + H_I$. The coupling with bath H_I in interaction picture can be written as

$$H_I(t) = \sum_{\alpha,\omega} A_\alpha(\omega) B_\alpha(t) e^{-i\omega t}, \tag{A.1}$$

with

$$A_\alpha(\omega) \equiv \sum_{\epsilon'-\epsilon=\omega} \Pi(\epsilon) A_\alpha \Pi(\epsilon'); A_\alpha^\dagger(\omega) = A_\alpha(-\omega); [H_0, A_\alpha(\omega)] = -\omega A_{\alpha(\omega)}; \tag{A.2}$$

$$B_\alpha(t) = e^{iH_0 t} B_\alpha e^{-iH_0 t}, \tag{A.3}$$

where the frequency-resolved operators are such that $A_\alpha(\omega) = \sum_{\epsilon,\epsilon'} \Pi_\epsilon A_\alpha \Pi_{\epsilon'} \delta_{\epsilon-\epsilon',\omega}$, where Π_ϵ is a projector onto eigenstates with energy ϵ.

After the Born-Markov approximation, the master equation is

$$\begin{aligned}
\frac{d\rho_I(t)}{dt} &= -\int_0^\infty d\tau Tr_B\left([H_I(t),[H_I(t-\tau),\rho_I(t)\otimes\rho_B]]\right) \\
&= -\sum_{\alpha,\beta,\omega',\omega} A_\alpha(\omega') A_\beta(\omega) \rho_I(t) \int_0^\infty d\tau \langle B_\alpha(t) B_\beta(t-\tau)\rangle_R e^{-i\omega' t} e^{-i\omega(t-\tau)} + h.c. \\
&\quad + \sum_{\alpha,\beta,\omega',\omega} A_\beta(\omega) \rho_I(t) A_\alpha(\omega') \int_0^\infty d\tau \langle B_\alpha(t) B_\beta(t-\tau)\rangle_R e^{-i\omega(t-\tau)} e^{-i\omega' t} + h.c. \\
&= \sum_{\alpha,\beta,\omega',\omega} e^{-i(\omega'+\omega)t} \Gamma_{\alpha\beta}(\omega) \left(A_\beta(\omega) \rho_I(t) A_\alpha(\omega') - A_\alpha(\omega') A_\beta(\omega) \rho_I(t)\right) + h.c.,
\end{aligned} \tag{A.4}$$

with the bath correlation function $g_{\alpha\beta}(\tau)$, and its one-sided Fourier transforms:

$$g_{\alpha\beta}(\tau) \equiv \langle B_\alpha(\tau) B_\beta(0)\rangle_R = \langle B_\alpha(t) B_\beta(t-\tau)\rangle_R = Tr_B\left(B_\alpha(t) B_\beta(t-\tau)\rho_B\right), \tag{A.5}$$

and

$$\Gamma_{\alpha\beta}(\omega) = \int_0^\infty d\tau g_{\alpha\beta}(\tau) e^{i\omega\tau}. \tag{A.6}$$

In the quantum optical master equation, $\tau_s \equiv 1/\left(|\omega' - \omega|\right) \ll \tau_R$. This means the time scale of the system is intrinsic evolution τ_S is much smaller than the open system relaxation time τ_R. We can use the rotating wave approximation (RWA) to neglect the terms $\omega' \neq \omega$. This is suitable for two-level system (TLS) with flat band. However, for the two band system with band structure, a small value for $\delta_\omega = |\omega' + \omega|$ is also allowed. Then the master equation can be written as

$$\frac{d\rho_I(t)}{dt} = \sum_{\alpha,\beta,\omega,\delta_\omega} e^{-i\delta_\omega t} \Gamma_{\alpha\beta}(\omega) \left(A_\beta(\omega) \rho_I(t) A_\alpha^\dagger(\omega + \delta_\omega) - A_\alpha^\dagger(\omega + \delta_\omega) A_\beta(\omega) \rho_I(t) \right) + h.c.$$

(A.7)

It is convenient to decompose the Fourier transforms of the reservoir correlation functions as follows

$$\Gamma_{\alpha\beta}(\omega) = \frac{1}{2}\gamma_{\alpha\beta}(\omega) + iS_{\alpha\beta}(\omega),$$

(A.8)

with

$$S_{\alpha\beta}(\omega) = \frac{1}{2i}\left(\Gamma_{\alpha\beta}(\omega) - \Gamma_{\beta\alpha}^*(\omega)\right),$$

(A.9)

$$\gamma_{\alpha\beta}(\omega) = \Gamma_{\alpha\beta}(\omega) + \Gamma_{\beta\alpha}^*(\omega) = \int_{-\infty}^{\infty} d\tau e^{i\omega\tau} \langle B_\alpha^\dagger(\tau) B_\beta(0) \rangle.$$

(A.10)

Finally, the master equation in the interaction picture is:

$$\frac{d\rho_I(t)}{dt} = -i\left[H_{LS}, \rho_I(t)\right] + \mathcal{L}_I\left[\rho_I(t)\right],$$

(A.11)

with the Hermitian operator

$$H_{LS} = \sum_{\alpha,\beta,\omega,\delta_\omega} e^{-i\delta_\omega t} S_{\alpha\beta}(\omega) A_\alpha^\dagger(\omega + \delta_\omega) A_\beta(\omega),$$

(A.12)

which is called Lamb shift Hamiltonian. This term leads to a Lamb-type renormalization of the unperturbed energy levels, induced by the system-reservoir coupling. The dissipator of the master equation takes the form

$$\mathcal{L}_I\left[\rho_I(t)\right] = \sum_{\alpha,\beta,\omega,\delta_\omega} e^{-i\delta_\omega t} \gamma_{\alpha\beta}(\omega) \left(A_\beta(\omega) \rho_I A_\alpha^\dagger(\omega + \delta_\omega) - \frac{1}{2}\left\{ A_\alpha^\dagger(\omega + \delta_\omega) A_\beta(\omega), \rho_I \right\} \right).$$

(A.13)

Appendix B

Two-band transformation and coherent Hamiltonian

B.1 Two-band polaron transformation

In this section, we derive the two-band polaron transformation in detail. The transformation operator $\hat{S}$ in Eq. (4.14) can be written as $\hat{S} = \sum_{i,\alpha,\beta} \hat{C}_i^{\alpha,\beta} \hat{a}_i^{\alpha\dagger} \hat{a}_i^{\beta}$ with $\hat{C}_i^{\alpha,\beta} \equiv \sum_{\mathbf{s}} \Lambda_{\mathbf{s}}^{\alpha,\beta} e^{i\cdot\mathbf{s}\cdot\mathbf{R}_i} \left(\hat{b}_{-\mathbf{s}}^{\dagger} - \hat{b}_{\mathbf{s}} \right)$ or in matrix form as $\hat{\mathbf{C}}_i \equiv \sum_{\mathbf{s}} \Lambda_{\mathbf{s}} \left(\hat{\mathbf{b}}_{-\mathbf{s}}^{\dagger} - \hat{\mathbf{b}}_{\mathbf{s}} \right) e^{i\cdot\mathbf{s}\cdot\mathbf{R}_i}$. By using the relation $\left[\hat{a}_i^{\alpha\dagger} \hat{a}_i^{\beta}, \hat{a}_j^{\gamma} \right] = -\delta_{ij}\delta_{\alpha\gamma}\hat{a}_i^{\beta}$, which is valid for both bosons and fermions, we obtain the transformed impurity annihilation operator as:

$$\left[\hat{S}, \hat{a}_i^{\alpha} \right] = -\sum_{\beta} \left(\hat{\mathbf{C}}_i \right)_{\alpha\beta} \hat{a}_i^{\beta}; \quad \left[\hat{S}, \left[\hat{S}, \hat{a}_i^{\alpha} \right] \right] = +\sum_{\beta} \left(\hat{\mathbf{C}}_i \hat{\mathbf{C}}_i \right)_{\alpha\beta} \hat{a}_i^{\beta}; \quad \cdots ; \tag{B.1}$$

$$e^{\hat{S}} \hat{a}_i^{\alpha} e^{-\hat{S}} = \sum_{\beta} \left(e^{-\hat{\mathbf{C}}_i} \right)_{\alpha\beta} \hat{a}_i^{\beta} = \sum_{\beta} \left(\hat{\mathbf{X}}_i \right)_{\alpha\beta} \hat{a}_i^{\beta}, \tag{B.2}$$

with $\hat{\mathbf{X}}_i = e^{-\hat{\mathbf{C}}_i}$ is defined in Eq. (4.17). The phonon annihilation operators can also be transformed in a similar way as:

$$\left[\hat{S}, \hat{b}_{\mathbf{s}} \right] = \sum_{i,\alpha,\beta} \left(\left[\hat{\mathbf{C}}_i, \hat{\mathbf{b}}_{\mathbf{s}} \right] \right)_{\alpha,\beta} \hat{a}_i^{\alpha\dagger} \hat{a}_i^{\beta}; \tag{B.3}$$

$$\left[\hat{S}, \left[\hat{S}, \hat{b}_{\mathbf{s}} \right] \right] = \left[\sum_{i,\alpha,\beta} \hat{C}_i^{\alpha,\beta} \hat{a}_i^{\alpha\dagger} \hat{a}_i^{\beta}, \sum_{i',\alpha',\beta'} \left(\left[\hat{\mathbf{C}}_{i'}, \hat{\mathbf{b}}_{\mathbf{s}} \right] \right)_{\alpha',\beta'} \hat{a}_{i'}^{\alpha'\dagger} \hat{a}_{i'}^{\beta'} \right] = \sum_{i,\alpha,\beta} \left(\left[\hat{\mathbf{C}}_i, \left[\hat{\mathbf{C}}_i, \hat{\mathbf{b}}_{\mathbf{s}} \right] \right] \right)_{\alpha\beta} \hat{a}_i^{\alpha\dagger} \hat{a}_i^{\beta}; \tag{B.4}$$

$$\vdots$$

and thus

$$e^{\hat{S}} \hat{b}_{\mathbf{s}} e^{-\hat{S}} = \hat{b}_{\mathbf{s}} + \sum_{i,\alpha,\beta} \left(e^{\hat{\mathbf{C}}_i} \hat{\mathbf{b}}_{\mathbf{s}} e^{-\hat{\mathbf{C}}_i} - \hat{b}_{\mathbf{s}} \right)_{\alpha\beta} \hat{a}_i^{\alpha\dagger} \hat{a}_i^{\beta} = \hat{b}_{\mathbf{s}} + \sum_{i,\alpha,\beta} \left(\hat{\mathbf{X}}_i^{\dagger} \hat{\mathbf{b}}_{\mathbf{s}} \hat{\mathbf{X}}_i - \hat{b}_{\mathbf{s}} \right)_{\alpha\beta} \hat{a}_i^{\alpha\dagger} \hat{a}_i^{\beta}. \tag{B.5}$$

Different from the single band case, all higher commutators in Eq. (B.5) are nonzero except when $[\boldsymbol{\Lambda_s}, \boldsymbol{\Lambda_{s'}}] = 0$. The Hamiltonian is transformed as:

$$\tilde{H} = -\sum_{\langle i,j \rangle} \sum_{\alpha\beta} \left(\hat{\mathbf{X}}_i^\dagger \mathbf{J} \hat{\mathbf{X}}_j\right)_{\alpha\beta} \hat{a}_i^{\alpha\dagger} \hat{a}_j^\beta + \sum_i \sum_{\alpha\beta} \left(\hat{\mathbf{X}}_i^\dagger \varepsilon \hat{\mathbf{X}}_i\right)_{\alpha\beta} \hat{a}_i^{\alpha\dagger} \hat{a}_i^\beta$$

$$+ \sum_{\mathbf{s}} \hbar\omega_{\mathbf{s}} \left(\hat{b}_{\mathbf{s}}^\dagger + \sum_{i,\alpha,\beta} \left(\hat{\mathbf{X}}_i^\dagger \hat{\mathbf{b}}_{\mathbf{s}}^\dagger \hat{\mathbf{X}}_i - \hat{\mathbf{b}}_{\mathbf{s}}^\dagger\right)_{\alpha\beta} \hat{a}_i^{\alpha\dagger} \hat{a}_i^\beta\right) \left(\hat{b}_{\mathbf{s}} + \sum_{j,\alpha',\beta'} \left(\hat{\mathbf{X}}_j^\dagger \hat{\mathbf{b}}_{\mathbf{s}} \hat{\mathbf{X}}_j - \hat{\mathbf{b}}_{\mathbf{s}}\right)_{\alpha'\beta'} \hat{a}_j^{\alpha'\dagger} \hat{a}_j^{\beta'}\right)$$

$$+ \sum_{i,\alpha,\beta} \sum_{\mathbf{s}} \hbar\omega_{\mathbf{s}} \left(\hat{b}_{-\mathbf{s}}^\dagger + \sum_{j,\alpha',\beta'} \left(\hat{\mathbf{X}}_j^\dagger \hat{\mathbf{b}}_{-\mathbf{s}}^\dagger \hat{\mathbf{X}}_j - \hat{\mathbf{b}}_{-\mathbf{s}}^\dagger\right)_{\alpha'\beta'} \hat{a}_j^{\alpha'\dagger} \hat{a}_j^{\beta'} + \hat{b}_{\mathbf{s}} + \sum_{j,\alpha',\beta'} \left(\hat{\mathbf{X}}_j^\dagger \hat{\mathbf{b}}_{\mathbf{s}} \hat{\mathbf{X}}_j - \hat{\mathbf{b}}_{\mathbf{s}}\right)_{\alpha'\beta'} \hat{a}_j^{\alpha'\dagger} \hat{a}_j^{\beta'}\right)$$

$$\cdot \left(\hat{\mathbf{X}}_i^\dagger \mathbf{M}_{i,\mathbf{s}} \hat{\mathbf{X}}_i\right)_{\alpha\beta} \hat{a}_i^{\alpha\dagger} \hat{a}_i^\beta. \tag{B.6}$$

The resulting polaron Hamiltonian is presented in Eq. (4.20).

B.2   Coherent Hamiltonian under thermal average

For completeness, we describe a general calculation of the coherent Hamiltonian after the two-band transformation. We apply a *shorthand notation* technique, which was used by Sibley and Munn [104, 105], to our two-band system. The transformed Hamiltonian in Eq. (4.13) is complicated since it has no assumptions for the variational parameters $\boldsymbol{\Lambda_s}$ except the symmetry relations in Eq. (4.10). On the other hand, for our specific choice assuming diagonal matrices for the variational parameters, all of the expressions in this section can be shown to be straightforward and simple.

     The coherent part $\langle \tilde{H} \rangle_T$ of Eq. (4.13) can be calculated by averaging over the phonon bath. Here we assume the phonon bath is thermally distributed at the BEC temperature. From Eq. (4.13) we find these calculations require several types of thermal average values such as (I) $\langle \left(\hat{\mathbf{X}}_i^\dagger \mathbf{J} \hat{\mathbf{X}}_j\right) \rangle_T$, (II) $\langle \left(\hat{\mathbf{X}}_i^\dagger \hat{\mathbf{b}}_{\mathbf{s}}^\dagger \mathbf{M}_{i,\mathbf{s}}^\dagger \hat{\mathbf{X}}_i\right) \rangle_T$, (III) $\langle \left(\hat{\mathbf{X}}_i^\dagger \hat{\mathbf{b}}_{\mathbf{s}}^\dagger \hat{\mathbf{b}}_{\mathbf{s}} \hat{\mathbf{X}}_i\right) \rangle_T$ and (IV) $\langle \left(\hat{\mathbf{X}}_i^\dagger \hat{\mathbf{b}}_{\mathbf{s}}^\dagger \hat{\mathbf{X}}_i - \hat{\mathbf{b}}_{\mathbf{s}}^\dagger\right)_{\alpha\beta} \cdot \left(\hat{\mathbf{X}}_i^\dagger \hat{\mathbf{b}}_{\mathbf{s}} \hat{\mathbf{X}}_i - \hat{\mathbf{b}}_{\mathbf{s}}\right)_{\alpha'\beta'} \rangle_T$. Note that some terms inside $\langle (\cdots) \rangle_T$ are 2×2 matrices. Here we will discuss these terms in details, without making any assumption for the parameters $\boldsymbol{\Lambda_s}$ except that they obey the same symmetry relations as for $\mathbf{M}_s$ as given in Eq. (4.10).

Part I: $\langle \left(\hat{\mathbf{X}}_i^\dagger \mathbf{J} \hat{\mathbf{X}}_j\right) \rangle_T$ and $\langle \left(\hat{\mathbf{X}}_i^\dagger \varepsilon \hat{\mathbf{X}}_j\right) \rangle_T$

The first coherent part describes a matrix $\mathbf{J}$ or ε transformed by the operator $\hat{\mathbf{X}}_i$. We use a general 2×2 matrix $\mathcal{F}$ instead of J or ε as:

$$\langle \left(\hat{\mathbf{X}}_i^\dagger \mathcal{F} \hat{\mathbf{X}}_j\right)_{\alpha\beta} \rangle_T = \sum_{\alpha'\beta'} (\mathcal{F})_{\alpha'\beta'} \langle \left(\hat{\mathbf{X}}_i^\dagger\right)_{\alpha\alpha'} \left(\hat{\mathbf{X}}_j\right)_{\beta'\beta} \rangle_T \equiv \sum_{\alpha'\beta'} (\mathcal{F})_{\alpha'\beta'} \langle \left(e^{\hat{\mathbf{C}}_i - \hat{\mathbf{C}}_j}\right)_{\alpha\alpha';\beta'\beta} \rangle_T. \tag{B.7}$$

In the last step, we apply the shorthand notation technique and imply the index α, α' for all functions of $\hat{\mathbf{C}}_i$ and the index β', β for all functions of $\hat{\mathbf{C}}_j$ [104, 90]. This shorthand notation ignores the commutation of matrices and collects all terms of $\hat{\mathbf{C}}_i$ together and all $\hat{\mathbf{C}}_j$ together, before applying the indices. For an arbitrary operator $\hat{\mathbf{C}}$ and an arbitrary type of averaging

involved, the expansion up to the second-order cumulant reads

$$\langle \exp \hat{\mathbf{C}} \rangle_T \simeq \exp \left\{ \langle \hat{\mathbf{C}} \rangle_T + \frac{1}{2} \left(\langle \hat{\mathbf{C}}^2 \rangle_T - \langle \hat{\mathbf{C}} \rangle_T^2 \right) \right\}.$$

This expansion is exact if applied without truncation directly to equation (B.7) when the matrices $\hat{\mathbf{C}}$ commute, i.e. $[\hat{\mathbf{C}}_i, \hat{\mathbf{C}}_j] = 0$. However, we make the approximation [104, 90], that the exponential in the short-hand notation also follows such a cumulant expansion. For small deviations from community, this will be a negligible approximation. Since the operators $\hat{\mathbf{C}}_i = \sum_{\mathbf{s}} \mathbf{\Lambda}_{\mathbf{s}} e^{i \cdot \mathbf{s} \cdot \mathbf{R}_i} \left(\hat{\mathbf{b}}_{-\mathbf{s}}^\dagger - \hat{\mathbf{b}}_{\mathbf{s}} \right)$ contain only creation and annihilation operators, the coherent part $\langle \hat{\mathbf{C}} \rangle_T = 0$. In this case, we have $\langle \exp \hat{\mathbf{C}} \rangle_T \simeq \exp \left(\langle \hat{\mathbf{C}}^2 \rangle_T / 2 \right)$.

For the single band calculation, this relation reduces to the *Bloch identity* and is valid exactly [150]. However, in the two band system this relation is only an approximation because higher order terms are also present. The accuracy depends on the commutator $[\mathbf{\Lambda}_{\mathbf{s}}, \mathbf{\Lambda}_{\mathbf{s}'}]$. Here we first apply this approximation with general parameters $\mathbf{\Lambda}_{\mathbf{s}}$:

$$\langle \left(e^{\hat{\mathbf{C}}_i - \hat{\mathbf{C}}_j} \right)_{\alpha\alpha';\beta'\beta} \rangle_T \simeq \left(e^{\frac{1}{2} \langle (\hat{\mathbf{C}}_i - \hat{\mathbf{C}}_j)^2 \rangle_T} \right)_{\alpha\alpha';\beta'\beta} = \left(e^{\frac{1}{2} \langle \hat{\mathbf{C}}_i^2 \rangle_T + \frac{1}{2} \langle -\hat{\mathbf{C}}_i \hat{\mathbf{C}}_j - \hat{\mathbf{C}}_j \hat{\mathbf{C}}_i \rangle_T + \frac{1}{2} \langle \hat{\mathbf{C}}_j^2 \rangle_T} \right)_{\alpha\alpha';\beta'\beta}$$
$$= \sum_{\alpha'',\beta''} \left(e^{\frac{1}{2} \langle \hat{\mathbf{C}}_i^2 \rangle_T} \right)_{\alpha\alpha''} \left(e^{\frac{1}{2} \langle -\hat{\mathbf{C}}_i \hat{\mathbf{C}}_j - \hat{\mathbf{C}}_j \hat{\mathbf{C}}_i \rangle_T} \right)_{\alpha''\alpha';\beta'\beta''} \left(e^{\frac{1}{2} \langle \hat{\mathbf{C}}_j^2 \rangle_T} \right)_{\beta''\beta}. \tag{B.8}$$

The exponents above contain matrices $\langle \hat{\mathbf{C}}_i^2 \rangle_T$, $\langle \hat{\mathbf{C}}_j^2 \rangle_T$, $\langle \hat{\mathbf{C}}_i \hat{\mathbf{C}}_j \rangle_T$, which do not commute with each other. Fortunately, by using the shorthand notation $(\cdots)_{\alpha\alpha';\beta'\beta}$, those matrix elements with index $\alpha\alpha';\beta'\beta$ do commute between each other. They can be separated into independent exponents. Thermal averages such as $\langle \hat{\mathbf{C}}_i^2 \rangle_T$ can be calculated easily:

$$\langle \hat{\mathbf{C}}_i^2 \rangle_T = \langle \sum_{\mathbf{s}} \sum_{\mathbf{s}'} \mathbf{\Lambda}_{i,\mathbf{s}}^\dagger \mathbf{\Lambda}_{i,\mathbf{s}'} \hat{\mathbf{b}}_{\mathbf{s}}^\dagger \hat{\mathbf{b}}_{\mathbf{s}'} + \sum_{\mathbf{s}} \sum_{\mathbf{s}'} \mathbf{\Lambda}_{i,\mathbf{s}'} \mathbf{\Lambda}_{i,\mathbf{s}}^\dagger \hat{\mathbf{b}}_{\mathbf{s}'} \hat{\mathbf{b}}_{\mathbf{s}}^\dagger \rangle_T = \sum_{\mathbf{s}} \left(\mathbf{\Lambda}_{i,\mathbf{s}}^\dagger \mathbf{\Lambda}_{i,\mathbf{s}} \right) (2N_{\mathbf{s}} + 1) \tag{B.9}$$

where $N_{\mathbf{s}} \equiv (\exp(\hbar\omega_{\mathbf{s}}/k_B T) - 1)^{-1}$ is the thermally averaged phonon occupation number. The result of $\langle \hat{\mathbf{C}}_i^2 \rangle_T$ is guaranteed to be a real number because of the symmetry relations $\mathbf{\Lambda}_{i,\mathbf{s}} = \mathbf{\Lambda}_{i,-\mathbf{s}}^\dagger$. The thermal averages in Eq. (B.8) can be calculated as:

$$\langle \left(e^{\hat{\mathbf{C}}_i - \hat{\mathbf{C}}_j} \right)_{\alpha\alpha';\beta'\beta} \rangle_T \simeq \sum_{\alpha'',\beta''} \left(e^{-\sum_{\mathbf{s}} \left(N_{\mathbf{s}} + \frac{1}{2}\right) \cdot \left(\mathbf{\Lambda}_{i,\mathbf{s}}^\dagger \mathbf{\Lambda}_{i,\mathbf{s}} \right)} \right)_{\alpha\alpha''} \left(e^{\sum_{\mathbf{s}} (2N_{\mathbf{s}} + 1) \left(\mathbf{\Lambda}_{i,\mathbf{s}}^\dagger \mathbf{\Lambda}_{j,\mathbf{s}} \right)} \right)_{\alpha''\alpha';\beta'\beta''}$$
$$\cdot \left(e^{-\sum_{\mathbf{s}} \left(N_{\mathbf{s}} + \frac{1}{2}\right) \cdot \left(\mathbf{\Lambda}_{j,\mathbf{s}}^\dagger \mathbf{\Lambda}_{j,\mathbf{s}} \right)} \right)_{\beta''\beta}. \tag{B.10}$$

The first and third term are easy to calculate. Then we expand the middle exponential under the shorthand notation $(\cdots)_{\alpha''\alpha';\beta'\beta''}$:

$$\left(e^{\sum_{\mathbf{s}} (2N_{\mathbf{s}} + 1) \left(\mathbf{\Lambda}_{i,\mathbf{s}}^\dagger \mathbf{\Lambda}_{j,\mathbf{s}} \right)} \right)_{\alpha''\alpha';\beta'\beta''} = \delta_{\alpha''\alpha'} \delta_{\beta'\beta''} + \frac{1}{1!} \sum_{\mathbf{s}} (2N_{\mathbf{s}} + 1) \left(\mathbf{\Lambda}_{i,\mathbf{s}}^\dagger \right)_{\alpha''\alpha'} (\mathbf{\Lambda}_{j,\mathbf{s}})_{\beta'\beta''}$$
$$+ \frac{1}{2!} \sum_{\mathbf{s}\mathbf{s}'} (2N_{\mathbf{s}} + 1)(2N_{\mathbf{s}'} + 1) \left(\mathbf{\Lambda}_{i,\mathbf{s}}^\dagger \mathbf{\Lambda}_{i,\mathbf{s}'}^\dagger \right)_{\alpha''\alpha'} (\mathbf{\Lambda}_{j,\mathbf{s}} \mathbf{\Lambda}_{j,\mathbf{s}'})_{\beta'\beta''} + \cdots$$
$$+ \frac{1}{k!} \sum_{\mathbf{s}\mathbf{s}'\cdots\mathbf{s}^{(k-1)}} \underbrace{(2N_{\mathbf{s}} + 1) \cdots (2N_{\mathbf{s}^{(k-1)}} + 1)}_{k} \underbrace{\left(\mathbf{\Lambda}_{i,\mathbf{s}}^\dagger \mathbf{\Lambda}_{i,\mathbf{s}'}^\dagger \cdots \mathbf{\Lambda}_{i,\mathbf{s}^{(k-1)}}^\dagger \right)_{\alpha''\alpha'}}_{k} \underbrace{\left(\mathbf{\Lambda}_{j,\mathbf{s}} \mathbf{\Lambda}_{j,\mathbf{s}'} \cdots \mathbf{\Lambda}_{j,\mathbf{s}^{(k-1)}} \right)_{\beta'\beta''}}_{k}.$$
$$\tag{B.11}$$

In each term, we combine elements with the same momentum $\mathbf{s}$:

$$
\left(e^{\sum_{\mathbf{s}}(2N_{\mathbf{s}}+1)\left(\boldsymbol{\Lambda}_{i,\mathbf{s}}^{\dagger}\boldsymbol{\Lambda}_{j,\mathbf{s}}\right)} \right)_{\alpha''\alpha';\beta'\beta''} = \delta_{\alpha''\alpha'}\delta_{\beta'\beta''} + \frac{1}{1!}\sum_{\mathbf{s}}(2N_{\mathbf{s}}+1)\left(\boldsymbol{\Lambda}_{i,\mathbf{s}}^{\dagger}\right)_{\alpha''\alpha'}(\boldsymbol{\Lambda}_{j,\mathbf{s}})_{\beta'\beta''}
$$

$$
+ \frac{1}{2!}\sum_{\alpha^{(3)},\beta^{(3)}}\left(\sum_{\mathbf{s}}(2N_{\mathbf{s}}+1)\left(\boldsymbol{\Lambda}_{i,\mathbf{s}}^{\dagger}\right)_{\alpha''\alpha^{(3)}}(\boldsymbol{\Lambda}_{j,\mathbf{s}})_{\beta'\beta^{(3)}}\right)\left(\sum_{\mathbf{s}'}(2N_{\mathbf{s}'}+1)\left(\boldsymbol{\Lambda}_{i,\mathbf{s}'}^{\dagger}\right)_{\alpha^{(3)}\alpha'}(\boldsymbol{\Lambda}_{j,\mathbf{s}'})_{\beta^{(3)}\beta''}\right) + \cdots
$$

$$
+ \frac{1}{k!}\underbrace{\sum_{\alpha^{(3)},\beta^{(3)}}\cdots\sum_{\alpha^{(k+1)},\beta^{(k+1)}}}_{k-1}
$$

$$
\cdot\underbrace{\left(\sum_{\mathbf{s}}(2N_{\mathbf{s}}+1)\left(\boldsymbol{\Lambda}_{i,\mathbf{s}}^{\dagger}\right)_{\alpha''\alpha^{(3)}}(\boldsymbol{\Lambda}_{j,\mathbf{s}})_{\beta'\beta^{(3)}}\right)\cdots\left(\sum_{\mathbf{s}^{(k-1)}}(2N_{\mathbf{s}^{(k-1)}}+1)\left(\boldsymbol{\Lambda}_{i,\mathbf{s}^{(k-1)}}^{\dagger}\right)_{\alpha^{(k+1)}\alpha'}\left(\boldsymbol{\Lambda}_{j,\mathbf{s}^{(k-1)}}\right)_{\beta^{(k+1)}\beta''}\right)}_{k}
$$

$$\tag{B.12}$$

In order to simplify the last part in Eq. (B.12), we define 4th rank tensors $\mathbf{G}_{ij}$ with elements:

$$
(\mathbf{G}_{ij})_{\alpha''\alpha'\beta'\beta''} \equiv \sum_{\mathbf{s}}(2N_{\mathbf{s}}+1)\left(\boldsymbol{\Lambda}_{i,\mathbf{s}}^{\dagger}\right)_{\alpha''\alpha'}(\boldsymbol{\Lambda}_{j,\mathbf{s}})_{\beta'\beta''}, \tag{B.13}
$$

and

$$
\left(\mathbf{G}_{ij}^{2}\right)_{\alpha\alpha'\beta\beta'} \equiv \sum_{\alpha''\beta''}(\mathbf{G}_{ij})_{\alpha\alpha''\beta\beta''}(\mathbf{G}_{ij})_{\alpha''\alpha'\beta''\beta'}. \tag{B.14}
$$

Then the Eq. (B.12) can be written as:

$$
\left(e^{\sum_{\mathbf{s}}(2N_{\mathbf{s}}+1)\left(\boldsymbol{\Lambda}_{i,\mathbf{s}}^{\dagger}\boldsymbol{\Lambda}_{j,\mathbf{s}}\right)} \right)_{\alpha''\alpha';\beta'\beta''}
$$

$$
= \delta_{\alpha''\alpha'}\delta_{\beta'\beta''} + \frac{1}{1!}(\mathbf{G}_{ij})_{\alpha''\alpha'\beta'\beta''} + \frac{1}{2!}\left(\mathbf{G}_{ij}^{2}\right)_{\alpha''\alpha'\beta'\beta''} + \frac{1}{k!}\left(\mathbf{G}_{ij}^{k}\right)_{\alpha''\alpha'\beta'\beta''}
$$

$$
= \left(e^{\mathbf{G}_{ij}} \right)_{\alpha''\alpha'\beta'\beta''}, \tag{B.15}
$$

where $\left(e^{\mathbf{G}_{ij}} \right)$ are also 4th rank tensors.

The tensors $\mathbf{G}_{ij}$ involve only numbers, and thus $\left(e^{\mathbf{G}_{ij}} \right)$ can be calculated exactly. Finally, the first thermal average term can be calculated as:

$$
\langle\left(\hat{\mathbf{X}}_{i}^{\dagger}\mathcal{F}\hat{\mathbf{X}}_{j}\right)_{\alpha\beta}\rangle_{T} = \sum_{\alpha'\beta'}(\mathcal{F})_{\alpha'\beta'}\langle\left(e^{\hat{\mathbf{C}}_{i}-\hat{\mathbf{C}}_{j}}\right)_{\alpha\alpha';\beta'\beta}\rangle_{T}
$$

$$
\langle\left(e^{\hat{\mathbf{C}}_{i}-\hat{\mathbf{C}}_{j}}\right)_{\alpha\alpha';\beta'\beta}\rangle_{T} = \sum_{\alpha'',\beta''}\left(e^{-\sum_{\mathbf{s}}\left(N_{\mathbf{s}}+\frac{1}{2}\right)\cdot\left(\boldsymbol{\Lambda}_{i,\mathbf{s}}^{\dagger}\boldsymbol{\Lambda}_{i,\mathbf{s}}\right)}\right)_{\alpha\alpha''}\left(e^{\mathbf{G}_{ij}}\right)_{\alpha''\alpha'\beta'\beta''}\left(e^{-\sum_{\mathbf{s}}\left(N_{\mathbf{s}}+\frac{1}{2}\right)\cdot\left(\boldsymbol{\Lambda}_{j,\mathbf{s}}^{\dagger}\boldsymbol{\Lambda}_{j,\mathbf{s}}\right)}\right)_{\beta''\beta}.
$$

$$\tag{B.16}$$

Part II: $\langle \left(\hat{\mathbf{X}}_i^\dagger \hat{\mathbf{b}}_{\mathbf{s}}^\dagger \mathbf{M}_{i,\mathbf{s}}^\dagger \hat{\mathbf{X}}_i \right) \rangle_T$

Here we calculate the second type of thermal averages by the relation $f(x=1) = \int_0^1 f'(x) \, dx + f(x=0)$:

$$
\langle \left(\hat{\mathbf{X}}_i^\dagger \hat{\mathbf{b}}_{\mathbf{s}}^\dagger \mathbf{M}_{i,\mathbf{s}}^\dagger \hat{\mathbf{X}}_i \right) \rangle_T = \langle \left(e^{\hat{\mathbf{C}}_i} \hat{\mathbf{b}}_{\mathbf{s}}^\dagger e^{-\hat{\mathbf{C}}_i} \right) \left(e^{\hat{\mathbf{C}}_i} \mathbf{M}_{i,\mathbf{s}}^\dagger e^{-\hat{\mathbf{C}}_i} \right) \rangle_T
$$

$$
= \langle \int_0^1 dx \frac{d}{dx} \left(e^{x\hat{\mathbf{C}}_i} \hat{\mathbf{b}}_{\mathbf{s}}^\dagger e^{-x\hat{\mathbf{C}}_i} e^{\hat{\mathbf{C}}_i} \mathbf{M}_{i,\mathbf{s}}^\dagger e^{-\hat{\mathbf{C}}_i} \right) \rangle_T + \langle \hat{\mathbf{b}}_{\mathbf{s}}^\dagger e^{\hat{\mathbf{C}}_i} \mathbf{M}_{i,\mathbf{s}}^\dagger e^{-\hat{\mathbf{C}}_i} \rangle_T
$$

$$
= - \int_0^1 dx \langle e^{x\hat{\mathbf{C}}_i} \mathbf{\Lambda}_{i,\mathbf{s}} e^{-x\hat{\mathbf{C}}_i} e^{\hat{\mathbf{C}}_i} \mathbf{M}_{i,\mathbf{s}}^\dagger e^{-\hat{\mathbf{C}}_i} \rangle_T + \langle \hat{\mathbf{b}}_{\mathbf{s}}^\dagger e^{\hat{\mathbf{C}}_i} \mathbf{M}_{i,\mathbf{s}}^\dagger e^{-\hat{\mathbf{C}}_i} \rangle_T \tag{B.17}
$$

where we have used the relation $\left[\hat{\mathbf{C}}_i, \ \hat{\mathbf{b}}_{\mathbf{s}}^\dagger \right] = -\mathbf{\Lambda}_{i,\mathbf{s}}$. The first term can be calculated by separating out the bath terms:

$$
\langle \left(e^{x\hat{\mathbf{C}}_i} \mathbf{\Lambda}_{i,\mathbf{s}} e^{-x\hat{\mathbf{C}}_i} e^{\hat{\mathbf{C}}_i} \mathbf{M}_{i,\mathbf{s}}^\dagger e^{-\hat{\mathbf{C}}_i} \right)_{\alpha\beta} \rangle_T
$$

$$
= \sum_{\alpha'\gamma\gamma'\beta'} \langle \left(e^{x\hat{\mathbf{C}}_i} \right)_{\alpha\alpha'} (\mathbf{\Lambda}_{i,\mathbf{s}})_{\alpha'\gamma} \left(e^{(1-x)\hat{\mathbf{C}}_i} \right)_{\gamma\gamma'} \left(\mathbf{M}_{i,\mathbf{s}}^\dagger \right)_{\gamma'\beta'} \left(e^{-\hat{\mathbf{C}}_i} \right)_{\beta'\beta} \rangle_T
$$

$$
= \sum_{\alpha'\gamma\gamma'\beta'} (\mathbf{\Lambda}_{i,\mathbf{s}})_{\alpha'\gamma} \left(\mathbf{M}_{i,\mathbf{s}}^\dagger \right)_{\gamma'\beta'} \cdot \langle \left(e^{x\hat{\mathbf{C}}_i} \right)_{\alpha\alpha'} \left(e^{(1-x)\hat{\mathbf{C}}_i} \right)_{\gamma\gamma'} \left(e^{-\hat{\mathbf{C}}_i} \right)_{\beta'\beta} \rangle_T. \tag{B.18}
$$

This element can be calculated by the same method as we applied for $\langle \left(e^{\hat{\mathbf{C}}_i} \right)_{\alpha\alpha'} \left(e^{-\hat{\mathbf{C}}_j} \right)_{\beta'\beta} \rangle_T$ in the previous section. Under the same shorthand notation:

$$
\langle \left(e^{x\hat{\mathbf{C}}_i} \right)_{\alpha\alpha'} \left(e^{(1-x)\hat{\mathbf{C}}_j} \right)_{\gamma\gamma'} \left(e^{-\hat{\mathbf{C}}_k} \right)_{\beta'\beta} \rangle_T = \langle \left(e^{x\hat{\mathbf{C}}_i + (1-x)\hat{\mathbf{C}}_j - \hat{\mathbf{C}}_k} \right)_{\alpha\alpha';\gamma\gamma';\beta'\beta} \rangle_T
$$

$$
\simeq \left(e^{\frac{1}{2}\langle \left(x\hat{\mathbf{C}}_i + (1-x)\hat{\mathbf{C}}_j - \hat{\mathbf{C}}_k \right)^2 \rangle_T} \right)_{\alpha\alpha';\gamma\gamma';\beta'\beta}
$$

$$
= \sum_{\alpha^2\alpha^3} \sum_{\gamma^2\gamma^3} \sum_{\beta^2\beta^3} \left(e^{\frac{1}{2}\langle x^2\hat{\mathbf{C}}_i^2 \rangle_T} \right)_{\alpha\alpha^{(2)}} \left(e^{\frac{1}{2}\langle (1-x)^2\hat{\mathbf{C}}_j^2 \rangle_T} \right)_{\gamma\gamma^{(2)}} \left(e^{\frac{1}{2}\langle \hat{\mathbf{C}}_k^2 \rangle_T} \right)_{\beta'\beta^{(2)}}
$$

$$
\cdot \left(e^{\frac{1}{2}\langle x\hat{\mathbf{C}}_i(1-x)\hat{\mathbf{C}}_j \rangle_T} \right)_{\alpha^{(2)}\alpha^{(3)};\gamma^{(2)}\gamma^{(3)}} \left(e^{-\frac{1}{2}\langle x\hat{\mathbf{C}}_i\hat{\mathbf{C}}_k \rangle_T} \right)_{\alpha^{(3)}\alpha';\beta^{(2)}\beta^{(3)}} \left(e^{-\frac{1}{2}\langle (1-x)\hat{\mathbf{C}}_j\hat{\mathbf{C}}_k \rangle_T} \right)_{\gamma^{(3)}\gamma';\beta^{(3)}\beta} \tag{B.19}
$$

with α, β, γ applied separately for $x\hat{\mathbf{C}}_i$, $(1-x)\hat{\mathbf{C}}_j$ and $-\hat{\mathbf{C}}_k$. We have introduced the different indices i, j and k so that we can keep track of the terms required in applying the short-hand notation. In the end, we will set $i = j = k$ to recover the desired result. Using the results from the previous section, these thermal averages will be:

$$
\langle \left(e^{x\hat{\mathbf{C}}_i} \right)_{\alpha\alpha'} \left(e^{(1-x)\hat{\mathbf{C}}_i} \right)_{\gamma\gamma'} \left(e^{-\hat{\mathbf{C}}_i} \right)_{\beta'\beta} \rangle_T
$$

$$
= \sum_{\alpha^2\alpha^3} \sum_{\gamma^2\gamma^3} \sum_{\beta^2\beta^3} \left(e^{-\sum_{\mathbf{s}}\left(N_{\mathbf{s}}+\frac{1}{2}\right)\cdot x^2 \cdot \mathbf{\Lambda}_{\mathbf{s}}^\dagger \mathbf{\Lambda}_{\mathbf{s}}} \right)_{\alpha\alpha^2} \left(e^{-\sum_{\mathbf{s}}\left(N_{\mathbf{s}}+\frac{1}{2}\right)\cdot(1-x)^2 \cdot \mathbf{\Lambda}_{\mathbf{s}}^\dagger \mathbf{\Lambda}_{\mathbf{s}}} \right)_{\gamma\gamma^2} \left(e^{-\sum_{\mathbf{s}}\left(N_{\mathbf{s}}+\frac{1}{2}\right)\cdot \mathbf{\Lambda}_{\mathbf{s}}^\dagger \mathbf{\Lambda}_{\mathbf{s}}} \right)_{\beta'\beta^2}
$$

$$
\cdot \left(e^{-x(1-x)\mathbf{G}_{ij}} \right)_{\alpha^{(2)}\alpha^{(3)}\gamma\gamma^{(3)}} \left(e^{x\mathbf{G}_{ik}} \right)_{\alpha^{(3)}\alpha'\beta^{(2)}\beta^{(3)}} \left(e^{(1-x)\mathbf{G}_{jk}} \right)_{\gamma^{(3)}\gamma'\beta^{(3)}\beta} \tag{B.20}
$$

with $\mathbf{G}_{ij}$ from Eq. (B.13).

On the other hand, the second term $\langle \hat{\mathbf{b}}_{\mathbf{s}}^\dagger e^{\hat{\mathbf{C}}_i} \mathbf{M}_{i,\mathbf{s}}^\dagger e^{-\hat{\mathbf{C}}_i} \rangle_T$ in Eq. (B.17) can be calculated as:

$$
\langle \left(\hat{\mathbf{b}}_{\mathbf{s}}^\dagger e^{\hat{\mathbf{C}}_i} \mathbf{M}_{i,\mathbf{s}}^\dagger e^{-\hat{\mathbf{C}}_i} \right)_{\alpha\beta} \rangle_T = \sum_{\alpha'\beta'} \left(\mathbf{M}_{i,\mathbf{s}}^\dagger \right)_{\alpha'\beta'} \langle \hat{b}_{\mathbf{s}}^\dagger \left(e^{\hat{\mathbf{C}}_i - \hat{\mathbf{C}}_i} \right)_{\alpha\alpha';\beta'\beta} \rangle_T. \tag{B.21}
$$

From the results in [105], the elements such as $\langle \hat{\mathbf{b}}_{\mathbf{s}}^{\dagger} \left(e^{\hat{\mathbf{C}}_i - \hat{\mathbf{C}}_i} \right) \rangle_T$ can be obtained by differentiating $\left(e^{\hat{\mathbf{C}}_i - \hat{\mathbf{C}}_i} \right)$ before taking the thermal average. On the other hand, since the thermal average only involves the phonon degrees of freedom, we can switch the order and differentiate $\langle \left(e^{\hat{\mathbf{C}}_i - \hat{\mathbf{C}}_i} \right) \rangle_T$ after taking the thermal average. By comparing the two steps, we obtain the relation:

$$\langle \hat{\mathbf{b}}_{\mathbf{s}}^{\dagger} \left(e^{\hat{\mathbf{C}}_i - \hat{\mathbf{C}}_i} \right) \rangle_T = -\langle \hat{\mathbf{b}}_{\mathbf{s}}^{\dagger} \sum_{\mathbf{s}'} \mathbf{\Lambda}_{i,\mathbf{s}'} \hat{\mathbf{b}}_{\mathbf{s}'} \rangle_T \langle \left(e^{\hat{\mathbf{C}}_i - \hat{\mathbf{C}}_i} \right) \rangle_T + \langle \left(e^{\hat{\mathbf{C}}_i - \hat{\mathbf{C}}_i} \right) \rangle_T \langle \hat{\mathbf{b}}_{\mathbf{s}}^{\dagger} \sum_{\mathbf{s}'} \mathbf{\Lambda}_{i,\mathbf{s}'} \hat{\mathbf{b}}_{\mathbf{s}'} \rangle_T, \quad \text{(B.22)}$$

which can be calculated by the results in Eq. (B.16). As an example, we show a simplified calculation in Eq.(C.11), where the transformation matrices $\mathbf{\Lambda}_{i,\mathbf{s}}$ are diagonal.

We finally obtain the second term in Eq. (B.17):

$$\langle \hat{\mathbf{b}}_{\mathbf{s}}^{\dagger} e^{\hat{\mathbf{C}}_i} \mathbf{M}_{i,\mathbf{s}}^{\dagger} e^{-\hat{\mathbf{C}}_i} \rangle_T$$
$$= \sum_{\alpha'\beta'} N_{\mathbf{s}} \left(\mathbf{M}_{i,\mathbf{s}}^{\dagger} \right)_{\alpha'\beta'} \left[\sum_{\alpha''} (-\mathbf{\Lambda}_{i,\mathbf{s}})_{\alpha\alpha''} \langle \left(e^{\hat{\mathbf{C}}_i - \hat{\mathbf{C}}_i} \right)_{\alpha''\alpha';\beta'\beta} \rangle_T + \sum_{\beta''} \langle \left(e^{\hat{\mathbf{C}}_i - \hat{\mathbf{C}}_i} \right)_{\alpha\alpha';\beta'\beta''} \rangle_T (\mathbf{\Lambda}_{i,\mathbf{s}})_{\beta''\beta} \right]. \quad \text{(B.23)}$$

Part III: $\langle \left(\hat{\mathbf{X}}_i^{\dagger} \hat{\mathbf{b}}_{\mathbf{s}}^{\dagger} \hat{\mathbf{b}}_{\mathbf{s}} \hat{\mathbf{X}}_i \right) \rangle_T$

This term can be calculated by a similar integral method as in the previous section:

$$\langle \left(\hat{\mathbf{X}}_i^{\dagger} \hat{\mathbf{b}}_{\mathbf{s}}^{\dagger} \hat{\mathbf{b}}_{\mathbf{s}} \hat{\mathbf{X}}_i \right) \rangle_T = \int_0^1 dy \langle \frac{d}{dy} \left(e^{y\hat{\mathbf{C}}_i} \hat{\mathbf{b}}_{\mathbf{s}}^{\dagger} \hat{\mathbf{b}}_{\mathbf{s}} e^{-y\hat{\mathbf{C}}_i} \right) \rangle_T + \langle \hat{\mathbf{b}}_{\mathbf{s}}^{\dagger} \hat{\mathbf{b}}_{\mathbf{s}} \rangle_T$$
$$= -\int_0^1 dy \langle e^{y\hat{\mathbf{C}}_i} \hat{\mathbf{b}}_{\mathbf{s}}^{\dagger} \mathbf{\Lambda}_{i,\mathbf{s}}^{\dagger} e^{-y\hat{\mathbf{C}}_i} + h.c. \rangle_T + \langle \hat{\mathbf{b}}_{\mathbf{s}}^{\dagger} \hat{\mathbf{b}}_{\mathbf{s}} \rangle_T \quad \text{(B.24)}$$

Here the thermal average $\langle e^{y\hat{\mathbf{C}}_i} \hat{\mathbf{b}}_{\mathbf{s}}^{\dagger} \mathbf{\Lambda}_{i,\mathbf{s}}^{\dagger} e^{-y\hat{\mathbf{C}}_i} \rangle_T$ can be obtained by changing $\hat{\mathbf{C}}_i$ to $y\hat{\mathbf{C}}_i$ and $\mathbf{M}_{i,\mathbf{s}}$ to $\mathbf{\Lambda}_{i,\mathbf{s}}$ in Eq. (B.17):

$$\langle \left(e^{y\hat{\mathbf{C}}_i} \hat{\mathbf{b}}_{\mathbf{s}}^{\dagger} \mathbf{\Lambda}_{i,\mathbf{s}}^{\dagger} e^{-y\hat{\mathbf{C}}_i} \right)_{\alpha\beta} \rangle_T$$
$$= -\int_0^1 dx \left[\sum_{\alpha'\gamma\gamma'\beta'} y (\mathbf{\Lambda}_{i,\mathbf{s}})_{\alpha'\gamma} \left(\mathbf{\Lambda}_{i,\mathbf{s}}^{\dagger} \right)_{\gamma'\beta'} \cdot \langle \left(e^{xy\hat{\mathbf{C}}_i} \right)_{\alpha\alpha'} \left(e^{(1-x)y\hat{\mathbf{C}}_i} \right)_{\gamma\gamma'} \left(e^{-y\hat{\mathbf{C}}_i} \right)_{\beta'\beta} \rangle_T \right]$$
$$+ N_{\mathbf{s}} \sum_{\alpha'\beta'} \left(\mathbf{\Lambda}_{i,\mathbf{s}}^{\dagger} \right)_{\alpha'\beta'} y \cdot \left[\sum_{\alpha''} (-\mathbf{\Lambda}_{i,\mathbf{s}})_{\alpha\alpha''} \langle \left(e^{y\hat{\mathbf{C}}_i - y\hat{\mathbf{C}}_i} \right)_{\alpha''\alpha';\beta'\beta} \rangle_T + \sum_{\beta''} \langle \left(e^{y\hat{\mathbf{C}}_i - y\hat{\mathbf{C}}_i} \right)_{\alpha\alpha';\beta'\beta''} \rangle_T (\mathbf{\Lambda}_{i,\mathbf{s}})_{\beta''\beta} \right]. \quad \text{(B.25)}$$

Part IV: $\langle \left(\hat{\mathbf{X}}_i^{\dagger} \hat{\mathbf{b}}_{\mathbf{s}}^{\dagger} \hat{\mathbf{X}}_i^{\dagger} - \hat{\mathbf{b}}_{\mathbf{s}}^{\dagger} \right)_{\alpha\beta} \left(\hat{\mathbf{X}}_i^{\dagger} \hat{\mathbf{b}}_{\mathbf{s}} \hat{\mathbf{X}}_i^{\dagger} - \hat{\mathbf{b}}_{\mathbf{s}} \right)_{\alpha'\beta'} \rangle_T$

This last term describes bath-induced interactions between polarons. By using a relation similar to Eq. (B.17) and applying it only to the $\hat{\mathbf{X}}_i^{\dagger} \hat{\mathbf{b}}_{\mathbf{s}}^{\dagger} \hat{\mathbf{X}}_i^{\dagger}$ term, we obtain

$$\left(\hat{\mathbf{X}}_i^{\dagger} \hat{\mathbf{b}}_{\mathbf{s}}^{\dagger} \hat{\mathbf{X}}_i^{\dagger} - \hat{\mathbf{b}}_{\mathbf{s}}^{\dagger} \right) = \int_0^1 dx \frac{d}{dx} \left(e^{x\hat{\mathbf{C}}_i} \hat{\mathbf{b}}_{\mathbf{s}}^{\dagger} e^{-x\hat{\mathbf{C}}_i} \right) = -\int_0^1 dx \left(e^{x\hat{\mathbf{C}}_i} \mathbf{\Lambda}_{i,\mathbf{s}} e^{-x\hat{\mathbf{C}}_i} \right), \quad \text{(B.26)}$$

and

$$\langle \left(\hat{\mathbf{X}}_i^\dagger \hat{\mathbf{b}}_{\mathbf{s}}^\dagger \hat{\mathbf{X}}_i^\dagger - \hat{\mathbf{b}}_{\mathbf{s}}^\dagger \right)_{\alpha\beta} \left(\hat{\mathbf{X}}_i^\dagger \hat{\mathbf{b}}_{\mathbf{s}} \hat{\mathbf{X}}_i^\dagger - \hat{\mathbf{b}}_{\mathbf{s}} \right)_{\alpha'\beta'} \rangle_T = \int_0^1 \int_0^1 dx dy \langle \left(e^{x\hat{\mathbf{C}}_i} \mathbf{\Lambda}_{i,\mathbf{s}} e^{-x\hat{\mathbf{C}}_i} \right)_{\alpha\beta} \left(e^{y\hat{\mathbf{C}}_i} \mathbf{\Lambda}_{i,\mathbf{s}}^\dagger e^{-y\hat{\mathbf{C}}_i} \right)_{\alpha'\beta'} \rangle_T$$

$$= \int_0^1 \int_0^1 dx dy \sum_{\gamma\gamma'} \sum_{\delta\delta'} (\mathbf{\Lambda}_{i,\mathbf{s}})_{\gamma\gamma'} \left(\mathbf{\Lambda}_{i,\mathbf{s}}^\dagger \right)_{\delta\delta'} \cdot \langle \left(e^{x\hat{\mathbf{C}}_i} \right)_{\alpha\gamma} \left(e^{-x\hat{\mathbf{C}}_i} \right)_{\gamma'\beta} \left(e^{y\hat{\mathbf{C}}_i} \right)_{\alpha'\delta} \left(e^{-y\hat{\mathbf{C}}_i} \right)_{\delta'\beta'} \rangle_T$$

$$(B.27)$$

This can thus be calculated by the same method as in Eqs. (B.19, B.20).

In addition, we would like to point out that the thermal average calculation in Eq. (B.8) is exact only when the matrices $\mathbf{\Lambda}_{\mathbf{s}}$ commute with each other: $[\mathbf{\Lambda}_{\mathbf{s}}, \mathbf{\Lambda}_{\mathbf{s}'}] = 0$, even though the other derivations are exact for an arbitrary choice of $\mathbf{\Lambda}_{\mathbf{s}}$. In order to maintain good control over our two-band polaron transformation method, we can also limit the variational parameters $\mathbf{\Lambda}_{\mathbf{s}}$ to be a set of *commuting matrices*. Though the ground state energy and the contribution from the incoherent part might thus increase, this transformation has the great advantage of an exactly solvable coherent part. Another benefit of using commuting matrices is that the transformed creation/annihilation operators take a simplified form $e^{\hat{S}} \hat{b}_{\mathbf{s}} e^{-\hat{S}} = \hat{b}_{\mathbf{s}} - \sum_{i,\alpha,\beta} \left(\Lambda_{i,\mathbf{s}}^{\alpha\beta} \right)^* \hat{a}_i^{\alpha\dagger} \hat{a}_i^\beta$.

Appendix C

Polaronic Lindblad equation in two-band system

After the polaron transformation, the Hamiltonian can be separated into a coherent part Eq. (4.21) and an incoherent part Eq. (4.33). This Hamiltonian describes a quantum system (coherent part) coupled to a bosonic bath via interactions (incoherent part). We apply the Lindblad master equation to include the incoherent part.

In the interaction picture, due to J^0; $J^1 \ll \varepsilon_{\mathrm{P}}^{\Delta}$ for a deep lattice, the polaron operators can be approximated as

$$\hat{a}_i^{\alpha}(t) \approx \hat{a}_i^{\alpha} e^{-i\varepsilon_{\mathrm{P}}^{\alpha} t/\hbar}; \quad \hat{a}_i^{\alpha\dagger}(t) \approx \hat{a}_i^{\alpha\dagger} e^{+i\varepsilon_{\mathrm{P}}^{\alpha} t/\hbar},$$

where $\varepsilon_{\mathrm{P}}^{\alpha}$ is the renormalized polaron on-site energy. The interaction (incoherent part) in Eq. (4.33) is given by:

$$H_{\mathrm{inc}}(t) \approx \sum_{\alpha} \sum_{i,j} \left\{ B_{i,j}^{\alpha\alpha}(t) \right\} \hat{a}_i^{\alpha\dagger} \hat{a}_j^{\alpha} + \sum_{\alpha \neq \beta} \sum_{i} \left\{ B_{i,i}^{\alpha\beta}(t) \right\} \hat{a}_i^{\alpha\dagger} \hat{a}_i^{\beta} e^{-i(\beta-\alpha)\varepsilon_{\mathrm{P}}^{\Delta} t/\hbar};$$

$$B_{i,j}^{\alpha\alpha}(t) \equiv -\delta_{j,i\pm1} J_{\mathrm{P}}^{\alpha} \hat{T}_{i,j}^{\alpha\alpha}(t) + \delta_{i,j} \sum_{\mathbf{s}} \hbar\omega_{\mathbf{s}} \left(\hat{b}_{\mathbf{s}}^{\dagger}(t) + \hat{b}_{-\mathbf{s}}(t) \right) \left(\mathbf{M}_{i,\mathbf{s}}^{\dagger} - \mathbf{\Lambda}_{i,\mathbf{s}}^{\dagger} \right)_{\alpha\alpha}; \qquad \text{(C.1)}$$

$$B_{i,i}^{\alpha\beta}(t) \equiv \sum_{\mathbf{s}} \hbar\omega_{\mathbf{s}} \left[\hat{b}_{\mathbf{s}}^{\dagger}(t) \left(\mathbf{M}_{i,\mathbf{s}}^{\dagger} \right)_{\alpha\beta} \left(\hat{K}_{i,i}^{\alpha\beta}(t) \right) + (\mathbf{M}_{i,\mathbf{s}})_{\beta\alpha} \left(\hat{K}_{i,i}^{\beta\alpha}(t) \right)^{*} \hat{b}_{\mathbf{s}}(t) \right]$$

$$+ \sum_{\mathbf{s}} \hbar\omega_{\mathbf{s}} \left[(\mathbf{\Lambda}_{\mathbf{s}}^{\alpha}) \left(\mathbf{M}_{\mathbf{s}}^{\dagger} \right)_{\alpha\beta} \left(\hat{T}_{i,i}^{\alpha\beta}(t) \right) + \left(\mathbf{\Lambda}_{\mathbf{s}}^{\beta} \right)^{*} (\mathbf{M}_{\mathbf{s}})_{\beta\alpha} \left(\hat{T}_{i,i}^{\beta\alpha}(t) \right)^{*} \right], \qquad \text{(C.2)}$$

where $\hat{K}_{i,i}^{\alpha\beta}(t)$ and $\hat{T}_{i,i}^{\alpha\beta}(t)$ are also in the interaction picture. The first term in $H_{\mathrm{inc}}(t)$ describes intra-band dynamics, while the second term describes inter-band dynamics. In both processes, the polaron will emit (absorb) phonons to (from) the bath. Using the general form of the Lindblad equation in Eq. (4.35), we can define the decoherence factor γ as:

$$\gamma_{ij;i'j'}^{\alpha\beta;\alpha'\beta'}(\omega) = \int_{-\infty}^{\infty} d\tau e^{i\omega\tau} \langle B_{ij}^{\alpha\beta\dagger}(\tau) B_{i'j'}^{\alpha'\beta'}(0) \rangle_T$$

$$= 2\mathrm{Re}\left(\Gamma_{ij;i'j'}^{\alpha\beta;\alpha'\beta'}(\omega) \right) \equiv 2\mathrm{Re} \int_0^{\infty} d\tau e^{i\omega\tau} g_{ij;i'j'}^{\alpha\beta;\alpha'\beta'}(\tau). \qquad \text{(C.3)}$$

By using the rotating wave approximation (RWA), we decouple intra- and inter-band dynam-

ics in the Lindblad equation:

$$\mathcal{L}_I\left[\rho\left(t\right)\right] = \sum_{\alpha,\alpha'} \sum_{ij} \sum_{i'j'} \gamma_{ij;i'j'}^{\alpha\alpha;\alpha'\alpha'} \left(C_{i'j'}^{\alpha'\alpha'} \rho C_{ij}^{\alpha\alpha\dagger} - \frac{1}{2}\left\{ C_{ij}^{\alpha\alpha\dagger} C_{i'j'}^{\alpha'\alpha'}, \rho \right\} \right)$$
$$+ \sum_{i} \sum_{i'} \gamma_{ii;i'i'}^{01;01} \left(C_{i'i'}^{01} \rho C_{ii}^{01\dagger} - \frac{1}{2}\left\{ C_{ii}^{01\dagger} C_{i'i'}^{01}, \rho \right\} \right)$$
$$+ \sum_{i} \sum_{i'} \gamma_{ii;i'i'}^{10;10} \left(C_{i'i'}^{10} \rho C_{ii}^{10\dagger} - \frac{1}{2}\left\{ C_{ii}^{10\dagger} C_{i'i'}^{10}, \rho \right\} \right). \tag{C.4}$$

The first part $\gamma_{ij;i'j'}^{\alpha\alpha;\alpha'\alpha'}$ describes intra-band decoherence effects. The second part $\gamma_{ii;i'i'}^{01;01}$ describes a polaron relaxation process from upper to lower band, while the third part $\gamma_{ii;i'i'}^{10;10}$ describes an excitation from lower to upper band. We use the short notation $\gamma_{i,j}^{01} \equiv \gamma_{ii;jj}^{01;01}$ and $C_i^{01} \equiv \left(\hat{a}_i^{0\dagger} \hat{a}_i^1\right)$ for the second term.

In this paper we focus on inter-band relaxation processes. The relaxation rate $\gamma_{i,j}^{01}$ is:

$$\gamma_{i,j}^{01} = 2 \cdot \mathrm{Re} \int_0^\infty d\tau e^{i\varepsilon_{\mathrm{P}}^\Delta \tau/\hbar} \langle B_{ii}^{01\dagger}\left(\tau\right) B_{jj}^{01}\left(0\right)\rangle_T \equiv 2 \cdot \mathrm{Re} \int_0^\infty d\tau e^{i\varepsilon_{\mathrm{P}}^\Delta \tau/\hbar} g_{ij}^{01}\left(\tau\right), \tag{C.5}$$

with the correlation function $g_{ij}^{01}\left(\tau\right) \equiv g_{ii;jj}^{01;01}\left(\tau\right)$:

$$g_{ij}^{01}\left(\tau\right) = \langle B_{ii}^{01\dagger}\left(\tau\right) B_{jj}^{01}\left(0\right)\rangle_T$$
$$= \sum_{\mathbf{s}\mathbf{s}'} \hbar^2 \omega_{\mathbf{s}} \omega_{\mathbf{s}'} \left(M_{i,\mathbf{s}}^{01}\right) \left(M_{j,\mathbf{s}'}^{01}\right)^*$$
$$\cdot \langle \left[\left(\hat{K}_{i,i}^{10}\left(\tau\right)\right) \hat{b}_{\mathbf{s}}\left(\tau\right) + \hat{b}_{-\mathbf{s}}^\dagger\left(\tau\right) \left(\hat{K}_{i,i}^{10}\left(\tau\right)\right) + \left(\Lambda_{i,\mathbf{s}}^0 - \Lambda_{i,\mathbf{s}}^1\right)^* \left(\hat{K}_{i,i}^{10}\left(\tau\right) - \langle\hat{K}_{i,i}^{10}\left(\tau\right)\rangle_T\right) \right]$$
$$\left[\hat{b}_{\mathbf{s}'}^\dagger\left(0\right) \left(\hat{K}_{j,j}^{01}\left(0\right)\right) + \left(\hat{K}_{j,j}^{01}\left(0\right)\right) \hat{b}_{-\mathbf{s}'}\left(0\right) + \left(\Lambda_{j,\mathbf{s}'}^0 - \Lambda_{j,\mathbf{s}'}^1\right) \left(\hat{K}_{j,j}^{01}\left(0\right) - \langle\hat{K}_{j,j}^{01}\left(0\right)\rangle_T\right) \right]\rangle_T. \tag{C.6}$$

From the definition of $\hat{K}_{i,j}^{\alpha\beta}$, we have

$$\hat{K}_{i,j}^{\alpha\beta}\left(t\right) \equiv \exp\left[\sum_{\mathbf{s}} \left(\mu_{ij,\mathbf{s}}^{\alpha\beta}\right)^* \hat{b}_{\mathbf{s}}^\dagger\left(t\right) - \sum_{\mathbf{s}} \left(\mu_{ij,\mathbf{s}}^{\alpha\beta}\right) \hat{b}_{\mathbf{s}}\left(t\right) \right];$$
$$\left(\mu_{ij,\mathbf{s}}^{\alpha\beta}\right) \equiv -\left(\Lambda_{i,\mathbf{s}}^{\alpha\alpha}\right) + \left(\Lambda_{j,\mathbf{s}}^{\beta\beta}\right), \tag{C.7}$$

and the thermal averaged results from Bloch identity:

$$\langle\hat{K}_{i,j}^{\alpha\beta}\left(t\right)\rangle_T = \exp\left[-\sum_{\mathbf{s}} \left(N_{\mathbf{s}} + \frac{1}{2}\right) \left(\mu_{ij,\mathbf{s}}^{\alpha\beta}\right)^* \left(\mu_{ij,\mathbf{s}}^{\alpha\beta}\right) \right], \tag{C.8}$$

as well as:

$$\langle\hat{K}_{i,j}^{\alpha\beta}\left(t\right) \hat{K}_{i',j'}^{\alpha'\beta'}\left(0\right)\rangle_T = \exp\left[-\sum_{\mathbf{s}} \left(N_{\mathbf{s}} + \frac{1}{2}\right) \left(\mu_{ij,\mathbf{s}}^{\alpha\beta}\right)^* \left(\mu_{ij,\mathbf{s}}^{\alpha\beta}\right) \right] \exp\left[-\sum_{\mathbf{s}} \left(N_{\mathbf{s}} + \frac{1}{2}\right) \left(\mu_{i'j',\mathbf{s}}^{\alpha'\beta'}\right)^* \left(\mu_{i'j',\mathbf{s}}^{\alpha'\beta'}\right) \right]$$
$$\cdot \exp\left[-\sum_{\mathbf{s}} \left(N_{\mathbf{s}}\right) \left(\mu_{ij,\mathbf{s}}^{\alpha\beta}\right)^* \left(\mu_{i'j',\mathbf{s}}^{\alpha'\beta'}\right) e^{i\omega_{\mathbf{s}} t} - \sum_{\mathbf{s}} \left(N_{\mathbf{s}} + 1\right) \left(\mu_{ij,\mathbf{s}}^{\alpha\beta}\right) \left(\mu_{i'j',\mathbf{s}}^{\alpha'\beta'}\right)^* e^{-i\omega_{\mathbf{s}} t} \right]. \tag{C.9}$$

The elements such as $\hat{b}_{\mathbf{s}}^{\dagger}(t)\,\hat{K}_{i,j}^{\alpha\beta}(t)\rangle_T$ can be obtained by using the Glauber formula $e^{\hat{A}+\hat{B}} = e^{\hat{A}}e^{\hat{B}}e^{-\frac{1}{2}[\hat{A},\hat{B}]}$ (with the condition $[\hat{A},[\hat{A},\hat{B}]] = [\hat{B},[\hat{A},\hat{B}]] = 0$) and differentiating $\hat{K}_{i,j}^{\alpha\beta}(t)$ in Eq. (C.7) as:

$$\frac{\partial}{\partial\left(\mu_{ij,\mathbf{s}}^{\alpha\beta}\right)^*}\hat{K}_{i,j}^{\alpha\beta}(t) = \left[\hat{b}_{\mathbf{s}}^{\dagger}(t) - \frac{1}{2}\left(\mu_{ij,\mathbf{s}}^{\alpha\beta}\right)\right]\hat{K}_{i,j}^{\alpha\beta}(t);$$

$$\frac{\partial}{\partial\left(\mu_{ij,\mathbf{s}}^{\alpha\beta}\right)}\hat{K}_{i,j}^{\alpha\beta}(t) = \hat{K}_{i,j}^{\alpha\beta}(t)\left[-\hat{b}_{\mathbf{s}}(t) - \frac{1}{2}\left(\mu_{ij,\mathbf{s}}^{\alpha\beta}\right)^*\right]. \tag{C.10}$$

As an example, averages of $\langle\hat{b}_{\mathbf{s}}^{\dagger}(t)\,\hat{K}_{i,j}^{\alpha\beta}(t)\rangle_T$ in Eq. (C.6) can then be obtained by using Eq. (C.10) and switching the order of differentiation and thermal averaging:

$$\langle\hat{b}_{\mathbf{s}}^{\dagger}(t)\,\hat{K}_{i,j}^{\alpha\beta}(t)\rangle_T = \frac{\partial}{\partial\left(\mu_{ij,\mathbf{s}}^{\alpha\beta}\right)^*}\langle\hat{K}_{i,j}^{\alpha\beta}(t)\rangle_T + \frac{1}{2}\left(\mu_{ij,\mathbf{s}}^{\alpha\beta}\right)\langle\hat{K}_{i,j}^{\alpha\beta}(t)\rangle_T$$

$$= -N_{\mathbf{s}}\left(\mu_{ij,\mathbf{s}}^{\alpha\beta}\right)\exp\left[-\sum_{\mathbf{s}}\left(N_{\mathbf{s}} + \frac{1}{2}\right)\left(\mu_{ij,\mathbf{s}}^{\alpha\beta}\right)^*\left(\mu_{ij,\mathbf{s}}^{\alpha\beta}\right)\right]. \tag{C.11}$$

Finally the correlation function Eq. (C.6) for inter-band relaxation is:

$$g_{ij}^{01}(\tau) = \sum_{\mathbf{s}}\left(\hbar\omega_{\mathbf{s}}|M_{\mathbf{s}}^{01}|\right)^2\cos\left[s_x(i-j)d\right]\left[(N_{\mathbf{s}}+1)e^{-i\omega_{\mathbf{s}}\tau} + (N_{\mathbf{s}})e^{+i\omega_{\mathbf{s}}\tau}\right]\langle\hat{K}_{i,i}^{10}(\tau)\,\hat{K}_{j,j}^{01}(0)\rangle_T$$

$$+ \sum_{\mathbf{s}\mathbf{s}'}\hbar^2\omega_{\mathbf{s}}\omega_{\mathbf{s}'}\left(M_{\mathbf{s}}^{01}\right)\left(M_{\mathbf{s}'}^{01}\right)\left(\Lambda_{\mathbf{s}}^0 - \Lambda_{\mathbf{s}}^1\right)\left(\Lambda_{\mathbf{s}'}^0 - \Lambda_{\mathbf{s}'}^1\right)\sin\left[s_x(i-j)d\right]\sin\left[s_x'(i-j)d\right]$$

$$\cdot\left[(N_{\mathbf{s}}+1)e^{-i\omega_{\mathbf{s}}\tau} - (N_{\mathbf{s}})e^{+i\omega_{\mathbf{s}}\tau}\right]\cdot\left[(N_{\mathbf{s}'}+1)e^{-i\omega_{\mathbf{s}'}\tau} - (N_{\mathbf{s}'})e^{+i\omega_{\mathbf{s}'}\tau}\right]\langle\hat{K}_{i,i}^{10}(\tau)\,\hat{K}_{j,j}^{01}(0)\rangle_T. \tag{C.12}$$

with

$$\langle\hat{K}_{i,i}^{10}(\tau)\,\hat{K}_{j,j}^{01}(0)\rangle_T$$

$$= \exp\left\{\sum_{\mathbf{s}}\left(\Lambda_{\mathbf{s}}^0 - \Lambda_{\mathbf{s}}^1\right)^2\left[-(2N_{\mathbf{s}}+1) + (N_{\mathbf{s}})\cos\left[s_x(i-j)d\right]e^{+i\omega_{\mathbf{s}}\tau} + (N_{\mathbf{s}}+1)\cos\left[s_x(i-j)d\right]e^{-i\omega_{\mathbf{s}}\tau}\right]\right\}. \tag{C.13}$$

The first term in the correlation function (C.12) is a single-phonon process, with the polaron absorbing (emitting) one phonon from (to) the bath. This term is similar to Fermi's Golden Rule except a renormalization factor $\langle\hat{K}_{i,i}^{10}(\tau)\,\hat{K}_{j,j}^{01}(0)\rangle_T$. The second term describes higher order correlations involving two phonons, which are absent in Fermi's Golden Rule.

The corresponding relaxation rate $\gamma_{i,j}^{01}$ is calculated by Eq. (C.5). At zero temperature, this corresponds to a spontaneous relaxation process:

$$\gamma_{i,j}^{01} = 2\cdot\text{Re}\int_0^\infty d\tau e^{i\varepsilon_{\mathrm{P}}^\Delta\tau/\hbar}\cdot\sum_{\mathbf{s}}\left(\hbar\omega_{\mathbf{s}}|M_{\mathbf{s}}^{01}|\right)^2\cos\left[s_x(i-j)d\right]e^{-i\omega_{\mathbf{s}}\tau}\cdot\langle\hat{K}_{i,i}^{10}(\tau)\,\hat{K}_{j,j}^{01}(0)\rangle_T$$

$$+ 2\cdot\text{Re}\int_0^\infty d\tau e^{i\varepsilon_{\mathrm{P}}^\Delta\tau/\hbar}\cdot\sum_{\mathbf{s}\mathbf{s}'}\hbar^2\omega_{\mathbf{s}}\omega_{\mathbf{s}'}\left(M_{\mathbf{s}}^{01}\right)\left(M_{\mathbf{s}'}^{01}\right)\left(\Lambda_{\mathbf{s}}^0 - \Lambda_{\mathbf{s}}^1\right)\left(\Lambda_{\mathbf{s}'}^0 - \Lambda_{\mathbf{s}'}^1\right)$$

$$\cdot\sin\left[s_x(i-j)d\right]\sin\left[s_x'(i-j)d\right]e^{-i\omega_{\mathbf{s}}\tau}e^{-i\omega_{\mathbf{s}'}\tau}\cdot\langle\hat{K}_{i,i}^{10}(\tau)\,\hat{K}_{j,j}^{01}(0)\rangle_T. \tag{C.14}$$

The terms with $i \neq j$ will rapidly decay with distance $|i-j|$. The leading term with $i = j$ only contains single phonon process.

Appendix D

Exact solution for single trapped ion

D.1 Solving the classical Mathieu equation

The classical equation of motion

$$\ddot{f}(t) + K(t) f(t) = 0, \tag{D.1}$$

with

$$K(t) = \frac{1}{4}\omega^2[a + 2q\cos(\omega t)], \tag{D.2}$$

has the following solution

$$f(t) = e^{i\mu t}\phi(t); \ \phi(t + T) = \phi(t), \tag{D.3}$$

and the complex conjugate $f^*(t)$ as another independent solution. The classical Floquet function $\phi(t)$ is periodic and can be represented as Fourier series:

$$\phi(t) = \sum_{n=-\infty}^{\infty} c_n e^{in\omega t}. \tag{D.4}$$

The value of the μ and coefficients c_n are found from numerically methods. These solutions are stable (bounded for arbitrary initial conditions) when μ/ω is a real non-integer number.

Then we end with the tridiagonal recurrence relation

$$\left[\omega^2 a - 4(\nu + n\omega)^2\right] c_n + \omega^2 q(c_{n+1} + c_{n-1}) = 0,$$

which can also be a tridiagonal matrix H_ν. The linear equations have non-trivial solution only if $\det(H_\nu) = 0$, which is an equation for ν. The solution of this equation will be

$$\nu = \frac{\omega}{\pi} \arcsin\left(\sqrt{\Delta(0)\sin^2\left(\pi\sqrt{a}/2\right)}\right) \quad \text{for } a \neq (n\omega)^2$$

$$\nu = \frac{\omega}{2\pi} \arccos\left(2\Delta\left(\frac{\omega}{2}\right) - 1\right) \quad \text{for } a = (n\omega)^2$$

with

$$
\Delta\left(\nu\right) \equiv \begin{pmatrix}
\ddots & \cdots & \cdots & \cdots & \cdots & \cdots & \cdots \\
\cdots & 1 & \frac{q}{(\nu-2\omega)^2-a} & 0 & 0 & 0 & \cdots \\
\cdots & \frac{q}{(\nu-\omega)^2-a} & 1 & \frac{q}{(\nu-\omega)^2-a} & 0 & 0 & \cdots \\
\cdots & 0 & \frac{q}{(\nu-0\omega)^2-a} & 1 & \frac{q}{(\nu-0\omega)^2-a} & 0 & \cdots \\
\cdots & 0 & 0 & \frac{q}{(\nu+\omega)^2-a} & 1 & \frac{q}{(\nu+\omega)^2-a} & \cdots \\
\cdots & 0 & 0 & 0 & \frac{q}{(\nu+2\omega)^2-a} & 1 & \cdots \\
\cdots & \cdots & \cdots & \cdots & \cdots & \cdots & \ddots
\end{pmatrix}
\tag{D.5}
$$

D.2   Unitary transformation

The Hamiltonian will be

$$
\hat{H}(t) = \frac{p^2}{2m_i} + \frac{1}{2}m_i x^2 K\left(t\right),
\tag{D.6}
$$

with the effective spring constant

$$
K\left(t\right) = \frac{1}{4}\omega^2[a + 2q\cos(\omega t)].
\tag{D.7}
$$

The classical solution gives us the initial conditions as

$$
f\left(0\right) = 1; \quad \dot{f}\left(0\right) = i\left(\mu + \omega\sum_n nc_n\nu\right)
\tag{D.8}
$$

Due to the equation of motion, we can define a time-independent Wronskian as

$$
2iW \equiv \dot{f}\left(t\right)f^*\left(t\right) - f\left(t\right)\dot{f}^*\left(t\right).
\tag{D.9}
$$

From the initial conditions, we have $W = \nu = \mu + \omega\sum_n nc_n$.

In order to solve the quantum-mechanical problem, we follow the method in [137, 138] and apply the canonical unitary transformation. The transformed Hamiltonian will be

$$
\tilde{H}\left(t\right) = U^{-1}H\left(t\right)U - i\hbar U^{-1}\frac{\partial}{\partial t}U
\tag{D.10}
$$

with the transformed wave function $|\tilde{\psi}\rangle = U^{-1}|\psi\rangle$. We apply the first unitary transformation

$$
U_1 = \exp\left[+\frac{i}{\hbar}\chi\left(t\right)x^2\right],
\tag{D.11}
$$

with

$$\chi(t) = \frac{m}{4}\left(\frac{\dot{f}(t)}{f(t)} + \frac{\dot{f}^*(t)}{f^*(t)}\right) = \frac{\text{Re}\left[\dot{f}(t)f^*(t)\right]}{2|f(t)|^2} = \frac{m}{4}\frac{d}{dt}\ln|f(t)|^2. \tag{D.12}$$

The coordinates are transformed as

$$U_1^{-1}xU_1 = x \tag{D.13}$$

$$U_1^{-1}\frac{\partial}{\partial x}U_1 = \frac{\partial}{\partial x} + 2\frac{i}{\hbar}\chi(t)x \tag{D.14}$$

and

$$U_1^{-1}\frac{\partial}{\partial t}U_1 = +\frac{i}{\hbar}x^2\frac{m}{4}\left(\frac{\ddot{f}(t)}{f(t)} - \frac{\dot{f}(t)\dot{f}(t)}{f(t)f(t)} + \frac{\ddot{f}^*(t)}{f^*(t)} - \frac{\dot{f}^*(t)\dot{f}^*(t)}{f^*(t)f^*(t)}\right)$$

$$= +\frac{i}{\hbar}x^2\frac{m}{4}\left(-2K(t) - \frac{\dot{f}(t)^2f^*(t)^2 + f(t)^2\dot{f}^*(t)^2}{f(t)f(t)f^*(t)f^*(t)}\right) \tag{D.15}$$

Then

$$\bar{H}(t) = \frac{(p + 2\chi(t)x)^2}{2m} + \frac{1}{2}mx^2K(t) - i\hbar U^{-1}\frac{\partial}{\partial t}U$$

$$= \frac{p^2}{2m} + \frac{\chi(t)}{m}(xp + px) + \frac{1}{2}m\left(\frac{W^2}{|f(t)|^4}\right)x^2. \tag{D.16}$$

The cross term involving $\chi(t)$ is removed by a scale changing transformation

$$U_2 = \exp\left[-\frac{i}{4\hbar}(px + xp)\ln|f(t)|^2\right]. \tag{D.17}$$

Then using the Baker-Campbell-Hausdorff formula

$$e^{\hat{S}}\hat{A}e^{-\hat{S}} = \hat{A} + \left[\hat{S},\,\hat{A}\right] + \frac{1}{2!}\left[\hat{S},\,\left[\hat{S},\,\hat{A}\right]\right] + \cdots, \tag{D.18}$$

we have:

$$U_2^{-1}xU_2 = x\cdot|f(t)| \tag{D.19}$$

$$U_2^{-1}pU_2 = p/|f(t)| \tag{D.20}$$

and

$$U_2^{-1}\frac{\partial}{\partial t}U_2 = -\frac{i\chi(t)}{m\hbar}(px + xp). \tag{D.21}$$

Then the final Hamiltonian is

$$\tilde{H}(t) = \frac{1}{|f(t)|^2}\left(\frac{p^2}{2m} + \frac{1}{2}mW^2x^2\right)$$

$$= \frac{W}{|f(t)|^2}\left(\hat{b}^\dagger\hat{b} + \frac{1}{2}\right), \tag{D.22}$$

with

$$\hat{b} \equiv \sqrt{\frac{mW}{2}}x + i\sqrt{\frac{1}{2mW}}p. \tag{D.23}$$

The transformed Hamiltonian $\tilde{H}(t)$ is time-dependent with period T.

In order to solve this equation, we defined a time-dependent factor $\vartheta(t)$ as:

$$\vartheta(t) \equiv -\frac{i}{2}\ln\left(\frac{f(t)}{f^*(t)}\right) = \mu t - \frac{i}{2}\ln\left(\frac{\phi(t)}{\phi^*(t)}\right) \tag{D.24}$$

$$\frac{d}{dt}\vartheta(t) = -\frac{i}{2}\left(\frac{\dot{f}(t)}{f(t)} - \frac{\dot{f}^*(t)}{f^*(t)}\right) = \frac{W}{|f(t)|^2} \tag{D.25}$$

The evolution operator for time-dependent Hamiltonian $\tilde{H}(t)$ can be formally written as

$$\hat{U}(t,t_0) = \mathcal{T}_t\exp\left[-i\int_{t_0}^t \tilde{H}(\tau)d\tau\right] = \mathcal{T}_t\exp\left[-i\int_{t_0}^t \frac{W}{|f(\tau)|^2}d\tau\left(\hat{b}^\dagger\hat{b} + \frac{1}{2}\right)\right] \tag{D.26}$$

$$\hat{U}(t,t_0) = \exp\left\{-i\left[\vartheta(t) - \vartheta(t_0)\right]\left(\hat{b}^\dagger\hat{b} + \frac{1}{2}\right)\right\} = \exp\left\{-i\left[\mu t - \frac{i}{2}\ln\left(\frac{\phi(t)}{\phi^*(t)}\right) - \vartheta(t_0)\right]\left(\hat{b}^\dagger\hat{b} + \frac{1}{2}\right)\right\} \tag{D.27}$$

with

$$\hat{U}(T + t_0, t_0) = \exp\left\{-i(\mu T)\left(\hat{b}^\dagger\hat{b} + \frac{1}{2}\right)\right\} = \exp(-iH_F T) \tag{D.28}$$

and

$$\hat{U}(nT + t_0, t_0) = \hat{U}(T + t_0, t_0)^n. \tag{D.29}$$

At the starting time t_0, the ground state can be defined as:

$$\hat{b}|0, t_0\rangle = 0,$$

and the excited states can be solved as usual harmonic oscillator wave function:

$$|n, t_0\rangle = \frac{1}{\sqrt{n!}}\left(\hat{b}^\dagger\right)^n|0, t_0\rangle.$$

The wave function at time t is

$$\begin{aligned}
|n, t\rangle &= \hat{U}(t, t_0)|n, t_0\rangle \\
&= \exp\left\{-i\left[\mu t - \frac{i}{2}\ln\left(\frac{\phi(t)}{\phi^*(t)}\right) - \vartheta(t_0)\right]\left(\hat{b}^\dagger\hat{b} + \frac{1}{2}\right)\right\}|n, t_0\rangle \\
&= \exp\left\{-i\left(n + \frac{1}{2}\right)\mu t\right\}\exp\left\{\left[-\frac{1}{2}\ln\left(\frac{\phi(t)}{\phi^*(t)}\right) + i\vartheta(t_0)\right]\left(n + \frac{1}{2}\right)\right\}|n, t_0\rangle \\
&= e^{-i\left(n+\frac{1}{2}\right)\mu t}\left\{\left[\frac{\phi^*(t)}{\phi(t)}\right]^{\frac{n}{2}+\frac{1}{4}}e^{+i\left(n+\frac{1}{2}\right)\vartheta(t_0)}|n, t_0\rangle\right\},
\end{aligned} \tag{D.30}$$

which takes the form as Floquet wave function.

In the (transformed) coordinate space, the wave function at $t_0 = 0$ is

$$\begin{aligned}
\tilde{\Psi}_n(x, t_0) &\equiv \langle x|n, t_0\rangle \\
&= \frac{1}{\sqrt{2^n n!}}\left(\frac{mW}{\pi\hbar}\right)^{\frac{1}{4}}e^{-\frac{mW}{2\hbar}x^2}H_n\left(\sqrt{\frac{mW}{\hbar}}x\right),
\end{aligned}$$

and at time t is

$$\tilde{\Psi}_n\left(x,t\right) = e^{-i\left(n+\frac{1}{2}\right)\mu t}\left\{\left[\frac{\phi^*\left(t\right)}{\phi\left(t\right)}\right]^{\frac{n}{2}+\frac{1}{4}}e^{+i\left(n+\frac{1}{2}\right)\vartheta(t_0)}\langle x|n,t_0\rangle\right\}.$$

In the original coordinate space, the wave function is transformed

$$\begin{aligned}\Psi_n\left(x,t\right) =&U_1U_2\tilde{\Psi}_n\left(x,t\right) = U_1U_2\langle x|n,t\rangle\\ =&\tilde{\Psi}_n\left(U_1U_2xU_2^{-1}U_1^{-1},t\right)U_1U_2\\ =&\tilde{\Psi}_n\left(\frac{x}{|f\left(t\right)|}\right)e^{+\frac{i}{\hbar}\chi(t)x^2}e^{-\frac{1}{4}\ln|f(t)|^2}\\ =&e^{-i\left(n+\frac{1}{2}\right)\mu t}\psi_n\left(x,t\right),\end{aligned}$$

with (at $t_0 = 0$)

$$\begin{aligned}\psi_n\left(x\right) =&\left[\frac{\phi^*\left(t\right)}{\phi\left(t\right)}\right]^{\frac{n}{2}+\frac{1}{4}}e^{+i\left(n+\frac{1}{2}\right)\vartheta(t_0)}\frac{1}{\sqrt{2^n n!}}\left(\frac{mW}{\pi\hbar}\right)^{\frac{1}{4}}e^{-\frac{mW}{2\hbar|f(t)|^2}x^2}e^{+\frac{i}{\hbar}\chi(t)x^2}e^{-\frac{1}{4}\ln|f(t)|^2}H_n\left(\sqrt{\frac{mW}{\hbar}}\frac{1}{|f\left(t\right)|}x\right)\\ =&\frac{1}{\sqrt{2^n n!}}\left(\frac{mW}{\pi\hbar}\right)^{\frac{1}{4}}\left(\left[\frac{\phi^*\left(t\right)}{\phi\left(t\right)}\right]^{\frac{n}{2}+\frac{1}{4}}\frac{1}{\sqrt{|f\left(t\right)|}}\right)H_n\left(\sqrt{\frac{mW}{\hbar|f\left(t\right)^2}}x\right)e^{i\frac{m}{2\hbar}\left(\dot{f}(t)/f(t)\right)x^2}\\ =&\frac{1}{\sqrt{2^n n!}}\left(\frac{mW}{\pi\hbar}\right)^{\frac{1}{4}}\frac{1}{\sqrt{\phi\left(t\right)}}\left[\frac{\phi^*\left(t\right)}{\phi\left(t\right)}\right]^{\frac{n}{2}+\frac{1}{4}}H_n\left(\sqrt{\frac{mW}{\hbar|f\left(t\right)^2}}x\right)\exp\left[-\frac{m\mu}{2\hbar}\left(1-\frac{i}{\mu}\frac{\dot{\phi}\left(t\right)}{\phi\left(t\right)}\right)x^2\right].\end{aligned}$$

Appendix E

Magnus expansion

We present the Magnus expansion for Floquet Hamiltonian up to second order by following the method in [142]. Using the Magnus expansion, the stroboscopic Floquet Hamiltonian is:

$$H_F[t_0] = \sum_{n=0}^{\infty} H_F^{(n)}[t_0]. \tag{E.1}$$

The super-index $^{(n)}$ means that $H_F^{(n)}[t_0]$ is of order ω^{-n}. The first few terms are given by

$$H_F^{(0)} = \frac{1}{T} \int_{t_0}^{T+t_0} dt \, H(t) = H_0; \tag{E.2}$$

$$H_F^{(1)} = \frac{1}{2!T(i\hbar)} \int_{t_0}^{T+t_0} dt_1 \int_{t_0}^{t_1} dt_2 \, [H(t_1), H(t_2)]; \tag{E.3}$$

$$H_F^{(2)} = \frac{1}{3!T(i\hbar)^2} \int_{t_0}^{T+t_0} dt_1 \int_{t_0}^{t_1} dt_2 \int_{t_0}^{t_2} dt_3$$
$$\cdot ([H(t_1), [H(t_2), H(t_3)]] + [H(t_3), [H(t_2), H(t_1)]]). \tag{E.4}$$

Let's take the gauge $t_0 = 0$ and expand the time-periodic Hamiltonian in its Fourier harmonics as:

$$H(t) = \sum_{l \in \mathbb{Z}} H_l e^{il\omega t} = \sum_{l=1}^{\infty} \left(H_l e^{il\omega t} + H_{-l} e^{-il\omega t} \right).$$

E.1   Zeroth-order

The zeroth-order term is simply the time-averaged Hamiltonian:

$$H_F^{(0)} = H_0. \tag{E.5}$$

E.2   First-order

For the first-order $H_F^{(1)}$ we use

$$
\int_0^T dt_1 \int_0^{t_1} dt_2 \sum_{m,n} [H_m,\, H_n]\, e^{im\omega t_1} e^{in\omega t_2} = [H_m,\, H_n] \cdot
\begin{cases}
2\pi^2/\left(\omega^2\right); & m=0, n=0; \\
-2i\pi/\left(m\omega^2\right); & m \neq 0, n=0; \\
2i\pi/\left(n\omega^2\right); & m=0, n \neq 0; \\
2i\pi/\left(n\omega^2\right); & m=-n, n \neq 0; \\
0 & \text{else.}
\end{cases}
$$

$$(E.6)$$

and thus

$$
H_F^{(1)} = \frac{1}{\omega} \sum_{l=1}^{\infty} \frac{1}{l} \left([H_l,\, H_{-l}] - [H_l,\, H_0] + [H_{-l},\, H_0]\right).
$$

$$(E.7)$$

E.3   Second-order

The second order of the Magnus expansion is quite complicated. For $H_F^{(2)}$ we need to calculate the integrals:

$$
\int_0^T dt_1 \int_0^{t_1} dt_2 \int_0^{t_2} dt_3 \sum_{l,m,n} [H_l,\, [H_m,\, H_n]] \left(e^{il\omega t_1} e^{im\omega t_2} e^{in\omega t_3} + e^{il\omega t_3} e^{im\omega t_2} e^{in\omega t_1}\right).
$$

$$
= [H_l,\, [H_m,\, H_n]] \cdot \left(\frac{\pi}{\omega^3}\right)
\begin{cases}
\begin{array}{ccc}
+4/\left(l^2\right) & +4/\left(n^2\right) & -8/\left(m^2\right) \\
(l;0;0); & (0;0;n); & (0;m;0); \\[1em]
+4/\left(l^2\right) & +4/\left(n^2\right) & -8/\left(l^2\right) \\
(l;-l;0); & (0;-n;n); & (l;0;-l); \\[1em]
-4/\left[m\left(m+l\right)\right] & -4/\left[m\left(m+n\right)\right] & +4/\left(l \cdot n\right) \\
(l;m \neq -l;0) & (0;m \neq -n;n) & (l;0;n \neq -l); \\[1em]
+4/\left(n^2\right) & +4/\left(n^2\right) & -8/\left(n^2\right) \\
(-n;n;n) & (-n;-n;n) & (n;-n;n) \\[1em]
-4/\left(l \cdot n\right) & -4/\left(l \cdot n\right) & -4/\left(l \cdot n\right) \\
(l \neq n;-n;n); & (l \neq n;-l;n); & (l \neq n;-\left(n+l\right);n);
\end{array}
\end{cases}
$$

$$(E.8)$$

with $(l;m;n)$ simply indicating the values of l, m and n.

The first few terms of the Magnus expansion for the stroboscopic Floquet Hamiltonian

take the form

$$H_F^{(0)} = H_0; \tag{E.9}$$

$$H_F^{(1)} = \frac{1}{\omega} \sum_{l=1}^{\infty} \frac{1}{l} \left([H_l,\, H_{-l}] - [H_l,\, H_0] + [H_{-l},\, H_0] \right); \tag{E.10}$$

$$H_F^{(2)} = \frac{1}{\omega^2} \sum_{l=1}^{\infty} \frac{1}{l^2} \left([H_0,\, [H_l,\, H_0]] + [H_0,\, [H_{-l},\, H_0]] \right)$$

$$- \frac{1}{\omega^2} \sum_{l=1}^{\infty} \frac{1}{l^2} \left([H_{-l},\, [H_l,\, H_0]] + [H_l,\, [H_{-l},\, H_0]] \right)$$

$$+ \frac{1}{\omega^2} \sum_{l=1}^{\infty} \sum_{n=1}^{\infty} \frac{1}{l\,(l+n)} \left([H_n,\, [H_l,\, H_0]] + [H_{-n},\, [H_{-l},\, H_0]] \right)$$

$$+ \frac{1}{\omega^2} \sum_{l=1}^{\infty} \sum_{n \neq l}^{\infty} \frac{1}{l\,(l-n)} \left([H_{-n},\, [H_l,\, H_0]] + [H_n,\, [H_{-l},\, H_0]] \right)$$

$$+ \frac{1}{\omega^2} \sum_{l=1}^{\infty} \sum_{n=1}^{\infty} \frac{1}{l \cdot n} \left([H_n,\, [H_{-l},\, H_l]] + [H_{-n},\, [H_l,\, H_{-l}]] \right)$$

$$+ \frac{1}{\omega^2} \sum_{l=1}^{\infty} \sum_{n=1}^{\infty} \frac{1}{n \cdot (n+l)} \left([H_n,\, [H_l,\, H_{-n-l}]] + [H_{-n},\, [H_{-l},\, H_{n+l}]] \right). \tag{E.11}$$

E.4 High frequency expansion (HFE)

We compare our results with the *High Frequency Expansion (HFE)* for the effective Floquet Hamiltonian up to $1/\omega^2$ order. The stroboscopic Magnus expansion Hamiltonian and non-stroboscopic *High Frequency Expansion (HFE)* Hamiltonian are connected to each other by the transformation

$$H_F[t_0] = e^{-iK_{\mathrm{eff}}(t_0)} H_{\mathrm{eff}} e^{iK_{\mathrm{eff}}(t_0)} \tag{E.12}$$

$$= H_{\mathrm{eff}} - i\left[K_{\mathrm{eff}}(t_0),\, H_{\mathrm{eff}}\right] - \frac{1}{2}\left[K_{\mathrm{eff}}(t_0),\, [K_{\mathrm{eff}}(t_0),\, H_{\mathrm{eff}}]\right] + \mathcal{O}\left(\omega^{-3}\right), \tag{E.13}$$

where $H_{\mathrm{eff}} = \sum_{n=0}^{\infty} H_{\mathrm{eff}}^{(n)}$ is the HFE effective Hamiltonian and $K_{\mathrm{eff}}(t) = \sum_{n=0}^{\infty} K_{\mathrm{eff}}^{(n)}(t)$ is the kick operator. The first few terms with the same $1/\omega$ order are:

$$H_F^{(0)}[t_0] = H_{\mathrm{eff}}^{(0)} = H_0; \tag{E.14}$$

$$H_F^{(1)}[t_0] = H_{\mathrm{eff}}^{(1)} - i\left[K_{\mathrm{eff}}^{(1)}(t_0),\, H_{\mathrm{eff}}^{(0)}\right]; \tag{E.15}$$

$$H_F^{(2)}[t_0] = H_{\mathrm{eff}}^{(2)} - i\left[K_{\mathrm{eff}}^{(1)}(t_0),\, H_{\mathrm{eff}}^{(1)}\right] - i\left[K_{\mathrm{eff}}^{(2)}(t_0),\, H_{\mathrm{eff}}^{(0)}\right] - \frac{1}{2}\left[K_{\mathrm{eff}}^{(1)}(t_0),\, \left[K_{\mathrm{eff}}^{(1)}(t_0),\, H_{\mathrm{eff}}^{(0)}\right]\right]. \tag{E.16}$$

and

$$K_F^{(1)}[t_0](t) = K_{\mathrm{eff}}^{(1)}(t) - K_{\mathrm{eff}}^{(1)}(t_0); \tag{E.17}$$

$$K_F^{(2)}[t_0](t) = K_{\mathrm{eff}}^{(2)}(t) - K_{\mathrm{eff}}^{(2)}(t_0) - \frac{1}{2}\left[K_{\mathrm{eff}}^{(1)}(t),\, K_{\mathrm{eff}}^{(1)}(t_0)\right]. \tag{E.18}$$

Up to $1/\omega^2$ order, these two methods give equivalent Floquet Hamiltonians.

The HFE effective Hamiltonian can be found in [140, 142] as:

$$H_{\text{eff}}^{(0)} = H_0; \tag{E.19}$$

$$H_{\text{eff}}^{(1)} = \frac{1}{\omega} \sum_{l=1}^{\infty} \frac{1}{l} \left([H_l, \, H_{-l}] \right); \tag{E.20}$$

$$H_{\text{eff}}^{(2)} = \frac{1}{\omega^2} \sum_{l \neq 0} \left(\frac{1}{2l^2} \cdot [H_{-l}, \, [H_0, \, H_l]] + \sum_{l' \neq 0, l} \frac{1}{3l \cdot l'} \cdot [H_{-l'}, \, [H_{l'-l}, \, H_l]] \right), \tag{E.21}$$

or equivalently:

$$\begin{aligned}
H_{\text{eff}}^{(2)} = & -\frac{1}{\omega^2} \sum_{l=1}^{\infty} \frac{1}{2} \cdot \frac{1}{l^2} \left([H_{-l}, \, [H_l, \, H_0]] + [H_l, \, [H_{-l}, \, H_0]] \right) \\
& + \frac{1}{\omega^2} \sum_{l=1}^{\infty} \sum_{n=1}^{\infty} \frac{1}{n \cdot (n+l)} \left([H_n, \, [H_l, \, H_{-n-l}]] + [H_{-n}, \, [H_{-l}, \, H_{n+l}]] \right).
\end{aligned}$$

The HFE effective kick operators can be found in [140, 151] as

$$K_{\text{eff}}^{(0)}(t) = 0; \tag{E.22}$$

$$K_{\text{eff}}^{(1)}(t) = \frac{1}{i\omega} \sum_{l=1}^{\infty} \frac{1}{l} \left(H_l e^{il\omega t} - H_{-l} e^{-il\omega t} \right); \tag{E.23}$$

$$\begin{aligned}
K_{\text{eff}}^{(2)}(t) = & \frac{1}{i\omega^2} \sum_{l=1}^{\infty} \frac{1}{l^2} \left([H_l, \, H_0] e^{il\omega t} - [H_0, \, H_{-l}] e^{-il\omega t} \right) \\
& + \frac{1}{2i\omega^2} \sum_{l,n=1}^{\infty} \frac{1}{l(l+n)} \left([H_l, \, H_n] e^{i(l+n)\omega t} - [H_{-n}, \, H_{-l}] e^{-i(l+n)\omega t} \right) \\
& + \frac{1}{2i\omega^2} \sum_{l \neq n=1}^{\infty} \frac{1}{l(l-n)} \left([H_l, \, H_{-n}] e^{i(l-n)\omega t} - [H_n, \, H_{-l}] e^{-i(l-n)\omega t} \right). \tag{E.24}
\end{aligned}$$

Appendix F

Excess micromotion

The single ion system with excess micromotion will be:

$$
\begin{aligned}
i\hbar\frac{\partial}{\partial t}\Psi(x,t) =&\Big\{ -\frac{\hbar^2}{2m_i}\frac{\partial^2}{\partial x^2} + \frac{1}{8}m_i\omega^2 x^2[a + 2q\cos(\omega t)] \\
&- eE_{\mathrm{dc}}x - eE_{\mathrm{ac}}x\sin(\omega t)\Big\}\Psi(x,t).
\end{aligned}
\tag{F.1}
$$

By using the same rotating frame as in the first section, we end up with the similar wave function:

$$
\Psi(x,t) = \exp\Big\{ -\frac{i}{\hbar}\Big[\frac{q}{4}m_i\omega x^2\sin(\omega t) + \frac{eE_{\mathrm{ac}}}{\omega}x\cos(\omega t)\Big]\Big\}\Phi(x,t),
\tag{F.2}
$$

with

$$
\begin{aligned}
i\hbar\frac{\partial}{\partial t}\Phi(x,t) =&\Big\{ -\frac{\hbar^2}{2m_i}\frac{\partial^2}{\partial x^2} + \frac{1}{2}m\omega_0^2 x^2 - eE_{dc}x \\
&- m_i(\gamma\omega_0)^2 x^2\cos(2\omega t) + 2i\hbar\gamma\omega_0\left(x\frac{\partial}{\partial x} + \frac{1}{2}\right)\sin(\omega t) \\
&+ \frac{\gamma\omega_0}{\omega}eE_{ac}x\sin(2\omega t) + i\hbar\frac{eE_{ac}}{m_i\omega}\cos(\omega t)\frac{\partial}{\partial x} + \frac{1}{2m_i}\left(\frac{eE_{\mathrm{ac}}}{\omega}\right)^2[\cos(\omega t)]^2\Big\}\Phi(x,t).
\end{aligned}
\tag{F.3}
$$

Effectively, the system with excess micromotion can be described as:

$$
H(t) = H_0 + H_{\mathrm{mm}}(t) + H_{\mathrm{ex}}(t),
$$

with

$$
\begin{aligned}
H_0 =&\frac{1}{2m_i}P^2 + \frac{1}{2}m_i\omega_0^2 X^2 - eE_{dc}X; \\
H_{\mathrm{mm}}(t) =& -m_i(\gamma\omega_0)^2 X^2\cos(2\omega t) - \gamma\omega_0\{X,\,P\}\sin(\omega t); \\
H_{\mathrm{ex}}(t) =&\frac{\gamma\omega_0}{\omega}eE_{ac}X\sin(2\omega t) - \frac{eE_{ac}}{m_i\omega}P\cos(\omega t).
\end{aligned}
$$

In order to get the similar form of H_0, we can define $\delta d \equiv eE_{dc}/\left(m_i\omega_0^2\right)$ and use $Y \equiv X - \delta d$. The position X was shifted by δd. Then we have:

$$H_0 = \frac{1}{2m_i}P^2 + \frac{1}{2}m_i\omega_0^2 Y^2 - \frac{1}{2}m_i\omega_0^2\left(\delta d\right)^2; \tag{F.4}$$

$$H_{\text{mm}}(t) = -m_i(\gamma\omega_0)^2 Y^2 \cos(2\omega t) - \gamma\omega_0\left\{Y,\ P\right\}\sin(\omega t); \tag{F.5}$$

$$H_{\text{ex}-\text{ac}}\left(t\right) = \frac{\gamma\omega_0}{\omega}eE_{ac}Y\sin(2\omega t) - \frac{eE_{ac}}{m_i\omega}P\cos(\omega t); \tag{F.6}$$

$$H_{\text{ex}-\text{dc}}\left(t\right) = -2m_i\left(\gamma\omega_0\right)^2\delta d \cdot Y\cos(2\omega t) - 2\gamma\omega_0\delta d \cdot P\sin(\omega t); \tag{F.7}$$

$$H_{\text{extra}}\left(t\right) = -m_i\left(\gamma\omega_0\right)^2\left(\delta d\right)^2 \cdot \cos(2\omega t) + \frac{\gamma\omega_0}{\omega}eE_{ac}\left(\delta d\right)\sin(2\omega t). \tag{F.8}$$

Let's take the gauge $t_0 = 0$ again and calculate the Magnus expansion for the ionic Hamiltonian. The Fourier expansion $H(t) = \sum_{l\in\mathbb{Z}}H_l e^{il\omega t}$ is:

$$H_0 = \frac{1}{2m_i}P^2 + \frac{1}{2}m_i\omega_0^2 Y^2 - \frac{1}{2}m_i\omega_0^2\left(\delta d\right)^2; \tag{F.9}$$

$$H_1 = \frac{i}{2}\gamma\omega_0\left\{Y,\ P\right\} - \frac{eE_{ac}}{2m_i\omega}P + i\gamma\omega_0\delta d \cdot P; \tag{F.10}$$

$$H_{-1} = \frac{-i}{2}\gamma\omega_0\left\{Y,\ P\right\} - \frac{eE_{ac}}{2m_i\omega}P - i\gamma\omega_0\delta d \cdot P; \tag{F.11}$$

$$H_2 = -\frac{1}{2}m_i(\gamma\omega_0)^2 Y^2 - \frac{i}{2}\frac{\gamma\omega_0}{\omega}eE_{ac}Y - m_i\left(\gamma\omega_0\right)^2\delta d \cdot Y; \tag{F.12}$$

$$H_{-2} = -\frac{1}{2}m_i(\gamma\omega_0)^2 Y^2 + \frac{i}{2}\frac{\gamma\omega_0}{\omega}eE_{ac}Y - m_i\left(\gamma\omega_0\right)^2\delta d \cdot Y. \tag{F.13}$$

The first two terms of the Magnus expansion will be:

$$\begin{aligned}H_F^{(1)} = &\frac{1}{2m_i}P^2\left(4\frac{\gamma\omega_0}{\omega}\right) - \frac{1}{2}m_i\omega_0^2 Y^2\left(4\frac{\gamma\omega_0}{\omega}\right)\\ &+ \frac{1}{2m_i}P\left(\frac{eE_{ac}}{\omega}\frac{\gamma\omega_0}{\omega}\right) - \frac{1}{2}m_i\omega_0^2 Y\left(4\delta d\frac{\gamma\omega_0}{\omega}\right);\end{aligned} \tag{F.14}$$

$$\begin{aligned}H_F^{(2)} = &\frac{1}{2m_i}P^2\left(11\right)\left(\frac{\gamma\omega_0}{\omega}\right)^2 + \frac{1}{2}m_i\omega_0^2 Y^2\left(13 - \frac{7}{2}\gamma^2\right)\left(\frac{\gamma\omega_0}{\omega}\right)^2\\ &+ \frac{1}{2m_i}P\left(\frac{eE_{ac}}{\omega}\right)\left(\frac{2}{\gamma^2} + \frac{2}{3}\right)\left(\frac{\gamma\omega_0}{\omega}\right)^2 + \frac{1}{2}m_i\omega_0^2 Y\delta d\left(19 - 7\gamma^2\right)\left(\frac{\gamma\omega_0}{\omega}\right)^2.\end{aligned} \tag{F.15}$$

Using the results in Eq. (6.58), we have

$$H_F = \frac{1}{2m_F}\left(P + \delta p_F\right)^2 + \frac{1}{2}m_F\omega_F^2\left(X - \delta d + \delta x_F\right)^2 + \text{Const} \tag{F.16}$$

with m_F, ω_F defined in Eqs. (6.59, 6.60). The constant term is

$$\text{Const} = -\frac{1}{2}m_i\omega_0^2\left(\delta d\right)^2 - \frac{1}{2m_F}\left(\delta p_F\right)^2 - \frac{1}{2}m_F\omega_F^2\left(\delta x_F\right)^2$$

with:

$$\begin{aligned}\delta p_F \equiv &\frac{1}{2}\frac{eE_{ac}}{\omega} \cdot \frac{\left(\gamma\omega_0/\omega\right) + \left(\frac{2}{\gamma^2} + \frac{2}{3}\right)\left(\gamma\omega_0/\omega\right)^2}{1 + 4\left(\gamma\omega_0/\omega\right) + 11\left(\gamma\omega_0/\omega\right)^2};\\ \delta x_F \equiv &\frac{1}{2}\delta d \cdot \frac{-4\left(\gamma\omega_0/\omega\right) + \left(19 - 7\gamma^2\right)\left(\gamma\omega_0/\omega\right)^2}{1 - 4\left(\gamma\omega_0/\omega\right) + \left(13 - \frac{7}{2}\gamma^2\right)\left(\gamma\omega_0/\omega\right)^2}.\end{aligned} \tag{F.17}$$

We notice that the energy levels $\hbar\omega_F \left(n + 1/2\right)$ are not modified by excess micromotion effects.

Then we look at the variance and kinetic energy in the presence of excess micromotion. The kinetic energy can be calculated as $\langle P\left(t\right)^2 \rangle / 2m_i$ and averaged over one micromotion period $2\pi/\omega$. The basis should be $\Psi\left(x,t\right)$ instead of $\Phi\left(x,t\right)$.

$$\Psi(x,t) = \exp\left\{ -\frac{i}{\hbar}\left[\frac{q}{4}m_i\omega x^2 \sin(\omega t) + \frac{eE_{\text{ac}}}{\omega}x\cos(\omega t)\right]\right\}\Phi(x,t).$$

The averaged kinetic energy will be:

$$\overline{\frac{\langle P\left(t\right)^2\rangle}{2m_i}} = \hbar\omega_F\left(n + \frac{1}{2}\right) + \frac{1}{2}m_i\omega_F^2\left(\delta d + \delta x_F\right)^2 + \frac{1}{2m_i}\left(\frac{1}{2}\right)\left(\frac{eE_{ac}}{\omega}\right)^2. \tag{F.18}$$

Appendix G

Numerov method

G.1 Formula

The one-dimensional Schrödinger equation is

$$\frac{d^2}{dx^2} u(x) = -\frac{2\mu}{\hbar^2} [E - V(x)] u(x) = -Q(x) u(x),$$

where $Q(x) > 0$ is the classically allowed region and $Q(x) < 0$ is the classically forbidden region. The bound state wave function will be $u(x \to \pm\infty) \to 0$. Here we follow the renormalized Numerov method from [152, 153].

With small step size $h_n = x_n - x_{n-1} = h$ and Taylor expansion of $u_{n\pm1} \equiv u(x \pm h)$ we have:

$$u_{n+1} = \sum_{k=0} \frac{(+h)^k}{k!} u_n^{(k)} = u_n + h u_n^{(1)} + \frac{h^2}{2!} u_n^{(2)} + \frac{h^3}{3!} u_n^{(3)} + \frac{h^4}{4!} u_n^{(4)} + \frac{h^5}{5!} u_n^{(5)} + \frac{h^6}{6!} u_n^{(6)} \quad \text{(G.1)}$$

$$u_{n-1} = \sum_{k=0} \frac{(-h)^k}{k!} u_n^{(k)} = u_n - h u_n^{(1)} + \frac{h^2}{2!} u_n^{(2)} - \frac{h^3}{3!} u_n^{(3)} + \frac{h^4}{4!} u_n^{(4)} - \frac{h^5}{5!} u_n^{(5)} + \frac{h^6}{6!} u_n^{(6)} \quad \text{(G.2)}$$

$$(u_{n+1} + u_{n-1}) = 2u_n + 2\frac{h^2}{2!} u_n^{(2)} + 2\frac{h^4}{4!} u_n^{(4)} + 2\frac{h^6}{6!} u_n^{(6)} \quad \text{(G.3)}$$

we differentiate the last line twice and multiply a factor αh^2:

$$\alpha h^2 \left(u_{n+1}^{(2)} + u_{n-1}^{(2)} \right) = \alpha \left(2h^2 u_n^{(2)} + 2\frac{h^4}{2!} u_n^{(4)} + 2\frac{h^6}{4!} u_n^{(6)} + 2\frac{h^8}{6!} u_n^{(7)} \right), \quad \text{(G.4)}$$

and then

$$(u_{n+1} + u_{n-1}) - \alpha h^2 \left(u_{n+1}^{(2)} + u_{n-1}^{(2)} \right) = 2u_n + \frac{2}{2!} h^2 u_n^{(2)} - 2\alpha h^2 u_n^{(2)}$$
$$+ 2\frac{h^4}{4!} u_n^{(4)} - 2\alpha \frac{h^4}{2!} u_n^{(4)}$$
$$+ 2\frac{h^6}{6!} u_n^{(6)} - 2\alpha \frac{h^6}{4!} u_n^{(6)} + \mathcal{O}\left(h^8\right), \quad \text{(G.5)}$$

keeping only the terms with u_n and $u_n^{(2)}$, we find $\alpha = 1/12$ and

$$(u_{n+1} + u_{n-1}) - \frac{1}{12} h^2 \left(u_{n+1}^{(2)} + u_{n-1}^{(2)} \right) = 2u_n + \frac{10}{12} h^2 u_n^{(2)} - \frac{h^6}{240} u_n^{(6)} + \mathcal{O}\left(h^8\right),$$

with the relations $u_n^{(2)} = -Q_n u_n$ and $u_n^{(6)} \sim Q_n^3 u_n$ we get the three term recurrence relations:

$$\left(1 - h^2 T_{n+1}\right) u_{n+1} = \left(2 + 10h^2 T_n\right) u_n - \left(1 - h^2 T_{n-1}\right) u_{n-1} - \frac{72}{10} h^6 T_n^3 u_n + \mathcal{O}\left(h^8\right),$$

here we use $T_n \equiv -Q_n/12$, which is different from [153].

G.2   Integrate

G.2.1   Outward

For outward from left to right, we define the ratio

$$R_n \equiv \frac{u_{n+1}}{u_n},$$

which is slightly different from [153]. Then we have

$$R_n = \frac{1}{\left(1 - h^2 T_{n+1}\right)} \left[\left(2 + 10h^2 T_n\right) - \left(1 - h^2 T_{n-1}\right) \frac{1}{R_{n-1}}\right] - \frac{72}{10} h^6 T_n^3$$

with error

$$\epsilon \approx \frac{72}{10} |h^6 T_n^3| \approx \frac{h^6 |Q_n^3|}{240}$$

in each step. In the calculation, we set the step size

$$h_n = \frac{(0.1\epsilon)^{1/6}}{\sqrt{Q_n}} \ll \frac{(240\epsilon)^{1/6}}{\sqrt{Q_n}}.$$

From [153], the cumulative error of the Numerov method at fixed value of x is of order h^4. The wave function

$$u_{n+1} = R_n u_n$$

needs to be normalized in the end.

For a very large Q_n in the classically allowed region (or larger $|Q_n|$ on the other hand), the wave function oscillates very fast with period

$$\Lambda \approx \frac{2\pi}{\sqrt{|Q_n|}}.$$

In order to keep the accuracy, we need at least $N \approx 20$ points in each period Λ as $h_n \approx \Lambda/N$. From previous results, we have $N (0.1\epsilon)^{1/6} \approx 2\pi$. The accuracy $\epsilon = 1E - 5$ corresponds to $N \approx 60$ points and $\epsilon = 1E - 6$ corresponds to $N \approx 90$ points.

G.2.2   Inward

For inward from right to left, we define the ratio

$$\tilde{R}_n \equiv \frac{u_{n-1}}{u_n},$$

and then

$$\tilde{R}_n = \frac{1}{\left(1 - h^2 T_{n-1}\right)} \left[\left(2 + 10h^2 T_n\right) - \left(1 - h^2 T_{n+1}\right) \frac{1}{R_{n+1}}\right]$$

with the same error as outward. The wave function should be $u_{n-1} = \tilde{R}_n u_n$.

G.2.3   Eigenenergies

The ratios from inward and outward should be matched at connection point $n = M$. We define

$$D\left(E\right) \equiv \tilde{R}_{M+1}^{-1} - R_M.$$

The eigenenergy is found by solving $D\left(E\right) = 0$ for each energy level. The node of the wave functions is given by the number of negative R_n and $\tilde{R}_n$. There is another $D\left(E\right)$ used in [153] , which works equally well.

G.3   Change step size

For the changing of step size, we always define

$$h_n = x_n - x_{n-1}; \quad c_n = \frac{h_{n+1}}{h_n}; \quad T_n \equiv -Q_n/12.$$

G.3.1   Doubling and halving:

G.3.1.1   Outward doubling:

When the outward step size is doubled as $c_n = h_{n+1}/h_n = 2$, we need to calculate $R_n = u_{n+1}/u_n$. In this case, we need the wave function u_{n-2} rather than u_{n-1} for the relation, with the new step size $h' = h_{n+1} = 2h_n$:

$$\left(1 + \frac{h'^2}{12}Q_{n+1}\right)u_{n+1} = \left(2 - 10\frac{h'^2}{12}Q_n\right)u_n - \left(1 + \frac{h'^2}{12}Q_{n-2}\right)u_{n-2},$$

then we have

$$R_n = \frac{1}{\left(1 - h'^2 T_{n+1}\right)}\left[\left(2 + 10h'^2 T_n\right) - \left(1 - h'^2 T_{n-2}\right)\frac{1}{R_{n-1}R_{n-2}}\right],$$

with $T_n = -Q_n/12$.

G.3.1.2   Outward halving:

When the outward step size is halved $c_n = h_{n+1}/h_n = 1/2$, we need $u_{n-\frac{1}{2}}$ rather than u_{n-1}, with the new step size $h' = h_{n+1} = \frac{1}{2}h_n$:

$$\left(1 + \frac{h'^2}{12}Q_{n+1}\right)u_{n+1} = \left(2 - 10\frac{h'^2}{12}Q_n\right)u_n - \left(1 + \frac{h'^2}{12}Q_{n-\frac{1}{2}}\right)u_{n-\frac{1}{2}},$$

$$\left(1 - h'^2 T_{n+1}\right)u_{n+1} = \left(2 + 10h'^2 T_n\right)u_n - \left(1 - h'^2 T_{n-\frac{1}{2}}\right)u_{n-\frac{1}{2}},$$

with $T_{n-\frac{1}{2}} = -Q\left(x_n - h'\right)/12$. From the relation:

$$u_{n-\frac{1}{2}} = \frac{1}{\left(2 - 10\frac{h'^2}{12}Q_{n-\frac{1}{2}}\right)}\left[\left(1 + \frac{h'^2}{12}Q_n\right)u_n + \left(1 + \frac{h'^2}{12}Q_{n-1}\right)u_{n-1}\right]$$

$$= \frac{1}{\left(2 + 10h'^2 T_{n-\frac{1}{2}}\right)}\left[\left(1 - h'^2 T_n\right)u_n + \left(1 - h'^2 T_{n-1}\right)u_{n-1}\right],$$

we have

$$R_n = \frac{1}{(1 - h'^2 T_{n+1})} \left\{ \left(2 + 10 h'^2 T_n\right) - \frac{\left(1 - h'^2 T_{n-\frac{1}{2}}\right)}{\left(2 + 10 h'^2 T_{n-\frac{1}{2}}\right)} \left[\left(1 - h'^2 T_n\right) + \left(1 - h'^2 T_{n-1}\right) \frac{1}{R_{n-1}} \right] \right\}.$$

G.3.1.3   Inward doubling:

When the outward step size is doubled as $c_n = h_{n+1}/h_n = 1/2$, we need to calculate $\tilde{R}_n = u_{n-1}/u_n$. In this case, we need the wave function u_{n+2} rather than u_{n+1} for the relation, with the new step size $h' = h_n = 2 h_{n+1} = 2 h_{n+2}$:

$$\left(1 + \frac{h'^2}{12} Q_{n-1}\right) u_{n-1} = \left(2 - 10 \frac{h'^2}{12} Q_n\right) u_n - \left(1 + \frac{h'^2}{12} Q_{n+2}\right) u_{n+2},$$

then we have

$$\tilde{R}_n = \frac{1}{(1 - h'^2 T_{n-1})} \left[\left(2 + 10 h'^2 T_n\right) - \left(1 - h'^2 T_{n+2}\right) \frac{1}{\tilde{R}_{n+1} \tilde{R}_{n+2}} \right].$$

G.3.1.4   Inward halving:

When the outward step size is halved $c_n = h_{n+1}/h_n = 2$, we need $u_{n+\frac{1}{2}}$ rather than u_{n+1}, with the new step size $h' = h_n = \frac{1}{2} h_{n+1}$:

$$\left(1 + \frac{h'^2}{12} Q_{n-1}\right) u_{n-1} = \left(2 - 10 \frac{h'^2}{12} Q_n\right) u_n - \left(1 + \frac{h'^2}{12} Q_{n+\frac{1}{2}}\right) u_{n+\frac{1}{2}},$$

$$\left(1 - h'^2 T_{n-1}\right) u_{n-1} = \left(2 + 10 h'^2 T_n\right) u_n - \left(1 - h'^2 T_{n+\frac{1}{2}}\right) u_{n+\frac{1}{2}},$$

with $T_{n+\frac{1}{2}} = -Q\left(x_n + h'\right)/12$. From the relation:

$$\begin{aligned}
u_{n+\frac{1}{2}} &= \frac{1}{\left(2 - 10 \frac{h'^2}{12} Q_{n+\frac{1}{2}}\right)} \left[\left(1 + \frac{h'^2}{12} Q_n\right) u_n + \left(1 + \frac{h'^2}{12} Q_{n+1}\right) u_{n+1} \right] \\
&= \frac{1}{\left(2 + 10 h'^2 T_{n+\frac{1}{2}}\right)} \left[\left(1 - h'^2 T_n\right) u_n + \left(1 - h'^2 T_{n+1}\right) u_{n+1} \right],
\end{aligned}$$

we have

$$\tilde{R}_n = \frac{1}{(1 - h'^2 T_{n-1})} \left\{ \left(2 + 10 h'^2 T_n\right) - \frac{\left(1 - h'^2 T_{n+\frac{1}{2}}\right)}{\left(2 + 10 h'^2 T_{n+\frac{1}{2}}\right)} \left[\left(1 - h'^2 T_n\right) + \left(1 - h'^2 T_{n+1}\right) \frac{1}{R_{n+1}} \right] \right\}.$$

G.3.2   General case

Here we consider the case when $c_n = h_{n+1}/h_n$ is arbitrary rather than 2 or 1/2. The Taylor expansion of $u_{n\pm 1}$ will be:

$$u_{n+1} = \sum_{k=0} \frac{(h_{n+1})^k}{k!} u_n^{(k)} = u_n + c_n h_n u_n^{(1)} + \frac{(c_n h_n)^2}{2!} u_n^{(2)} + \frac{(c_n h_n)^3}{3!} u_n^{(3)} + \frac{(c_n h_n)^4}{4!} u_n^{(4)}$$

$$+ \frac{(c_n h_n)^5}{5!} u_n^{(5)} + \frac{(c_n h_n)^6}{6!} u_n^{(6)}; \tag{G.6}$$

$$u_{n-1} = \sum_{k=0} \frac{(-h_n)^k}{k!} u_n^{(k)} = u_n - h u_n^{(1)} + \frac{h^2}{2!} u_n^{(2)} - \frac{h^3}{3!} u_n^{(3)} + \frac{h^4}{4!} u_n^{(4)}$$

$$- - \frac{h^5}{5!} u_n^{(5)} + \frac{h^6}{6!} u_n^{(6)}; \tag{G.7}$$

$$(A u_{n+1} + B u_{n-1}) = (A + B) u_n + (A c_n - B) h_n u_n^{(1)} + (A c_n^2 + B) \frac{h_n^2}{2!} u_n^{(2)}$$

$$+ (A c_n^3 - B) \frac{h_n^3}{3!} u_n^{(3)} + (A c_n^4 + B) \frac{h_n^4}{4!} u_n^{(4)}. \tag{G.8}$$

We differentiate the last term twice and multiply with a factor h^2 to get $h^2 \left(A u_{n+1}^{(2)} + B u_{n-1}^{(2)} \right)$. Then we end with the relation:

$$(u_{n+1} + c_n \cdot u_{n-1}) - h_n^2 \left(A u_{n+1}^{(2)} + B u_{n-1}^{(2)} \right)$$

$$= (1 + c_n) u_n + \left[\frac{(c_n^2 + c_n)}{2!} - (A + B) \right] h_n^2 u_n^{(2)}$$

$$+ \left[\frac{(c_n^3 - c_n)}{3!} - (A c_n - B) \right] h_n^3 u_n^{(3)} + \left[\frac{(c_n^4 + c_n)}{4!} - \frac{(A c_n^2 + B)}{2!} \right] h_n^4 u_n^{(4)}$$

$$+ \left[\frac{(c_n^5 - c_n)}{5!} - \frac{(A c_n^3 - B)}{3!} \right] h_n^5 u_n^{(5)} + \left[\frac{(c_n^6 + c_n)}{6!} - \frac{(A c_n^4 + B)}{4!} \right] h_n^6 u_n^{(6)} + \mathcal{O}\left(h^7 \right).$$

Keeping only the terms with u_n and $u_n^{(2)}$, we find

$$A_n = \frac{1}{12} \left(-1 + c_n + c_n^2 \right); \quad B_n = \frac{1}{12} \left(c_n + c_n^2 - c_n^3 \right),$$

and then use the relations $u_n^{(2)} = -Q_n u_n$ and

$$\left(1 + A_n Q_{n+1} h_n^2 \right) u_{n+1} = \left((1 + c_n) + \left[\frac{(c_n^2 + c_n)}{2!} - (A + B) \right] Q_n h_n^2 \right) u_n$$

$$- \left(c_n + B_n Q_{n-1} h_n^2 \right) u_{n-1} + \left(\frac{(c_n^5 - c_n)}{5!} - \frac{(A c_n^3 - B)}{3!} \right) h_n^5 u_n^{(5)}. \tag{G.9}$$

1. For $c_n = 1$, the formula reduces to the fixed-step size Numerov method with error $\epsilon \approx \frac{|Q_n^3|}{240} h_n^6$ in each step.

2. For $c_n = 2$, doubling the size, we have an error $\epsilon \approx \frac{|Q_n|^{5/2}}{3} h_n^5$ in each step.

3. For $c_n = 1/2$, having the size, we have an error $\epsilon \approx \frac{|Q_n|^{5/2}}{192} h_n^5$ in each step. Fortunately, the step size only changes few times with $c_n \neq 1$. The cumulative error is as good as for the fixed-step size Numerov method.

4. It is possible to use a four-point formula involving u_n, u_{n-1}, u_{n-2} to calculate u_{n+1}. The formula has an error $\epsilon \approx \mathcal{O}\left(h_n^7\right)$ in each step. However, the result is not better than for the fixed-step size since the errors are also arising from Numerov method itself.

Bibliography

[1] S. Lloyd, Science **273**, 1073 (1996).

[2] D. Jaksch, C. Bruder, J. Cirac, C. Gardiner, and P. Zoller, Phys. Rev. Lett. **81**, 3108 (1998).

[3] J. I. Cirac and P. Zoller, Nat. Phys. **8**, 264 (2012).

[4] I. Bloch, J. Dalibard, and S. Nascimbène, Nat. Phys. **8**, 267 (2012).

[5] I. Bloch, J. Dalibard, and W. Zwerger, Rev. Mod. Phys. **80**, 885 (2008).

[6] T. Gericke, P. Würtz, D. Reitz, T. Langen, and H. Ott, Nat. Phys. **4**, 949 (2008).

[7] W. S. Bakr, J. I. Gillen, A. Peng, S. Fölling, and M. Greiner, Nature **462**, 74 (2009).

[8] J. F. Sherson, C. Weitenberg, M. Endres, M. Cheneau, I. Bloch, and S. Kuhr, Nature **467**, 68 (2010).

[9] F. Serwane, G. Zürn, T. Lompe, T. B. Ottenstein, a. N. Wenz, and S. Jochim, Science **332**, 336 (2011).

[10] R. P. Feynman, Int. J. Theor. Phys. **21**, 467 (1982).

[11] Y.-J. Lin, R. L. Compton, K. Jiménez-García, J. V. Porto, and I. B. Spielman, Nature **462**, 628 (2009).

[12] D. Cocks, P. P. Orth, S. Rachel, M. Buchhold, K. Le Hur, and W. Hofstetter, Phys. Rev. Lett. **109**, 205303 (2012).

[13] U. Bissbort, *Dynamical Effects and Disorder in Ultracold Bosonic Matter*, Phd thesis (2012).

[14] M. Greiner, *Ultracold quantum gases in three-dimensional optical lattice potential*, Phd thesis (2003).

[15] C. Chin, R. Grimm, P. Julienne, and E. Tiesinga, Rev. Mod. Phys. **82**, 1225 (2010).

[16] M. Greiner, O. Mandel, T. Esslinger, T. W. Hänsch, and I. Bloch, Nature **415**, 39 (2002).

[17] S. Diehl, E. Rico, M. a. Baranov, and P. Zoller, Nat. Phys. **7**, 15 (2011).

[18] A. J. Daley, Adv. Phys. **63**, 77 (2014).

[19] W. D. Phillips, Rev. Mod. Phys. **70**, 721 (1998).

[20] C. J. Pethick and H. Smith, *Bose-Einstein Condensation in Dilute Gases* (Cambridge University Press, 2008).

[21] F. Ferlaino and R. Grimm, Physics). **3**, 9 (2010).

[22] M. Olshanii, Phys. Rev. Lett. **81**, 938 (1998).

[23] E. Haller, R. Hart, M. J. Mark, J. G. Danzl, L. Reichsöllner, and H.-C. Nägerl, Phys. Rev. Lett. **104**, 200403 (2010).

[24] Y. Nishida and S. Tan, Phys. Rev. Lett. **101**, 170401 (2008).

[25] G. Lamporesi, J. Catani, G. Barontini, Y. Nishida, M. Inguscio, and F. Minardi, Phys. Rev. Lett. **104**, 153202 (2010).

[26] I. Bloch, Nature **453**, 1016 (2008).

[27] M. Holthaus, J. Phys. B At. Mol. Opt. Phys. **49**, 13001 (2016).

[28] C. W. Gardiner, A. S. Parkins, and P. Zoller, Phys. Rev. A **46**, 4363 (1992).

[29] R. Dum, P. Zoller, and H. Ritsch, Phys. Rev. A **45**, 4879 (1992).

[30] J. Dalibard, Y. Castin, and K. Mølmer, Phys. Rev. Lett. **68**, 580 (1992).

[31] Y. Castin and K. Mo/lmer, Phys. Rev. A **54**, 5275 (1996).

[32] F. Herrera and R. V. Krems, Phys. Rev. A **84**, 051401 (2011).

[33] S. Mostame, P. Rebentrost, A. Eisfeld, A. J. Kerman, D. I. Tsomokos, and A. Aspuru-Guzik, New J. Phys. **14**, 105013 (2012).

[34] J. P. Hague and C. MacCormick, Phys. Rev. Lett. **109**, 223001 (2012).

[35] J. P. Hague and C. MacCormick, New J. Phys. **14**, 033019 (2012).

[36] L. Mathey, D.-W. Wang, W. Hofstetter, M. Lukin, and E. Demler, Phys. Rev. Lett. **93**, 120404 (2004).

[37] D. J. J. Marchand, G. De Filippis, V. Cataudella, M. Berciu, N. Nagaosa, N. V. Prokof'ev, A. S. Mishchenko, and P. C. E. Stamp, Phys. Rev. Lett. **105**, 266605 (2010).

[38] T. Holstein, Ann. Phys. (N. Y). **8**, 343 (1959).

[39] G. D. Mahan, *Many-particle physics* (Springer US, 2000).

[40] D. Golež, J. Bonča, L. Vidmar, and S. A. Trugman, Phys. Rev. Lett. **109**, 236402 (2012).

[41] W. Zwerger, Z. Phys. B - Condens. Matter **53**, 53 (1983).

[42] A. Leggett, S. Chakravarty, A. T. Dorsey, M. P. A. Fisher, A. Garg, and W. Zwerger, Rev. Mod. Phys. **59**, 1 (1987).

[43] K. Agarwal, I. Martin, M. Lukin, and E. Demler, Phys. Rev. B **87**, 144201 (2013).

[44] J. Zaanen and A. M. Oles, Phys. Rev. B **37**, 9423 (1988).

[45] A. Lanzara, P. V. Bogdanov, X. J. Zhou, S. A. Kellar, D. L. Feng, E. D. Lu, T. Yoshida, H. Eisaki, A. Fujimori, K. Kishio, J. I. Shimoyama, T. Noda, S. Uchida, Z. Hussain, and Z. X. Shen, Nature **412**, 510 (2001).

[46] J. Devreese and S. Alexandrov, Reports Prog. Phys. **72**, 066501 (2009).

[47] A. S. Alexandrov and J. T. Devreese, *Advances in Polaron Physics*, Springer Series in Solid-State Sciences, Vol. 159 (2010).

[48] V. M. Stojanović, T. Shi, C. Bruder, and J. I. Cirac, Phys. Rev. Lett. **109**, 250501 (2012).

[49] A. Grier, M. Cetina, F. Oručević, and V. Vuletić, Phys. Rev. Lett. **102**, 223201 (2009).

[50] C. Zipkes, S. Palzer, C. Sias, and M. Köhl, Nature **464**, 388 (2010).

[51] S. Schmid, A. Härter, and J. H. Denschlag, Phys. Rev. Lett. **105**, 133202 (2010).

[52] L. Ratschbacher, C. Zipkes, C. Sias, and M. Köhl, Nat. Phys. **8**, 649 (2012).

[53] J. Casanova, A. Mezzacapo, L. Lamata, and E. Solano, Phys. Rev. Lett. **108**, 190502 (2012).

[54] K. Günter, T. Stöferle, H. Moritz, M. Köhl, and T. Esslinger, Phys. Rev. Lett. **96**, 180402 (2006).

[55] S. Ospelkaus, C. Ospelkaus, O. Wille, M. Succo, P. Ernst, K. Sengstock, and K. Bongs, Phys. Rev. Lett. **96**, 180403 (2006).

[56] T. Best, S. Will, U. Schneider, L. Hackermüller, D. van Oosten, I. Bloch, and D.-S. Lühmann, Phys. Rev. Lett. **102**, 030408 (2009).

[57] S. Will, T. Best, S. Braun, U. Schneider, and I. Bloch, Phys. Rev. Lett. **106**, 115305 (2011).

[58] W. Casteels, J. Tempere, and J. T. Devreese, Phys. Rev. A **86**, 043614 (2012).

[59] C. Mora and F. Chevy, Phys. Rev. A **80**, 033607 (2009).

[60] A. Schirotzek, C.-H. Wu, A. Sommer, and M. W. Zwierlein, Phys. Rev. Lett. **102**, 230402 (2009).

[61] S. Nascimbène, N. Navon, K. J. Jiang, L. Tarruell, M. Teichmann, J. McKeever, F. Chevy, and C. Salomon, Phys. Rev. Lett. **103**, 170402 (2009).

[62] W. Yi and W. Zhang, Phys. Rev. Lett. **109**, 140402 (2012).

[63] P. Massignan, M. Zaccanti, and G. M. Bruun, Reports Prog. Phys. **77**, 034401 (2014).

[64] M. Cetina, M. Jag, R. S. Lous, J. T. M. Walraven, R. Grimm, R. S. Christensen, and G. M. Bruun, Phys. Rev. Lett. **115**, 135302 (2015).

[65] F. M. Cucchietti and E. Timmermans, Phys. Rev. Lett. **96**, 210401 (2006).

[66] M. Bruderer, A. Klein, S. Clark, and D. Jaksch, Phys. Rev. A **76**, 011605 (2007).

[67] J. Tempere, W. Casteels, M. Oberthaler, S. Knoop, E. Timmermans, and J. Devreese, Phys. Rev. B **80**, 184504 (2009).

[68] A. Privitera and W. Hofstetter, Phys. Rev. A **82**, 063614 (2010).

[69] T. Fukuhara, A. Kantian, M. Endres, M. Cheneau, P. Schauß, S. Hild, D. Bellem, U. Schollwöck, T. Giamarchi, C. Gross, I. Bloch, and S. Kuhr, Nat. Phys. **9**, 235 (2013).

[70] R. S. Christensen, J. Levinsen, and G. M. Bruun, Phys. Rev. Lett. **115**, 160401 (2015).

[71] J. Levinsen, M. M. Parish, and G. M. Bruun, Phys. Rev. Lett. **115**, 125302 (2015).

[72] M. Hohmann, F. Kindermann, B. Gänger, T. Lausch, D. Mayer, F. Schmidt, and A. Widera, EPJ Quantum Technol. **2**, 23 (2015).

[73] F. Grusdt and E. Demler, arXiv:1510.04934 (2015).

[74] M.-G. Hu, M. J. Van de Graaff, D. Kedar, J. P. Corson, E. A. Cornell, and D. S. Jin, arXiv:1605.00729 (2016).

[75] G. Pupillo, A. Griessner, A. Micheli, M. Ortner, D.-W. Wang, and P. Zoller, Phys. Rev. Lett. **100**, 050402 (2008).

[76] M. Ortner, A. Micheli, G. Pupillo, and P. Zoller, New J. Phys. **11**, 055045 (2009).

[77] F. Herrera, K. W. Madison, R. V. Krems, and M. Berciu, Phys. Rev. Lett. **110**, 223002 (2013).

[78] M. Gullans, T. G. Tiecke, D. E. Chang, J. Feist, J. D. Thompson, J. I. Cirac, P. Zoller, and M. D. Lukin, Phys. Rev. Lett. **109**, 235309 (2012).

[79] R. Mottl, F. Brennecke, K. Baumann, R. Landig, T. Donner, and T. Esslinger, Science **336**, 1570 (2012).

[80] U. Bissbort, D. Cocks, A. Negretti, Z. Idziaszek, T. Calarco, F. Schmidt-Kaler, W. Hofstetter, and R. Gerritsma, Phys. Rev. Lett. **111**, 080501 (2013).

[81] D. K. K. Lee and J. M. F. Gunn, Phys. Rev. B **46**, 301 (1992).

[82] E. Braaten and H. W. Hammer, Phys. Rep. **428**, 259 (2006).

[83] P. Massignan and Y. Castin, Phys. Rev. A **74**, 013616 (2006).

[84] M. Bruderer, A. Klein, S. R. Clark, and D. Jaksch, New J. Phys. **10**, 033015 (2008).

[85] A. Daley, P. Fedichev, and P. Zoller, Phys. Rev. A **69**, 022306 (2004).

[86] F. Grusdt, A. Shashi, D. Abanin, and E. Demler, Phys. Rev. A **90**, 063610 (2014).

[87] F. Grusdt, Y. E. Shchadilova, A. N. Rubtsov, and E. Demler, Sci. Rep. **5**, 12124 (2015).

[88] R. A. Harris and R. Silbey, J. Chem. Phys. **83**, 1069 (1985).

[89] J. Chatterjee and A. N. Das, Phys. Rev. B **61**, 4592 (2000).

[90] V. M. Stojanović, P. A. Bobbert, and M. A. J. Michels, Phys. Rev. B **69**, 144302 (2004).

[91] P. Barone, R. Raimondi, M. Capone, and C. Castellani, Phys. Rev. B **73**, 085120 (2006).

[92] D. Benjamin and E. Demler, Phys. Rev. A **89**, 033615 (2014).

[93] S. Dutta and E. J. Mueller, Phys. Rev. A **88**, 053601 (2013).

[94] C. Kohstall, M. Zaccanti, M. Jag, a. Trenkwalder, P. Massignan, G. M. Bruun, F. Schreck, and R. Grimm, Nature **485**, 615 (2012).

[95] A. Wenz, G. Zürn, S. Murmann, I. Brouzos, T. Lompe, and S. Jochim, Science **342**, 457 (2013).

[96] F. Chevy, Phys. Rev. A **74**, 29 (2006).

[97] F. Chevy and C. Mora, Reports Prog. Phys. **73**, 112401 (2010).

[98] R. Combescot, A. Recati, C. Lobo, and F. Chevy, Phys. Rev. Lett. **98**, 180402 (2007).

[99] J. Heinze, S. Götze, J. S. Krauser, B. Hundt, N. Fläschner, D. S. Lühmann, C. Becker, and K. Sengstock, Phys. Rev. Lett. **107**, 135303 (2011).

[100] N. Spethmann, F. Kindermann, S. John, C. Weber, D. Meschede, and A. Widera, Phys. Rev. Lett. **109**, 235301 (2012).

[101] R. Scelle, T. Rentrop, A. Trautmann, T. Schuster, and M. K. Oberthaler, Phys. Rev. Lett. **111**, 070401 (2013).

[102] D. Chen, C. Meldgin, and B. DeMarco, Phys. Rev. A **90**, 013602 (2014).

[103] R. Silbey and R. W. Munn, J. Chem. Phys. **72**, 2763 (1980).

[104] R. W. Munn and R. Silbey, J. Chem. Phys. **83**, 1843 (1985).

[105] R. W. Munn and R. Silbey, J. Chem. Phys. **83**, 1854 (1985).

[106] D. Chen, J. Ye, H. Zhang, and Y. Zhao, J. Phys. Chem. B **115**, 5312 (2011).

[107] C. A. Parra-Murillo, J. Madroñero, and S. Wimberger, Phys. Rev. A **88**, 032119 (2013).

[108] C. A. Parra-Murillo, J. Madroñero, and S. Wimberger, Phys. Rev. A **89**, 053610 (2014).

[109] D. H. Santamore and E. Timmermans, New J. Phys. **13**, 103029 (2011).

[110] T. Yin, P. Zhang, and W. Zhang, Phys. Rev. A **84**, 052727 (2011).

[111] E. Malatsetxebarria, Z. Cai, U. Schollwöck, and M. Cazalilla, Phys. Rev. A **88**, 063630 (2013).

[112] Z. Lan and C. Lobo, Phys. Rev. A **90**, 033627 (2014).

[113] Z. Cai, U. Schollwöck, and L. Pollet, Phys. Rev. Lett. **113**, 260403 (2014).

[114] A. Griessner, A. Daley, S. Clark, D. Jaksch, and P. Zoller, Phys. Rev. Lett. **97**, 220403 (2006).

[115] A. Griessner, A. J. Daley, S. R. Clark, D. Jaksch, and P. Zoller, New J. Phys. **9**, 44 (2007).

[116] R. Kalas and D. Blume, Phys. Rev. A **73**, 043608 (2006).

[117] D.-S. Lühmann, K. Bongs, K. Sengstock, and D. Pfannkuche, Phys. Rev. Lett. **101**, 050402 (2008).

[118] M. Bruderer, W. Bao, and D. Jaksch, EPL **82**, 7 (2008).

[119] D. Roberts and S. Rica, Phys. Rev. Lett. **102**, 025301 (2009).

[120] D. W. Wang, M. D. Lukin, and E. Demler, Phys. Rev. A **72**, 051604(R) (2005).

[121] F. D. Klironomos and S. W. Tsai, Phys. Rev. Lett. **99**, 100401 (2007).

[122] P. Anders, P. Werner, M. Troyer, M. Sigrist, and L. Pollet, Phys. Rev. Lett. **109**, 206401 (2012).

[123] M. Bukov and L. Pollet, Phys. Rev. B - Condens. Matter Mater. Phys. **89**, 094502 (2014).

[124] S. Rica and D. C. Roberts, Phys. Rev. A **80**, 013609 (2009).

[125] T. Yin, D. Cocks, and W. Hofstetter, Phys. Rev. A **92**, 063635 (2015).

[126] B. Liu and L. Yin, Phys. Rev. A **84**, 043630 (2011).

[127] T. Koponen, J.-P. Martikainen, J. Kinnunen, and P. Törmä, Phys. Rev. A **73**, 033620 (2006).

[128] R. Micnas, J. Ranninger, S. Robaszkiewicz, and S. Tabor, Phys. Rev. B **37**, 9410 (1988).

[129] M. Bukov, *Bose-Fermi Mixtures: A Mean-Field Study*, Master thesis, LMU Munich (2013).

[130] A. B. Eriksson, T. Einarsson, and S. Ostlund, Phys. Rev. B **52**, 3662 (1995).

[131] R. Micnas, J. Ranninger, and S. Robaszkiewicz, Rev. Mod. Phys. **62**, 113 (1990).

[132] D. Leibfried, R. Blatt, C. Monroe, and D. Wineland, Rev. Mod. Phys. **75**, 281 (2003).

[133] B. P. Lanyon, C. Hempel, D. Nigg, M. Müller, R. Gerritsma, F. Zähringer, P. Schindler, J. T. Barreiro, M. Rambach, G. Kirchmair, M. Hennrich, P. Zoller, R. Blatt, and C. F. Roos, Science **334**, 13 (2011).

[134] R. Blatt and C. F. Roos, Nat. Phys. **8**, 277 (2012).

[135] M. Cetina, A. T. Grier, and V. Vuletić, Phys. Rev. Lett. **109**, 253201 (2012).

[136] S. Earnshaw, Trans. Camb. Phil. Soc., **7**, 97 (1842).

[137] L. Brown, Phys. Rev. Lett. **66**, 527 (1991).

[138] S. Brouard and J. Plata, Phys. Rev. A **63**, 043402 (2001).

[139] R. J. Cook, D. G. Shankland, and A. L. Wells, Phys. Rev. A **31**, 564 (1985).

[140] A. Eckardt and E. Anisimovas, New J. Phys. **17**, 093039 (2015).

[141] S. Blanes, F. Casas, J. a. Oteo, and J. Ros, Phys. Rep. **470**, 151 (2009).

[142] M. Bukov, L. D'Alessio, and A. Polkovnikov, Adv. Phys. **64**, 139 (2015).

[143] L. D'Alessio and M. Rigol, Phys. Rev. X **4**, 041048 (2014).

[144] P. Ponte, A. Chandran, Z. Papić, and D. a. Abanin, Ann. Phys. (N. Y). **353**, 196 (2015).

[145] M. Rigol, V. Dunjko, and M. Olshanii, Nature **452**, 854 (2008).

[146] E. Khatami, G. Pupillo, M. Srednicki, and M. Rigol, Phys. Rev. Lett. **111**, 050403 (2013).

[147] Z. Idziaszek, T. Calarco, and P. Zoller, Phys. Rev. A **76**, 033409 (2007).

[148] H. Doerk, Z. Idziaszek, and T. Calarco, Phys. Rev. A **81**, 012708 (2010).

[149] L. H. Nguyên, A. Kalev, M. D. Barrett, and B.-G. Englert, Phys. Rev. A **85**, 052718 (2012).

[150] G. Grosso and G. P. Parravicini, *Solid State Physics, 2nd Edition* (2013) p. 434.

[151] N. Goldman and J. Dalibard, Phys. Rev. X **4**, 31027 (2014).

[152] J. M. Blatt, J. Comput. Phys. **1**, 382 (1967).

[153] B. R. Johnson, J. Chem. Phys. **67**, 4086 (1977).

Acknowledgments

First of all, I would like to express my sincere gratitude to my supervisor Professor Dr. Walter Hofstetter for giving me the opportunity to write my Ph.D. thesis in his group. I appreciate for his helpfulness supports, fruitful discussions, and various opportunities to participate conferences and workshops. All of these, as well as the great research environment in the institute, make me benefit a lot.

I would also like to use this opportunity to thank Professor Dr. Roser Valentí for taking time from her busy schedule to referee this thesis.

I would like to thank Professor Wei Zhang, who bring me to this fantastic research field six years ago. I am very grateful to Professor Peng Zhang for his instructions. I also very much appreciate Immanuel Bloch, Andrew Daley, Eugen Demler, Rene Gerritsma, Ferdinand Schmidt-Kaler and Artur Widera for fruitful discussions.

There are great experiences to collaborate with Daniel Cocks and Tao Qin, who help me a lot during my Ph.D. studies. I also appreciate them for proofreading this thesis and providing valuable suggestions. Many gratitudes also go to Andreas Geißler and Thomas Mertz, who translate "Zussamenfassung" in German.

I would like to thank all the people in our group, for making a pleasant and enjoyable atmosphere. Special thanks go to Marie Haußels and Liang He for settling me down when I first arrived Frankfurt. The same gratitudes go to Ulf Bissbort, Andrii Sotnikov, Ivana Vasic, and Dandan Su, who provide valuable helpfulness during the past years.

I am particularly grateful to my parents and family for their unconditional support and encouragement. Special gratitude goes to Jingnan Hu, who always encourages me and stands together with me. Last but not least, I would like to thank all my friends for supporting me and making precious memories in my life.

Curriculum Vitae

Tao Yin

Institute for Theoretical Physics,
Johann Wolfgang Goethe-University
Max-von-Laue-Strasse 1,
60438, Frankfurt am Main, Germany
taoyin@itp.uni-frankfurt.de

Research Interests

- Polaronic effects in single- and multi-band ultracold quantum system

- Dynamics in ultracold atomic system out of equilibrium

- Decoherence in open quantum system

- Hybrid atom-ion simulator and periodically driven system

Education

09/2012-present	Ph.D. Candidate in Theoretical Physics, Goethe-University, Frankfurt am Main, Germany Quantum Matter Theory Group (Prof. Dr. Walter Hofstetter) Thesis: *Polaronic and dynamical effects in ultracold quantum gases*
09/2009-07/2012	Master of Science in Theoretical Physics, Renmin University of China, Beijing, China Cold Atom Group (Prof. Wei Zhang) Thesis: *Stable heteronuclear atoms bound states in mixed dimensions*
09/2004-07/2008	Bachelor of Science in Applied Physics, Nanjing University of Aeronautics and Astronautics, Jiangsu, China Condensed Matter Group (Prof. Changgeng Ding) Thesis: *Magnetic properties and electronic orbital of transition-metal clusters*

Teaching Experience

04/2016-08/2016	Teaching assistant for "Quantum Mechanics"

10/2015-02/2016   Teaching assistant for "Thermodynamic and Statistical Mechanics"

04/2015-08/2015   Teaching assistant for "Computational Physics and Simulations in Matlab"

10/2014-02/2015   Teaching assistant for "Theoretical Electrodynamics"

10/2013-02/2014   Teaching assistant for "Computational Physics and Simulations in Matlab"

04/2013-08/2013   Teaching assistant for "Quantum Mechanics"

10/2012-02/2013   Teaching assistant for "Computational Physics and Simulations in Matlab"

Honors & Awards

2012   Excellent Master Thesis (1/16), Renmin University of China

2011   Excellent Graduate Student (1/10), Renmin University of China

2011   Best Poster Presentation (3/18), The 5th National Conference on Cold
                    Atomic Gases and Quantum Information of China

2009, 2010, 2011   First-Grade Scholarship, Renmin University of China

Personal

Language skills: Chinese (native); English (fluent); German (basic A1)

Computer skills: Matlab; Mathematica; C;
                    LaTex; Microsoft Office; Mendeley; Adobe Illustrator;

Publications

Peer reviewed journals

1.   Tao Yin, Daniel Cocks, and Walter Hofstetter
     Polaronic effects in one- and two-band quantum systems
     Physical Review A **92**, 063635 (2015). (Editor's suggestion)

2.   Tao Yin, Peng Zhang, and Wei Zhang
     Stable heteronuclear few-atom bound states in mixed dimensions
     Physical Review A **84**, 052727 (2011).

Work in progress

3.   Tao Yin and Walter Hofstetter
     Interacting polarons and exotic phases in Bose-Fermi mixtures

4.   Tao Yin, Tao Qin, and Walter Hofstetter
     Micromotion induced heating and decoherence in a hybrid atom-ion system

5.   Tao Yin, Daniel Cocks, and Walter Hofstetter
     Polaronic phenomena in an interacting neutral atom-ion system